

**Charles University**

**Faculty of Science**

Developmental and Cell Biology



**Ing. Markéta Končická**

Role and regulation of nuclear membrane during meiotic maturation of mammalian oocyte

Role a regulace jaderné membrány během meiotického zrání savčího oocyty

Doctoral thesis

Supervisor: Ing. Michal Kubelka, CSc.

Advisor: Ing. Andrej Šušor, Ph.D.

Prague, 2019

**Prohlášení:**

Prohlašuji, že jsem závěrečnou práci vypracovala samostatně a že jsem uvedla všechny použité informační zdroje a literaturu. Také prohlašuji, že tato práce ani její podstatná část nebyla předložena k získání jiného nebo stejného akademického titulu.

I hereby declare that I wrote this thesis independently, using the cited literature. This work or a substantial part of it has not been submitted elsewhere to obtain any other academic degree.

V Praze, 2019

Markéta Končická

Podpis:

## **Acknowledgement**

At first place I would like to thank my supervisor Ing. Michal Kubelka, CSc. who gave me an opportunity to elaborate my PhD study in his lab, and for his guidance. Also I am grateful to my advisor Andrej Susor for helpful ideas and for considerable time spent discussing my project.

I would like to thank to other PhD students from our lab, namely: Anna Tetkova, Denisa Jansova and Edgar Del Llano for discussion of every problem and also for helping with experiments. Great thanks is to our technician assistants Jaroslava Supolikova and Marketa Hancova for the help with operation of the laboratory and experiments.

Finally, I would like to thank to my family and especially to Ondra for endless support and help.

## Abstract

Meiotic division of a female germ cell, an oocyte, is more prone to segregation errors and consequently to aneuploidies than meiosis of a sperm. Aneuploidies and chromosomal aberrations in oocytes increase with higher maternal age in humans and also in mice. Meiotic maturation onset is connected with activity of cyclin dependent kinase 1 (CDK1) that leads to dissociation of nuclear membrane. Moreover regulation of translation of key transcripts is necessary for proper meiotic progression. In thesis findings from four scientific publications are interpreted.

We have analyzed the timing of nuclear envelope breakdown (NEBD) and polar body extrusion in mouse oocytes originating from two distinct female age groups: young (2 months old) and aged (12 months old). We found that meiotic maturation happens faster in aged females' oocytes due to early phosphorylation of Lamin A/C, a component of nuclear lamina, and rapid dissociation of nuclear membrane. Moreover aged females' oocytes presented unique characteristic invaginations of nuclear membrane and thus significantly increased circumference of the nuclear envelope compared to the oocytes from young females. These data combined with increased activity of CDK1 and Cyclin B, as well as increased translation of factors that regulate the translation itself, suggest that oocytes from aged females undergo a precocious meiotic division that can contribute to chromosomal errors in meiosis I.

To study the influence of CDK1 function during meiotic maturation in oocytes we have also elucidated the role of cyclin-dependent kinase subunit protein 2 (CKS2). *Cks2*<sup>-/-</sup> mice are infertile in both sexes with oocytes and spermatocytes arrested in metaphase of meiotic division I. These oocytes display reduced and delayed maturation-promoting factor (MPF) activity, leading to the delay of NEBD and defects in activation of the anaphase-promoting complex/cyclosome (APC/C) and meiotic spindle assembly. In *Cks2*<sup>-/-</sup> germ cells the expression of CDK1 and Cyclin A1/B1 is reduced.

We have observed that active CDK1 phosphorylates and activates mammalian target of rapamycin (mTOR). Activation of mTOR kinase leads to hyperphosphorylation and inhibition of translational repressor 4E-BP1. Inactive 4E-BP1 is released from eukaryotic initiation factor 4E (eIF4E), which can in turn form functional initiation complex eIF4F and start cap-dependent translation. In this manner CDK1 influences translation of a pool of RNAs during the meiosis onset. In addition to ongoing translation in the area of forming spindle we have observed specific localization of number of RNAs within the nucleus of oocytes before NEBD. Apart from RNAs, also active inhibitor of cap-dependent translation 4E-BP1 is localized in the nucleus, as well as the proteins connected with mRNA processing (hnRNPA1 and eIF4A3). As the specific localization of RNAs is a prerequisite for their subsequent translation, we propose that RNAs stored in the nucleus are translationally dormant and can be translated subsequently after NEBD.

Altogether, these observations show that MPF is an important regulator of many processes during meiotic maturation. It is also needed for full activation of mTOR, which inhibits 4E-BP1 and in this way allows initiation of translation. Inhibition of 4E-BP1 occurs post NEBD when previously dormant RNAs are available for cap-dependent translation. Aberrant MPF activity that occur in oocytes from aged females or in oocytes with *Cks2* deletion can lead to the increase in frequency of chromosome segregation errors, delay in the progression of meiotic maturation, or problems with polar body extrusion. Our findings should help to better understand the molecular basis of female reproductive physiology and can find usage in further research or practice.



## Abstrakt (česky)

Meiotické dělení samičí zárodečné buňky, oocyty, je více náchylné k chybám a následně k aneuploidii, než je tomu během meiózy spermií. Aneuploidie a chromozomální aberace se u oocytů zvyšují se zvyšujícím se věkem matky a to jak u lidí, tak u myši. Zahájení meiotického zrání je spojeno s aktivací cyklin-dependentní kinázy 1 (CDK1), což vede k rozpadu jaderné membrány. Kromě toho je pro správný průběh meiózy nezbytná regulace translace klíčových transkriptů. V této disertační práci jsou shrnuty poznatky ze čtyř vědeckých publikací.

Analyzovali jsme čas rozpadu jaderné membrány (NEBD) a vydělení prvního pólóvého tělíška u oocytů pocházejících od samic 2 rozdílných věkových kategorií: mladých (2 měsíce věku) a starých (12 měsíců věku). Zjistili jsme, že meiotické zrání u oocytů starých samic probíhá výrazně rychleji díky dřívější fosforylaci Laminu A/C, který je komponentem jaderné laminy, a rychlému rozpadu jaderného obalu. Mimo to oocyty starých samic vykazují unikátní charakteristické invaginace jaderné membrány a také signifikantně delší obvod jaderného obalu v porovnání s oocyty mladých samic. Tato data spolu se zvýšenou aktivitou CDK1 a Cyklinu B a také se zvýšenou translací faktorů účastnících se regulace translace naznačují, že oocyty starých samic procházejí předčasným meiotickým dělením, které může přispívat k chromozomálním chybám během meiózy I.

Pro zjištění vlivu funkce CDK1 během meiotického zrání jsme také objasnili úlohu cyklin-dependentní kinázy vázajícího proteinu 2 (CKS2). *Cks2*<sup>-/-</sup> myši obou pohlaví jsou neplodné a jejich oocyty a spermatocyty zastaví meiotické dělení v metafázi I. Tyto oocyty mají sníženou a zpožděnou aktivaci metafázi podporujícího faktoru (MPF), což vede ke zpoždění NEBD a poruchám v aktivaci anafázi podporujícího komplexu/cyklozomu (APC/C) a také k chybnému utváření meiotického vřeténka. U *Cks2*<sup>-/-</sup> zárodečných buněk je snížená exprese CDK1 a Cyklinů A1/B1.

Zjistili jsme že aktivní CDK1 fosforyluje a aktivuje protein „mammalian target of rapamycin“ (mTOR). Aktivita mTOR kinázy vede k hyperfosforylaci a inhibici translačního represoru 4E-BP1. Inaktivní 4E-BP1 je uvolněn z vazby s eukaryotním iniciačním faktorem 4E (eIF4E), který v tuto chvíli může formovat funkční iniciační komplex a cap-dependentní translaci může být zahájena. Tímto způsobem CDK1 ovlivňuje translaci RNA důležitých při zahájení meiózy. Kromě translace probíhající v oblasti vznikajícího meiotického vřeténka jsme pozorovali specifickou jadernou lokalizaci množství RNA před rozpadem jádra. Mimo RNA je v jádře uložen aktivní inhibitor cap-dependentní translace 4E-BP1 a také proteiny spojené s posttranskripčními modifikacemi mRNA (hnRNPA1 a eIF4A3). Jelikož je specifická lokalizace RNA předpokladem pro její následnou translaci, je pravděpodobné, že RNA uložená v jádře je translačně dormantní a následně dochází k její translaci po NEBD.

Tyto výsledky ukazují, že MPF je důležitým regulátorem mnoha procesů meiotického zrání. Také je potřebný pro úplnou aktivaci mTOR kinázy, která inhibuje represor cap-dependentní translace 4E-BP1. Inhibice 4E-BP1 probíhá po NEBD, kdy jsou původně dormantní RNA přístupné pro cap-dependentní translaci. Aberantní aktivita MPF, která se vyskytuje u oocytů starých samic nebo u oocytů s delecí *Cks2* může vést k nárůstu chromozomálních chyb během dělení, zpoždění průběhu meiotického zrání nebo k problémům s vydělením pólóvého tělíška. Naše zjištění přináší lepší porozumění molekulárním základům samičí/ženské reprodukční fyziologie a mohou najít uplatnění v dalším výzkumu či praxi.

## Obsah

Abstract.....	4
Abstrakt (česky).....	5
1. Introduction.....	7
1.1. Oocyte.....	7
1.2. Meiotic maturation and MPF regulation.....	7
1.3. Nuclear membrane and lamina.....	11
1.4. Ageing.....	12
2. Aims of the thesis.....	14
3. Comments on publications.....	15
3.1. Regulation of 4E-BP1 activity in the mammalian oocyte.....	16
3.2. Localization of RNA and translation in the mammalian oocyte and embryo.....	17
3.3. Increased Expression of Maturation Promoting Factor Components Speeds Up Meiosis in Oocytes from Aged Females.....	18
3.4. CKS1 Germ Line Exclusion is Essential for the Transition from Meiosis to Early Embryonic Development.....	19
4. Discussion of thesis.....	20
5. Conclusions of thesis.....	24
6. References.....	25
7. Abbreviations.....	34
8. Curriculum vitae.....	37
9. Attachment - research papers.....	39

# 1. Introduction

## 1.1. Oocyte

Oogenesis is a process, during which developmentally competent female germ cells (oocytes/eggs) are created from primordial germ cells (PGCs). Oogenesis occurs during embryonic development of female. PGCs migrate from extra embryonal mesoderm through allantois to right and left genital ridges (Gilbert and Gilbert, 2000; Saitou et al., 2002; Tam and Snow, 1981). Before invagination to the genital ridges the PGCs are surrounded by epithelial pregranulosa cells and after this invagination they become oogonia. Oogonia together with pregranulosa cells in ovaries form primordial follicles. Oogonia are mitotically active until E13.5, when they reach the maximum number of cells and subsequently can start replication of chromosomes in pre-leptotene stage (S phase) (Hernández-Hernández et al., 2012; Marston and Amon, 2004) and subsequently prophase of the first meiotic division can start (McLaren and Southee, 1997; Vanderhyden, 2002).

Before the birth of a female, oocytes enter the prophase of the first meiotic division and undergo leptotene, zygotene, pachytene and are arrested in diplotene (dictyate) stage of prophase of the first meiotic division. In zygotene stage chromosomes are attached by telomeres to nuclear membrane and centromeres of homolog chromosomes are bound together by synaptonemal complex (Cook, 1997). In this phase, all four chromatids hold together and form so-called bivalent (tetrad). During pachytene stage the chromosomes condense, and crossing over (recombination) can start. Process of recombination can continue until diplotene stage. The diplotene chromosomes remain held together by chiasmata in place where crossing over has occurred. Chiasmata hold homolog chromosomes together during first meiotic division (Székvölgyi and Nicolas, 2010). Oocytes in ovaries are after birth arrested in prophase of the first meiotic division and this stage is called germinal vesicle (GV) that corresponds to G2 phase of the cell cycle in mitotic cells (Hernández-Hernández et al., 2012; Tsafiriri et al., 1982). With the puberty onset part of the oocytes periodically start their resumption of meiotic maturation upon hormonal stimulation

## 1.2. Meiotic maturation and MPF regulation

Meiosis consists of two divisions: reduction division (meiosis I) and equational division (meiosis II) with just one DNA replication before, and results in formation of cells with haploid number of chromosomes. In meiosis I, homologous chromosomes are separated, while in meiosis II sister chromatids become segregated (Marston and Amon, 2004; Roeder, 1997). Meiosis in oocytes results in one large egg and two small polar bodies and it is finished after fertilization. The result of meiosis of a female germ cell is just one oocyte, in contrast to a sperm, where four sperm cells become formed from one precursor (Hassold and Hunt, 2001).

In GV stage the oocytes undergo growth period, during which they gradually acquire meiotic and developmental competence and during which new RNAs are massively transcribed (fig.1.). Oocytes become meiotically competent after reaching their full size by the end of the growth period. In the same time transcription is ceased and meiotic maturation of the oocytes is regulated exclusively on the level of translation and posttranslational modification(s) of proteins (De La Fuente et al., 2004). It means that oocytes have to prepare and store all the essential RNAs before meiotic maturation starts (fig.1.). Transcription is reactivated again in mouse 2-cell embryo (Matova and Cooley, 2001; Schultz, 1993).

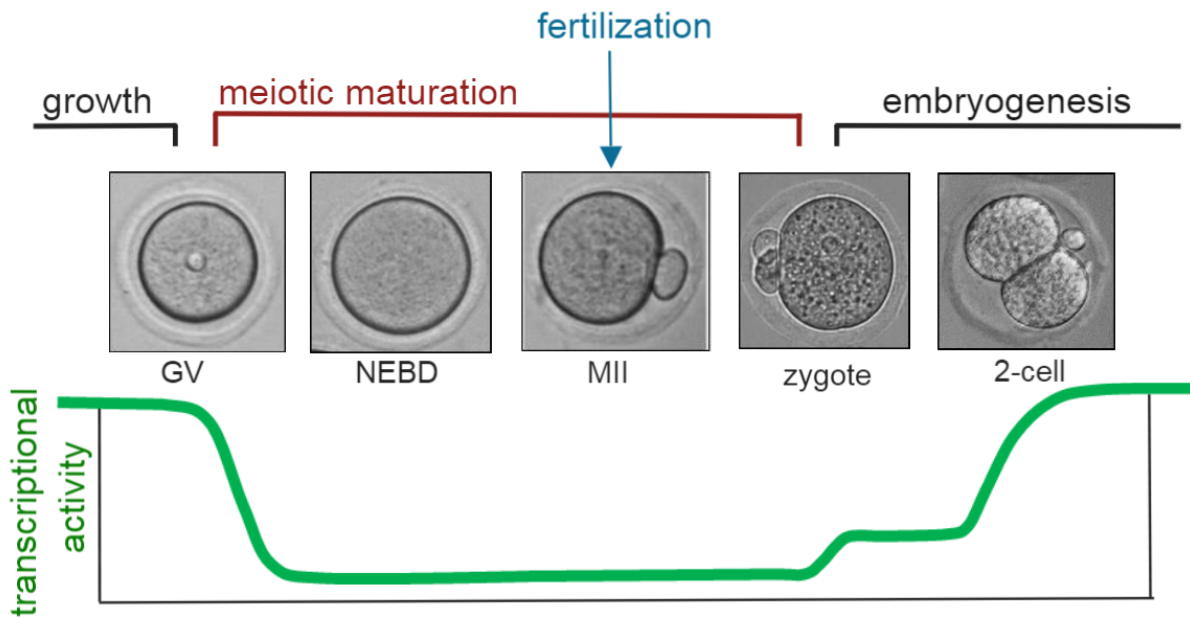


**Fig.1. Meiotic maturation of mouse oocyte.** Oocytes in GV stage reach their meiotic competence by transcribing and accumulating macromolecules. During meiotic maturation oocytes are transcriptionally ceased until the stage of 2-cell embryos. Meiotic maturation consists of nuclear envelope break down (NEBD), subsequent asymmetric division with first polar body extrusion and formation of metaphase II (MII) spindle. When MII stage oocyte is fertilized, it becomes a zygote, meiosis is completed and pronuclei are formed. Activation of embryonic genome is in 2-cell embryo coupled with increase of translation. (Created with Biorender.com)

Oocyte development occurs inside a follicle where the supporting cells are sensitive to gonadotropin hormones. Follicle-stimulating hormone (FSH) supports growing of small cohort of follicles that grow with the oocytes reaching their meiotic competence inside. Development of antral (ovulatory) follicle is dependent on FSH and luteinizing hormone (LH) stimulation, which cause growth of the follicle and changes in cumulus and follicular cells (Harman et al., 1975; Soules et al., 1984; Tsafiriri et al., 1976).

On the molecular level meiosis resumption is effectively blocked by cyclic adenosine monophosphate (cAMP) in oocyte of: *Xenopus* (Ferrell, 1999), hamster (Racowsky, 1985),

bovine (Aktas et al., 1995), rat (Dekel et al., 1981) and mouse (Cho et al., 1974). Increased cAMP is important for prevention of release from the first meiotic block of mouse and human oocyte (Cho et al., 1974). Meiotic block is supported by cumulus cells which produce cyclic guanosine monophosphate (cGMP). cGMP prevents the activation of phosphodiesterase 3A (PDE3A), which is responsible for degradation of cAMP. cGMP is distributed from cumulus cells through gap junction to the oocyte. Surge of LH decreases cGMP level in cumulus cells and subsequently, PDE3A can cause degradation of cAMP (Norris et al., 2009; Vaccari et al., 2009). Meiotic resumption of oocytes *in vivo* is controlled by LH but in mammalian oocyte the resumption can be initiated also spontaneously after release of the oocytes from the follicles to culture medium (Sato and Koide, 1984; Szybek, 1972). When the level of cAMP is decreased and PKA is inhibited, Maturation or M-phase promoting factor (MPF) can become activated (Duncan et al., 2006; Schultz et al., 1983).

Meiotic maturation is initiated by nuclear envelope breakdown (NEBD; dissociation of the nuclear membrane) and condensation of chromosomes. During prometaphase the spindle becomes formed. After all the chromosomes are attached to spindle microtubules and metaphase plate is formed, anaphase I can start followed by telophase I and the first polar body extrusion. Before fertilization the oocytes are arrested in metaphase of second meiotic division and meiosis is completed when sperm gets inside the oocyte, which in turn causes the release of  $Ca^{2+}$  ions (Cuthbertson and Cobbold, 1985; Cuthbertson et al., 1981).

Meiotic maturation is regulated by so-called maturation or M-phase promoting factor (MPF), which is composed of catalytic subunit CDK1 kinase and regulatory subunit Cyclin B (Gautier et al., 1990; Labbé et al., 1989). For its activation it is important to reach threshold of Cyclin B, whose level increases from S phase. During meiotic arrest in prophase I CDK1 is inhibited by phosphorylation at Thr14 and Tyr15 located on its ATP-binding loop (*fig.2.*) (Han et al., 2005; Nurse, 1997). Upon meiosis resumption, firstly CDK1 and Cyclin B form pre-MPF and after dephosphorylation of CDK1 at Thr14 and Tyr15 MPF becomes active (*fig.2.*) (Fattaey and Booher, 1997). The inhibition of CDK1 by phosphorylation at Thr14 and Tyr15 is maintained by WEE1B/MYT1 kinases, which are activated by protein kinase A (PKA) by phosphorylation at Ser15. WEE1B/MYT1 are important for the first meiosis arrest and down regulation of *Wee1b* RNA causes resumption of meiotic maturation in growing oocytes. On the other hand, overexpression of WEE1B can cause delay in meiotic maturation (Han et al., 2005; Kovo et al., 2006). Initiation of meiotic resumption is mediated by CDC25B phosphatase via removal of inhibitory CDK1 phosphorylation. Oocytes from *Cdc25b*<sup>-/-</sup> mouse are not able to activate CDK1 and also cannot resume meiosis (Lincoln et al., 2002). Active CDK1 also phosphorylates CDC25C, which stimulates phosphatase activity of CDC25B and this mechanism represents autocatalytic activation of CDK1 (Hoffmann et al., 1993).

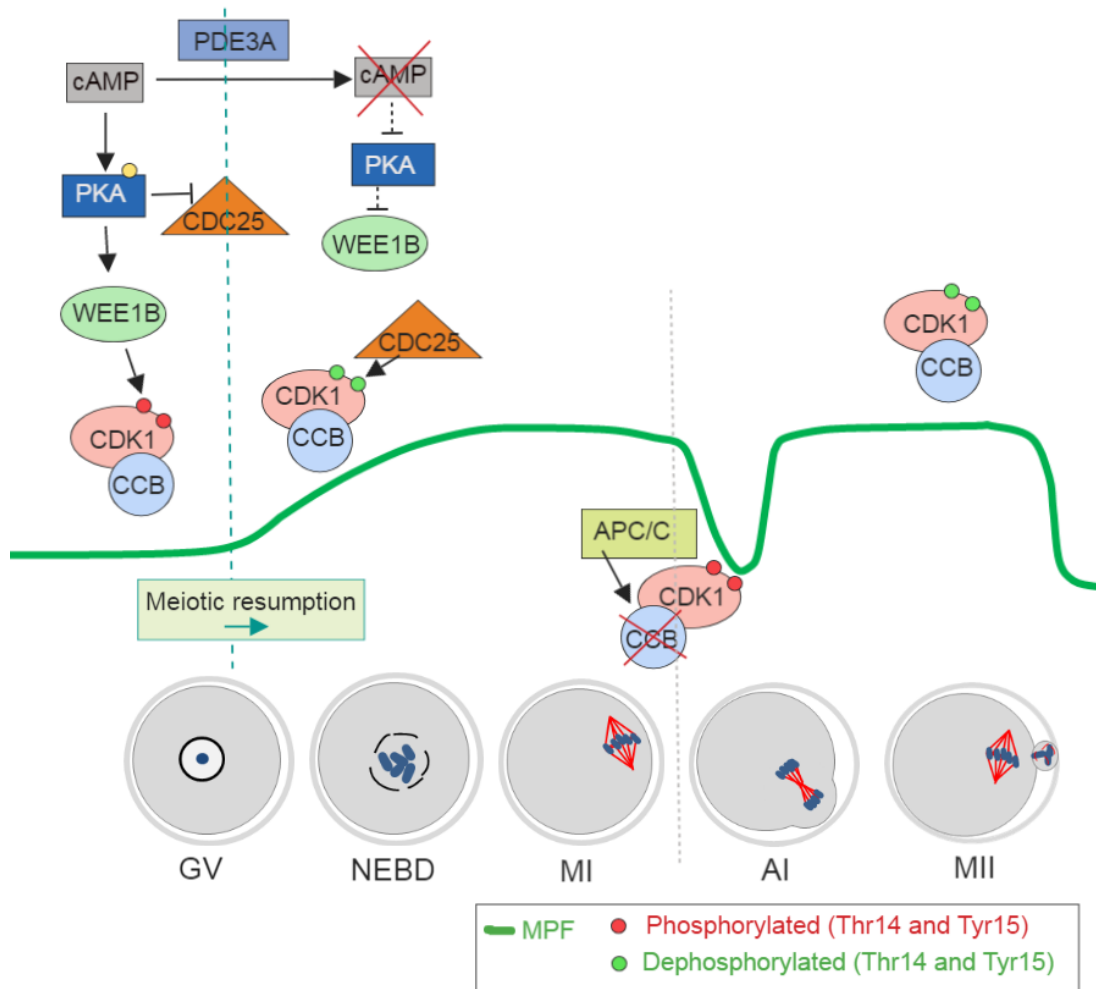


**Fig.2. MPF activity during meiotic maturation.** Resumption of meiotic maturation in GV stage is blocked by activity of cyclic adenosine monophosphate (cAMP). cAMP mediates activation of protein kinase A (PKA) which is responsible for inhibition of phosphatase CDC25 and activation of kinase WEE1B. WEE1B phosphorylates CDK1 on its inhibition sites Thr14 and Tyr15. Upon resumption of meiotic maturation cAMP is degraded by phosphodiesterase 3A (PDE3A) and PKA together with WEE1B become inactivated. Active CDC25 dephosphorylates Thr14 and Tyr15 of CDK1 and at this time MPF activity increases. Green curve shows MPF activity during the meiotic maturation of oocytes. Before anaphase I (AI) MPF activity drops down, Cyclin B (CCB) is degraded by anaphase promoting complex (APC/C) and CDK1 is newly phosphorylated at Thr14 and Tyr15. After polar body extrusion in metaphase of second meiotic division (MII) MPF is newly activated. (Created with Biorender.com)

Level of activated MPF falls down in anaphase I, which is caused by degradation of cyclin B by Anaphase-promoting complex (APC/C) (fig.2.) (Holt et al., 2010). MPF is active during first metaphase and inactivated during the first polar body extrusion, then it becomes activated in metaphase II stage and remains active until fertilization (Choi et al., 1991).

### 1.3. Nuclear membrane and lamina

Nuclear membrane (nuclear envelope) is a barrier, which separates nuclear and cytoplasmic components. Nuclear envelope is composed of inner and outer nuclear membranes, furthermore it contains nuclear pore complex and nuclear lamina. Nuclear membranes are formed of phospholipid bilayer (Mazzanti et al., 2001). Lamina protein meshwork lining the nucleoplasmic surface of inner membrane is thought to provide a framework for organizing nuclear envelope structure and an anchoring site at the nuclear periphery for interphase chromatin (Aebi et al., 1986). Based on biochemical classification and cDNA cloning nuclear Lamins belong to V group of intermediated filament proteins (Goldman et al., 1986; McKeon et al., 1986).

Lamins are encoded by three genes: *Lmna*, *Lmnb1* and *Lmnb2*. *Lmna* gene produces at least four proteins by alternative splicing: Lamin A, Lamin C, Lamin C2 and Lamin A $\Delta$ 10. *Lmnb1* codes for Lamin B1. The *Lmnb2* gene gives rise to two splicing variants: Lamin B2 and germ cell specific Lamin B3 (Dittmer and Misteli, 2011; Furukawa and Hotta, 1993).

Nuclear lamina plays role also in chromosomal organization and chromosomes segregation. During transcription and DNA replication Lamins serve as a structural support (Kennedy et al., 2000; Moir et al., 2000). Lamins of type A and C (Lamin A/C; LMN A/C) are destabilized during mitosis and meiosis, however, B type lamins are associated with nuclear membrane all the time (Gerace and Blobel, 1980).

LMN A/C can be detected in fertilized egg but after further embryonic cleavages are undetectable. Newly expressed LMN A/C are present in extraembryonic cells of mouse embryo at day 9 and in embryonal cells at day 12 (Constantinescu et al., 2006; Röber et al., 1989; Stewart and Burke, 1987). LMN A/C contains more than 30 known and conserved phosphorylation sites, which are phosphorylated by multiple kinases (Mitsubishi et al., 2010; "PhosphoSitePlus," n.d.). LMN A/C is disassembled after hyperphosphorylation that is induced by activation of MPF, which starts phosphorylation cascade of Lamin A/C. Three main kinases influencing the activity of LMN A/C are: CDK1, protein kinase C (PKC) and protein kinase A (PKA). The key phosphorylation sites, which are responsible for depolymerization of Lamin filaments in mitosis and meiosis are Thr19, Ser22 and Ser392 (Heald and McKeon, 1990; Peter et al., 1990; Ward and Kirschner, 1990). Mutation in Ser22 phosphorylation site leads to unusual phenotype in 35 % of mitotic cells – in these cells the nuclear lamina remains compact. Mutation in Ser22 together with Ser392 leads to block of disassembly of lamina in almost every cell (Heald and McKeon, 1990).

It is known that Hutchinson-Gilford Progeria Syndrome (HGPS) and Atypical Werner Syndrome cause premature aging in humans via mutation of Lamin (Kudlow et al., 2007). These cells in cell culture manifest age dependent changes in nuclear structure. Moreover, the similar markers of nuclear architecture senescence show cells of *Ceanorhabditis elegans* during normal aging. In these cells, age dependent changes manifest themselves: folding of nuclear lamina, less distinct nuclear periphery and increase of cytoplasmic localization of Lamin (Haithcock et al., 2005). Human mesenchymal stem cells show change in lamina morphology and form telomere aggregates after limited number of division. Changes in

morphology are present before expression of Hayflick-senescence-associated factors. These findings show that Lamin changes are early markers of senescence and can be also useful for detection of aging (Hayflick and Moorhead, 1961; Raz et al., 2008).

#### **1.4. Ageing**

From the reproduction point of view, ageing is accompanied by increased incidence of infertility and pregnancy loss. Especially in aged women, lower pregnancy rates and increasing numbers of pregnancy loss can be found. When these women receive oocytes from younger donors, embryo implantation and pregnancy rates are restored to normal level (Navot et al., 1994; Sauer, 1998).

Woman after birth has 500 000 - 1 000 000 follicles with oocytes in ovaries, but in puberty follicular reserve decreases to 300 000 follicles. Follicular reserve is critical when around 25 000 of follicles are present in the ovaries and this corresponds to number of follicles found in ovaries of women around 37 years of age. Women in menopause have a low number of follicles in ovaries, in age 50 around 1000 of follicles. During the whole female life some oocytes undergo atresia but with higher age number of ovulated a degraded oocytes increases and the ovarian reserve decreases (Block, 1953, 1952; Faddy et al., 1992). Previously, it was thought that number of follicles rapidly fell down in women around 37 years, but new findings show that with higher age the number of follicles decay increase gradually (Hansen et al., 2008).

The main factor responsible for increased infertility in connection of mother age is aneuploidy. The errors during first meiotic division can lead to aneuploidy and subsequently to pregnancy loss (Kusch et al., 2003). Chromosome segregation errors are frequent in mammalian female meiosis, and their incidence gradually increases with maternal age (Hassold and Chiu, 1985; Hassold and Hunt, 2001). Mammalian female meiosis is more prone to segregation errors than meiosis of sperm (more than two times higher frequency of chromosomal abnormalities). They differ also in types of abnormalities, as oocytes usually have wrong number of chromosomes, while sperms fail in chromosomal structure (Martin, 2008). The spindles of aged females (40 - 45 years old women) exhibit in 79 % abnormal tubulin placement and one or more chromosomes out of metaphase plate. Spindle abnormalities and faults in chromosome congression on the metaphase plate are associated with advanced maternal age and they likely contribute to the observed increased incidence of aneuploidy (Battaglia et al., 1996). Mouse and human have similar incidence of chromosomal segregation errors and their incidence gradually increases with maternal age (Pan et al., 2008; Sebestova et al., 2012). Young women around 20 years have aneuploidy rate around 2 % and similarly low is aneuploidy in 3 months old mouse female (~5 %). However, after 35 years of age, aneuploidy is increased to 35 % and in mouse after 12 months aneuploidy increases to 30-50 % (Chiang et al., 2010; Hassold and Hunt, 2001; Hunt, 2017; Merriman et al., 2012; Pan et al., 2008).

When a chromosome is not attached to the meiotic spindle or its attachment is wrong, this may result in uneven distribution of chromosomes. Most of aneuploidies are lethal already



during embryonic development, but trisomies of 21, 18 and 13 chromosomes (respectively Down, Edwards, Patau syndromes) are most common viable autosomal trisomies. However, trisomies 18 and 13 cause multi system disorders and frequent fetus death during pregnancy or within few weeks after birth. Frequency of these trisomies increase in women between 35 – 45 years of age (Savva et al., 2010). Trisomies and monosomies are most frequent aneuploidies in oocyte and it is also known that Down syndrome rate significantly increases with increasing maternal age (Allen et al., 2009; Hassold and Hunt, 2001).

Aneuploidy in human oocytes is caused by two main pathways: nondisjunction (NDJ) and premature separation of sister chromatids (PSSC). “Nondisjunction” means a failure of the segregation of homologous chromosomes (meiosis I), while PSSC happens when sister chromatids are separated earlier than they should (meiosis II). Moreover, so-called reverse segregation can occur in meiosis I when sister chromatids are segregated instead of homologous chromosomes. These oocytes have correct number of chromosomes but chromosomes are from different parents and are not held together, which can lead to errors during metaphase II.

In studies analyzing donor oocytes and polar bodies from woman between 33 and 41 years, at least one oocyte from each woman displayed reverse segregation (Ottolini et al., 2015). But in other study, oocytes from younger donors (25 – 35years) reverse segregation was not detected (Hou et al., 2013). Studies of trisomies and monosomies indicated that 80 to 90 % of them resulted from nondisjunction in oocyte MI stage (Hassold and Hunt, 2001). Most human aneuploidies observed after analysis of the first or the second polar bodies showed aneuploidy for chromosome 16, 22, 21 and 15 (Fragouli et al., 2011; Gabriel et al., 2011; Handyside et al., 2012).

With higher age the cohesion between sister chromatids gradually decreases and frequency of their separation also increases. Distance between chromatids of young mouse oocyte is 0.2 – 0.4  $\mu\text{m}$  and in aged female it increases to double size. This distance increases with age also in human oocytes (Chiang et al., 2010; Duncan et al., 2012; Merriman et al., 2012).

Proper MPF activity is important for correct disassembly of nuclear membrane in NEBD and also for regulation of whole meiotic maturation. With higher maternal age the frequency of errors caused during meiotic division is increased. Changes in regulation of meiotic maturation can cause non-equal chromosomal division which can lead to loss of pregnancy or fetus disorder.

## 2. Aims of the thesis

During the growth phase, before the oocytes reinitiate meiosis, they store transcribed RNAs and reach meiotic competence. Meiotic maturation onset is initiated by increased MPF activity which leads to phosphorylation of Lamin A/C and consequently to dissociation of nuclear envelope in NEBD (nuclear envelope breakdown) stage.

The objectives of my work were to investigate the role of nuclear membrane and nuclear lamina during meiotic maturation and factors which regulate their functions. Moreover, I have also focused my study to the alterations in MPF during meiotic maturation of aged females' oocytes and oocytes from *Cks2*<sup>-/-</sup> mice (as CKS2 protein associates with cyclin dependent kinases).

The particular aims of my thesis are following:

### 1. To investigate dynamics and regulators of nuclear envelope in the aged females' oocytes

- 1.1. To compare dissociation of nuclear envelope during meiotic maturation in mouse oocytes of two age groups: young females (2 months) and aged females (12 months).
- 1.2. To visualize nuclear membrane morphology in oocytes of the two age groups of mice.
- 1.3. Morphological evaluation of nucleus as a prerequisite of intracellular patterning/gradient of RNA and translational factors in GV oocytes and 2-cell embryos.

### 2. To study changes during meiotic division in oocytes from *Cks2*<sup>-/-</sup> mice and aged females in connection with altered MPF levels

- 2.1. To observe if MPF levels are altered in aged (12 months old) females' oocytes in comparison to young (2 months old) females' oocytes during meiotic division.
- 2.2. To detect if *Cks2*<sup>-/-</sup> mice have decreased MPF levels during meiotic maturation in comparison to the wild type mice.
- 2.3. In case of MPF levels being abnormal in *Cks2*<sup>-/-</sup> oocytes, to try to rescue NEBD by microinjection of active MPF.
- 2.4. To determine if and how MPF regulates cap-dependent translation repressor 4E-BP1.

### 3. Comments on publications

During my PhD study I have published three scientific papers in peer reviewed journals. Based on rules set by the committee of Department of Developmental and Cell Biology of Charles University my cumulative impact factor (CIF) is 5.7215. My fourth publication was submitted and is now under second revision. All my publications are listed below:

**3.1** Jansova D, **Koncicka M**, Tatkova A, Cerna R, Malik R, Del Llano E, Kubelka M, Susor A. Regulation of 4E-BP1 activity in the mammalian oocyte, **Cell Cycle**, 2017. DOI: 10.1080/15384101.2017.1295178. **IF: 3.304 (2018)**

- M.K. performed RNA microinjections and contributed to the sample preparation and manuscript writing.

**3.2** Jansova D, Tatkova A, **Koncicka M**, Susor A. Localization of RNA and translation in the mammalian oocyte and embryo, **PLoS One**, 2018. DOI: 10.1371/journal.pone.0192544. **IF 2.766 (2018)**

- M.K. contributed to experiments and prepared samples of NIH3T3 cells.

**3.3** **Koncicka M**, Tatkova A, Jansova D, Del Llano E, Gahurova L, Kracmarova J, Prokesova S, Masek T, Pospisek M, Bruce AW, Kubelka M, Susor A. Increased Expression of Maturation Promoting Factor Components Speeds Up Meiosis in Oocytes from Aged Females. **International Journal of Molecular Sciences**, 2018. DOI: 10.3390/ijms19092841. **IF: 3.687 (2018)**

- M.K. designed and performed experiments (microinjection, western blots, immunocytochemistry), analyzed data and wrote the manuscript.

#### **Publication under revision**

**3.4** Ellederova Z, del Rincon S, **Koncicka M**, Susor A, Kubelka M, Sun D, Spruck Ch. CKS1 Germ Line Exclusion is Essential for the Transition from Meiosis to Early Embryonic Development. **Molecular and Cellular Biology**, Submitted: 20.12.2018, first revision 25.1.2019

- M.K. performed all oocyte microinjections and live-cell imaging.

### 3.1. Regulation of 4E-BP1 activity in the mammalian oocyte

Initiation of cap-dependent translation is regulated by formation of eukaryotic translation initiation factor 4F (eIF4F) complex. Eukaryotic initiation factor 4E (eIF4E) is bound to translational repressor eIF4E-binding protein (4E-BP1) and this binding block/inhibits formation of eIF4F complex needed for cap-dependent translation initiation. After hyperphosphorylation of 4E-BP1, eIF4E is released from block and eIF4F complex can be formed.

Using quantitative RT-PCR we observed that in oocytes all 3 forms of *4e-bp* transcripts (*4e-bp1*, *4e-bp2* and *4e-bp3*) are expressed. Global amount of all three mRNAs is uniform during meiotic maturation (from GV to MII stage) but at the protein level only one form is expressed: 4E-BP1. In this study we investigated the localization and timing of 4E-BP1 phosphorylation in the oocytes. Global 4E-BP1 antibody which detected phosphorylated and unphosphorylated 4E-BP1 showed by immunocytochemistry staining (ICC) localization in whole cytoplasm of GV, NEBD, MI and MII stage of oocytes. In GV oocytes total 4E-BP1 was also localized in the nucleoplasm. After NEBD, we observed increased localization of global 4E-BP1 in spindle area. 4E-BP1 phosphorylated on Thr37/46 showed similar localization pattern as global 4E-BP1 after NEBD. 4E-BP1(Ser65) showed post NEBD increased expression around chromosomes, on the spindle in MI and on spindle poles in MII. 4E-BP1(Thr70) had strong localization on the forming spindle after NEBD and on the bipolar spindles in MI and MII. Antibodies to the phosphorylated forms of 4E-BP1 did not show fluorescent signal in GV oocytes. These results were confirmed by western blot analysis with global 4E-BP1 antibody, which showed one band in GV oocyte (non-phosphorylated form) and one upper shifted band (phosphorylated form) in MII, while NEBD stage contained both bands (non-phosphorylated and phosphorylated). Previously we showed that treatment with rapamycin, an mTOR inhibitor, significantly decreased expression phosphorylation of 4E-BP1 but did not stop meiotic maturation of the oocytes (Susor et al., 2015). In this study we showed that mTOR and CDK1 exhibit similar localization of fluorescent signal in oocytes after NEBD as phosphorylated 4E-BP1. Moreover, CDK1 inhibition using roscovitine in the beginning of oocyte maturation caused arrest of meiosis in GV stage. Inhibition of CDK1 after NEBD resulted in decrease of mTOR phosphorylation at Ser2448 and also significantly repressed phosphorylation of 4E-BP1. These data suggest that mTOR is regulated and activated by MPF activity and consequently cause initiation of cap-dependent translation. PLK1 is a known regulator of 4E-BP1 phosphorylation during mitosis in somatic cells (Shang et al., 2012). Also in oocytes, PLK1 is localized after NEBD in spindle assembly area. But inhibition of PLK1 by BI2536 inhibitor didn't show any effect on phosphorylation of 4E-BP1 in oocyte. This result showed that in meiosis PLK1 didn't work in a similar way as in mitosis. We further microinjected RNA coding 4E-BP1 with mutated 4 phospho-sites (Thr36/47/70 and Ser65), which cannot be phosphorylated to down-regulate phosphorylation of 4E-BP1. MII oocytes, which expressed this mutant RNA showed on western blot unphosphorylated (lower) and also phosphorylated (upper) bands in contrast to oocytes microinjected with wild type RNA, which showed just phosphorylated band, validating the mRNA microinjection. In oocytes with mutant *4e-bp1* RNA cap-dependent translation was decreased compared to control *4e-bp1* RNA, which was tested by *Renilla* Luciferase reporter

with canonical TOP motive on *Eef2*. Oocytes injected with mutant *4e-bp1* RNA, extruded polar body, but ICC analysis showed increased number of aberrant spindles, in 59% chromosomal alignment to metaphase plate was absent in comparison to 3% of WT *4e-bp1* injected oocytes.

This study reveals the localization of meiotic regulators, which play an important role in activation of cap-dependent translation after NEBD. These regulators, active CDK1 as MPF component, mTOR and inactivated 4E-BP1, concentrate to spindle area after NEBD, which is also a place with increased translation activity.

### **3.2. Localization of RNA and translation in the mammalian oocyte and embryo**

In oocytes all RNAs are transcribed before resumption of meiosis, and afterwards the oocytes remain transcriptionally inactive and utilize stored RNAs. In this study we examined localization of RNAs by different methods: RNA fluorescent in situ hybridization (FISH), rolling circle amplification (RCA), proximity ligation assay (PLA) and immunocytochemistry (ICC).

We compared localization of global and specific RNA between nucleus and cytoplasm of GV oocytes, 2-cell embryos and NIH3T3 cells. In this study we observed that poly(A) RNA was increased in nucleus of GV oocytes compared to oocyte cytoplasm, however, embryos showed 2-fold higher intensity in nucleus than oocytes. By rolling circle amplification (RCA) using random hexamers probes and detection by antibody against m7G-cap and m3G-cap we detected similar localization of RNA as by poly(A) RNA approach. After detection of abundant global RNA in nucleus we tried to localize some specific transcripts. Nuclear-enriched abundant transcript 2/metastasis associated lung adenocarcinoma transcript 1 (*Neat2/Malat1*, long noncoding RNA) known as specifically localized in nuclear speckles of HeLa cells. In accordance with this localization we found that *Neat2/Malat1* was present exclusively in the nucleus of oocytes and NIH3T3 cells, but in embryos it was localized only in the cytoplasm. Deleted in azoospermia-like RNA (*Dazl*) was localized equally in both compartments of oocytes but in embryos it was abundantly localized in cytoplasm.

Also interesting for us was localization of proteins, participating on mRNA processing and, also localization of regulators of translation. Heterogeneous nuclear ribonucleoproteins (hnRNP) represent a group of proteins, which participate on the processing, export, translation and stabilization of mRNAs. hnRNPA1 was present in nucleus of oocyte in higher abundance than in cytoplasm, but in embryos it was expressed on a similar level throughout the whole cells. Component of exon junction protein complex, eIF4A3 was released from RNA during first round of translation and it was localized mainly in the nucleus of GV oocytes and of embryos. Repressor of cap-dependent translation 4E-BP1 had increased signal in nucleus compared to cytoplasm, where it was observed in granular pattern. These results show that nucleus may work as a repository for translationally dormant mRNAs and these RNAs can be translated after NEBD, when they are released from nucleus. In addition, after NEBD cap-dependent translation starts to be more and more activated as its repressors become inhibited.

### 3.3. Increased Expression of Maturation Promoting Factor Components Speeds Up Meiosis in Oocytes from Aged Females

Aged females' (AF) oocytes undergo meiosis faster than young females' (YF) oocytes. Nuclear envelope breaks down (NEBD) and polar body extrusion happens earlier in AF oocytes than in YF oocytes. By immunocytochemistry we have detected that AF oocytes in metaphase I (6h post-IBMX-wash) have more stably end-on attached kinetochores (95.5%) than YF oocytes (75.8%,  $p < 0.01$ ). Nuclear envelope breakdown is preceded by phosphorylation of Lamin A/C, which is responsible for degradation of nuclear membrane. Phosphorylation of Lamin A/C at Ser22 is increased earlier in AF oocytes than in YF oocytes. As Lamin A/C is phosphorylated by active CDK1 we have observed also increased expression of MPF components. Our results show that CDK1, Cyclin B and activating phosphorylation of CDK1 (at Thr161) are significantly increased in aged females' oocytes. By quantitative RT-PCR we have detected significantly increased *Cdk1* and *Ccnb* transcripts in AF oocytes in comparison to YF oocytes. When we have treated oocytes 3h post NEBD by 20 $\mu$ M of roscovitine (CDK1 inhibitor) decreased phosphorylation of Lamin A/C at Ser22 can be seen when compared to non-treated oocytes. This result confirms that phosphorylation of Lamin A/C at Ser22 is dependent on CDK1 activity. By injection of RNA coding Cyclin B to YF oocytes we have been able to induce phenocopy of aged oocytes. Injected YF oocytes show similar timing of meiotic progression and also similar manner of chromosome attachment like AF oocytes.

Disrupted Lamin structures in oocytes 3h post NEBD still surround chromosomal area in YF, but in AF Lamin structures are more dissociated from chromosomal area. Electron microscopy examinations of oocytes cryosections show changes in shape of nuclear membrane in AF oocytes. AF oocytes show high number of deep invaginations, which decreases the compactness of nuclear membrane. This morphology of nuclear membrane results in significantly increased circumference in AF oocytes compared to YF oocytes. Together, these changes of nuclear membrane and increasing of CDK1 activity lead to earlier dissociation of nuclear membrane in aged females' oocytes.

By analyzing polysomal fractions we have observed up-regulation of number of mRNAs involved in translational regulation in aged females' oocytes compared to young female oocytes. Products of increased transcripts belong to following groups: eukaryotic translation initiation factors (eIF2D, eIF3E, eIF4B, eIF4E3 and eIF4G1), polyadenylation factors (PABPN1L and PABPN1), elongation factor (eEF2) and ribosomal proteins (60S-RPL6, RPL10, RPL10A, RPL17, RPL19, RPL23A, RPL24, RPL37, RPL38; 40S-RPS6, RPS8, RPS9, RPS13, RPS16 and RPS25)

This study shows that AF oocytes have altered expression and also earlier activation of MPF, which leads to faster progression of oocytes through meiosis. This precocious meiosis progression can be one of the reasons why AF oocytes have higher level of aneuploidy and can explain increased incidence of reproductive disorders in higher age females.

### 3.4. CKS1 Germ Line Exclusion is Essential for the Transition from Meiosis to Early Embryonic Development

CKS1 and CKS2 are proteins associated with cyclin dependent kinases and are important for cell division control and development. CKS1 is expressed in somatic cells whereas CKS2 is germ line specific. *Cks2*<sup>-/-</sup> knockout mice are sterile in both sexes and germ cells are arrested at metaphase of first meiotic division. Oocytes show a prolonged division during meiotic maturation and they are not able to extrude the polar body. Kinase assay shows later activation of MPF 6h post IBMX wash with maximum activation level at 8h in *Cks2*<sup>-/-</sup> oocytes in contrast to activation of MPF after 4h with maximum at 6h in wild type (WT) mouse oocytes. Also activation of mitogen-activated protein kinases (MAPK), which is important for meiotic spindle assembly, is delayed (*Cks2*<sup>-/-</sup> 6h, WT 4h). MAPK is activated by MPF through induction of expression of MOS. ICC analysis shows that 8h after meiotic resumption securin still persists in *Cks2*<sup>-/-</sup> oocytes. Normally, CDC27 is activated by MPF and consequently activation of APC/C complex leads to degradation of securin. RT-PCR analysis shows that *Cks2*<sup>-/-</sup> oocytes have reduced levels of *Cdk1*, *Ccnb1* and *Ccnal* in comparison to WT oocytes. In knockout mice the level of inhibiting phosphorylation of CDK1 at Tyr15 is also increased. By microinjection of active MPF and as a control inactive MPF we have not been able to rescue meiotic maturation of *Cks2*<sup>-/-</sup> oocytes and oocytes still arrest in MI. However, oocytes injected with active MPF make NEBD 1h earlier than *Cks2*<sup>-/-</sup> oocytes injected with inactive MPF. In oocytes injected with active MPF together with CKS2 or CKS1 protein, timing of NEBD is similar to WT oocytes. Oocytes of transgenic mice with *Cks1* expressed under *Cks2* promoter are able rescue meiosis and they are not arrested in MI. These heterozygote mice (*Cks2*<sup>cks1/-</sup>) are able to produce offspring, but they don't produce homozygote *Cks2*<sup>cks1/cks1</sup> offspring. Our additional observation show that *Cks2*<sup>cks1/cks1</sup> homozygote mice have problem with early embryonic development and they die at 2-5-cell stage embryonic development.

Our results show that CKS1 under *Cks2* promoter can rescue meiotic maturation and oocytes can be also fertilized but they have problems during early embryonic development. The role of CKS2, which is associated with CDK1 role, is essential for meiosis but also for early embryonic development in mouse.

## 4. Discussion of thesis

In my dissertation I address a question of a role of the nuclear membrane in regulation of meiotic maturation in mammalian oocyte. Nuclear membrane dissociation is the key process during meiotic maturation of oocytes. Without dissociation of nuclear membrane which is induced by active MPF, meiotic maturation cannot continue (Heald and McKeon, 1990; Peter et al., 1990). This process is altered in oocytes originating from females with increased age and also in oocytes from *Cks2*<sup>-/-</sup> mice. In both, regulation of CDK1 activity is affected. Nuclear membrane in oocytes is also important for compartmentation of different regulatory factors in nucleus and cytoplasm.

Precise timing of nuclear envelope breakdown is important for proper meiotic progression but in aged females' (AF) oocytes NEBD occurs earlier than in young females' (YF) oocytes. This findings are consistent with previously published results (Chiang et al., 2011; Eichenlaub-Ritter et al., 1988; Eichenlaub-Ritter and Boll, 1989a, 1989b; Sebestova et al., 2012). On the other hand, other reports suggested no differences in meiotic progression timing (NEBD timing) in AF oocytes (Duncan et al., 2009; Lister et al., 2010). These discrepancies can be explained by different selection of meiotically competent oocytes or different manipulation with the oocytes (e.g., microinjection, removal of cumulus cells, etc.). In YF oocytes 3h after NEBD nuclear envelope structures still persist around chromosomal area and possibly make a boundary between two translational areas (Katsani et al., 2008; Maiato et al., 2006; Schweizer et al., 2015; Susor et al., 2015). But in AF oocytes, nuclear envelope structures after NEBD (3h) visibly disassemble. We have found that oocytes from AF are more meiotically competent than oocytes from young females. From oocytes, which resume meiosis (reach metaphase II) in 12 hours period: 94% of aged females' oocytes in comparison with 84% of young female oocytes. Cui et al., (2013) show similar significantly increased meiotic competency in aged females' oocytes. But aged females' have lower number of oocytes in ovaries in comparison to young females (in average: 3 oocytes and 22 oocytes, respectively).

Earlier phosphorylation of Lamin A/C at Ser22 occurs in AF oocytes, which leads to earlier NEBD compared to YF oocytes. On the basis of these observations in AF oocytes we have tested activity of MPF. It is known that phosphorylation of Lamin A/C at Ser22 is dependent on activity of CDK1 (Heald and McKeon, 1990; Peter et al., 1990). We show that in AF GV oocytes transcripts coding for MPF components *Cdk1*, *Ccnb* and especially *Ccnb2*, which are important for prophase/metaphase transition in mouse oocytes (Gui and Homer, 2013) are significantly increased. This increased *Ccnb2* expression could be connected to accelerated meiotic maturation. Furthermore, it was also shown earlier that premature activation of MPF activity by *Ccnb* microinjection lead to precocious spindle formation, which is consistent with our observation in AF oocytes (Davydenko et al., 2013). We show that premature activation of MPF activity in AF oocytes can result in segregation errors. Additionally, we have observed that activating CDK1 phosphorylation at Thr161 is increased earlier in AF oocytes. This increased activating phosphorylation of CDK1 also participates in increased MPF activity (De Smedt et al., 2002). It is known that in addition to Cyclin B1, also Cyclin



B2 works as regulatory subunit of CDK1 and that the activity of MPF is dependent on the overall amount of Cyclins B present in the oocyte (Félix et al., 1990; Li et al., 2018; Solomon, 1993). These findings are in good agreement with our results showing that the increased expression of MPF components and activation of MPF and consequent more rapid progression of meiotic maturation (in AF versus YF) contributes to accelerated division of AF oocytes.

Using electron microscopy we have also examined changes in morphology of nuclear membrane in different age groups. AF oocytes display higher number of deep invagination and membranes have significantly increased circumference. Similar senescence changes of nuclear membrane morphology display aged somatic cells (Haithcock et al., 2005; Righolt et al., 2011). We expect that aneuploidy in the oocytes can be a consequence of the quick progress through meiosis and of early phosphorylation and dissociation of Lamin A/C in oocytes from old females. The precocious progression through meiosis can be the cause of higher rate of aneuploidy and infertility in older females. The correct timing of NEBD is likely to be required for normal spindle architecture and accurate chromosome segregation.

CKS proteins are components of MPF and their precise role or roles in regulation of MPF during meiotic maturation are not fully understood. Previously it was shown that *Cks2*<sup>-/-</sup> oocytes were arrested in metaphase I stage (Spruck et al., 2003). In our experiments we have extended previous results by showing that *Cks2*<sup>-/-</sup> oocytes have delayed NEBD in comparison to wild type oocytes. NEBD is normally induced by surge of active MPF and the activity reach maximum in metaphase I (Adhikari et al., 2012; Adhikari and Liu, 2014). In connection with observed NEBD delay in *Cks2*<sup>-/-</sup> oocytes, also decreased activity of MPF and MAPK occurs, which is in good correlation with the observations published earlier showing that MAPK is activated by MPF during the whole meiotic maturation (Minshull et al., 1994). Our findings suggest that CKS2 dependent function of MPF promotes NEBD in mammalian oocytes. However, injection of active MPF into *Cks2*<sup>-/-</sup> oocytes is not able to rescue NEBD delay completely. CDK1 is the main CDK involved in the regulation of meiotic maturation and deletion of CDK1 causes permanent arrest in the GV stage of the oocytes (Adhikari et al., 2012). Santamaría et al., (2007) show that microinjection of CDK1 to *Cdk1*<sup>-/-</sup> oocytes leads to meiotic progression, but meiosis is stopped in metaphase I and oocytes are not able to rescue meiotic maturation, which is similar to our observation from *Cks2*<sup>-/-</sup> oocytes. Our observations show that NEBD is delayed in *Cks2*<sup>-/-</sup> oocytes suggesting that absence of CKS2 can decrease CDK1 function or change targeted substrates important for promotion of NEBD. However, MPF-CKS2 substrates are currently not known. In yeast it is known that CKS proteins are important for regulation of translation by promoting the recruitment of CDK1 and the proteasome to the coding region (Yu et al., 2005). Deletion of CKS1 + CKS2 in mammalian cells disrupt transcription of *Ccnb1*, *Ccna2* and *Cdk1* (Martinsson-Ahlzén et al., 2008). Different accumulation of CKS1 (G1/S phase) and CKS2 (G2/M phase) in human cells show that these proteins have different roles during mitosis. Since CKS2 is the only CKS expressed in oocytes and spermatocytes, it is likely that they perform a specialized role in regulation of CDK1 function (Spruck et al., 2003). *Cks1* expression under *Cks2* promoter in (*Cks2*<sup>cks1/cks1</sup>) mouse can compensate for CKS2 in meiosis *in vivo*, but embryos homozygote

for *Cks1* are arrested at the 2-5-cell stage. These results show that CKS1 can rescue meiotic maturation but is lethal for embryonic development and this can be the reason for their exclusion from germ line. Homolog of CKS in *Xenopus* (Xe-p9) promotes CDK1-dependent phosphorylation of CDC25, MYT1 and WEE1 which in turn induces MPF activation (Patra et al., 1999).

These observations from *Cks2*<sup>-/-</sup> oocytes show that CKS2 is in oocytes important for regulation of CDK1 function during meiotic maturation and that CKS1 can compensate CKS2 deletion during meiosis but not in embryonic development.

MPF regulates many of molecular events during meiotic maturation: phosphorylation of nuclear lamina, nuclear envelope breakdown (NEBD), spindle assembly, activation of cap-dependent translation by inactivation of 4E-BP1, APC/C mediated deactivation of Cyclin B1 and securin and polar body extrusion and spindle assembly (Choi et al., 1991; Verlhac et al., 1994).

We have also analyzed regulation of 4E-BP1 phosphorylation during meiotic maturation of mouse oocytes. Oocytes' meiotic progression is dependent on rapid inactivation/phosphorylation of 4E-BP1, which leads to high activation of cap-dependent translation in oocytes after NEBD. Similarly as Mayer et al., (2014), we haven't detected 4E-BP2 and 4E-BP3 proteins in oocytes, which documents that only 4E-BP1 is highly expressed in mouse and bovine oocytes. However, RNA expression of all three proteins might indicate that the other members of this family can be important after fertilization or can be translated in the case when the expression of 4E-BP1 is insufficient (Tsukiyama-Kohara et al., 2001). We have found that main regulators of 4E-BP1 are mTOR and CDK1. These kinases start to be highly activated after resumption of meiotic maturation in mouse, human and, bovine oocytes (Hampl and Eppig, 1995; Mayer et al., 2014; Susor et al., 2015). Earlier, it was shown that PLK1 promoted phosphorylation of 4E-BP1 in mitosis (Shang et al., 2012). However, our results show that inhibition of PLK1 in oocytes does not induce any changes in phosphorylation of 4E-BP1, suggesting that 4E-BP1 is regulated by different mechanisms in meiosis and mitosis. Inhibition of CDK1 results in decreased mTOR phosphorylation at the activation site (Ser2448). Similarly as Heesom et al. (2001) our observations show that mTOR is the main regulator of 4E-BP1 and CDK1 in mouse oocyte is important for the full mTOR activation rather than for direct 4E-BP1 phosphorylation. Increased phosphorylation of 4E-BP1 post NEBD was earlier detected in porcine, bovine and mouse oocytes (Ellederova et al., 2006; Romasko et al., 2013; Tomek et al., 2002b, 2002a), however, localization of different forms of phosphorylated 4E-BP1 was documented only during meiotic maturation of mouse oocytes (Romasko et al., 2013). We show that 4E-BP1 forms phosphorylated at Ser65 and Thr70 are localized post NEBD in spindle formation area, and similar localization was previously shown by Romasko et al., (2013), who showed in addition also 4E-BP1 phosphorylation at Ser-112. Phosphorylation of 4E-BP1 is increased at the onset of meiotic maturation and is inactivated after fertilization (Susor et al., 2015). At the time when the activity of 4E-BP1 is inhibited by hyperphosphorylation cap-dependent translation can be activated.

After resumption of meiosis, the oocytes are transcriptionally inactive and regulation of meiotic maturation is dependent on storage and utilization of maternal RNAs and also on regulation of their translation. After disassembly of nuclear membrane, Lamin structures still persist in gap between two translation areas: chromosomal translational area-CTA and perispindular translational area-PTA (Susor et al., 2015). By staining of RNAs with several methods we have elucidated localization of global RNAs and we have observed localization of some specific RNAs in nucleus of oocytes. Exon junction protein complex eIF4A3 is also localized in nucleus and is deposited on mRNA during splicing and after first round of translation it is released from mRNA (Chan et al., 2004; Maquat et al., 2010; Shibuya et al., 2006). Heterogenous nuclear ribonucleoprotein A1 (hnRNPA1) participating in pre-mRNA processing has abundant localization in the nucleus. Despite observation showing the occurrence of translation in the nucleus (Belgrader et al., 1993; Reid and Nicchitta, 2012), our findings show inactive translation in the oocyte nucleus. RNA staining of oocytes and embryos show that nucleus of oocytes has large amount of RNAs. These stored maternal RNAs are probably dormant (Ford et al., 1999) and this prediction is supported by nuclear localization of 4E-BP1, which inhibits translation (Jansova et al., 2017), hnRNPA1 and eIF4A3. Also the absence of phosphorylated RPS6 which is involved in translational activation in the nucleus argue that dormant RNAs are present in the nucleus (Puighermanal et al., 2017; Roux et al., 2007). Phosphorylation of RPS6 on Ser235/236 increases its affinity to the cap structure and also leads to translation initiation (Roux et al., 2007). Our results show that RPS6 (Ser235/236) is localized dominantly in cytoplasm with decreased signal in nucleus of oocytes and 2-cell embryos.

In this work we document that MPF is the main regulator of nuclear membrane dissociation dynamics and that it also participates in regulation of cap-dependent translation. Increase or decrease of MPF activity behind certain limit during meiotic maturation leads to problems in meiotic division. MPF causes disassembly of nuclear membrane by phosphorylation of Lamin A/C at Ser22. It is known that increased female age leads to increasing rates of aneuploidies in human and mouse oocytes. In this study we show that increased levels of MPF activity seen in AF oocytes lead to more rapid progression of meiosis, which can be the reason for more frequent chromosome segregation errors. In addition, we have studied CDK1 aberrant activity in *Cks2*<sup>-/-</sup> oocytes which display significant decrease in MPF activity accompanied by the delay in NEBD and arrest in metaphase I. Absence of CKS2 protein is associated with the decrease of CDK1 activity and this suggests that CKS2 is important for proper regulation of CDK1.

During the growth phase of GV oocytes numerous RNAs are transcribed. Substantial part of these RNAs is localized in the nucleus of GV oocytes and they are probably translationally dormant. We propose that these RNAs post NEBD can be available for initiation of cap-dependent translation. Initiation of cap-dependent translation is also influenced by MPF activation, which leads to activation of mTOR kinase, which in turn causes inhibition of 4E-BP1 by hyperphosphorylation.

## 5. Conclusions of thesis

- In AF oocytes nuclear membrane becomes dissociated earlier than in YF oocytes. YF oocytes, 3h post NEBD show some dissociated Lamin structures localized around chromosomes, but in aged female oocytes the Lamin structures are substantially more dissociated from chromosomes.
- Electron microscopy of nuclear membrane shows its changed morphology in AF oocytes. AF oocytes display many invaginations in nuclear membrane and significantly increased circumference of the nuclear membrane in comparison to YF oocytes. This leads to lower stability of nuclear membrane, which is similar to senescence changes of nuclear envelope of somatic cells.
- We show increased expression of MPF components, both on mRNA level - *Ccnb* and *Cdk1*, and on protein level - Cyclin B and CDK1 in oocytes from aged females in comparison with young female oocytes. Accordingly, also increased level of activating phosphorylation of CDK1 at Thr161, as well as premature activation of CDK1 have been found by us in aged females when compared to young female oocytes.
- Meiotic division of *Cks2*<sup>-/-</sup> oocytes is arrested in MI stage with significant delay in NEBD. Kinase assay shows prolonged activation of CDK1 in *Cks2*<sup>-/-</sup> oocytes in comparison to wild type oocytes. *Cks2*<sup>-/-</sup> oocytes have also decreased RNA levels of *Cdk1*, *Ccnb1* and *Ccnal* when compared to WT oocytes.
- *Cks2*<sup>-/-</sup> oocytes microinjected with active MPF are not able to fully rescue NEBD delay, however, injection of active MPF together with CKS2 or CKS1 protein results in similar timing of NEBD as in WT oocytes.
- Our observations also show that CDK1 kinase induces hyperphosphorylation of 4E-BP1 through activation of mTOR, which in turn leads to release of eIF4E from its inhibition making it available for creation of an active translation initiation complex eIF4F. By this mechanism cap-dependent translation becomes activated after NEBD when CDK1/MPF is active.
- Staining of global RNAs shows abundant localization of number of RNAs in the nucleus of GV oocytes. However, the presence of active repressor of translation 4E-BP1, as well as of other proteins which participate in RNA processing (hnRNP1A, eIF4A3) within the nucleus suggest that RNAs localized in the nucleus are dormant. We suppose that these RNAs can be translated after NEBD when they are released from the nucleus.

Our findings should help to better understand the regulation of meiotic maturation in oocytes and can find usage in further research or practice. Further studies are needed to elucidate the influence of female age on regulation of meiosis in connection with the role of MPF regulation in this process.

## 6. References

- Adhikari, D., Liu, K., 2014. The regulation of maturation promoting factor during prophase I arrest and meiotic entry in mammalian oocytes. *Mol. Cell. Endocrinol.* 382, 480–487. <https://doi.org/10.1016/j.mce.2013.07.027>
- Adhikari, D., Zheng, W., Shen, Y., Gorre, N., Ning, Y., Halet, G., Kaldis, P., Liu, K., 2012. Cdk1, but not Cdk2, is the sole Cdk that is essential and sufficient to drive resumption of meiosis in mouse oocytes. *Hum. Mol. Genet.* 21, 2476–2484. <https://doi.org/10.1093/hmg/dds061>
- Aebi, U., Cohn, J., Buhle, L., Gerace, L., 1986. The nuclear lamina is a meshwork of intermediate-type filaments. *Nature* 323, 560–564. <https://doi.org/10.1038/323560a0>
- Aktas, H., Wheeler, M.B., Rosenkrans, C.F., First, N.L., Leibfried-Rutledge, M.L., 1995. Maintenance of bovine oocytes in prophase of meiosis I by high [cAMP]<sub>i</sub>. *J. Reprod. Fertil.* 105, 227–235.
- Allen, E.G., Freeman, S.B., Druschel, C., Hobbs, C.A., O’Leary, L.A., Romitti, P.A., Royle, M.H., Torfs, C.P., Sherman, S.L., 2009. Maternal age and risk for trisomy 21 assessed by the origin of chromosome nondisjunction: a report from the Atlanta and National Down Syndrome Projects. *Hum Genet* 125, 41–52. <https://doi.org/10.1007/s00439-008-0603-8>
- Battaglia, D.E., Goodwin, P., Klein, N.A., Soules, M.R., 1996. Influence of maternal age on meiotic spindle assembly in oocytes from naturally cycling women. *Hum. Reprod.* 11, 2217–2222.
- Belgrader, P., Cheng, J., Maquat, L.E., 1993. Evidence to implicate translation by ribosomes in the mechanism by which nonsense codons reduce the nuclear level of human triosephosphate isomerase mRNA. *Proc. Natl. Acad. Sci. U.S.A.* 90, 482–486.
- Block, E., 1953. A quantitative morphological investigation of the follicular system in newborn female infants. *Acta Anat (Basel)* 17, 201–206.
- Block, E., 1952. Quantitative morphological investigations of the follicular system in women; variations at different ages. *Acta Anat (Basel)* 14, 108–123.
- Chan, C.C., Dostie, J., Diem, M.D., Feng, W., Mann, M., Rappsilber, J., Dreyfuss, G., 2004. eIF4A3 is a novel component of the exon junction complex. *RNA* 10, 200–209.
- Chiang, T., Duncan, F.E., Schindler, K., Schultz, R.M., Lampson, M.A., 2010. Evidence that weakened centromere cohesion is a leading cause of age-related aneuploidy in oocytes. *Curr. Biol.* 20, 1522–1528. <https://doi.org/10.1016/j.cub.2010.06.069>
- Chiang, T., Schultz, R.M., Lampson, M.A., 2011. Age-dependent susceptibility of chromosome cohesion to premature separase activation in mouse oocytes. *Biol. Reprod.* 85, 1279–1283. <https://doi.org/10.1095/biolreprod.111.094094>
- Cho, W.K., Stern, S., Biggers, J.D., 1974. Inhibitory effect of dibutyryl cAMP on mouse oocyte maturation in vitro. *J. Exp. Zool.* 187, 383–386. <https://doi.org/10.1002/jez.1401870307>
- Choi, T., Aoki, F., Mori, M., Yamashita, M., Nagahama, Y., Kohmoto, K., 1991. Activation of p34cdc2 protein kinase activity in meiotic and mitotic cell cycles in mouse oocytes and embryos. *Development* 113, 789–795.
- Constantinescu, D., Gray, H.L., Sammak, P.J., Schatten, G.P., Csoka, A.B., 2006. Lamin A/C expression is a marker of mouse and human embryonic stem cell differentiation. *Stem Cells* 24, 177–185. <https://doi.org/10.1634/stemcells.2004-0159>
- Cook, P.R., 1997. The transcriptional basis of chromosome pairing. *Journal of Cell Science* 110, 1033–1040.

- Cui, L.-B., Zhou, X.-Y., Zhao, Z.-J., Li, Q., Huang, X.-Y., Sun, F.-Z., 2013. The Kunming mouse: as a model for age-related decline in female fertility in human. *Zygote* 21, 367–376. <https://doi.org/10.1017/S0967199412000123>
- Cuthbertson, K.S., Cobbold, P.H., 1985. Phorbol ester and sperm activate mouse oocytes by inducing sustained oscillations in cell Ca<sup>2+</sup>. *Nature* 316, 541–542.
- Cuthbertson, K.S.R., Whittingham, D.G., Cobbold, P.H., 1981. Free Ca<sup>2+</sup> increases in exponential phases during mouse oocyte activation. *Nature* 294, 754. <https://doi.org/10.1038/294754a0>
- Davydenko, O., Schultz, R.M., Lampson, M.A., 2013. Increased CDK1 activity determines the timing of kinetochore-microtubule attachments in meiosis I. *J. Cell Biol.* 202, 221–229. <https://doi.org/10.1083/jcb.201303019>
- De La Fuente, R., Viveiros, M.M., Burns, K.H., Adashi, E.Y., Matzuk, M.M., Eppig, J.J., 2004. Major chromatin remodeling in the germinal vesicle (GV) of mammalian oocytes is dispensable for global transcriptional silencing but required for centromeric heterochromatin function. *Developmental Biology* 275, 447–458. <https://doi.org/10.1016/j.ydbio.2004.08.028>
- De Smedt, V., Poulhe, R., Cayla, X., Dessauge, F., Karaiskou, A., Jesus, C., Ozon, R., 2002. Thr-161 phosphorylation of monomeric Cdc2. Regulation by protein phosphatase 2C in *Xenopus* oocytes. *J. Biol. Chem.* 277, 28592–28600. <https://doi.org/10.1074/jbc.M202742200>
- Dekel, N., Lawrence, T.S., Gilula, N.B., Beers, W.H., 1981. Modulation of cell-to-cell communication in the cumulus-oocyte complex and the regulation of oocyte maturation by LH. *Dev. Biol.* 86, 356–362.
- Dittmer, T.A., Misteli, T., 2011. The lamin protein family. *Genome Biol* 12, 222. <https://doi.org/10.1186/gb-2011-12-5-222>
- Duncan, F.E., Chiang, T., Schultz, R.M., Lampson, M.A., 2009. Evidence That a Defective Spindle Assembly Checkpoint Is Not the Primary Cause of Maternal Age-Associated Aneuploidy in Mouse Eggs<sup>1</sup>. *Biology of Reproduction* 81, 768–776. <https://doi.org/10.1095/biolreprod.109.077909>
- Duncan, F.E., Hornick, J.E., Lampson, M.A., Schultz, R.M., Shea, L.D., Woodruff, T.K., 2012. Chromosome cohesion decreases in human eggs with advanced maternal age. *Aging Cell* 11, 1121–1124. <https://doi.org/10.1111/j.1474-9726.2012.00866.x>
- Duncan, F.E., Moss, S.B., Williams, C.J., 2006. Knockdown of the cAMP-dependent protein kinase (PKA) Type Ialpha regulatory subunit in mouse oocytes disrupts meiotic arrest and results in meiotic spindle defects. *Dev. Dyn.* 235, 2961–2968. <https://doi.org/10.1002/dvdy.20930>
- Eichenlaub-Ritter, U., Boll, I., 1989a. Age-related non-disjunction, spindle formation and progression through maturation of mammalian oocytes. *Prog. Clin. Biol. Res.* 318, 259–269.
- Eichenlaub-Ritter, U., Boll, I., 1989b. Nocodazole sensitivity, age-related aneuploidy, and alterations in the cell cycle during maturation of mouse oocytes. *Cytogenetic and Genome Research* 52, 170–176. <https://doi.org/10.1159/000132871>
- Eichenlaub-Ritter, U., Chandley, A.C., Gosden, R.G., 1988. The CBA mouse as a model for age-related aneuploidy in man: studies of oocyte maturation, spindle formation and chromosome alignment during meiosis. *Chromosoma* 96, 220–226.
- Ellederova, Z., Kovarova, H., Melo-Sterza, F., Livingstone, M., Tomek, W., Kubelka, M., 2006. Suppression of translation during in vitro maturation of pig oocytes despite enhanced formation of cap-binding protein complex eIF4F and 4E-BP1 hyperphosphorylation. *Mol. Reprod. Dev.* 73, 68–76. <https://doi.org/10.1002/mrd.20368>

- Faddy, M.J., Gosden, R.G., Gougeon, A., Richardson, S.J., Nelson, J.F., 1992. Accelerated disappearance of ovarian follicles in mid-life: implications for forecasting menopause. *Hum. Reprod.* 7, 1342–1346.
- Fattaey, A., Booher, R.N., 1997. Myt1: a Wee1-type kinase that phosphorylates Cdc2 on residue Thr14. *Prog Cell Cycle Res* 3, 233–240.
- Félix, M.A., Cohen, P., Karsenti, E., 1990. Cdc2 H1 kinase is negatively regulated by a type 2A phosphatase in the *Xenopus* early embryonic cell cycle: evidence from the effects of okadaic acid. *EMBO J.* 9, 675–683.
- Ferrell, J.E., 1999. *Xenopus* oocyte maturation: new lessons from a good egg. *Bioessays* 21, 833–842. [https://doi.org/10.1002/\(SICI\)1521-1878\(199910\)21:10<833::AID-BIES5>3.0.CO;2-P](https://doi.org/10.1002/(SICI)1521-1878(199910)21:10<833::AID-BIES5>3.0.CO;2-P)
- Ford, C.L., Randal-Whitis, L., Ellis, S.R., 1999. Yeast Proteins Related to the p40/Laminin Receptor Precursor Are Required for 20S Ribosomal RNA Processing and the Maturation of 40S Ribosomal Subunits. *Cancer Res* 59, 704–710.
- Fragouli, E., Alfarawati, S., Goodall, N., Sánchez-García, J.F., Colls, P., Wells, D., 2011. The cytogenetics of polar bodies: insights into female meiosis and the diagnosis of aneuploidy. *Mol Hum Reprod* 17, 286–295. <https://doi.org/10.1093/molehr/gar024>
- Furukawa, K., Hotta, Y., 1993. cDNA cloning of a germ cell specific lamin B3 from mouse spermatocytes and analysis of its function by ectopic expression in somatic cells. *EMBO J* 12, 97–106.
- Gabriel, A.S., Thornhill, A.R., Ottolini, C.S., Gordon, A., Brown, A.P.C., Taylor, J., Bennett, K., Handyside, A., Griffin, D.K., 2011. Array comparative genomic hybridisation on first polar bodies suggests that non-disjunction is not the predominant mechanism leading to aneuploidy in humans. *Journal of Medical Genetics* 48, 433–437. <https://doi.org/10.1136/jmg.2010.088070>
- Gautier, J., Minshull, J., Lohka, M., Glotzer, M., Hunt, T., Maller, J.L., 1990. Cyclin is a component of maturation-promoting factor from *Xenopus*. *Cell* 60, 487–494.
- Gerace, L., Blobel, G., 1980. The nuclear envelope lamina is reversibly depolymerized during mitosis. *Cell* 19, 277–287.
- Gilbert, S.F., Gilbert, S.F., 2000. *Developmental Biology*, 6th ed. Sinauer Associates.
- Goldman, A.E., Maul, G., Steinert, P.M., Yang, H.Y., Goldman, R.D., 1986. Keratin-like proteins that coisolate with intermediate filaments of BHK-21 cells are nuclear lamins. *Proc Natl Acad Sci U S A* 83, 3839–3843.
- Gui, L., Homer, H., 2013. Hec1-dependent cyclin B2 stabilization regulates the G2-M transition and early prometaphase in mouse oocytes. *Dev. Cell* 25, 43–54. <https://doi.org/10.1016/j.devcel.2013.02.008>
- Haithecock, E., Dayani, Y., Neufeld, E., Zahand, A.J., Feinstein, N., Mattout, A., Gruenbaum, Y., Liu, J., 2005. Age-related changes of nuclear architecture in *Caenorhabditis elegans*. *Proc. Natl. Acad. Sci. U.S.A.* 102, 16690–16695. <https://doi.org/10.1073/pnas.0506955102>
- Hampl, A., Eppig, J.J., 1995. Translational regulation of the gradual increase in histone H1 kinase activity in maturing mouse oocytes. *Mol. Reprod. Dev.* 40, 9–15. <https://doi.org/10.1002/mrd.1080400103>
- Han, S.J., Chen, R., Paronetto, M.P., Conti, M., 2005. Wee1B is an oocyte-specific kinase involved in the control of meiotic arrest in the mouse. *Curr. Biol.* 15, 1670–1676. <https://doi.org/10.1016/j.cub.2005.07.056>
- Handyside, A.H., Montag, M., Magli, M.C., Repping, S., Harper, J., Schmutzler, A., Vesela, K., Gianaroli, L., Geraedts, J., 2012. Multiple meiotic errors caused by predivision of chromatids in women of advanced maternal age undergoing *in vitro* fertilisation.

- European Journal of Human Genetics 20, 742–747.  
<https://doi.org/10.1038/ejhg.2011.272>
- Hansen, K.R., Knowlton, N.S., Thyer, A.C., Charleston, J.S., Soules, M.R., Klein, N.A., 2008. A new model of reproductive aging: the decline in ovarian non-growing follicle number from birth to menopause. *Hum. Reprod.* 23, 699–708. <https://doi.org/10.1093/humrep/dem408>
- Harman, S.M., Louvet, J.P., Ross, G.T., 1975. Interaction of estrogen and gonadotrophins on follicular atresia. *Endocrinology* 96, 1145–1152. <https://doi.org/10.1210/endo-96-5-1145>
- Hassold, T., Chiu, D., 1985. Maternal age-specific rates of numerical chromosome abnormalities with special reference to trisomy. *Human Genetics* 70, 11–17. <https://doi.org/10.1007/BF00389450>
- Hassold, T., Hunt, P., 2001. To err (meiotically) is human: the genesis of human aneuploidy. *Nat. Rev. Genet.* 2, 280–291. <https://doi.org/10.1038/35066065>
- Hayflick, L., Moorhead, P.S., 1961. The serial cultivation of human diploid cell strains. *Experimental Cell Research* 25, 585–621. [https://doi.org/10.1016/0014-4827\(61\)90192-6](https://doi.org/10.1016/0014-4827(61)90192-6)
- Heald, R., McKeon, F., 1990. Mutations of phosphorylation sites in lamin A that prevent nuclear lamina disassembly in mitosis. *Cell* 61, 579–589. [https://doi.org/10.1016/0092-8674\(90\)90470-Y](https://doi.org/10.1016/0092-8674(90)90470-Y)
- Heesom, K.J., Gampel, A., Mellor, H., Denton, R.M., 2001. Cell cycle-dependent phosphorylation of the translational repressor eIF-4E binding protein-1 (4E-BP1). *Curr. Biol.* 11, 1374–1379.
- Hernández-Hernández, A., Hernández, R.O., Vázquez-Nin, G.H., 2012. Epigenetics of the Synaptonemal Complex. *Meiosis - Molecular Mechanisms and Cytogenetic Diversity.* <https://doi.org/10.5772/29752>
- Hoffmann, I., Clarke, P.R., Marcote, M.J., Karsenti, E., Draetta, G., 1993. Phosphorylation and activation of human cdc25-C by cdc2--cyclin B and its involvement in the self-amplification of MPF at mitosis. *EMBO J* 12, 53–63.
- Holt, J.E., Weaver, J., Jones, K.T., 2010. Spatial regulation of APCCdh1-induced cyclin B1 degradation maintains G2 arrest in mouse oocytes. *Development* 137, 1297–1304. <https://doi.org/10.1242/dev.047555>
- Hou, Y., Fan, W., Yan, L., Li, R., Lian, Y., Huang, J., Li, J., Xu, L., Tang, F., Xie, X.S., Qiao, J., 2013. Genome Analyses of Single Human Oocytes. *Cell* 155, 1492–1506. <https://doi.org/10.1016/j.cell.2013.11.040>
- Hunt, P., 2017. Oocyte Biology: Do the Wheels Fall Off with Age? *Current Biology* 27, R266–R269. <https://doi.org/10.1016/j.cub.2017.02.035>
- Jansova, D., Koncicka, M., Tetkova, A., Cerna, R., Malik, R., Del Llano, E., Kubelka, M., Susor, A., 2017. Regulation of 4E-BP1 activity in the mammalian oocyte. *Cell Cycle* 16, 927–939. <https://doi.org/10.1080/15384101.2017.1295178>
- Katsani, K.R., Karess, R.E., Dostatni, N., Doye, V., 2008. In vivo dynamics of *Drosophila* nuclear envelope components. *Mol. Biol. Cell* 19, 3652–3666. <https://doi.org/10.1091/mbc.E07-11-1162>
- Kennedy, B.K., Barbie, D.A., Classon, M., Dyson, N., Harlow, E., 2000. Nuclear organization of DNA replication in primary mammalian cells. *Genes Dev.* 14, 2855–2868. <https://doi.org/10.1101/gad.842600>
- Kovo, M., Kandli-Cohen, M., Ben-Haim, M., Galiani, D., Carr, D.W., Dekel, N., 2006. An active protein kinase A (PKA) is involved in meiotic arrest of rat growing oocytes. *Reproduction* 132, 33–43. <https://doi.org/10.1530/rep.1.00824>



- Kudlow, B.A., Kennedy, B.K., Monnat, R.J., 2007. Werner and Hutchinson-Gilford progeria syndromes: mechanistic basis of human progeroid diseases. *Nat. Rev. Mol. Cell Biol.* 8, 394–404. <https://doi.org/10.1038/nrm2161>
- Kusch, J., Liakopoulos, D., Barral, Y., 2003. Spindle asymmetry: a compass for the cell. *Trends in Cell Biology* 13, 562–569. <https://doi.org/10.1016/j.tcb.2003.09.008>
- Labbé, J.C., Capony, J.P., Caput, D., Cavadore, J.C., Derancourt, J., Kaghad, M., Lelias, J.M., Picard, A., Dorée, M., 1989. MPF from starfish oocytes at first meiotic metaphase is a heterodimer containing one molecule of cdc2 and one molecule of cyclin B. *EMBO J.* 8, 3053–3058.
- Li, J., Tang, J.-X., Cheng, J.-M., Hu, B., Wang, Y.-Q., Aalia, B., Li, X.-Y., Jin, C., Wang, X.-X., Deng, S.-L., Zhang, Y., Chen, S.-R., Qian, W.-P., Sun, Q.-Y., Huang, X.-X., Liu, Y.-X., 2018. Cyclin B2 can compensate for Cyclin B1 in oocyte meiosis I. *J. Cell Biol.* 217, 3901–3911. <https://doi.org/10.1083/jcb.201802077>
- Lincoln, A.J., Wickramasinghe, D., Stein, P., Schultz, R.M., Palko, M.E., De Miguel, M.P., Tessarollo, L., Donovan, P.J., 2002. Cdc25b phosphatase is required for resumption of meiosis during oocyte maturation. *Nat. Genet.* 30, 446–449. <https://doi.org/10.1038/ng856>
- Lister, L.M., Kouznetsova, A., Hyslop, L.A., Kalleas, D., Pace, S.L., Barel, J.C., Nathan, A., Floros, V., Adelfalk, C., Watanabe, Y., Jessberger, R., Kirkwood, T.B., Höög, C., Herbert, M., 2010. Age-Related Meiotic Segregation Errors in Mammalian Oocytes Are Preceded by Depletion of Cohesin and Sgo2. *Current Biology* 20, 1511–1521. <https://doi.org/10.1016/j.cub.2010.08.023>
- Maiato, H., Hergert, P.J., Moutinho-Pereira, S., Dong, Y., Vandenbeldt, K.J., Rieder, C.L., McEwen, B.F., 2006. The ultrastructure of the kinetochore and kinetochore fiber in *Drosophila* somatic cells. *Chromosoma* 115, 469–480. <https://doi.org/10.1007/s00412-006-0076-2>
- Maquat, L.E., Tarn, W.-Y., Isken, O., 2010. The pioneer round of translation: features and functions. *Cell* 142, 368–374. <https://doi.org/10.1016/j.cell.2010.07.022>
- Marston, A.L., Amon, A., 2004. Meiosis: cell-cycle controls shuffle and deal. *Nat. Rev. Mol. Cell Biol.* 5, 983–997. <https://doi.org/10.1038/nrm1526>
- Martin, R.H., 2008. Meiotic errors in human oogenesis and spermatogenesis. *Reproductive BioMedicine Online* 16, 523–531. [https://doi.org/10.1016/S1472-6483\(10\)60459-2](https://doi.org/10.1016/S1472-6483(10)60459-2)
- Martinsson-Ahlzén, H.-S., Liberal, V., Grünfelder, B., Chaves, S.R., Spruck, C.H., Reed, S.I., 2008. Cyclin-dependent kinase-associated proteins Cks1 and Cks2 are essential during early embryogenesis and for cell cycle progression in somatic cells. *Mol. Cell Biol.* 28, 5698–5709. <https://doi.org/10.1128/MCB.01833-07>
- Matova, N., Cooley, L., 2001. Comparative Aspects of Animal Oogenesis. *Developmental Biology* 231, 291–320. <https://doi.org/10.1006/dbio.2000.0120>
- Mayer, S., Wrenzycki, C., Tomek, W., 2014. Inactivation of mTOR arrests bovine oocytes in the metaphase-I stage, despite reversible inhibition of 4E-BP1 phosphorylation. *Mol. Reprod. Dev.* 81, 363–375. <https://doi.org/10.1002/mrd.22305>
- Mazzanti, M., Bustamante, J.O., Oberleithner, H., 2001. Electrical dimension of the nuclear envelope. *Physiol. Rev.* 81, 1–19. <https://doi.org/10.1152/physrev.2001.81.1.1>
- McKeon, F.D., Kirschner, M.W., Caput, D., 1986. Homologies in both primary and secondary structure between nuclear envelope and intermediate filament proteins. *Nature* 319, 463–468. <https://doi.org/10.1038/319463a0>
- McLaren, A., Southee, D., 1997. Entry of mouse embryonic germ cells into meiosis. *Dev. Biol.* 187, 107–113. <https://doi.org/10.1006/dbio.1997.8584>
- Merriman, J.A., Jennings, P.C., McLaughlin, E.A., Jones, K.T., 2012. Effect of aging on superovulation efficiency, aneuploidy rates, and sister chromatid cohesion in mice

- aged up to 15 months. *Biol. Reprod.* 86, 49.  
<https://doi.org/10.1095/biolreprod.111.095711>
- Minshull, J., Sun, H., Tonks, N.K., Murray, A.W., 1994. A MAP kinase-dependent spindle assembly checkpoint in *Xenopus* egg extracts. *Cell* 79, 475–486.
- Mitsuhashi, H., Hayashi, Y.K., Matsuda, C., Noguchi, S., Wakatsuki, S., Araki, T., Nishino, I., 2010. Specific phosphorylation of Ser458 of A-type lamins in LMNA-associated myopathy patients. *J. Cell. Sci.* 123, 3893–3900. <https://doi.org/10.1242/jcs.072157>
- Moir, R.D., Spann, T.P., Herrmann, H., Goldman, R.D., 2000. Disruption of Nuclear Lamin Organization Blocks the Elongation Phase of DNA Replication. *The Journal of Cell Biology* 149, 1179–1192. <https://doi.org/10.1083/jcb.149.6.1179>
- Navot, D., Drews, M.R., Bergh, P.A., Guzman, I., Karstaedt, A., Scott, R.T., Garrisi, G.J., Hofmann, G.E., 1994. Age-related decline in female fertility is not due to diminished capacity of the uterus to sustain embryo implantation. *Fertil. Steril.* 61, 97–101.
- Norris, R.P., Ratzan, W.J., Freudzon, M., Mehlmann, L.M., Krall, J., Movsesian, M.A., Wang, H., Ke, H., Nikolaev, V.O., Jaffe, L.A., 2009. Cyclic GMP from the surrounding somatic cells regulates cyclic AMP and meiosis in the mouse oocyte. *Development* 136, 1869–1878. <https://doi.org/10.1242/dev.035238>
- Nurse, P., 1997. Checkpoint pathways come of age. *Cell* 91, 865–867.
- Ottolini, C.S., Newnham, L.J., Capalbo, A., Natesan, S.A., Joshi, H.A., Cimadomo, D., Griffin, D.K., Sage, K., Summers, M.C., Thornhill, A.R., Housworth, E., Herbert, A.D., Rienzi, L., Ubaldi, F.M., Handyside, A.H., Hoffmann, E.R., 2015. Genome-wide maps of recombination and chromosome segregation in human oocytes and embryos show selection for maternal recombination rates. *Nature Genetics* 47, 727–735. <https://doi.org/10.1038/ng.3306>
- Pan, H., Ma, P., Zhu, W., Schultz, R.M., 2008. Age-associated increase in aneuploidy and changes in gene expression in mouse eggs. *Dev. Biol.* 316, 397–407.  
<https://doi.org/10.1016/j.ydbio.2008.01.048>
- Patra, D., Wang, S.X., Kumagai, A., Dunphy, W.G., 1999. The *xenopus* *Suc1/Cks* protein promotes the phosphorylation of G(2)/M regulators. *J. Biol. Chem.* 274, 36839–36842.
- Peter, M., Nakagawa, J., Dorée, M., Labbé, J.C., Nigg, E.A., 1990. In vitro disassembly of the nuclear lamina and M phase-specific phosphorylation of lamins by *cdc2* kinase. *Cell* 61, 591–602.
- PhosphoSitePlus [WWW Document], n.d. URL  
<https://www.phosphosite.org/homeAction.action> (accessed 3.1.19).
- Puighermanal, E., Biever, A., Pascoli, V., Melser, S., Pratlong, M., Cutando, L., Rialle, S., Severac, D., Boubaker-Vitre, J., Meyuhas, O., Marsicano, G., Lüscher, C., Valjent, E., 2017. Ribosomal Protein S6 Phosphorylation Is Involved in Novelty-Induced Locomotion, Synaptic Plasticity and mRNA Translation. *Front Mol Neurosci* 10.  
<https://doi.org/10.3389/fnmol.2017.00419>
- Racowsky, C., 1985. Effect of forskolin on the spontaneous maturation and cyclic AMP content of hamster oocyte-cumulus complexes. *J. Exp. Zool.* 234, 87–96.  
<https://doi.org/10.1002/jez.1402340111>
- Raz, V., Vermolen, B.J., Garini, Y., Onderwater, J.J.M., Mommaas-Kienhuis, M.A., Koster, A.J., Young, I.T., Tanke, H., Dirks, R.W., 2008. The nuclear lamina promotes telomere aggregation and centromere peripheral localization during senescence of human mesenchymal stem cells. *J. Cell. Sci.* 121, 4018–4028. <https://doi.org/10.1242/jcs.034876>

- Reid, D.W., Nicchitta, C.V., 2012. Primary role for endoplasmic reticulum-bound ribosomes in cellular translation identified by ribosome profiling. *J. Biol. Chem.* 287, 5518–5527. <https://doi.org/10.1074/jbc.M111.312280>
- Righolt, C.H., van 't Hoff, M.L.R., Vermolen, B.J., Young, I.T., Raz, V., 2011. Robust nuclear lamina-based cell classification of aging and senescent cells. *Aging (Albany NY)* 3, 1192–1201. <https://doi.org/10.18632/aging.100414>
- Röber, R.A., Weber, K., Osborn, M., 1989. Differential timing of nuclear lamin A/C expression in the various organs of the mouse embryo and the young animal: a developmental study. *Development* 105, 365–378.
- Roeder, G.S., 1997. Meiotic chromosomes: it takes two to tango. *Genes Dev.* 11, 2600–2621. <https://doi.org/10.1101/gad.11.20.2600>
- Romasko, E.J., Amarnath, D., Midic, U., Latham, K.E., 2013. Association of Maternal mRNA and Phosphorylated EIF4EBP1 Variants With the Spindle in Mouse Oocytes: Localized Translational Control Supporting Female Meiosis in Mammals. *Genetics* 195, 349–358. <https://doi.org/10.1534/genetics.113.154005>
- Roux, P.P., Shahbazian, D., Vu, H., Holz, M.K., Cohen, M.S., Taunton, J., Sonenberg, N., Blenis, J., 2007. RAS/ERK signaling promotes site-specific ribosomal protein S6 phosphorylation via RSK and stimulates cap-dependent translation. *J. Biol. Chem.* 282, 14056–14064. <https://doi.org/10.1074/jbc.M700906200>
- Saitou, M., Barton, S.C., Surani, M.A., 2002. A molecular programme for the specification of germ cell fate in mice. *Nature* 418, 293–300. <https://doi.org/10.1038/nature00927>
- Santamaría, D., Barrière, C., Cerqueira, A., Hunt, S., Tardy, C., Newton, K., Cáceres, J.F., Dubus, P., Malumbres, M., Barbacid, M., 2007. Cdk1 is sufficient to drive the mammalian cell cycle. *Nature* 448, 811–815. <https://doi.org/10.1038/nature06046>
- Sato, E., Koide, S.S., 1984. Forskolin and mouse oocyte maturation in vitro. *Journal of Experimental Zoology* 230, 125–129. <https://doi.org/10.1002/jez.1402300116>
- Sauer, M.V., 1998. The impact of age on reproductive potential: lessons learned from oocyte donation. *Maturitas* 30, 221–225.
- Savva, G.M., Walker, K., Morris, J.K., 2010. The maternal age-specific live birth prevalence of trisomies 13 and 18 compared to trisomy 21 (Down syndrome). *Prenat. Diagn.* 30, 57–64. <https://doi.org/10.1002/pd.2403>
- Schultz, R.M., 1993. Regulation of zygotic gene activation in the mouse. *BioEssays* 15, 531–538. <https://doi.org/10.1002/bies.950150806>
- Schultz, R.M., Montgomery, R.R., Belanoff, J.R., 1983. Regulation of mouse oocyte meiotic maturation: Implication of a decrease in oocyte cAMP and protein dephosphorylation in commitment to resume meiosis. *Developmental Biology* 97, 264–273. [https://doi.org/10.1016/0012-1606\(83\)90085-4](https://doi.org/10.1016/0012-1606(83)90085-4)
- Schweizer, N., Pawar, N., Weiss, M., Maiato, H., 2015. An organelle-exclusion envelope assists mitosis and underlies distinct molecular crowding in the spindle region. *J Cell Biol* 210, 695–704. <https://doi.org/10.1083/jcb.201506107>
- Sebestova, J., Danylevska, A., Novakova, L., Kubelka, M., Anger, M., 2012. Lack of response to unaligned chromosomes in mammalian female gametes. *Cell Cycle* 11, 3011–3018. <https://doi.org/10.4161/cc.21398>
- Shang, Z.-F., Yu, L., Li, B., Tu, W.-Z., Wang, Y., Liu, X.-D., Guan, H., Huang, B., Rang, W.-Q., Zhou, P.-K., 2012. 4E-BP1 participates in maintaining spindle integrity and genomic stability via interacting with PLK1. *Cell Cycle* 11, 3463–3471. <https://doi.org/10.4161/cc.21770>
- Shibuya, T., Tange, T.Ø., Stroupe, M.E., Moore, M.J., 2006. Mutational analysis of human eIF4AIII identifies regions necessary for exon junction complex formation and

- nonsense-mediated mRNA decay. *RNA* 12, 360–374.  
<https://doi.org/10.1261/rna.2190706>
- Solomon, M.J., 1993. Activation of the various cyclin/cdc2 protein kinases. *Curr. Opin. Cell Biol.* 5, 180–186.
- Soules, M.R., Steiner, R.A., Clifton, D.K., Cohen, N.L., Aksel, S., Bremner, W.J., 1984. Progesterone modulation of pulsatile luteinizing hormone secretion in normal women. *J. Clin. Endocrinol. Metab.* 58, 378–383. <https://doi.org/10.1210/jcem-58-2-378>
- Spruck, C.H., de Miguel, M.P., Smith, A.P.L., Ryan, A., Stein, P., Schultz, R.M., Lincoln, A.J., Donovan, P.J., Reed, S.I., 2003. Requirement of Cks2 for the first metaphase/anaphase transition of mammalian meiosis. *Science* 300, 647–650. <https://doi.org/10.1126/science.1084149>
- Stewart, C., Burke, B., 1987. Teratocarcinoma stem cells and early mouse embryos contain only a single major lamin polypeptide closely resembling lamin B. *Cell* 51, 383–392.
- Susor, A., Jansova, D., Cerna, R., Danylevska, A., Anger, M., Toralova, T., Malik, R., Supolikova, J., Cook, M.S., Oh, J.S., Kubelka, M., 2015. Temporal and spatial regulation of translation in the mammalian oocyte via the mTOR-eIF4F pathway. *Nat Commun* 6, 6078. <https://doi.org/10.1038/ncomms7078>
- Székvölgyi, L., Nicolas, A., 2010. From meiosis to postmeiotic events: homologous recombination is obligatory but flexible. *FEBS J.* 277, 571–589.  
<https://doi.org/10.1111/j.1742-4658.2009.07502.x>
- Szybek, K., 1972. In-vitro maturation of oocytes from sexually immature mice. *J. Endocrinol.* 54, 527–528.
- Tam, P.P.L., Snow, M.H.L., 1981. Proliferation and migration of primordial germ cells during compensatory growth in mouse embryos. *Development* 64, 133–147.
- Tomek, W., Melo Sterza, F.A., Kubelka, M., Wollenhaupt, K., Torner, H., Anger, M., Kanitz, W., 2002a. Regulation of translation during in vitro maturation of bovine oocytes: the role of MAP kinase, eIF4E (cap binding protein) phosphorylation, and eIF4E-BP1. *Biol. Reprod.* 66, 1274–1282.
- Tomek, W., Torner, H., Kanitz, W., 2002b. Comparative analysis of protein synthesis, transcription and cytoplasmic polyadenylation of mRNA during maturation of bovine oocytes in vitro. *Reprod. Domest. Anim.* 37, 86–91.
- Tsafriiri, A., Dekel, N., Bar-Ami, S., 1982. The role of oocyte maturation inhibitor in follicular regulation of oocyte maturation. *J. Reprod. Fertil.* 64, 541–551.
- Tsafriiri, A., Lieberman, M.E., Koch, Y., Bauminger, S., Chobsieng, P., Zor, U., Lindner, H.R., 1976. Capacity of immunologically purified FSH to stimulate cyclic AMP accumulation and steroidogenesis in Graafian follicles and to induce ovum maturation and ovulation in the rat. *Endocrinology* 98, 655–661. <https://doi.org/10.1210/endo-98-3-655>
- Tsukiyama-Kohara, K., Poulin, F., Kohara, M., DeMaria, C.T., Cheng, A., Wu, Z., Gingras, A.C., Katsume, A., Elchebly, M., Spiegelman, B.M., Harper, M.E., Tremblay, M.L., Sonenberg, N., 2001. Adipose tissue reduction in mice lacking the translational inhibitor 4E-BP1. *Nat. Med.* 7, 1128–1132. <https://doi.org/10.1038/nm1001-1128>
- Vaccari, S., Weeks, J.L., Hsieh, M., Menniti, F.S., Conti, M., 2009. Cyclic GMP signaling is involved in the luteinizing hormone-dependent meiotic maturation of mouse oocytes. *Biol. Reprod.* 81, 595–604. <https://doi.org/10.1095/biolreprod.109.077768>
- Vanderhyden, B., 2002. Molecular basis of ovarian development and function. *Front. Biosci.* 7, d2006-2022.
- Verlhac, M.H., Kubiak, J.Z., Clarke, H.J., Maro, B., 1994. Microtubule and chromatin behavior follow MAP kinase activity but not MPF activity during meiosis in mouse oocytes. *Development* 120, 1017–1025.

- Ward, G.E., Kirschner, M.W., 1990. Identification of cell cycle-regulated phosphorylation sites on nuclear lamin C. *Cell* 61, 561–577.
- Yu, V.P.C.C., Baskerville, C., Grünenfelder, B., Reed, S.I., 2005. A kinase-independent function of Cks1 and Cdk1 in regulation of transcription. *Mol. Cell* 17, 145–151. <https://doi.org/10.1016/j.molcel.2004.11.020>

## 7. Abbreviations

4E-BP1	Eukaryotic translation initiation factor 4E (eIF4E)-binding protein1
4E-BP2	Eukaryotic translation initiation factor 4E (eIF4E)-binding protein 2
4E-BP3	Eukaryotic translation initiation factor 4E (eIF4E)-binding protein 3
AF	aged females (1 years old)
APC/C	Anaphase-promoting complex
ATP	Adenosintrifosfát
cAMP	cyclic adenosine monophosphate
CCNB (CCB)	Cyclin B1
CDC25 (C, B)	Cell division cycle 25 phosphatases
CDK1	Cyclin dependent kinase 1
cGMP	cyclic guanosine monophosphate
CKS2	Cyclin-dependent kinase subunit protein 2
CKS1	Cyclin-dependent kinase subunit protein 1
<i>Dazl</i>	Deleted in azoospermia-like
DNA	Deoxyribonucleic acid
eIF4A3	initiation factor, exon junction complex component
eIF4E	eukaryotic translation initiation factor 4E
eIF4F	eukaryotic translation initiation factor 4F coplex
FISH	Fluorescent in situ hybridization
FSH	Folicle stimulated hormone
GV	germinal vesicle
HGPS	Hutchinson-Gilford Progeria Syndrome
hnRNP	heterogeneous Nuclear Ribonucleoprotein
hnRNPA1	heterogeneous Nuclear Ribonucleoprotein A1
ICC	immunocytochemistry

IVF	in vitro fertilization
LH	luteinizing hormone
LMNA,	Lamin A/C
<i>Malat1</i>	Metastasis associated lung adenocarcinoma transcript 1
MAPK	Mitogen-activated protein kinases
MI	metaphase I
MII	metaphase II
MPF	M-phase- or maturation-promoting factor
mTOR	mammalian target of rapamycin
MYT1	Myelin transcription factor 1
NDJ	nondisjunction
<i>Neat2</i>	Noncoding nuclear-enriched abundant transcript 2
NEBD	nuclear envelope breakdown
NIH3T3	mouse embryo fibroblast cell line
PDE3A	Phosphodiesterase 3A
PGCs	primordial germ cells
PKA	Protein kinase A
PKC	Protein kinase C
PLA	proximity ligation assay
PLK1	Polo like kinase 1
Poly(A)	polyadenylated
PSSC	premature separation of sister chromatids
RCA	rolling circle amplification
RNA	Ribonucleic acid
RPS14	40S ribosomal protein S14
RPS6	40S ribosomal protein S6
RT-PCR	reverse transcription polymerase chain reaction

WEE1B

Wee1-like protein kinase 1B

YF

aged females (2 months old)



## 8. Curriculum vitae

Marketa Koncicka, Ing.

Institute of Animal Physiology and Genetics CAS, v. v. i.

Department: Laboratory of Biochemistry and Molecular Biology of Germ Cells

Rumburská 89, 277 21 Liběchov

Phone number: +420 739 723 165

Laboratory phone num.: +420 315 639 580

Email: koncicka@iapg.cas.cz

### Education/Qualifications

2015-Present Charles University in Prague, Czech Republic; Faculty of Science

A PhD student at the Developmental Biology Program

Laboratory of Biochemistry and Molecular Biology of Germ Cells

PhD Thesis: Role and regulation of nuclear membrane during meiotic maturation of mammalian oocyte

2013-2015 Czech University of Life Sciences Prague, Czech Republic; Faculty of

Agrobiolology, Food and Natural Resources, *Master's study program*

Diploma Thesis: The role of 4E-BP1 in regulation of cap-dependent translation in mammalian oocyte

2010 – 2013 Czech University of Life Sciences Prague, Czech Republic; Faculty of

Agrobiolology, Food and Natural Resources, *Bachelor's study program*

Bachelor's thesis: The role of Bcl-2 proteins in organism

### Other Experience/Presentation and conferences

2018 – Inaugural Meeting of the Visegrad Group Society for Developmental Biology (V4SDB), Brno, Czech Republic, poster presentation: Detection of Lamin C2 in the mouse oocyte

7 – 9.9.2018

- 2017 - Summer School on RNA-protein interactions RNA Structure and Biology workshop  
CEITEC, Brno, Czech Republic  
2 – 6.10.2017
- 2016 - Certificate of professional competence for designing experiments and experimental projects according to § 15d paragraph 3 of Act no. 246/1992 Coll., on the protection of animals against cruelty  
8 – 12.2.2016
- 2015 - EMBO Conference: Protein Synthesis and Translational Control,  
Heidelberg, Germany  
9 – 13.9.2015
- 2014 - Course in Introduction to Immunochemistry  
Prague Institute of Chemical Technology
- 2012 - Course on Primate Sociobiology, Husbandry & Nutrition  
German Primate Centre (DPZ) in Göttingen, Germany

#### **Publications:**

- Jansova D, **Koncicka M**, Tetkova A, Cerna R, Malik R, Del Llano E, Kubelka M, Susor A. Regulation of 4E-BP1 activity in the mammalian oocyte, **Cell Cycle**, 2017. DOI: 10.1080/15384101.2017.1295178. **IF: 3.304 (2018)**
- Jansova D, Tetkova A, **Koncicka M**, Susor A. Localization of RNA and translation in the mammalian oocyte and embryo, **PLoS One**, 2018. DOI: 10.1371/journal.pone.0192544. **IF: 2.766 (2018)**
- **Koncicka M**, Tetkova A, Jansova D, Del Llano E, Gahurova L, Kracmarova J, Prokesova S, Masek T, Pospisek M, Bruce AW, Kubelka M, Susor A. Increased Expression of Maturation Promoting Factor Components Speeds Up Meiosis in Oocytes from Aged Females. **International Journal of Molecular Sciences**, 2018. DOI: 10.3390/ijms19092841. **IF: 3.687 (2018)**
- Ellederova Z, del Rincon S, **Koncicka M**, Susor A, Kubelka M, Sun D, Spruck Ch. CKS1 Germ Line Exclusion is Essential for the Transition from Meiosis to Early Embryonic Development. **Molecular and Cellular Biology**, Submitted: 20.12.2018

## 9. Attachment - research papers

1. Jansova D, **Koncicka M**, Tetkova A, Cerna R, Malik R, Del Llano E, Kubelka M, Susor A. Regulation of 4E-BP1 activity in the mammalian oocyte, **Cell Cycle**, 2017.

DOI:

10.1080/15384101.2017.1295178.

2. Jansova D, Tetkova A, **Koncicka M**, Susor A. Localization of RNA and translation in the mammalian oocyte and embryo, **PLoS One**, 2018. DOI:

10.1371/journal.pone.0192544.

**Koncicka M**, Tetkova A, Jansova D, Del Llano E, Gahurova L, Kracmarova J, Prokesova S, Masek T, Pospisek M, Bruce AW, Kubelka M, Susor A. Increased Expression of Maturation Promoting Factor Components Speeds Up Meiosis in Oocytes from Aged Females. **International Journal of Molecular Sciences**, 2018. DOI:



10.3390/ijms19092841.

4. Ellederova Z, del Rincon S, **Koncicka M**, Susor A, Kubelka M, Sun D, Spruck Ch. CKS1 Germ Line Exclusion is Essential for the Transition from Meiosis to Early Embryonic Development. **Molecular and Cellular Biology**, Submitted: 20.12.2018 (now under revision)

REPORT

 OPEN ACCESS

## Regulation of 4E-BP1 activity in the mammalian oocyte

Denisa Jansova<sup>a</sup>, Marketa Koncicka<sup>a</sup>, Anna Tetkova<sup>a</sup>, Renata Cerna<sup>a</sup>, Radek Malik <sup>b</sup>, Edgar del Llano<sup>a</sup>, Michal Kubelka <sup>a</sup>, and Andrej Susor<sup>a</sup>

<sup>a</sup>Institute of Animal Physiology and Genetics, ASC, Libechov, Czech Republic; <sup>b</sup>Institute of Molecular Genetics, ASCR, Prague, Czech Republic

### ABSTRACT

Fully grown mammalian oocytes utilize transcripts synthesized and stored during earlier development. RNA localization followed by a local translation is a mechanism responsible for the regulation of spatial and temporal gene expression. Here we show that the mouse oocyte contains 3 forms of cap-dependent translational repressor expressed on the mRNA level: 4E-BP1, 4E-BP2 and 4E-BP3. However, only 4E-BP1 is present as a protein in oocytes, it becomes inactivated by phosphorylation after nuclear envelope breakdown and as such it promotes cap-dependent translation after NEBD. Phosphorylation of 4E-BP1 can be seen in the oocytes after resumption of meiosis but it is not detected in the surrounding cumulus cells, indicating that 4E-BP1 promotes translation at a specific cell cycle stage. Our immunofluorescence analyses of 4E-BP1 in oocytes during meiosis I showed an even localization of global 4E-BP1, as well as of its 4E-BP1 (Thr37/46) phosphorylated form. On the other hand, 4E-BP1 phosphorylated on Ser65 is localized at the spindle poles, and 4E-BP1 phosphorylated on Thr70 localizes on the spindle. We further show that the main positive regulators of 4E-BP1 phosphorylation after NEBD are mTOR and CDK1 kinases, but not PLK1 kinase. CDK1 exerts its activity toward 4E-BP1 phosphorylation via phosphorylation and activation of mTOR. Moreover, both CDK1 and phosphorylated mTOR co-localize with 4E-BP1 phosphorylated on Thr70 on the spindle at the onset of meiotic resumption. Expression of the dominant negative 4E-BP1 mutant adversely affects translation and results in spindle abnormality. Taken together, our results show that the phosphorylation of 4E-BP1 promotes translation at the onset of meiosis to support the spindle assembly and suggest an important role of CDK1 and mTOR kinases in this process. We also show that the mTOR regulatory pathway is present in human oocytes and is likely to function in a similar way as in mouse oocytes.

### ARTICLE HISTORY

Received 10 October 2016  
Revised 31 January 2017  
Accepted 8 February 2017

### KEYWORDS

4E-BP1; CDK1; cumulus cells; kinase; mTOR; mRNA; meiosis; oocyte; spindle; translation

## Introduction

Translational control of specific mRNAs is a widespread mechanism of gene regulation and contributes to diverse biologic processes in many cell types. During the meiotic division of mammalian oocytes (so called oocyte maturation) protein synthesis plays an important role in controlling the progress of meiosis, since the regulation of gene expression on the level of transcription is ceased. At the onset of the first meiotic division, nuclear envelope breakdown (NEBD; G2/M transition) occurs, chromosomes condense and a bipolar spindle forms from the microtubule organizing centers.<sup>1</sup> During meiosis I, the spindle migrates from the center of the oocyte to the cortex, and the oocyte undergoes an asymmetric division resulting in a large egg competent for fertilization and a relatively small polar body. Proper positioning of the spindle during asymmetric cell division ensures correct partitioning of cellular determinants.<sup>2</sup> How these events are orchestrated in detail remains unclear.


The importance of protein synthesis for meiotic and mitotic progression has been shown previously. Those published results revealed that protein synthesis is not required for NEBD in mouse

oocytes, although the formation of the spindle and progression to metaphase II requires active protein synthesis.<sup>3</sup> In contrast, positive regulators of the cap-dependent translational pathway become activated post NEBD and inactivated after fertilization.<sup>4–9</sup>

Regulation of translation occurs mainly at the initiation step, which was shown to be rate limiting for overall protein synthesis.<sup>10</sup> Protein factors that bind to the cap structure at the 5<sup>0</sup>UTR (untranslated region) and to the 3<sup>0</sup>UTR-poly(A) sequence of mRNAs have been identified as being essential for this process. Most of the interactions of these proteins are regulated by phosphorylation.<sup>11,12</sup> The best described protein kinase regulating translation initiation is the mTOR/FRAP kinase, the targets of which are the Eukaryotic initiation factor 4E-binding protein 1 (4E-BP1)<sup>13</sup> and the S6 kinase.<sup>14</sup> Hypo-phosphorylated 4E-BP1 binds eIF4E and in such a way inhibits the formation of a translation initiation complex (eIF4F) at the cap structure. EIF4F contains eIF4E (the cap-binding protein), eIF4G1 (the scaffold protein) and eIF4A (an RNA helicase). This complex is probably critical for the translation of mRNAs with extensive secondary structure in their 5<sup>0</sup>UTR. Upon resumption of meiosis, 4E-BP1

**CONTACT** Andrej Susor  [susor@iapg.cas.cz](mailto:susor@iapg.cas.cz)  Institute of Animal Physiology and Genetics, ASC, Rumburska 89, Libechov, Czech Republic.

Color versions of one or more of the figures in this article can be found online at [www.tandfonline.com/kccy](http://www.tandfonline.com/kccy).

 Supplemental data for this article can be accessed on the [publisher's website](#).

© 2017 Denisa Jansova, Marketa Koncicka, Anna Tetkova, Renata Cerna, Radek Malik, Edgar del Llano, Michal Kubelka, and Andrej Susor. Published with license by Taylor & Francis. This is an Open Access article distributed under the terms of the Creative Commons Attribution License (<http://creativecommons.org/licenses/by/3.0/>), which permits unrestricted use, distribution, and reproduction in any medium, provided the original work is properly cited. The moral rights of the named author(s) have been asserted.

becomes phosphorylated at several sites resulting in its release from eIF4E, allowing eIF4F formation. Phosphorylation at Ser65 and Thr70 modulates the binding of 4E-BP1 to eIF4E directly. Phosphorylation of these sites depends upon 4E-BP1s C-terminal TOR signaling motif that binds Raptor, a component of the mTORC1. Phosphorylation at Thr37/46, which is known to be mediated by mTOR, is required for the modification of Thr70 and Ser65, reflecting the hierarchical phosphorylation of 4E-BP1,<sup>15</sup> and depends upon 4E-BP1s N-terminal RAIP motif.<sup>16</sup> Phosphorylation of Thr37/46 is profoundly inhibited by starving cells of amino acids, which inactivates mTOR signaling.<sup>17</sup> mTORC1 signaling is activated via phosphatidylinositol 3-kinase and protein kinase B (PKB, also termed AKT) and by the Ras/Raf/ERK pathway.<sup>18</sup> AKT plays a substantial role during the progression of meiosis from GV-stage (germinal vesicle – nucleus in the oocytes) to the MII/MIII-stage.<sup>19,20</sup> Involvement of the mTOR/4F axis in translational regulation during mitosis might be used as a model case for the meiotic cell. Increased phosphorylation of 4E-BP1 has been detected during the meiotic progression of mammalian oocytes,<sup>4,21,22</sup> and different phosphorylated forms of 4E-BP1 have been shown to co-localize with the meiotic spindle in mouse oocytes.<sup>9,22</sup> Blocking of 4E-BP1 phosphorylation during maturation has also resulted in the irreversible arrest of metaphase I in bovine oocytes,<sup>23</sup> abnormal formation of MII spindles in mouse oocytes<sup>9</sup> or affected asymmetric division.<sup>24</sup>

The aim of this work was to study the metabolic pathways which are involved in 4E-BP1 phosphorylation during in vitro meiotic maturation of mouse oocytes. We discovered that 4E-BP1 becomes phosphorylated in post-NEBD stage oocytes and this phosphorylation remains constant until the MII stage of oocyte maturation and promotes specific translation, which affects spindle assembly. Furthermore, we have uncovered the involvement of different kinases which are potentially involved in the phosphorylation of 4E-BP1.

## Results

### Only 4E-BP1 is present in the mouse oocyte

In mammals 3 genes code 4E-BP1, 2 and 3.<sup>25</sup> Our first objective was to determine which form is dominant during mouse oocyte meiotic maturation from the GV to MII stage on the mRNA level. Quantitative RT-PCR analysis showed the presence of all 3 forms of *4e-bps* but with a slightly higher abundance of *4e-bp3*. The global amount of the mRNAs for the 3 different *4e-bps* remained constant throughout meiosis from GV to MII oocytes (Fig. 1A).

Next, we analyzed the presence of all 3 isoforms on the protein level. Our WB analyses showed an absence of 4E-BP2 and 4E-BP3 proteins in the oocytes, which is in the contrary to the results obtained from WB analyses of brain lysate (Fig. 1B and C). However, 4E-BP1 was highly abundant in mouse oocytes with an increased mobility shift post-NEBD (Fig. 1B). Our data showed higher presence of the 4E-BP1 protein in the oocytes than in the brain sample (Fig. 1B and C; Supplementary Fig. 1A). WB also showed that whole population of 4E-BP1 in MII stage oocytes is present as the upper (presumably phosphorylated) band. Treatment of MII oocyte lysate with lambda protein phosphatase (LPP) resulted in the disappearance of the

upper band and mobility shift toward lower band, similar pattern to that seen in the GV stage oocytes (Fig. 1D). The experiment in the Fig. 1D shows that mobility shift represents phosphorylation of the 4E-BP1. Moreover, the appearance of mobility shift was confirmed by microinjection of oocytes with RNA coding for 4E-BP1 protein tagged with hemagglutinin (HA). The oocytes were kept in the GV stage or matured for 3 h to NEBD and to MII for 12 h and analyzed by WB, using HA antibody. Our data showed no phosphorylation shift in the GV oocytes, appearance of 2 bands in the NEBD oocytes and whole expressed exogenous HA-4E-BP1 was phosphorylated in the MII stage (Supplementary Fig. 1B).

It is well established that phosphorylation of 4E-BP1 plays an important role in the regulation of cap-dependent translation.<sup>25–30</sup> We thus investigated the localization of 4E-BP1 and its phosphorylated forms (Thr37/46/70 and Ser65) during meiosis I. We analyzed different meiotic stages of maturing oocytes; a germinal vesicle (nucleus is present, prophase I) stage was collected directly post isolation; oocytes underwent NEBD following release from the 3-Isobutyl-1-methylxanthine (IBMX) block, oocytes undergone naturally NEBD within 1 h, a group post-NEBD was collected 3 h post IBMX wash (PIW); a metaphase I (MI) stage was collected 7 h PIW and metaphase II (MII) oocytes were collected 12 h PIW. Cell cycle progression was monitored by timing and by immunocytochemistry (ICC) using DNA staining with DAPI. Pan 4E-BP1 antibody was used to analyze the localization of global 4E-BP1 during GV to MII (Fig. 2A). In GV oocytes global 4E-BP1 was evenly distributed throughout the cytoplasm but with a higher signal visible in the nucleoplasm (Fig. 2A and Supplementary Fig. 3), without staining in the nucleolus (marked by asterisk). In the post-NEBD stages the global 4E-BP1 was also spread evenly with just a slight increase at the spindle. ICC experiments using phospho-specific antibody against the Thr37/46 form showed no signal in the GV and a similar localization was seen as total 4E-BP1 protein in the post-NEBD. Antibody recognizing 4E-BP1 phosphorylated at Ser65 showed an increased fluorescence signal in the vicinity of chromosomes, at the spindle assembly area and later at the spindle poles. The pattern of 4E-BP1 phosphorylation at Thr70 showed significant localization at the newly forming spindle post-NEBD or bipolar spindle at MI and MII, and was also present in the extruded polar body. The phospho-specific antibodies did not show a positive signal in the GV stage, which is in a good agreement with our WB data (Fig. 1B and Supplementary Fig. 1A, B). Moreover, double staining of 4E-BP1 phosphorylated at Ser65 or Thr70 with marker of microtubule organizing centers  $\alpha$ -tubulin showed significant enrichment of the 4E-BP1(Ser65) signal in the region with stained  $\alpha$ -tubulin; however, 4E-BP1(Thr70) was distributed along the whole spindle (Fig. 2B).

As 4E-BP1 phosphorylated at the Thr70 was found to be exclusively localized at the forming spindle, we therefore speculated whether this localization was tubulin-dependent. We disrupted the spindle by treatment with 1 mM Nocodazole (Noco) for 1h post-NEBD. Although the dissolved spindle changed the 4E-BP1 (Thr70) pattern, the fluorescence signal still persisted at the chromosomal area (Fig. 2C).

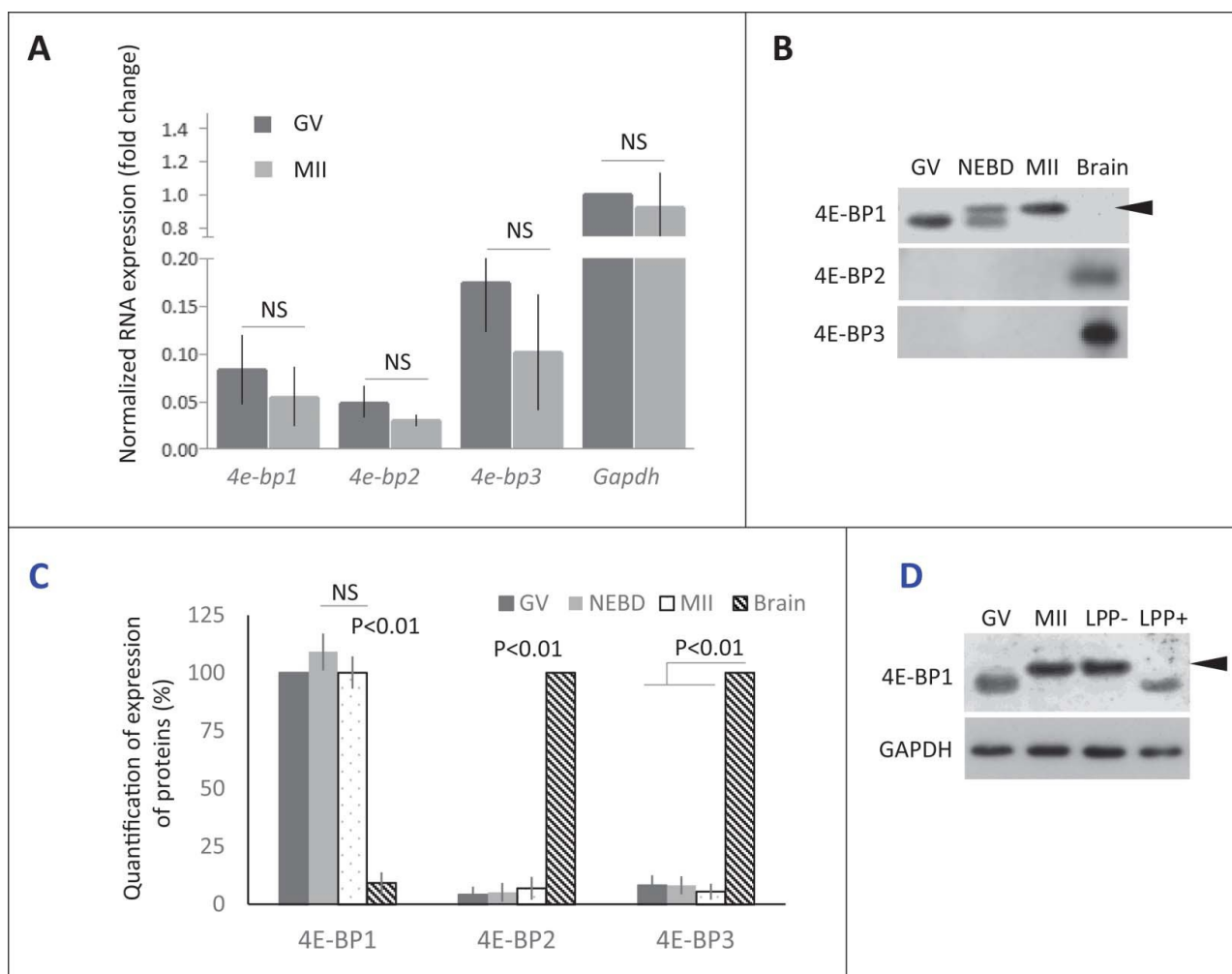


**Figure 1.** Expression of 4E-BP forms in mouse oocytes. (A) Quantitative RT-PCR analysis shows all 3 forms of *4e-bp* mRNA, which are stable during oocyte maturation (NS D non-significant,  $r^2 = 3$ ). Results were normalized to the relative internal standard *Gapdh* mRNA in GV. (B) Immunoblotting shows presence of only 4E-BP1 form on the protein level. Both 4E-BP2 and 4E-BP3 are absent in the oocytes, although they are present in the brain. Expression of the 4E-BP1 in the brain sample is significantly lower in comparison with oocytes (See Fig. S1A). 4E-BP1 displays visible phosphorylation shift (arrowhead) post-NEBD (a typical experiment from at least 3 replicates is shown). (C) Quantification of protein expression of the 4E-BP1-3 in the oocytes during maturation and brain samples. Data are presented as mean  $\pm$  SD, Student's t-test. (D) Treatment of the lysate from MII oocytes with Lambda Protein Phosphatase (LPPC) suppressed mobility shift of the 4E-BP1 on the WB. Arrowhead points to phospho 4E-BP1 form. See Figure S1A and B.

#### Activity of mTOR is increased in the human oocyte post-NEBD

As the mouse oocyte is a model organism for the study of human oocytes, we speculated whether mTOR(Ser2448) in human oocytes would be activated similarly as in the mouse oocyte, with a comparable localization pattern. ICC staining of human oocytes in GV, NEBD and MII stages showed that there was no signal for phospho-specific antibody against mTOR (Ser2448) in the GV stage (Supplementary Fig. 3) but increased fluorescence was visible in the NEBD and MII stage. The MII oocyte produced normally formed spindle stained with anti-tubulin antibody with a strong signal for mid-body structure positive for mTOR(Ser2448) (Supplementary Fig. 3).

#### 4E-BP1 phosphorylation requires mTOR and CDK1 activity

The timing of increased phosphorylation of 4E-BP1 positively correlates with increased cap-dependent translation after

NEBD in the mouse, porcine and bovine oocyte.<sup>5,9,21</sup> Also, the timing of the increased phosphorylation of mTOR after NEBD,<sup>9,31</sup> suggests a potential role for mTOR in 4E-BP1 phosphorylation during mammalian meiosis.

Previously we have shown that suppression of mTOR activity using 100 nM mTOR inhibitor Rapamycin (Rapa) significantly represses phosphorylation of 4E-BP1, however, it does not prevent the oocytes to reach MII stage.<sup>18</sup> Phosphorylation of 4E-BP1 by CDK1 kinase<sup>32-34</sup> has been also described in other systems, in which it becomes activated at the onset of both mitosis,<sup>34,35</sup> and meiosis.<sup>36</sup> In mammalian oocytes, CDK1 activity is essential for the major morphological events occurring during meiotic maturation (including NEBD, chromosome congression and condensation, formation of the meiotic spindle) and its inhibition in the beginning of maturation results in the complete block of meiosis with oocytes arresting in the GV stage.<sup>37</sup> We therefore investigated the ability of the CDK1 inhibitor 10 mM Roscovitine (Rosco), as well as 100 nM mTOR inhibitor Rapa, to suppress phosphorylation of 4E-BP1 post



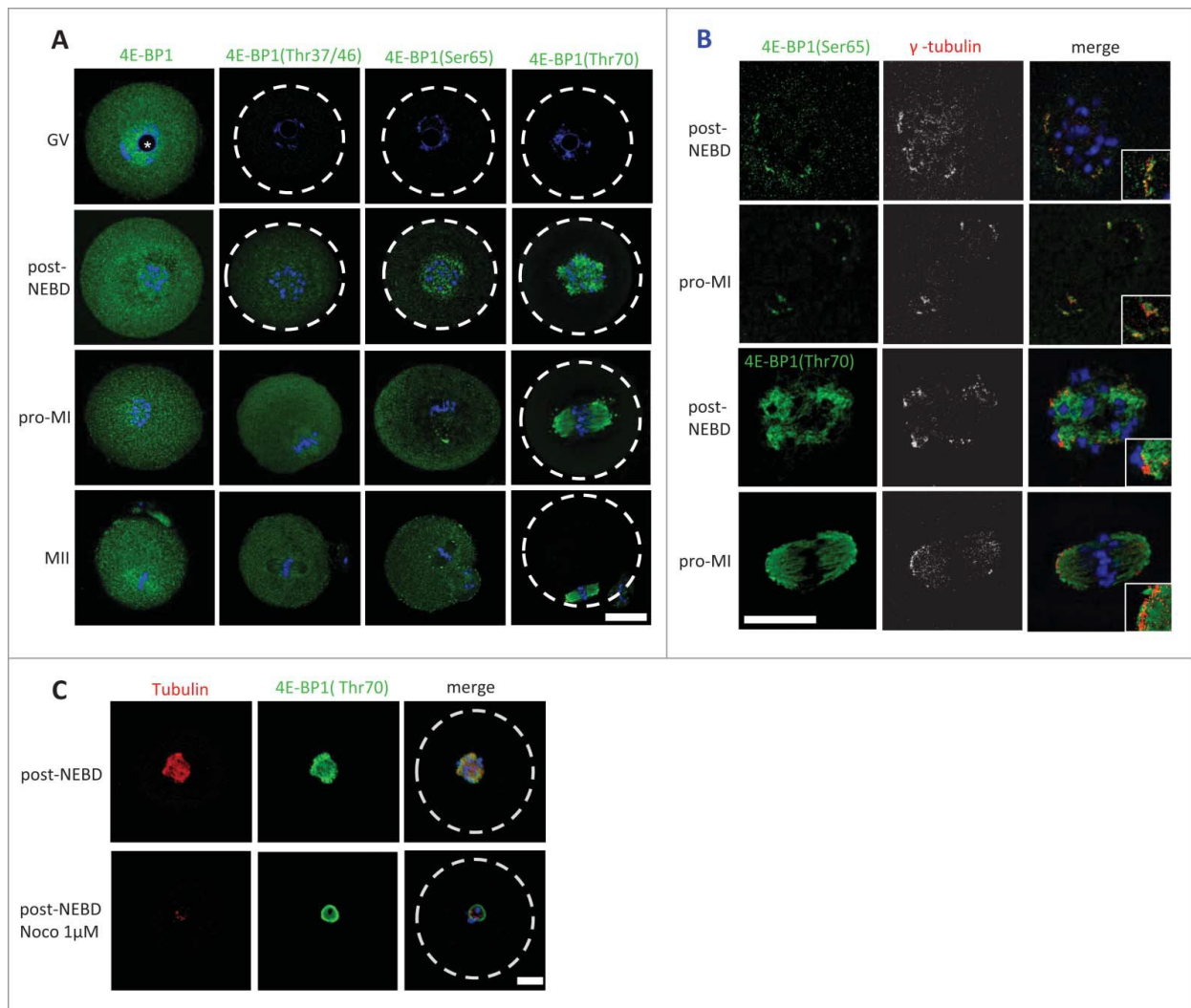


**Figure 2.** Localization of 4E-BP1 and its phosphorylated forms in the oocytes. (A) Confocal images of different meiotic stages GV (germinal vesicle), post-NEBD (3 h post IBMX wash, PIW), pro-MI (7 h PIW) and MII (12 h) stained with phospho-specific antibody (green) and DAPI (blue), white line indicates oocyte edge. Scale bar D 25  $\mu$ m. Nucleolus is depicted by asterisk, from at least 3 replicates and n 2: 30. (B) Marker of the microtubule-organizing centers, gamma tubulin (pseudo-colored and red) co-localizes with 4E-BP1 (Ser65) and (Thr70). Scale bar D 25  $\mu$ m, n D 10. Enlarged detail in the right bottom corner. (C) Confocal images of control oocytes and oocytes treated with 1 mM Noco for 1 h in the post-NEBD stage (n 2: 28), tubulin (red), 4E-BP1 (green) and DNA (blue). Scale bar D 20  $\mu$ m.

NEBD. Rapa or Rosco were added to the culture media 1h PIW. Similarly to Rapa, the inhibition of CDK1 also showed significant suppression of phosphorylation shift (Fig. 3A). Next, based on its activity described in mitotic cells, we decided to determine whether PLK1 is also involved in the phosphorylation of 4E-BP1.<sup>38</sup> We added 100 nM specific PLK1 inhibitor BI2536<sup>39</sup> to the oocytes 1h PIW. However, no effect of BI2536 on 4E-BP1 phosphorylation was seen after 2h of culture (Fig. 3A and B).

Our study supports other published research<sup>32-34</sup> documenting that CDK1/CYCB1 (MPF) kinase is also involved in 4E-BP1 phosphorylation and in the inactivation of its suppressor function. Mitosis is commonly thought to be associated with reduced cap-dependent protein translation, however, our previously published results<sup>4,5,9</sup> show that the main regulators of cap-dependent translation initiation become activated at the onset of meiosis in pig oocytes. Therefore, we elucidated whether MPF had an impact on the activation of mTOR in mouse oocytes. By downregulation of CDK1 using Rosco treatment (added post-NEBD)

we found a significant decrease in phosphorylation of mTOR(Ser2448) (Fig. 3C and D). On the other hand, treatment with Okadaic Acid (OA) substantially increased phosphorylation/activation of mTOR in the treated oocytes, when compared with control oocytes (Fig. 3C and D). Our WB data revealed that MPF influenced the activity of mTOR in the mammalian oocyte after the re-initiation of meiosis. We expected a positive correlation between the localization of the kinases and that of the phosphorylated forms of 4E-BP1. The ICC experiments indeed showed that fluorescence for both mTOR(Ser2448) and CDK1 kinases are present at the newly forming spindle or bipolar spindle (Fig. 3E), which was in good agreement with the localization of phosphorylated 4E-BP1 (Fig. 2).

Reduced cap-dependent protein translation is believed to be connected with mitosis. However, Heesom et al.<sup>32</sup> and Huda et al.<sup>34</sup> have demonstrated that cap-dependent translation is generally sustained during mitosis and 4E-BP1 becomes phosphorylated after entry to mitosis. Thus we isolated cumulus cells (CCs) from GV and MII oocyte-

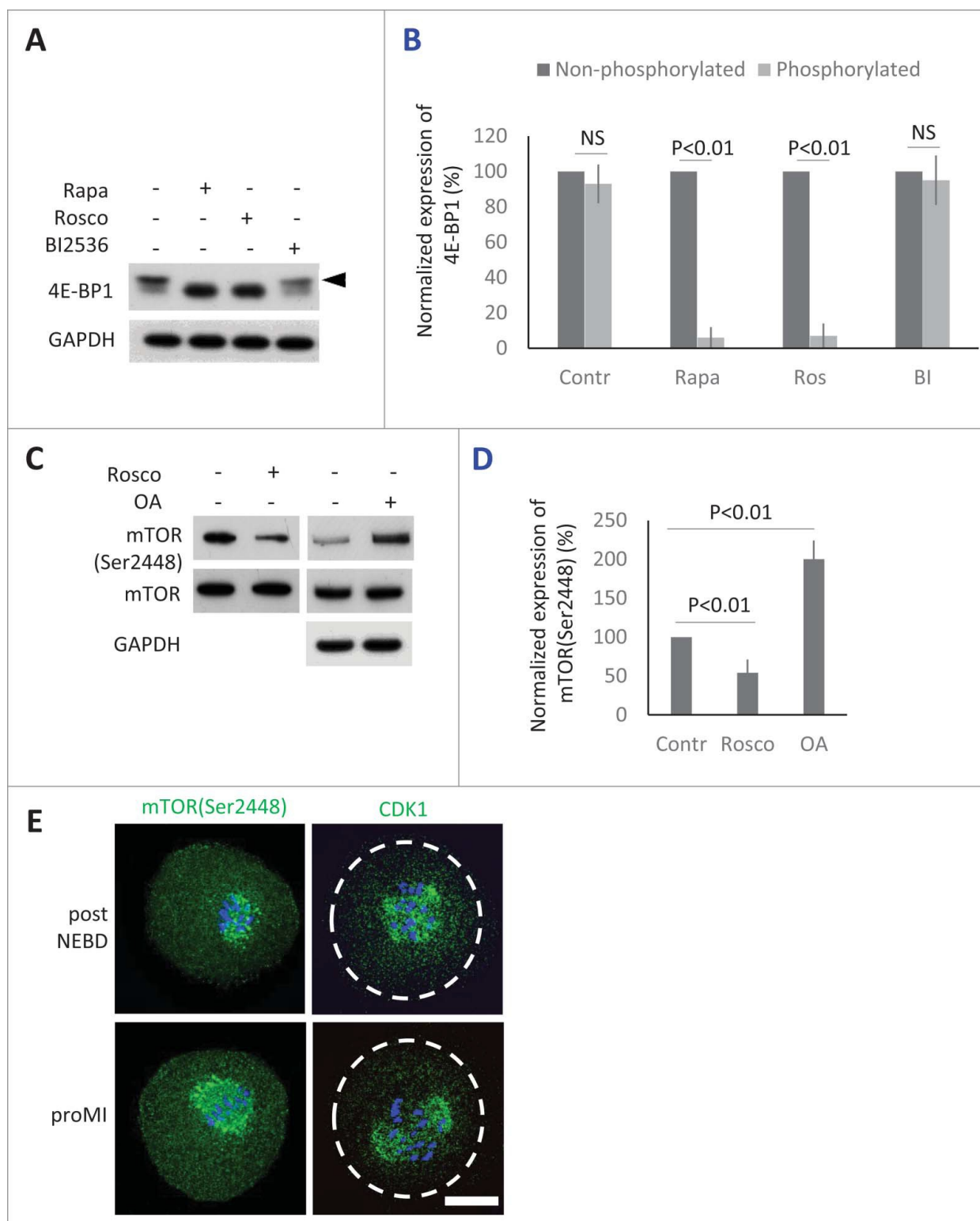


**Figure 3.** Protein kinases phosphorylating 4E-BP1 in the oocytes. (A) Detection of 4E-BP1 by immunoblotting in the oocytes treated with specific inhibitors Rapa (100 nM), Rosco (10 mM), or BI2536 (100 nM) post-NEBD. Arrowhead marks the presence of upper band (phosphorylation shift) of 4E-BP1 in the oocytes treated for 2 h post-NEBD. GAPDH was used as a loading control, a typical experiment from at least 3 replicates is shown. (B) Quantification of non-phosphorylated and phosphorylated form of 4E-BP1 in the post-NEBD oocytes. Data are presented as mean  $\pm$  SD, Student's t-test, NS, non-significant. (C) CDK1 effect on mTOR phosphorylation in the oocytes treated by Rosco (10 mM) or OA (1 mM). Immunoblot was probed with mTOR(Ser2448) and control (mTOR and GAPDH) antibodies. Twenty oocytes were used per sample. (D) Presence of mTOR(Ser2448) normalized to the mTOR in the Rosco or OA treated oocytes. Data are presented as mean  $\pm$  SD, Student's t-test. (E) Localization of mTOR(Ser2448) and CDK1 in the post-NEBD and pro-MI stage oocytes,  $n=30$ , phospho-specific antibody (green) and DNA (blue). Scale bar D 20  $\mu$ m.

cumulus complexes to investigate the phosphorylated status of 4E-BP1 in other cells that are naturally present in the G0 or G1 stage<sup>40</sup> of the cell cycle. WB data from CCs

lysates revealed that 4E-BP1 was not phosphorylated in the CCs isolated either from GV or from MII CCs (Supplementary Fig. 4A). Oocytes in GV and MII stages were used as a



control of the protein mobility shift. Accordingly, in the ICC experiments there was no 4E-BP1 phosphorylation signal observed for Thr37/46/70 and Ser65 in the CCs, although 4E-BP1 was present in this cell type (Supplementary Fig. 4B).

Altogether, our results suggest that upon exit from prophase the activity of CDK1/CYCB1 (MPF) is required for the phosphorylation of 4E-BP1, most likely via activation of mTOR.

#### Expression of a dominant negative 4E-BP1 mutant promotes aberrant spindle formation

4E-BP1 phosphorylation releases eIF4E binding to permit translation initiation; the overall increase in phospho-4E-BP1 in the cytoplasm may facilitate maternal mRNA translational recruitment in the cytoplasm. To down-regulate phosphorylation of 4E-BP1, we expressed RNA coding for 4E-BP1 with all 4 phospho-sites mutated - Thr37/46/70 and

Ser65 (4E-BP1-4Ala; Fig. 4A). Microinjection (Fig. 4B) of the *in vitro* transcribed (IVT) RNA coding for 4E-BP1-wild type (4E-BP1-Wt) or 4E-BP1-4Ala showed that the whole population of endogenous and exogenous 4E-BP1-Wt was phosphorylated in the MII oocytes (Fig. 4C; also see Fig. 1A and D), however, in MII oocytes microinjected with 4E-BP1-4Ala RNA 2 not phosphorylated bands were present (depicted by arrowhead) and upper band of phosphorylated endogenous 4E-BP1 (Fig. 4C). Moreover, ICC detection with 4E-BP1 antibody in the microinjected oocytes showed significant increase of the intensity of the 4E-BP1 protein level for both injected constructs in comparison with no injected group (Supplementary Fig. 5; mean value 29 % in the 4E-BP1-Wt and mean value 23 % in the 4E-BP1-4Ala,  $P < 0.001$  Student's *t*-test). Microinjected oocytes with 4E-BP1-4Ala RNA extruded a polar body, however, ICC analysis showed significant increase in aberrant spindles accompanied by the absence of chromosome alignment to the

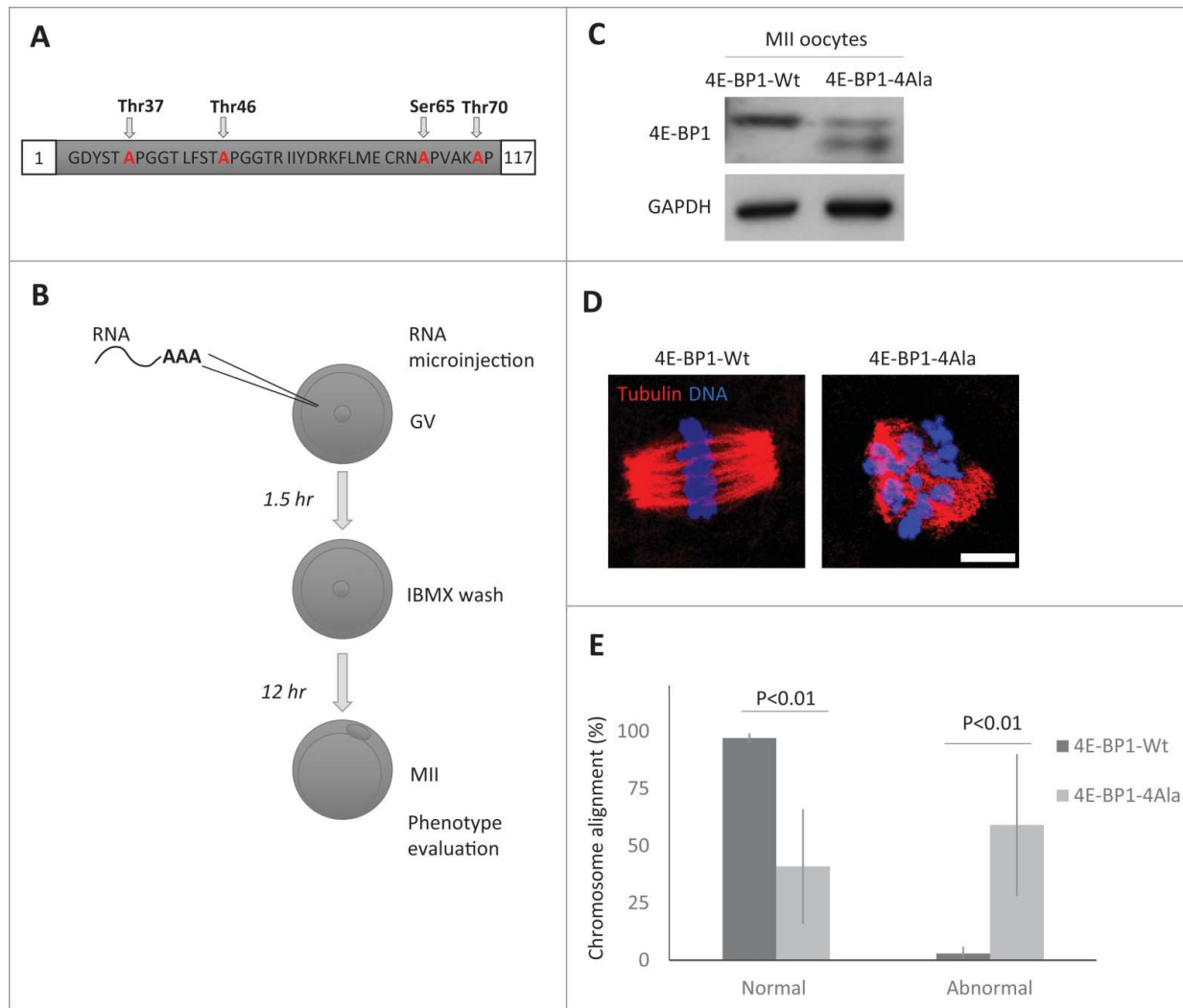


**Figure 4.** Down-regulation of 4E-BP1 phosphorylation in oocytes results in defects in the MII spindle assembly. (A) Scheme of dominant negative mutant construct of 4E-BP1-4Ala used for *in vitro* transcription. (B) Scheme of experimental procedure to express 4E-BP1 RNA constructs in the oocyte. (C) Immunoblotting evaluation of expression of microinjected non-phosphorylatable form (marked by arrowhead) of 4E-BP1 in the matured MII oocytes n D 2. GAPDH was used as a loading control. See Figure S5. (D) Confocal images of MII spindles of oocytes microinjected with 4E-BP1-Wt or dominant negative mutant 4E-BP1-4Ala, Tubulin (red) and DNA (blue). Scale bar D 10  $\mu$ m. (E) Quantification of chromosome alignment in the metaphase plate, MII oocytes expressing 4E-BP1-Wt or 4E-BP1-4Ala RNA. Data are presented as mean  $\pm$  SD, Student's *t*-test, n 2:25.

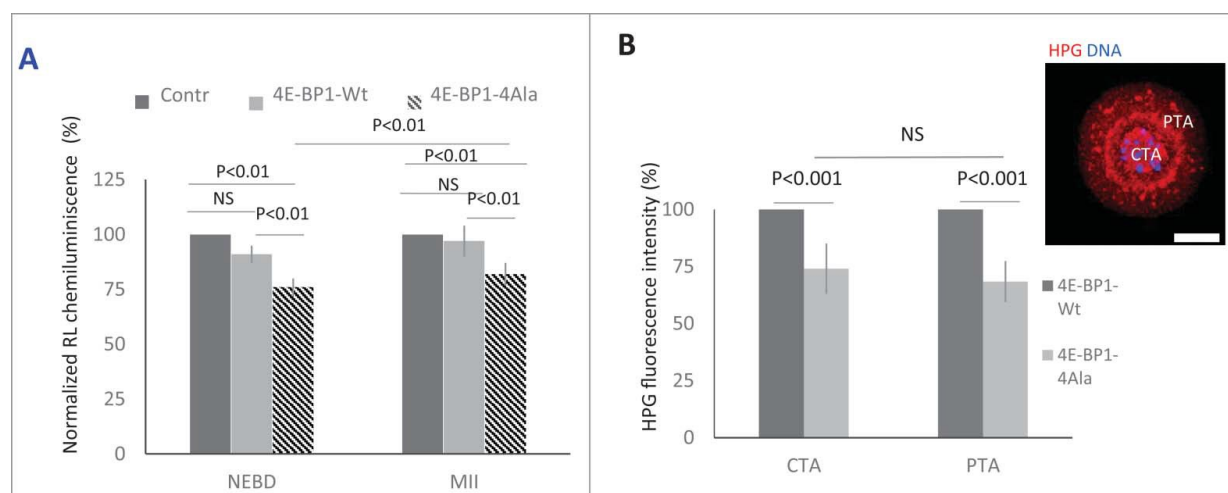


**Figure 5.** 4E-BP1 effects on protein synthesis in the oocytes. (A) Renilla luciferase reporter carrying 5'UTR TOP motive of *Eef2* co-injected with 4E-BP1-Wt or 4E-BP1-4Ala RNA. In the control no 4E-BP1 RNA was used and the IRES motive Firefly Luciferase was used as a loading control. Chemiluminescence was measured in the post NEBD stage (mean value  $\pm$  SD, Student's *t*-test, NS, non-significant) and MII stage oocytes (mean values  $\pm$  SD, Student's *t*-test). Data are presented as mean  $\pm$  SD, n 20 replicates. (B) Measurement of *in situ* translation intensity in the chromosomal area (CTA, mean value  $\pm$  SD, Student's *t*-test, NS, non-significant) and perispindular translational area (PTA, mean value  $\pm$  SD, Student's *t*-test) in the post NEBD oocytes, HPG (red) and DNA (blue). Data are presented as mean  $\pm$  SD, n 221. Scale bar = 20  $\mu$ m.

metaphase plate in 59% of the 4E-BP1-4Ala injected oocytes (mean value  $\pm$  SD, 31%;  $P < 0.01$ , Student's *t*-test), whereas only 3% of the 4E-BP1-Wt injected oocytes produced them (mean value  $\pm$  SD, 3%;  $P < 0.01$ , Student's *t*-test, Fig. 4E).

It is accepted that 4E-BP1 is a key player in cap-dependent translation<sup>27</sup> which predominantly utilizes mRNA with TOP motif.<sup>41</sup> To further investigate this, we examined the expression of a dominant negative mutant of 4E-BP1<sup>41</sup> and its influence on the translation of the *Renilla* Luciferase (RL) reporter with canonical TOP motive of the *Eef2*<sup>41</sup>. We performed microinjection of IVT RNA coding 4E-BP1-Wt or 4E-BP1-4Ala with RL reporter RNA and *Firefly* Luciferase (FL) with IRES motif as a microinjection loading control. Analysis of chemiluminescence showed a significant decrease of RL expression in the oocytes expressing 4E-BP1-4Ala in comparison with the control injected with RL and FL (Fig. 5A). Decrease of RL expression was non-significant in 4E-BP1-Wt RNA injected (mean value  $\pm$  SD, 6%,  $P > 0.05$ , Student's *t*-test) in the post-NEBD stage in comparison with 24% significant decrease in the 4E-BP1-4Ala RNA injected groups (mean value  $\pm$  SD, 4%,  $P < 0.01$ , Student's *t*-test). RL expression in the MII oocytes showed significant (18%) decrease in the oocytes injected with 4E-BP1-4Ala RNA in comparison with the control group (mean value  $\pm$  SD, 5%,  $P < 0.01$ , Student's *t*-test). Moreover, we analyzed *in situ* translation (Fig. 5B) in the 2 distinct areas of the oocyte after expression of 4E-BP1-Wt or 4E-BP1-4Ala, one at the area of the newly forming spindle (Chromosomal Translational Area; CTA) and the second at the Perispindular Translational Area (PTA). We detected a significant decrease of translation at the CTA (26%, mean  $\pm$  SD, 11%;  $P < 0.01$ , Student's *t*-test) and PTA (32%, mean  $\pm$  SD, 9%;  $P < 0.01$ , Student's *t*-test), however, without significant differences between CTA and PTA ( $P > 0.05$ ; Fig. 5B).

## Discussion

Here we present an analysis of regulation of 4E-BP1 phosphorylation during meiotic division of the mammalian oocyte, a cell

that naturally undergoes NEBD, then enters prometaphase and resumes meiosis further by asymmetric cytokinesis creating a fertilizable egg and a polar body. The progress of oocytes through cell cycle is highly synchronized, with rapid inactivation/phosphorylation of 4E-BP1, which suggests that cap-dependent translation is highly active in this cell type and stage. In accordance with Mayer et al.<sup>23</sup> we were not able to detect 4E-BP2 and 4E-BP3 proteins suggesting that 4E-BP1 is the only form of eIF4E-binding protein present in mouse and bovine oocytes. However, mRNAs coding all 3 isoforms are present and stable in mouse oocytes during maturation indicating their role post-fertilization during early embryonic development, or alternatively, they might be translated to substitute 4E-BP1 in case of an insufficiency of the 4E-BP1 form.<sup>42</sup>

Here we show that the main effector kinases of 4E-BP1 phosphorylation are mTOR and CDK1, which become highly active after the resumption of meiosis both in mouse, human and, also bovine oocytes (mTOR,<sup>9,23</sup> and MPF<sup>26</sup>), which is similar to mitosis.<sup>43</sup> It has been reported that also PLK1 promotes phosphorylation of 4E-BP1 in mitotic cells,<sup>44</sup> however, inhibition of PLK1 in mammalian oocytes did not show any effect on 4E-BP1 phosphorylation in our model system. Inhibition of mTOR or CDK1, on the other hand, strongly affects 4E-BP1 phosphorylation in a very similar manner. These findings suggest the existence of a different mechanism of 4E-BP1 phosphorylation in the meiotic cell. We further show that inhibition of CDK1 kinase activity results in inhibition of mTOR phosphorylation on the site activation (Ser2448), suggesting that CDK1 exerts its effect on 4E-BP1 phosphorylation via activation of mTOR, although we cannot exclude the possibility that CDK1 phosphorylates 4E-BP1 directly. So, in accordance with Heesom et al.<sup>32</sup> we show that the main regulator of 4E-BP1 phosphorylation in mouse oocytes is mTOR, on the other hand, CDK1 activity is in our system required for the full mTOR activation rather than for direct 4E-BP1 phosphorylation. It is known that mTOR is phosphorylated and activated in mitotic cells by AKT,<sup>45</sup> however, according to our results, it

seems that during mammalian meiosis this pathway is not sufficient for full mTOR activation, which is likely to be mediated by CDK1.

An increase in 4E-BP1 phosphorylation has been previously seen in porcine, bovine and mouse oocytes,<sup>4,8,9,21,22</sup> however, only recently the localization of the differently phosphorylated forms of 4E-BP1 has been described in mouse oocytes.<sup>38</sup> The nature and role of Ser65 and Thr70 phosphorylation for spindle localization is unclear at the present time, although it should be noted that cap-dependent translation becomes elevated at the onset of meiosis and is inactivated later when it exits meiosis (fertilization).<sup>6</sup> Romasko et al.<sup>22</sup> show that 4E-BP1(Ser112) has similar localization as 4E-BP1(Ser65) in our study. Regulation of 4E-BP1 phosphorylation at the spindle is likely to be temporally and mechanistically distinct from its regulation in the rest of the oocyte. The dynamic spatial and temporal pattern of localization of phosphorylated 4E-BP1 that forms at the spindle is indicative of a novel mechanism promoting localized protein production related to transcripts localized at the spindle. Depolymerization of the newly forming spindle by Noco treatment changed the 4E-BP1(Thr70) pattern, however, phosphorylation still persisted at the chromosomal area. This suggests the existence of a mechanism, which maintains phosphorylation at this position, most likely involving Lamin A/C and/or endoplasmic reticulum structures surrounding the spindle assembly area. Such a mechanism would promote the accumulation of specific proteins by microtubule-independent machinery, involving some sort of semipermeable membrane<sup>46</sup> formed from microfilaments,<sup>47,48</sup> ER,<sup>49-51</sup> LMN<sup>9</sup> and possibly other constituents.

A number of studies,<sup>22,52-57</sup> have reported the enrichment of specific mRNAs at the spindle, which may contribute to the local proteome. Beside the enrichment of global translation at the oocyte spindle,<sup>9</sup> Romasko et al.<sup>22</sup> has also shown that *Mis18a* mRNA coding MIS18 Kinetochore Protein A is localized at the oocyte spindle, which is required for metaphase alignment and proper chromosome segregation.<sup>58</sup> Another example of localized translation has been documented by Bomar et al.<sup>52</sup> who identified the localization of *Akap95* (A kinase-anchoring protein) mRNA at the MII spindle without protein expression at this stage, but the mRNA was then translated after fertilization and the protein was present in the female pronucleus causing an unequal distribution between maternal and paternal nuclei in the zygote. Local transcriptome coupled with its translation suggests the role of translational machineries, where mTOR, CDK1 and 4E-BP1 are key players, the mechanism that is used by meiotic and mitotic cells of various species. However, differences between the cell types suggest there are distinct modes of regulation.

There are various factors involved in spindle formation. Apart from the specific transport of mRNA to the spindle, a population of RNA might already be present in the nucleus,<sup>9,56,59,60</sup> which indicates a significant contribution of the local transcriptome to the formation of spindle directly post-NEBD. In accordance with this, 4E-BP1 is enriched in the nucleus in its non-phosphorylated state. 4E-BP1 in the nucleus might be bound to the 5'UTR of mRNAs, where it probably functions as a translational repressor. Consequently, after its hyperphosphorylation following NEBD, it becomes inactivated and in such a way promotes the

translation of specific mRNAs at the newly forming spindle. These results suggest that the function of mRNA retention in the nucleus may be to sustain translational repression, and that their subsequent translation can be regulated in a spatiotemporally restricted manner in response to cell cycle events.

We propose that meiotic phosphorylation of 4E-BP1 on Ser65 and Thr70 by mTOR acts to stimulate cap-dependent translation as the oocyte proceeds through meiosis (particularly after NEBD) and that specific localization of the key cap-dependent translation regulatory factors,<sup>22,61</sup> is essential for the translation of specific mRNAs at the spindle area to ensure errorless meiotic progression. We identify the 2 kinases mTOR and CDK1 involved in the inactivation of the 4E-BP1 at the spindle where all the important regulators are present. Using PLK1 inhibitor BI2536 we show that PLK1 kinase is not involved in 4E-BP1 phosphorylation in mouse oocytes and also, that CDK1 exerts its influence via the phosphorylation (and as such further activation) of mTOR, which as a result is likely to phosphorylate Ser65 and Thr70 of 4E-BP1. However, we cannot exclude the possibility that CDK1 phosphorylates at least one of these sites directly, as was previously reported by Heesom et al.<sup>32</sup> and Shuda et al.<sup>34</sup> Since the effect of CDK1 inhibition on the level of 4E-BP1 phosphorylation is less pronounced in later stages of meiosis (data not shown) it is tempting to speculate that the increased activation of mTOR mediated by CDK1 might be temporally and possibly also spatially restricted to the most critical process during early meiosis, i.e. formation of the meiotic spindle. Such hypothesis is supported also by the data obtained by us and other studies<sup>38</sup> showing the increased presence of 4E-BP1 phosphorylated forms at the spindle and in the chromosomal area. It is also interesting to note that CDK1 has been shown to directly phosphorylate the key mTOR binding partner Raptor during mitosis.<sup>62</sup> This reinforces our conclusions and those from other studies suggesting that mTOR activity is highly regulated by cell cycle progression. A number of other proteins involved in the regulation of translation have also been described previously. Papst<sup>63</sup> reported that Ribosomal Protein S6 Kinase is a substrate for CDK1/CYCB1 in mitosis and Elongation factor-1<sup>64</sup> in the *Xenopus* oocytes during meiotic cell division is a physiologic substrate of CDK1/CYCB1 in mitosis.

After fertilization when the nuclear envelope is reformed again at the end of meiosis, phosphorylation of 4E-BP1 disappears.<sup>59</sup> This indicates a specific/exclusive role of this pathway in meiotic maturation, which is also supported by our findings showing that no phosphorylated 4E-BP1 is present in the CCs, naturally occurring in the G0 or G1 stage. We might conclude that phosphorylation of 4E-BP1 follows exit from prophase of the cell cycle. It has been reported previously that overall protein synthesis becomes reduced during meiosis.<sup>4,9,65</sup> However, studies in synchronized HeLa cells have shown that this inhibition ceases by late telophase<sup>66</sup> and that overall protein synthesis increases rapidly as cells enter G1-phase.<sup>67</sup>

Here we show that the presence of a non-phosphorylated 4E-BP1 population in an oocyte that progresses through meiosis results in aberrant morphology of the metaphase II spindle that is most likely the result of impaired translation of a subset of RNAs. Previously, we have described the effect of mTOR/4F



pathway downregulation on in situ translation at the chromosomal area.<sup>9</sup> Our current finding shows that a non-phosphorylated mutant does not display significant differences in the level of translation between the chromosomal and perispindular areas. This might be explained by the fact that exogenous 4E-BP1, which is loaded to the cytoplasm in the form of RNA, and its consequent 4E-BP1 protein, lacks endogenous localization in this large cell and so influences both translational areas within the cell. On the other hand, the expression of a mutant in the cytoplasm which is unable to be phosphorylated leads to downregulation of translation in the cytoplasm and at the chromosomal area.

4E-BP1 null mice are viable and fertile.<sup>42</sup> However, we have observed aberrant spindle formation in the MII oocytes expressing a non-phosphorylatable 4E-BP1 form, which might suggest that the role of 4E-BP1 is rather in the fine tuning of meiotic progression. Regulation of 4E-BP1 in the oocyte might be affected by cell stress or by the age of the female. Moreover, insulin stimulates the mTOR signaling pathway<sup>68</sup> and insulin signaling promotes the production of high-quality oocytes.<sup>69</sup> Consistently, oocytes from diabetic mice display spindle abnormalities, which can be reversed by pancreatic islet transplantation.<sup>70</sup> Our findings showing localization of phosphorylated/inactivated 4E-BP1 at the spindle also suggest the existence of a mechanism that links maternal age and environmental exposures to diminished oocyte quality arising from defective spindle formation and function. We show that mTOR becomes also activated post NEBD in the human oocyte, with strong signal at midbody in the MII oocyte, suggesting its similar role in the human oocyte meiosis in specific translational regulation, as it plays in the mouse oocyte. Here, mTOR pathway might contribute to the age related chromosome segregation errors in the woman oocytes, similarly as it has been documented in the mouse model,<sup>9</sup> as well as in mammalian and yeast cells.<sup>71</sup> Lapasset et al.<sup>7</sup> showed that the treatment with Rapa resulted in the prevention of extrusion of second polar body in starfish oocytes. They present the absence of eIF4E dissociation from 4E-BP in the presence of Rapa without the effect on translation of Cyclin B1 or Mos. Taken together, mTOR involvement is indispensable for inactivation of translational repressor 4E-BP1, which prevents the synthesis of essential proteins necessary for a correct completion of the meiotic and mitotic divisions. In addition to translational initiation factors, Ribosomal protein S3 (RPS3) is present at the mitotic<sup>72</sup> or newly forming meiotic spindle.<sup>73</sup> RPS3 knockdown causes arrest in mitotic metaphase,<sup>72</sup> which resembles the effect of mTOR inhibition<sup>23</sup> in the bovine oocyte. The influence of known effector kinases in the inactivation of the translational repressor 4E-BP1 might be essential for the temporal and spatial translation of specific mRNAs at the spindle area to ensure errorless meiotic progression.

In this study we propose that localized translational regulation at the oocyte spindle regulated through an mTOR/CDK1 pathway might represent a mechanism which links spindle formation and function with the temporal and spatial regulation of the local transcriptome in the particular subcellular areas, which affects oocyte quality. There is still much to learn about

the dynamics of distribution of mRNA and translational regulatory components, as well as how exactly these are regulated in the different cellular compartments. Further elucidation of the relationship between cytoskeletal elements and translation machinery may help to explain the logistics of translational control of spindle assembly and chromosome segregation.

## Material and methods

### Oocytes isolation and maturation

Mouse ovaries were obtained from CD1 mice at least 6 weeks old which were stimulated to by intraperitoneal injection of 5 UI of pregnant mare serum gonadotropin (PMSG; Folligon, Merck Animal Health) 46 h before collection. GV oocytes were isolated into transfer medium Tetkova et al.<sup>74</sup> supplemented with 100 mM of 3-isobutyl-1-methylxanthine (IBMX) used to prevent spontaneous resumption of meiosis. Selected oocytes were stripped of the cumulus cells and cultured in M16 medium (Millipore) without IBMX at 37°C, 5% CO<sub>2</sub>. After 70 min post IBMX wash (PIW) at least 90% of oocytes underwent nuclear envelope breakdown (NEBD, resumption of meiosis; G2/M transition) and oocytes arrested in the GV were discarded. Pro-metaphase I (pro-MI) and metaphase I (MI) stage oocytes were collected after post IBMX wash at 3 h (post-NEBD), 7 h (pro-MI) and 12 h (MII). All animal work was conducted according to Act No 246/1992 on the protection of animals against cruelty. Human oocytes, not used in human reproduction, were obtained from the Obstetrics and Gynecology Clinic of the General University Hospital in Prague. The project was accredited (#30/12) by the Ethical Committee of the General Hospital, Prague.

### Oocyte treatments

Mouse oocytes were treated with 100nM BI2536 for 2 hours post NEBD (Axon Medchem), 1 mM Nocodazole for 1 h (M1404, Sigma-Aldrich), 100 nM Rapamycin (#9904, CST) or 10 mM Roscovitine (R7772, Sigma-Aldrich); 1 mM Okadaic acid (OA, CAS 459616, Millipore) for 2 h after NEBD. For nascent protein synthesis specific stage NEBD-2 h, oocytes were cultured in methionine-free medium (Gibco) supplemented with 1% dialyzed fetal bovine serum (10,000MW; Sigma) and 50 mM L-homopropargylglycine (HPG) for 30 min. HPG was detected by using a Click-iT Cell Reaction Kit (Life Technologies). *In situ* translation detection showed increased incorporation of HPG in the chromosomal area (CTA) and perispindular area (PTA)<sup>9</sup>

### RNA isolation and quantitative RT-PCR

RNA was extracted with RNeasy Plus Micro kit (Qiagen) according to manufacturer's instructions. Genomic DNA was depleted using guide columns. H<sub>2</sub>O for qRT-PCR was used for RNA elution in amount of 25 mL for 25 oocytes. Samples were stored at -80°C until expression analysis. mRNA equivalent for 1 oocyte was amplified by a One-step RT-PCR kit (Qiagen) with real-time detection using SybrGreenI fluorescent dye on a Rotor Gene 3000 instrument (Corbett Research, Australia). The qRT-PCR reactions were prepared in duplicates in one

run. Reaction conditions were: reverse transcription at 50°C for 30 min, initial activation at 95°C for 15 min, cycling: denaturation at 95°C for 20 sec, annealing at a temperature specific for each set of primers (see Table S1) for 20 sec, extension at 7°C for 30 sec. Products were verified by melting analysis and gel electrophoresis on 1.2% agarose gel with ethidium bromide staining. The relative concentration of templates in different samples was determined using comparative analysis software (Corbett Research). The results for individual target genes were normalized according to the relative internal standard GAPDH. The data are presented from at least 3 biologic replicates. The significant differences between GV and MII were evaluated using *t*-test (PrismaGraph5).

### Immunocytochemistry

Mouse and human oocytes were fixed for 20 min in 4% PFA in phosphate saline buffer (PBS). Oocytes were permeabilized for 10 min in 0.2% Triton X-100 in PBS, then washed with PVA/PBS. Oocytes were incubated with primary antibodies at 4°C overnight. We are using human 4E-BP1 nomenclature to unify the text discussing human and mouse systems. The human 4E-BP1 sequence of amino acid numbers is greater by one. The following antibodies were used in 1:100 dilution: rabbit anti-4E-BP1 (#9452, CST), rabbit anti-phospho-4E-BP1(Thr70) (#13396, CST), rabbit anti-phospho-4E-BP1(T37/46) (#9459, CST), rabbit anti-phospho-4E-BP1(Ser65) (#9451, CST), rabbit anti-CDK1 (#9112, CST), mouse anti-tubulin (#T6793, Sigma) and  $\alpha$ -tubulin (#T6557, Sigma), rabbit anti-phospho-mTOR(Ser2448, #2971, CST) and mouse anti-LMNA/C (SAB4200236, Sigma Aldrich). After washing in PBS, detection of the primary antibodies was performed by cultivation of the oocytes with relevant Alexa Fluor 488, 594 or 647 conjugates (diluted 1: 250) for 1 h at room temperature. Oocytes were then washed 2 times for 15 min in PVA/PBS and mounted using Vectashield Mounting Medium with DAPI (H-1200, Vector Laboratories). Samples were visualized using a Leica SP5 inverted confocal microscope (Leica Microsystems) in 16 bit depth. Images were assembled in LEICA LasAFIX (Leica Microsystems) software and equatorial sections were quantified by Image J software (<http://rsbweb.nih.gov/ij/>).

### Western blot

Oocytes were lysed with 6 ml of Millipore H<sub>2</sub>O and 2, 5 ml of 4x lithium dodecyl sulfate, sample buffer NP 0007 and 1 ml reduction buffer NP 0004 (Novex, Thermo Fisher Scientific) and boiled at 100°C for 5 min. If not stated otherwise, sample of 50 oocytes per sample was used. To detect phosphorylation shift, oocytes were dissolved in the 20 ml of the 1x NEBuffer with 800 U of LPP enzyme (P0753, New England BioLabs) and incubated overnight at 30°C, LPP was omitted in the control sample (LPP-). Lysates were separated using a 4–12% gradient polyacrylamide gel SDS (NP323BOX, Life Technologies) page and transferred to an immobilon P membrane (PVDF; Millipore) using semidry blotting system (Biometra GmbH). Membranes were blocked for 1 h, in 1–5% skimmed milk dissolved in Tween-Tris-buffer saline (TTBS, pH 7.4) according to antibody (list of primary antibodies and dilutions is below). After 3 cycles for 10 min washing in TTBS, membranes were incubated

at 4°C overnight in 1% milk/TTBS with the following primary antibodies: GAPDH (rabbit, G9545, Sigma-Aldrich) and Tubulin (mouse, T6793, Sigma-Aldrich) antibodies were diluted 1:30 000 and 4E-BP1 (rabbit, 9452, CST), 4E-BP1(T69) (rabbit, 9455S, CST), 4E-BP1(T36/45) (rabbit, 9459, CST), 4E-BP1(S64) (rabbit, 9451S, CST), anti HA (rabbit, 3724, CST) antibodies were diluted 1:500; mTOR(Ser2448) (rabbit, 2971S, CST), mTOR (rabbit, 2972, CST) antibodies were diluted 1:8 000 and 1:2 000 respectively. After 3 cycles of 10 min washing in TTBS the membrane was incubated for 1 h with secondary antibody Peroxidase Anti-Rabbit Donkey (711-035-152, Jackson immunoresearch) or Peroxidase Anti-mouse Donkey (715-035-151, Jackson immunoresearch) in 1:7.500 dilution in 1% milk/TTBS 1 h at room temperature. Immunodetected proteins were visualized by ECL (Amersham, GE Healthcare life science), films were scanned using a GS-800 calibrated densitometer (Bio-Rad) and quantified using Image J software (<http://rsbweb.nih.gov/ij/>).

### Microinjection

GV stage mouse oocytes were microinjected in transfer medium with IBMX on an inverted microscope Leica DMI 6000B with Transferman NK2 and Femtojet (Eppendorf). Oocytes were injected with *in vitro* transcribed RNA (mMessage, Ambion) from mutant plasmid pCW57.1-4E-BP1-4Ala<sup>41</sup> and pCMV3-N-HA-4E-BP1 (generous gift of professor Nahum Sonenberg, McGill University, Montreal, Canada; Gingras et al.<sup>27</sup>). Approximately 5 pl of RNA solutions of 4E-BP1-Ala or 4E-BP1-Wt diluted in RNase free water, to concentration 50 ng/ml were microinjected into oocytes.

### Dual-luciferase assay

Oocytes were injected in the presence of IBMX with 50 ng/ml of IVT RNA (mMessage, Ambion) from *Renilla Luciferase* constructs (*Eef2*-5'UTR - RL; #38235; Addgene) with combination of injection amount control *Firefly Luciferase* (FL; #18964; Addgene<sup>75</sup>) and RNA for 4E-BP1-Wt or 4E-BP1-4Ala in the presence of IBMX. Oocytes were cultured for 5 h without IBMX. At least 5 oocytes were lysed in 5 ml of Passive Lysis Buffer and stored at 80°C until measurement of chemiluminescence by Dual-Luciferase Assay System (Promega) according to the manufacturer's instructions. Signal intensities were measured using a Glomax Luminometer (Promega). Activity of RL was normalized to the FL luciferase.

### Statistical analysis

Experiments were repeated at least 3 times unless stated. Mean and SD values were calculated using MS Excel, statistical significance of the differences between the groups was tested using Student's *t*-test (PrismaGraph5) and *P*<0.05 was considered as statistically significant.

### Abbreviations

Akap95	Kinase (PRKA) anchor protein 8
CCs	Cumulus cells

CDK1	Cyclin dependent kinase 1
CTA	Chromosomal translational area
CYCB1	Cyclin B1
DAPI	4', 6-diamidino-2-phenylindole
ER	Endoplasmic reticulum
eIF4E	Eukaryotic initiation factor 4E
eIF4G1	Eukaryotic initiation factor 4G1
eIF4A	Eukaryotic initiation factor 4A
FL	Firefly Luciferase
FRAP kinase	FKBP-12-rapamycin-associated protein
G1-phase	Gap 1 phase
GV	Germinal vesical stage
HPG	L-homopropargylglycine
HA	Hemagglutinin
IBMX	3-Isobutyl-1-methylxanthine
IRES	Internal ribosome entry site
IVT	<i>In vitro</i> transcribed
LMN	Lamin A/C
Mis18a	MIS18 kinetochore protein A
mTOR	Mammalian target of rapamycin
MI	Metaphase of first meiotic maturation
MII	Metaphase of second meiotic maturation
MPF	Maturation promoting factor
Noco	Nocodazole
NEBD	Nuclear envelope breakdown
OA	Okadaic acid
PTA	Perispindular translational area
PVA	Polyvinylalcohol
PIW	Post IBMX wash
PLK1	Polo-like kinase1
PKB/ AKT	Protein kinase B/ serine/threonine-specific protein kinase
PBE	Polar body extrusion.
Ras/Raf/ERK pathway	Mitogen-activated protein kinases pathway
Rosco	Roscovitine
RL	Renilla Luciferase
Rapa	Rapamycin
S6 kinase	Ribosomal s6 kinase
TOP	Terminal oligopyrimidine motif
3' UTR	Three prime untranslated region
4E-BP1	Eukaryotic translation initiation factor 4E-binding protein 1
4E-BP2	Eukaryotic translation initiation factor 4E-binding protein 2
4E-BP3	Eukaryotic translation initiation factor 4E-binding protein 3
5' UTR	Five prime untranslated region

## Disclosure of potential conflicts of interest

No potential conflicts of interest were disclosed.

## Acknowledgments

We thank Jaroslava Suplikova and Marketa Hancova for their exceptional assistance with experiments and Nahum Sonenberg and his laboratory for kindly providing the pCMV3-N-HA- 4E-BP1 plasmid.

## Funding

This work was supported by GACR13-12291S, GACR15-22765S, EXCELLENCE CZ.02.1.01/0.0/0.0/15\_003/0000460 OP RDE and Institutional Research Concept RVO67985904.

## ORCID

Radek Malik  <http://orcid.org/0000-0002-6783-1146>  
Michal Kubelka  <http://orcid.org/0000-0002-2264-5884>

## References

- [1] Schuh M, Ellenberg J. Self-organization of MTOCs replaces centrosome function during acentrosomal spindle assembly in live mouse Oocytes. *Cell* 2007; 130:484-98
- [2] Kusch J, Liakopoulos D, Barral Y. Spindle asymmetry: a compass for the cell. *Trends Cell Biol* 2003; 13:562-9
- [3] Hashimoto N, Kishimoto T. Regulation of meiotic metaphase by a cytoplasmic maturation-promoting factor during mouse oocyte maturation. *Dev Biol* 1988; 126:242-52; PMID:3350209
- [4] Ellederova Z, Kovarova H, Melo-Sterza F, Livingstone M, Tomek W, Kubelka M. Suppression of translation during in vitro maturation of pig oocytes despite enhanced formation of cap-binding protein complex eIF4F and 4E-BP1 hyperphosphorylation. *Mol Reprod Dev* 2006; 73:68-76; PMID:16211600
- [5] Ellederova Z, Cais O, Susor A, Uhlířová K, Kovářová H, Jeřnková L, Tomek W, Kubelka M. ERK1/2 map kinase metabolic pathway is responsible for phosphorylation of translation initiation factor eIF4E during in vitro maturation of pig oocytes. *Mol Reprod Dev* 2008; 75:309-17; PMID:17290414
- [6] Susor A, Jeřnková L, Karabínová P, Torner H, Tomek W, Kovářová H, Kubelka M. Regulation of cap-dependent translation initiation in the early stage porcine parthenotes. *Mol Reprod Dev* 2008; 75:1716-25; PMID:18386287
- [7] Lapasset L, Pradet-Balade B, Vergé V, Lozano J-C, Oulhen N, Cormier P, Peaucellier G. Cyclin B synthesis and rapamycin-sensitive regulation of protein synthesis during starfish oocyte meiotic divisions. *Mol Reprod Dev* 2008; 75:1617-26; PMID:18361417
- [8] Tomek W, Torner H, Kanitz W. Comparative analysis of protein synthesis, transcription and cytoplasmic polyadenylation of mRNA during maturation of bovine oocytes in vitro. *Reprod Domest Anim Zuchthyg* 2002; 37:86-91
- [9] Susor A, Jansova D, Cerna R, Danylevska A, Anger M, Toralova T, Malik R, Supolikova J, Cook MS, Oh JS, et al. Temporal and spatial regulation of translation in the mammalian oocyte via the mTOR-eIF4F pathway. *Nat Commun* 2015; 6:6078; PMID:25629602
- [10] Jackson RJ, Hellen CUT, Pestova TV. The mechanism of eukaryotic translation initiation and principles of its regulation. *Nat Rev Mol Cell Biol* 2010; 11:113-27; PMID:20094052
- [11] Gingras AC, Gygi SP, Raught B, Polakiewicz RD, Abraham RT, Hoekstra MF, Aebersold R, Sonenberg N. Regulation of 4E-BP1 phosphorylation: a novel two-step mechanism. *Genes Dev* 1999; 13:1422-37; PMID:10364159
- [12] Gingras AC, Raught B, Sonenberg N. Regulation of translation initiation by FRAP/mTOR. *Genes Dev* 2001; 15:807-26; PMID:11297505
- [13] Raught B, Gingras AC, Sonenberg N. The target of rapamycin (TOR) proteins. *Proc Natl Acad Sci U S A* 2001; 98:7037-44; PMID:11416184
- [14] Tavares MR, Pavan ICB, Amaral CL, Meneguello L, Luchessi AD, Simabuco FM. The S6K protein family in health and disease. *Life Sci* 2015; 131:1-10; PMID:25818187
- [15] Gingras AC, Raught B, Gygi SP, Niedzwiecka A, Miron M, Burley SK, Polakiewicz RD, Wyslouch-Cieszynska A, Aebersold R, Sonenberg N. Hierarchical phosphorylation of the translation inhibitor 4E-BP1. *Genes Dev* 2001; 15:2852-64; PMID:11691836
- [16] Tee AR, Proud CG. Caspase cleavage of initiation factor 4E-binding protein 1 yields a dominant inhibitor of cap-dependent translation and reveals a novel regulatory motif. *Mol Cell Biol*



- 2002; 22:1674-83; PMID:11865047; <http://dx.doi.org/10.1128/MCB.22.6.1674-1683.2002>
- [17] Wang X, Beugnet A, Murakami M, Yamanaka S, Proud CG. Distinct signaling events downstream of mTOR cooperate to mediate the effects of amino acids and insulin on initiation factor 4E-binding proteins. *Mol Cell Biol* 2005; 25:2558-72; PMID:15767663; <http://dx.doi.org/10.1128/MCB.25.7.2558-2572.2005>
- [18] Corradetti MN, Guan K-L. Upstream of the mammalian target of rapamycin: do all roads pass through mTOR? *Oncogene* 2006; 25:6347-60; PMID:17041621; <http://dx.doi.org/10.1038/sj.onc.1209885>
- [19] Kalous J, Kubelka M, Solc P, Susor A, Mot'ik J. AKT (protein kinase B) is implicated in meiotic maturation of porcine oocytes. *Reprod Camb Engl* 2009; 138:645-54
- [20] Tomek W, Smiljakovic T. Activation of Akt (protein kinase B) stimulates metaphase I to metaphase II transition in bovine oocytes. *Reprod Camb Engl* 2005; 130:423-30
- [21] Tomek W, Melo Sterza FA, Kubelka M, Wollenhaupt K, Torner H, Anger M, Kanitz W. Regulation of translation during in vitro maturation of bovine oocytes: the role of MAP kinase, eIF4E (cap binding protein) phosphorylation, and eIF4E-BP1. *Biol Reprod* 2002; 66:1274-82; PMID:11967187; <http://dx.doi.org/10.1095/biolreprod66.5.1274>
- [22] Romasko EJ, Amarnath D, Midic U, Latham KE. Association of maternal mRNA and phosphorylated EIF4EBP1 variants with the spindle in mouse oocytes: localized translational control supporting female meiosis in mammals. *Genetics* 2013; 195:349-58; PMID:23852387; <http://dx.doi.org/10.1534/genetics.113.154005>
- [23] Mayer S, Wrenzycki C, Tomek W. Inactivation of mTOR arrests bovine oocytes in the metaphase-I stage, despite reversible inhibition of 4E-BP1 phosphorylation. *Mol Reprod Dev* 2014; 81:363-75; PMID:24459013; <http://dx.doi.org/10.1002/mrd.22305>
- [24] Lee S-E, Sun S-C, Choi H-Y, Uhm S-J, Kim N-H. mTOR is required for asymmetric division through small GTPases in mouse oocytes. *Mol Reprod Dev* 2012; 79:356-66; PMID:22407942; <http://dx.doi.org/10.1002/mrd.22035>
- [25] Poulin F, Gingras A-C, Olsen H, Chevalier S, Sonenberg N. 4E-BP3, a New Member of the Eukaryotic Initiation Factor 4E-binding Protein Family. *J Biol Chem* 1998; 273:14002-7; PMID:9593750; <http://dx.doi.org/10.1074/jbc.273.22.14002>
- [26] Pause A, Belsham GJ, Gingras AC, Donzè O, Lin TA, Lawrence JC, Sonenberg N. Insulin-dependent stimulation of protein synthesis by phosphorylation of a regulator of 5<sup>0</sup>-cap function. *Nature* 1994; 371:762-7; PMID:7935836; <http://dx.doi.org/10.1038/371762a0>
- [27] Gingras AC, Raught B, Sonenberg N. eIF4 initiation factors: effectors of mRNA recruitment to ribosomes and regulators of translation. *Annu Rev Biochem* 1999; 68:913-63; PMID:10872469; <http://dx.doi.org/10.1146/annurev.biochem.68.1.913>
- [28] Mader S, Lee H, Pause A, Sonenberg N. The translation initiation factor eIF-4E binds to a common motif shared by the translation factor eIF-4 gamma and the translational repressors 4E-binding proteins. *Mol Cell Biol* 1995; 15:4990-7; PMID:7651417; <http://dx.doi.org/10.1128/MCB.15.9.4990>
- [29] Tsukiyama-Kohara K, Vidal SM, Gingras AC, Glover TW, Hanash SM, Heng H, Sonenberg N. Tissue distribution, genomic structure, and chromosome mapping of mouse and human eukaryotic initiation factor 4E-binding proteins 1 and 2. *Genomics* 1996; 38:353-63; PMID:8975712; <http://dx.doi.org/10.1006/geno.1996.0638>
- [30] Fadden P, Haystead TA, Lawrence JC. Identification of phosphorylation sites in the translational regulator, PHAS-I, that are controlled by insulin and rapamycin in rat adipocytes. *J Biol Chem* 1997; 272:10240-7; PMID:9092573; <http://dx.doi.org/10.1074/jbc.272.15.10240>
- [31] Kogasaka Y, Hoshino Y, Hiradate Y, Tanemura K, Sato E. Distribution and association of mTOR with its cofactors, raptor and rictor, in cumulus cells and oocytes during meiotic maturation in mice. *Mol Reprod Dev* 2013; 80:334-48; PMID:23440873; <http://dx.doi.org/10.1002/mrd.22166>
- [32] Heesom KJ, Gampel A, Mellor H, Denton RM. Cell cycle-dependent phosphorylation of the translational repressor eIF-4E binding protein-1 (4E-BP1). *Curr Biol* 2001; 11:1374-9; PMID:11553333; [http://dx.doi.org/10.1016/S0960-9822\(01\)00422-5](http://dx.doi.org/10.1016/S0960-9822(01)00422-5)
- [33] Greenberg VL, Zimmer SG. Paclitaxel induces the phosphorylation of the eukaryotic translation initiation factor 4E-binding protein 1 through a Cdk1-dependent mechanism. *Oncogene* 2005; 24:4851-60; PMID:15897904; <http://dx.doi.org/10.1038/sj.onc.1208624>
- [34] Shuda M, Velásquez C, Cheng E, Cordek DG, Kwun HJ, Chang Y, Moore PS. CDK1 substitutes for mTOR kinase to activate mitotic cap-dependent protein translation. *Proc Natl Acad Sci U S A* 2015; 112:5875-82; PMID:25883264; <http://dx.doi.org/10.1073/pnas.1505787112>
- [35] Velásquez C, Cheng E, Shuda M, Lee-Oesterreich PJ, Pogge von Strandmann L, Gritsenko MA, Jacobs JM, Moore PS, Chang Y. Mitotic protein kinase CDK1 phosphorylation of mRNA translation regulator 4E-BP1 Ser83 may contribute to cell transformation. *Proc Natl Acad Sci U S A* 2016; 113:8466-71; PMID:27402756; <http://dx.doi.org/10.1073/pnas.1607768113>
- [36] Hampl A, Eppig JJ. Analysis of the mechanism(s) of metaphase I arrest in maturing mouse oocytes. *Development* 1995; 121:925-33; PMID:7743936
- [37] Wang X, Swain JE, Bollen M, Liu X-T, Ohl DA, Smith GD. Endogenous regulators of protein phosphatase-1 during mouse oocyte development and meiosis. *Reproduction* 2004; 128:493-502; PMID:15509695; <http://dx.doi.org/10.1530/rep.1.00173>
- [38] Shang ZF, Yu L, Li B, Tu WZ, Wang Y, Liu XD, Guan H, Huang B, Rang WQ, Zhou PK. 4E-BP1 participates in maintaining spindle integrity and genomic stability via interacting with PLK1. *Cell Cycle* 2012; 11:3463-71; PMID:22918237; <http://dx.doi.org/10.4161/cc.21770>
- [39] Lenárt P, Petronczki M, Steegmaier M, Di Fiore B, Lipp JJ, Hoffmann M, Rettig WJ, Kraut N, Peters J-M. The small-molecule inhibitor BI 2536 reveals novel insights into mitotic roles of polo-like kinase 1. *Curr Biol CB* 2007; 17:304-15; PMID:17291761; <http://dx.doi.org/10.1016/j.cub.2006.12.046>
- [40] Katska L, Bochenek M, Kania G, Ryńska B, Smorag Z. Flow cytometric cell cycle analysis of somatic cells primary cultures established for bovine cloning. *Theriogenology* 2002; 58:1733-44; PMID:12472143; [http://dx.doi.org/10.1016/S0093-691X\(02\)01043-9](http://dx.doi.org/10.1016/S0093-691X(02)01043-9)
- [41] Thoreen CC, Chantranupong L, Keys HR, Wang T, Gray NS, Sabatini DM. A unifying model for mTORC1-mediated regulation of mRNA translation. *Nature* 2012; 485:109-13; PMID:22552098; <http://dx.doi.org/10.1038/nature11083>
- [42] Tsukiyama-Kohara K, Poulin F, Kohara M, DeMaria CT, Cheng A, Wu Z, Gingras AC, Katsume A, Elchebly M, Spiegelman BM, et al. Adipose tissue reduction in mice lacking the translational inhibitor 4E-BP1. *Nat Med* 2001; 7:1128-32; PMID:11590436; <http://dx.doi.org/10.1038/nm1001-1128>
- [43] Vazquez-Martin A, Oliveras-Ferraro C, Bernadó L, López-Bonet E, Menendez JA. The serine 2481-autophosphorylated form of mammalian Target Of Rapamycin (mTOR) is localized to midzone and midbody in dividing cancer cells. *Biochem Biophys Res Commun* 2009; 380:638-43; PMID:19285014; <http://dx.doi.org/10.1016/j.bbrc.2009.01.153>
- [44] He Z, Wu J, Dang H, Lin H, Zheng H, Zhong D. Polo-like kinase 1 contributes to the tumorigenicity of BEL-7402 hepatoma cells via regulation of Survivin expression. *Cancer Lett* 2011; 303:92-8; PMID:21330050; <http://dx.doi.org/10.1016/j.canlet.2011.01.007>
- [45] Makker A, Goel MM, Mahdi AA. PI3K/PTEN/Akt and TSC/mTOR signaling pathways, ovarian dysfunction, and infertility: an update. *J Mol Endocrinol* 2014; 53:R103-118; PMID:25312969; <http://dx.doi.org/10.1530/JME-14-0220>
- [46] Schweizer N, Pawar N, Weiss M, Maiato H. An organelle-exclusion envelope assists mitosis and underlies distinct molecular crowding in the spindle region. *J Cell Biol* 2015; 210:695-704; PMID:26304726; <http://dx.doi.org/10.1083/jcb.201506107>
- [47] Yu Y, Dumollard R, Rossbach A, Lai FA, Swann K. Redistribution of mitochondria leads to bursts of ATP production during spontaneous mouse oocyte maturation. *J Cell Physiol* 2010; 224:672-80; PMID:20578238; <http://dx.doi.org/10.1002/jcp.22171>
- [48] Yi K, Rubinstein B, Unruh JR, Guo F, Slaughter BD, Li R. Sequential actin-based pushing forces drive meiosis I chromosome migration

- and symmetry breaking in oocytes. *J Cell Biol* 2013; 200:567-76; PMID:23439682; <http://dx.doi.org/10.1083/jcb.201211068>
- [49] FitzHarris G, Marangos P, Carroll J. Changes in endoplasmic reticulum structure during mouse oocyte maturation are controlled by the cytoskeleton and cytoplasmic dynein. *Dev Biol* 2007; 305:133-44; PMID:17368610; <http://dx.doi.org/10.1016/j.ydbio.2007.02.006>
- [50] Dalton CM, Carroll J. Biased inheritance of mitochondria during asymmetric cell division in the mouse oocyte. *J Cell Sci* 2013; 126:2955-64; PMID:23659999; <http://dx.doi.org/10.1242/jcs.128744>
- [51] Schlaitz A-L, Thompson J, Wong CCL, Yates JR, Heald R. REEP3/4 ensure endoplasmic reticulum clearance from metaphase chromatin and proper nuclear envelope architecture. *Dev Cell* 2013; 26:315-23; PMID:23911198; <http://dx.doi.org/10.1016/j.devcel.2013.06.016>
- [52] Bomar J, Moreira P, Balise JJ, Collas P. Differential regulation of maternal and paternal chromosome condensation in mitotic zygotes. *J Cell Sci* 2002; 115:2931-40; PMID:12082153
- [53] Blower MD, Feric E, Weis K, Heald R. Genome-wide analysis demonstrates conserved localization of messenger RNAs to mitotic microtubules. *J Cell Biol* 2007; 179:1365-73; PMID:18166649; <http://dx.doi.org/10.1083/jcb.200705163>
- [54] Elisacovich C, Peset I, Vernos I, Méndez R. Spindle-localized CPE-mediated translation controls meiotic chromosome segregation. *Nat Cell Biol* 2008; 10:858-65; PMID:18536713; <http://dx.doi.org/10.1038/ncb1746>
- [55] Mili S, Macara IG. RNA localization and polarity: from A(PC) to Z (BP). *Trends Cell Biol* 2009; 19:156-64; PMID:19251418; <http://dx.doi.org/10.1016/j.tcb.2009.02.001>
- [56] Lécuyer E, Yoshida H, Parthasarathy N, Alm C, Babak T, Cerovina T, Hughes TR, Tomancak P, Krause HM. Global Analysis of mRNA localization reveals a prominent role in organizing cellular architecture and function. *Cell* 2007; 131:174-87; PMID:17923096; <http://dx.doi.org/10.1016/j.cell.2007.08.003>
- [57] Bolton EM, Tuzova AV, Walsh AL, Lynch T, Perry AS. Noncoding RNAs in prostate cancer: the long and the short of it. *Clin Cancer Res Off J Am Assoc Cancer Res* 2014; 20:35-43; <http://dx.doi.org/10.1158/1078-0432.CCR-13-1989>
- [58] Fujita Y, Hayashi T, Kiyomitsu T, Toyoda Y, Kokubu A, Obuse C, Yanagida M. Priming of centromere for CENP-A recruitment by human hMis18alpha, hMis18beta, and M18BP1. *Dev Cell* 2007; 12:17-30; PMID:17199038; <http://dx.doi.org/10.1016/j.devcel.2006.11.002>
- [59] Jambor H, Surendranath V, Kalinka AT, Mejstrik P, Saalfeld S, Tomancak P. Systematic imaging reveals features and changing localization of mRNAs in Drosophila development. *Elife* 2015; 4:e05003; PMID:25838129; <http://dx.doi.org/10.1080/15384101.2017.1295178>
- [60] Susor A, Jansova D, Anger M, Kubelka M. Translation in the mammalian oocyte in space and time. *Cell Tissue Res* 2016; 363:69-84; PMID:26340983; <http://dx.doi.org/10.1007/s00441-015-2269-6>
- [61] Guertin DA, Sabatini DM. Defining the role of mTOR in cancer. *Cancer Cell* 2007; 12:9-22; PMID:17613433; <http://dx.doi.org/10.1016/j.ccr.2007.05.008>
- [62] Gwinn DM, Asara JM, Shaw RJ. Raptor is phosphorylated by cdc2 during mitosis. *PLoS One* 2010; 5:e9197; PMID:20169205; <http://dx.doi.org/10.1371/journal.pone.0009197>
- [63] Papst PJ, Sugiyama H, Nagasawa M, Lucas JJ, Maller JL, Terada N. Cdc2-Cyclin B Phosphorylates p70 S6 Kinase on Ser411at Mitosis. *J Biol Chem* 1998; 273:15077-84; PMID:9614117; <http://dx.doi.org/10.1074/jbc.273.24.15077>
- [64] Bellé R, Minella O, Cormier P, Morales J, Poulhe R, Mulner-Lorillon O. Phosphorylation of elongation factor-1 (EF-1) by cdc2 kinase [Internet]. In: Meijer L, Guidet S, Tung HYL, editors. *Progress in Cell Cycle Research*. Boston, MA: Springer US; 1995 [cited 2016 Aug 2]. 265-70. Available from: [http://link.springer.com/10.1007/978-1-4615-1809-9\\_21](http://link.springer.com/10.1007/978-1-4615-1809-9_21)
- [65] Schultz RM, LaMarca MJ, Wassarman PM. Absolute rates of protein synthesis during meiotic maturation of mammalian oocytes in vitro. *Proc Natl Acad Sci* 1978; 75:4160-4; PMID:279905; <http://dx.doi.org/10.1073/pnas.75.9.4160>
- [66] King DW, Barnhisel ML. Synthesis of RNA in mammalian cells during mitosis and interphase. *J Cell Biol* 1967; 33:265-72; PMID:6039370; <http://dx.doi.org/10.1083/jcb.33.2.265>
- [67] Pyronnet S, Pradayrol L, Sonenberg N. A cell cycle-dependent internal ribosome entry site. *Mol Cell* 2000; 5:607-16; PMID:10882097; [http://dx.doi.org/10.1016/S1097-2765\(00\)80240-3](http://dx.doi.org/10.1016/S1097-2765(00)80240-3)
- [68] Vander Haar E, Lee S-I, Bandhakavi S, Griffin TJ, Kim D-H. Insulin signalling to mTOR mediated by the Akt/PKB substrate PRAS40. *Nat Cell Biol* 2007; 9:316-23; PMID:17277771; <http://dx.doi.org/10.1038/ncb1547>
- [69] Wang Q, Ratchford AM, Chi MM-Y, Schoeller E, Frolova A, Schedl T, Moley KH. Maternal diabetes causes mitochondrial dysfunction and meiotic defects in murine oocytes. *Mol Endocrinol* 2009; 23:1603-12; PMID:19574447; <http://dx.doi.org/10.1210/me.2009-0033>
- [70] Chen J, Chen S, Chen Y, Zhang C, Wang J, Zhang W, Liu G, Zhao B, Chen Y. Circulating endothelial progenitor cells and cellular membrane microparticles in db/db diabetic mouse: possible implications in cerebral ischemic damage. *Am J Physiol Endocrinol Metab* 2011; 301:E62-71; PMID:21505143; <http://dx.doi.org/10.1152/ajpendo.00026.2011>
- [71] Bonatti S, Simili M, Galli A, Bagnato P, Pigullo S, Schiestl RH, Abbondandolo A. Inhibition of the Mr 70,000 S6 kinase pathway by rapamycin results in chromosome malsegregation in yeast and mammalian cells. *Chromosoma* 1998; 107:498-506; PMID:9914383; <http://dx.doi.org/10.1007/s004120050335>
- [72] Jang C-Y, Kim HD, Zhang X, Chang J-S, Kim J. Ribosomal protein S3 localizes on the mitotic spindle and functions as a microtubule associated protein in mitosis. *Biochem Biophys Res Commun* 2012; 429:57-62; PMID:23131551; <http://dx.doi.org/10.1016/j.bbrc.2012.10.093>
- [73] Susor A, Kubelka M. Translational regulation in the mammalian oocyte. In: *Oocytes - Maternal information and functions. Results and problems in cell differentiation*. Boston, MA: Springer US; 2017.
- [74] Tetkova A, Hancova M. Mouse Oocyte Isolation, Cultivation and RNA Microinjection —BIO-PROTOCOL; 6:e1729; <https://dx.doi.org/10.21769/BioProtoc.1729>
- [75] Safran M, Kim WY, O'Connell F, Flippin L, Günzler V, Horner JW, Depinho RA, Kaelin WG. Mouse model for noninvasive imaging of HIF prolyl hydroxylase activity: assessment of an oral agent that stimulates erythropoietin production. *Proc Natl Acad Sci U S A* 2006; 103:105-10; PMID:16373502; <http://dx.doi.org/10.1073/pnas.0509459103>



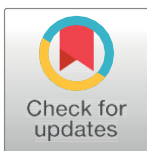
RESEARCH ARTICLE

# Localization of RNA and translation in the mammalian oocyte and embryo

Denisa Jansova<sup>1,2\*</sup>, Anna Tetkova<sup>1,2</sup>, Marketa Koncicka<sup>1,2</sup>, Michal Kubelka<sup>1</sup>, Andrej Susor<sup>1\*</sup>

**1** Institute of Animal Physiology and Genetics, CAS, Libechov, Czech Republic, **2** Department of Cell Biology, Faculty of Science, Charles University in Prague, Prague 2, Czech Republic

\* [jansova@iapg.cas.cz](mailto:jansova@iapg.cas.cz) (DJ); [susor@iapg.cas.cz](mailto:susor@iapg.cas.cz) (AS)



**OPEN ACCESS**

**Citation:** Jansova D, Tetkova A, Koncicka M, Kubelka M, Susor A (2018) Localization of RNA and translation in the mammalian oocyte and embryo. PLoS ONE 13(3): e0192544. <https://doi.org/10.1371/journal.pone.0192544>

**Editor:** Alexander F. Palazzo, University of Toronto, CANADA

**Received:** August 14, 2017

**Accepted:** January 25, 2018

**Published:** March 12, 2018

**Copyright:** © 2018 Jansova et al. This is an open access article distributed under the terms of the [Creative Commons Attribution License](https://creativecommons.org/licenses/by/4.0/), which permits unrestricted use, distribution, and reproduction in any medium, provided the original author and source are credited.

**Data Availability Statement:** All relevant data are within the paper and its Supporting Information files.

**Funding:** This work was supported by Charles University in Prague, Faculty of Cell Biology-GAUK 243-227026 to DJ, The Academy of Sciences of the Czech Republic, <http://www.cas.cz/>, GACR13-12291S to AS, GACR15-22765S to MK, EXCELLENCE CZ.02.1.01/0.0/0.0/15\_003/0000460 OPRDE and Institutional Research Concept RVO67985904.

## Abstract

The tight correlation between mRNA distribution and subsequent protein localization and function indicate a major role for mRNA localization within the cell. RNA localization, followed by local translation, presents a mechanism for spatial and temporal gene expression regulation utilized by various cell types. However, little is known about mRNA localization and translation in the mammalian oocyte and early embryo. Importantly, fully-grown oocyte becomes transcriptionally inactive and only utilizes transcripts previously synthesized and stored during earlier development. We discovered an abundant RNA population in the oocyte and early embryo nucleus together with RNA binding proteins. We also characterized specific ribosomal proteins, which contribute to translation in the oocyte and embryo. By applying selected markers to mouse and human oocytes, we found that there might be a similar mechanism of RNA metabolism in both species. In conclusion, we visualized the localization of RNAs and translation machinery in the oocyte, that could shed light on this *terra incognita* of these unique cell types in mouse and human.

## Introduction

Meiotic maturation of mammalian oocytes and oocyte-to-zygote transition proceed without transcription and depend entirely on the post-transcriptional regulation of maternal mRNAs. The overall translation gradually decreases during oocyte meiotic maturation [1], but the activators of cap-dependent translation become more active during this period, implying a role for translation of specific mRNAs in the regulation of meiosis [2,3]. These mRNAs need to be recruited to translational machinery and subsequently degraded in a tightly controlled temporal manner [4]. Spatial segregation of protein synthesis in cells involves the positioning of mRNAs according to where their protein products are required, and results in local or compartmentalized gene expression. mRNA localization can occur during different stages of development. While these processes were studied in other cell types [5–7], little is known about mRNA localization and translation in the mammalian oocyte or early embryo.

Our previous study indicated that the oocyte nucleus contains an RNA population in the fully grown oocyte that most likely contributes to translation in the vicinity of chromosomes after nuclear envelope break down (NEBD) [8,9]. Localization of mRNAs at the spindle is

**Competing interests:** The authors have declared that no competing interests exist.

evolutionarily conserved in mammals and has also been seen in mitotic cells [10,11]. The differences in enrichment of 384 mRNAs between the meiotic spindle area and cortical regions have been analyzed by microarrays [12]. Investigations of mRNA localization have been conducted in the oocytes of *Drosophila* [13,14], *Xenopus* [15,16] and mouse [4]. The localization of mRNA molecules within the cytoplasm provides a basis for cell polarization, underlying developmental processes such as asymmetric cell division during meiosis, and embryonic patterning [17].

Endogenous mRNAs do not exist alone; they bind to a number of proteins to form mRNA-protein complexes [18]. RNA-binding proteins (RBPs) and molecular motors mediate the transport of mRNAs along the cytoskeleton of cells, resulting in an asymmetric distribution of RNAs. RBPs are capable of regulating mRNA stability and translation. Some RBPs, such as CPE-binding protein (CPEB), Deleted in azoospermia-like (DAZL), post-transcriptionally regulate mRNA by binding to its 7-methylguanosine cap structure at the 5'-untranslated end (5'UTR) or to 3'-+ regions (3'UTRs). Regulation of the initiation of cap dependent translation is controlled via the translational repressor 4E-binding protein 1 (4E-BP1). Hierarchical phosphorylation of 4E-BP1 leads to its dissociation from eIF4E. In a previous study [19], we detected enriched localization of 4E-BP1 in the nucleus of fully grown oocytes. Another common mechanism regulating the recruitment and stability of dormant maternal mRNAs is reversible polyadenylation, which is controlled by cytoplasmic polyadenylation elements (CPEs) [20]. CPEs are specific sequences in 3'UTRs of dormant maternal mRNAs that serve as a binding platform for the CPE-binding proteins (CPEBs), which control polyadenylation-induced translation. The CPEBs family has four members. The most studied is CPE-binding protein 1 (CPEB1), which functions as a translational activator or repressor according to its phosphorylation state [21]. Other RBPs that regulate RNA processing are known as heterogeneous nuclear ribonucleoproteins (hnRNPs) [22]. This family contains more than 20 members. The key characteristic of the hnRNPs is their nucleocytoplasmic shuttling [23]. The hnRNP proteins A0, A1, A2/B1 and A3 were considered to be the prime constituents of 40S heterogeneous nuclear ribonucleoprotein particles, which bind to and stabilize nascent pre-mRNA [24,25]. The exon junction complex consists of RNA binding proteins and contains Eukaryotic initiation factor 4A-III (eIF4A3), a DEAD-box RNA helicase—a member of the eIF4A family of translation initiation factors [26]. Exon junction complex proteins play important roles in post-splicing events—including mRNA export, cytoplasmic localization, and non-sense-mediated decay [26,27,28]. The presence of assembled ribosomes is directly linked to protein synthesis during crucial periods of development and is tightly associated with the developmental competence of oocytes. It has been proposed that the mRNAs for 27 ribosomal proteins are expressed at higher levels in developmentally competent oocytes compared to non-competent ones [29].

A remarkable feature of mammalian oocyte maturation is the significant elimination of rRNA and ribosomes [30]. Moreover, genome-wide transcriptome analysis has shown that mRNAs coding for ribosomal proteins are degraded during oocyte maturation and after fertilization [31,32]. The eukaryotic ribosome contains 4 RNAs and ~80 ribosomal proteins (RPs), forming its two subunits: small 40S and large 60S. RPL24 is positioned between the two subunits with an N-terminal domain in 60S [33], while its C-terminal part interacts with RPS6 [34]. Mitogens and growth factors are responsible for RPS6 phosphorylation on five residues [35,36]. It was shown that RPS6 phosphorylation has an important function in the translational control of the subclass of mRNAs that harbor the 5' tract oligopyrimidine (5' TOP) sequence and this level of regulation may imbue the ribosome with greater specificity [37]. Similar to RPS6, RPS14 also plays a role in the regulation of the MDM2-p53 pathway [38,39].

In this study we focus on the visualization of transcriptome in association with the regulation of translation and visualization of translation in the mammalian oocyte and early embryo. Extensive analyses of the transcriptionally inactive germinal vesicle (GV) oocytes and the 2-cell embryos during transcriptional reprogramming show substantial measurements of both similarities and differences between the two cell types, as well as between mouse and human. Here, we also present the distribution and expression of specific components of translational machinery in the mammalian oocyte and early embryo.

## Methods

### Oocyte isolation and cultivation

Mouse ovaries were obtained from CD1 mice which were at least 6 weeks old and had been stimulated to superovulate by intraperitoneal injection of 5 UI pregnant mare serum gonadotropin (PMSG; Folligon, Merck Animal Health) 46 h prior to collection. Growing and fully grown GV oocytes were isolated subsequently into M2 medium (Millipore) supplemented with 100  $\mu$ M of 3-isobutyl-1-methylxanthine (IBMX, Sigma Aldrich) to prevent resumption of meiosis. Selected oocytes were stripped of cumulus cells and cultured in M16 medium (Millipore) without IBMX at 37°C, 5% CO<sub>2</sub>. Zygotes were obtained by mating females with males after injections of 5 UI PMSG and then (after 46 h) 5 UI of human chorionic gonadotropin (hCG; Merck Animal Health). Zygotes were isolated 17 h after mating and cultured *in vitro* in M16 under mineral oil for 20 h, then 2-cell embryos were collected. All animal work was conducted according to Act No 246/1992 on the protection of animals against cruelty. Human oocytes, not used in human reproduction, were obtained from the Obstetrics and Gynecology Clinic of the General University Hospital in Prague. The project was accredited (#30/12) by the Ethical Committee of the General Hospital, Prague.

### Immunocytochemistry

Oocytes were fixed 15 min in 4% paraformaldehyde (PFA, Sigma Aldrich) in PBS and permeabilized 10 min in 0.1% Triton X-100 in PBS with one drop of ActinGreen probe Phalloidin488 (Thermo Fisher). Then the oocytes were incubated overnight at 4°C with primary antibodies diluted in PBS/0.2% normal bovine serum. The following antibodies were used in 1:150 dilution: rabbit anti-4E-BP1 (CST); rabbit anti-Ribosomal S14 (Santa Cruz); rabbit anti-Ribosomal S3 (CST); rabbit anti-RPL24 (Thermo Fisher); mouse anti-RPS6 (Santa Cruz); rabbit anti-CPEB4 (Thermo Fisher); mouse anti-hnRNPA1 (Sigma Aldrich); mouse anti-eIF4A3 (Abcam), rabbit anti-RPL7 (Abcam); mouse anti-m3G cap/m7G cap (Thermo Fisher). Mouse anti-5.8S rRNA antibody (Abcam), was also diluted 1:150 and incubated at room temperature for 2 h. After washing in PBS for 2x15 min, detection of the primary antibodies was performed by cultivation of the oocytes with relevant Alexa Fluor 488/594 conjugates (diluted 1:250) for 1 h at room temperature. Oocytes were then washed 2x15 min in PBS and mounted using Vectashield Mounting Medium with DAPI (Vector Laboratories). For nascent protein synthesis oocytes and embryos were incubated 1 h with 1  $\mu$ gml<sup>-1</sup> puromycin (Sigma Aldrich) or 1  $\mu$ M cycloheximide, specific stage (GV, 2-cell embryo). For measuring nascent translation oocytes were cultured in methionine-free medium (Gibco) supplemented with 1% dialyzed fetal bovine serum (10,000MW; Sigma) and 50 mM HPG for 30 min. HPG was detected by using Click-iT Cell Reaction Kit (Life Technologies) according manufacture instruction. Samples were visualized using Leica SP5 inverted confocal microscope in 16 bit depth. Images were assembled in Photoshop CS3 and quantified by Image J software (<http://rsbweb.nih.gov/ij/>). Experiments were performed three times with 25 oocytes/embryos per experiment.

## Preparation of slides for imaging

Nunc Lab-Tek II Chamber Slide System (Thermo Fisher) glass coverslips were coated at 37°C for 2 h with poly-L-ornithine (Sigma Aldrich) diluted in RNase-free water 1:250 and then overnight with laminin (Sigma Aldrich) diluted in PBS 1:1000 also at 37°C.

## RNA fluorescent in situ hybridization (FISH)

RNA FISH was performed with small changes according to [40]. Oocytes were fixed for 10 min in 4% paraformaldehyde and permeabilized in 0.1% Triton X-100 in PBS with 40 units/20 µl of RNaseOut (Invitrogen), then mounted to pre-coated Lab-Tek II Chamber Slide System slides using 80% methanol pre-frozen to -20°C. Oocytes were washed in Wash Buffer A (Biosearch Technologies) and incubated overnight at 30°C in hybridization buffer (Biosearch Technologies) with 75 nM oligo-d(T) probe (Biotech Generi); *Neat2* CalFluorRed610 (Biosearch Technologies); *Dazl* (Biosearch Technologies) and  $\beta$ -*actin* labelled with Cy5 (Biotech Generi); GFP CalFluorRed635 (Biosearch Technologies) with 75 nM (protected from light). Oocytes were then washed 3x in Wash Buffer A and 2x in 2xSSC (Sigma Aldrich). For visualization of chromatin structure the oocytes were incubated 1 min with 10 nM DAPI (Sigma Aldrich) in 2xSSC; then washed 1x with 2xSSC and scanned in 2xSSC. For negative control RNase A (Ambion) was used for 2 h at 37°C after the permeabilization step. Forty-five oocytes and embryos was analyzed using ImageJ/FIJI (<http://rsbweb.nih.gov/ij/>) for quantification of fluorescence intensity in the cytoplasm and the nucleus.

## Rolling circle amplification (RCA) FISH

RCA FISH was performed according to [41] protocol with the following changes: oocytes were fixed 10 min in 4% PFA (Sigma Aldrich) and permeabilized in 0.1% Triton X-100 in PBS for 10 min and subsequently in 70% ethanol, pre-frozen to -20°C, for 10 seconds. The whole transcriptome was converted into cDNA by M-MuLV reverse transcriptase (Enzymatics) and the reaction mix was prepared according to the mentioned protocol. The cDNA fragments were fixed to the cellular protein matrix using a nonreversible amine cross-linker BS(PEG)9 (Sigma Aldrich) and circularized after degrading the RNA residues. The circular templates were amplified using RCA primers 100 µM (TCTTCAGCGTTCCCGA\*G\*A; where \* is phosphorothioate, Generi Biotech) complementary to the adapter sequence in the presence of aminoalanyl-dUTP and stably cross-linked. For visualization of endogenous cDNA we used fluorescently labeled random octamers, which were labeled by two fluorophore (green-488 nm) or (red-561 nm). Chromatin was visualized by incubation (1min) with 10 nM DAPI (Sigma Aldrich) in 2xSSC; then washed 1x with 2xSSC. We scanned the samples in 2xSSC. Quantification of fluorescent intensity between cytoplasm and nucleus was used ImageJ/FIJI (<http://rsbweb.nih.gov/ij/>). Per one experiment was used 12 oocyte and 10 embryos, we quantified 3 experiments.

## In situ proximity ligation assay (PLA)

Proximity ligation assay was performed according to manual instructions of PLA Duolink kit (Sigma Aldrich). Oocytes and embryos were incubated 1 h with 1 µgml<sup>-1</sup> puromycin (Sigma Aldrich) to decrease translation, then fixed 15 min in 4% paraformaldehyde in PBS and permeabilized 10 min in 0.1% Triton X-100 in PBS. We added PLA Duolink kit blocking solution to each sample. Oocytes were incubated with primary antibodies rabbit anti-RPL24 (Thermo Fisher) and mouse anti-RPS6 (Santa Cruz) at 4°C overnight. The samples were washed in PBS and then in Wash Buffer A (Sigma Aldrich). The samples were incubated with 40 µl reaction

mixture (8  $\mu$ l PLA probe MINUS stock, 8  $\mu$ l PLA probe PLUS stock and 24  $\mu$ l PBS) in a chamber for 1 h at 37°C. The slides were washed in 1x Wash Buffer A for 6x2 min and ligation was performed in 40  $\mu$ l reaction: 1  $\mu$ l of ligase to 39  $\mu$ l of ligation solution. Samples were incubated in ligation reaction mixture for 30 min at 37°C then washed 6x2 min in Wash Buffer A. 40  $\mu$ l of amplification reaction (0.5  $\mu$ l polymerase and 39.5  $\mu$ l amplification solution) was added to each sample before incubation at 37°C for 100 min. Next, the samples were washed in Wash Buffer B (Sigma Aldrich) for 3x5 min and in 0.01 Wash Buffer B for 2 min. The samples were mounted by Vectashield Mounting Medium with DAPI (Vector Laboratories). Quantification of interaction foci was performed using ImageJ/FIJI. We performed 5 experiments with 150 oocytes/embryos.

### Live cell imaging of nascent translation (ReAsH method)

The ReAsH method [42] was used to detect *in situ* translation. For the ReAsH we used plasmid #27123 (Adgene; [43]). The growing oocytes were injected according to the protocol by [44] with a plasmid diluted to ~40 ng/ $\mu$ l into nuclei. Oocytes were incubated overnight in 1  $\mu$ M cycloheximide (CHX; Sigma Aldrich) in M16 medium to prevent translation. After CHX wash oocytes were incubated for 30 min in M16 supplemented with ReAsH dye (final concentration 20  $\mu$ M, Thermo Fisher) and then transferred into 250  $\mu$ M 2,3-dimercaptopropanol (BAL buffer, Thermo Fisher) in M16 and immediately scanned on confocal microscope Leica TCS SP5. Thirty oocytes was quantified from three independent experiments.

### Western blot (WB)

Lysates of embryos and oocytes was analysed on 4–12% gradient acrylamide gel. Samples were transferred to polyvinylidene-fluoride membrane (Immobilon P; Merckmillipore) using blotting system (Biometra GmbH) at 5 mA/cm<sup>2</sup> during 25 minute. Membranes were blocked for 1 h, at room temperature and then they were incubated at 4°C overnight with the following primary antibodies: rabbit anti-4E-BP1 (CST); rabbit anti-Ribosomal S14 (Santa Cruz); rabbit anti-Ribosomal S3 (CST); rabbit anti-RPL24 (Thermo Fisher); mouse anti-RPS6 S235/236 (Santa Cruz); rabbit anti-CPEB4 (Thermo Fisher); mouse anti-hnRNPA1 (Sigma Aldrich); mouse anti-eIF4A3 (Abcam), rabbit anti-RPL7 (Abcam), with 1% milk/TTBS (Tween-Tris-buffer saline; NaCl, Tween 20, 2M; Tris pH 7,6; dH<sub>2</sub>O). After 3 cycles of 10 minute washing in 0,05% TTBS membrane was incubated at room temperature for 1 h in 3% milk with secondary antibody conjugated with peroxidase (Jackson Immunoresearch). Following washing step with 0,05% TTBS. Immunodetected proteins were visualized by ECL (Amersham, GE Healthcare Life Science) according instruction from supplier. Films were scanned using a GS-800 calibrated densitometer (Bio-Rad) and quantified 3 independent experiment for each protein for one experiment was used 100 oocytes/embryos, we normalized quantification to GAPDH, using ImageJ/FIJI (<http://rsbweb.nih.gov/ij/>).

### Statistical analysis

Mean and SD values were calculated using MS Excel, statistical significance of the differences between the groups was tested using Student's t-test (PrismaGraph5) and  $P < 0.05$  was considered as statistically significant (marked by asterisk) \* $p < 0.05$ ; \*\* $p < 0.01$ ; \*\*\* $p < 0.001$ .

## Results

### Detection of global transcriptome in the oocyte and embryo

mRNA localization generally leads to targeted translation [45]. We have asked how the transcriptome is distributed in the mammalian oocyte and 2-cell embryo. It is known that 70% of



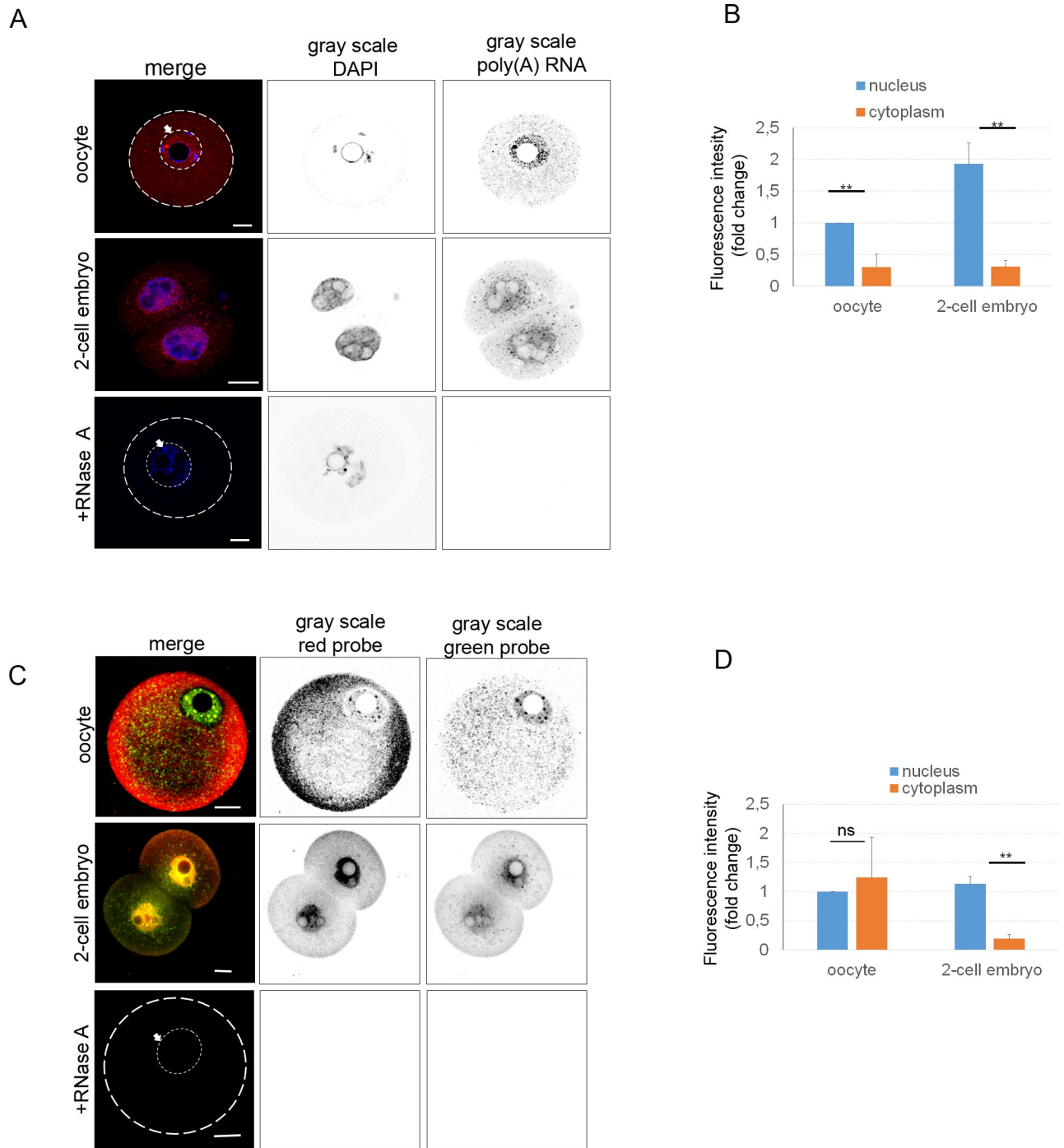


**Fig 1. Localization of transcriptome in oocyte and embryo.** A) Single Z-stack from confocal images of GV (germinal vesicle) oocyte stage and 2-cell embryo. RNA FISH detecting poly(A) RNA subpopulation (red; oligo(dT) probe), and the gray scale shows separated light channels (DAPI and oligo(dT) probe). The arrow with the white line indicates the nucleus of the oocyte. As a negative control RNA was digested by RNase A after the cell permeabilization step. Scale bars 20  $\mu$ m. The cortex of the oocyte is indicated by the white line. B) Quantification of fluorescence intensity of poly(A) RNA of equatorial Z-stack, in the nucleus and cytoplasm of oocyte and embryo, relatively compared to the nucleus of the oocyte. The experiment was repeated 3 times, with 15 oocytes and embryos per experiment. Data are represented as mean  $\pm$  s.d.; the values bars with *ns* are not significant, and the asterisk denotes statistically significant differences \* $p$ <0.05; \*\* $p$ <0.01; \*\*\* $p$ <0.001. C) Rolling circle amplification FISH using random hexamers probes showing distribution of global RNA. The arrow with the white line indicates the nucleus of the oocyte. The gray scale shows separated channels (red and green probe). The cortex of the oocyte is indicated by the white line. As a negative control RNA was digested by RNase A after cell permeabilization step. Scale bars 20  $\mu$ m. D) Quantification of fluorescence intensity of whole transcriptome in the nucleus and cytoplasm. The value of the nucleus was set as 1. The experiment was repeated 3 times, with 12 oocytes and 10 embryos per experiment. Data are represented as mean  $\pm$  s.d.; the values bars with *ns* are not significant, and the asterisk denotes statistically significant differences \* $p$ <0.05; \*\* $p$ <0.01; \*\*\* $p$ <0.001.

<https://doi.org/10.1371/journal.pone.0192544.g001>

RNAs are polyadenylated [46]. To detect this subpopulation, i.e. to detect RNA localization in the oocyte and 2-cell embryo, fluorescently (CY5) labeled oligo(dT) probes were used (Fig 1A). Treatment by RNase A eliminated the fluorescence signal, thus confirming its RNA origin in the rest of the experiments (Fig 1A). PolyA RNA was detected in the cytoplasm with a significant decrease (0.7-fold) compared to the nucleus of the oocyte. The nucleus of the 2-cell embryo shows higher (2-fold) presence of polyA RNA in the comparison with the oocyte. However, cytoplasmic signal intensity of poly(A) RNA is similar in both cell types (Fig 1B).

Rolling circle amplification (RCA) [41,47] was used to visualize the whole cellular transcriptome, the method comprising reverse *in situ* transcription followed by hybridization of fluorescently labeled random octamers, which were labeled by fluorophore, green (488 nm) and red (561 nm). By RCA, we observed a similar localization of RNA as with RNA FISH (Fig 1A and 1C). The different color pattern might be the result of a different affinity of the labeled probes. Similarly, the degradation of RNA by RNase A treatment significantly decreased the fluorescence signal (Fig 1C). Fluorescence intensity of global transcriptome was at the same level in both compartments of the oocyte (Fig 1D). However, in the cytoplasm of the 2-cell embryo RNA intensity was significantly lower (about 0.8-fold; Fig 1D). In addition to the previous methods for visualization of the global transcriptome, we used an antibody detecting the 5' UTR cap both m7G-cap (present in most RNAs) and m3G-cap (present in small nuclear RNAs, snRNAs) structures [48]. We were able to detect these cap structures (Fig 2A) with similar RNA distribution in both oocytes and 2-cell embryos, again comparable to RNA FISH and RCA methods (Fig 2A). Similar to RNA FISH and RCA results, we observed significantly higher fluorescence intensity of the m3G/m7G-cap in the nuclei of the oocytes and embryos (about 0.7-fold; Fig 2B).

Using RNA FISH, RCA and an antibody against RNA cap structure produced results showing a high uniformity concerning the localization of global transcriptome. We found the nuclei significantly enriched with RNA in both cell types.

In addition, using immunocytochemistry (ICC) with antibody against 5.8S ribosomal RNA, which is a structural component of 40S subunit of ribosome [49,50], we found a strong fluorescence signal in the cytoplasm of the oocyte and the embryo, with a decrease in the nucleoplasm of both stages (Fig 2C). Treatment with RNase A led to the loss of fluorescent signal. Quantification of 5.8S rRNA signal showed similar intensities in both cellular compartments in the oocyte/embryo. We observed a significant decrease of global 5.8S ribosomal RNA (about 0.8-fold) in the 2-cell embryo compared to the oocyte (Fig 2D).

Using direct detection of whole transcriptome by RCA, RNA FISH and ICC, we detected the localization of various RNA types and ribosomal rRNA in the mammalian oocyte and early embryo.

## Identification of specific RNAs in the oocyte and embryo

Pinpointing the subcellular localization of specific RNA species might lead to the unveiling of their potential molecular role in such large cells. Single molecule RNA FISH (smRNA FISH) was used to visualize specific RNAs. First, we determined the localization of Deleted in azoospermia-like RNA (*Dazl*)—a germ cell specific transcript. smRNA FISH showed an even distribution of the mRNA in the cytoplasm and a weak signal in the nucleoplasm of both, the oocyte and the early embryo (Fig 3A and 3D) with increased levels in the cytoplasm of the 2-cell embryo (Fig 3A and 3D), suggesting early transcription of *Dazl* mRNA in the embryo. Cumulus cells (depicted by asterisk, Fig 3A) and mouse fibroblasts NIH3T3 (Fig 3A) were negative and RNase A treatment of the oocyte and embryo resulted in the absence of a fluorescent signal (S1B Fig), supporting the specificity of *Dazl* mRNA detection in the oocyte and early

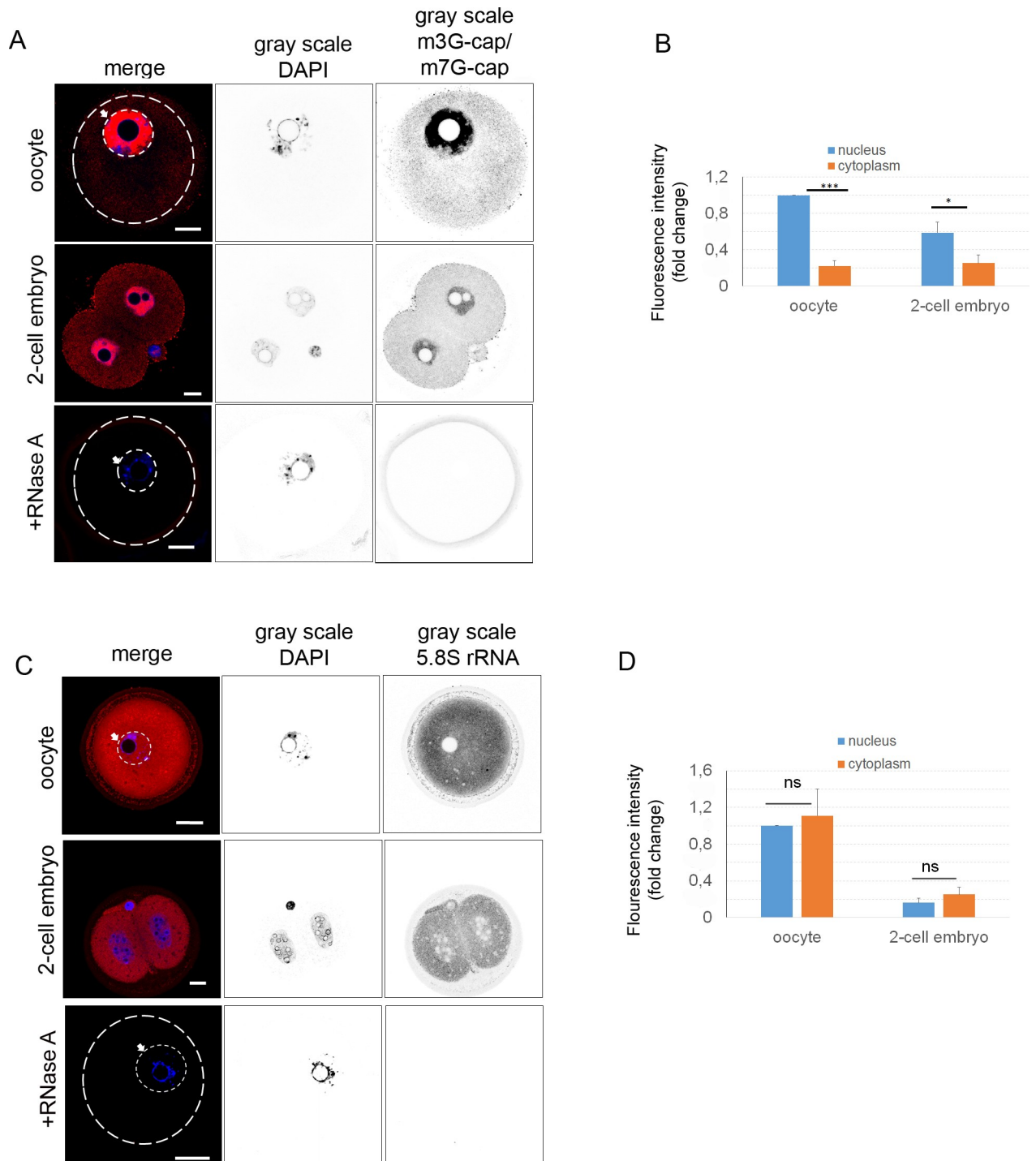


**Fig 2. Localization of rRNA and RNA in oocyte and embryo.** A) Antibody detecting m3G-cap and m7G-cap indicates cap-structure at the 5'UTR of mRNA (red). DNA stained with DAPI (blue). The gray scale shows separated light channels. The arrow with the white line indicates the nucleus of the oocyte. As a negative control RNA was digested by RNase A after the cell permeabilization step. The cortex of the oocyte is indicated by the white line. Scale bars 20  $\mu$ m. The experiments were repeated 3 times, with 25 oocytes/embryos per experiment. B) Quantification of fluorescence intensity of 5'UTR cap-structure of equatorial Z-stacks, in the nucleus and cytoplasm of oocyte and embryo, relatively compared to nucleus of oocyte. The experiment was repeated 3 times, with 25 oocytes/embryos per experiment. Data are represented as mean  $\pm$  s.d.; the value bars with *ns* are not significant, and the asterisk denotes statistically significant differences \*  $p < 0.05$ ; \*\*  $p < 0.01$ ; \*\*\*  $p < 0.001$ . C) Distribution of 5.8S rRNA in the oocyte and early embryo (red). DNA stained with DAPI (blue). The gray scale shows separated light channels. The arrow with the white line indicates the nucleus of the oocyte. As a negative control RNase A digestion was used after the cell permeabilization step. The white line indicates the oocyte cortex. The experiment was repeated 3 times, with 25 oocytes/embryos per experiment. D) Quantification of fluorescence intensity of 5.8S rRNA in



the nucleus and cytoplasm from equatorial Z-stacks. The value of the oocyte nucleus was set as 1; other values are represented as a ratio to the intensity of the oocyte nucleus. The experiment was repeated 3 times, with 25 oocytes/embryos per experiment. Data are represented as mean  $\pm$  s.d.; the value bars with *ns* are not significant, and the asterisk denotes statistically significant differences \*  $p < 0.05$ ; \*\*  $p < 0.01$ ; \*\*\*  $p < 0.001$ .

<https://doi.org/10.1371/journal.pone.0192544.g002>

embryo. Another detected mRNA was  $\beta$ -*actin*, which was present in both subcellular compartments, nucleus and cytoplasm of the oocyte, and as dot-like structures in the cytoplasm of the early embryo (Fig 3B and 3E). The localization in the NIH3T3 was mostly at the leading edges (Fig 3B). Next, we also detected long noncoding RNA *Neat2/Malat1* (Nuclear-Enriched Abundant Transcript 2/Metastasis Associated Lung Adenocarcinoma Transcript 1) which is known to be localized in the nuclear speckles of HeLa cells [51]. *Neat2/Malat1* was exclusively localized in the nucleus of the GV oocyte and NIH3T3 cells. However, localized in the cytoplasm of the embryo (Fig 3C and 3E). RNase A treatment eliminated the fluorescent signal (S1B Fig) which corroborates the specificity of our RNA detection. The quantification of the intensity of the specific RNA signal shows that *Dazl* mRNA is distributed in both compartments, i.e. the nucleus and cytoplasm, of the oocyte (Fig 3D). However, in the embryo, this mRNA is elevated and localized predominantly in the cytoplasm (1.3-fold; Fig 3D).  $\beta$ -*actin* mRNA shows equal localization in the nucleus and embryo in both cell types (Fig 3E). *Neat2* lncRNA shows significant presence in the nucleus (about 0.85-fold) of the oocyte. In contrast, in the embryo, the fluorescence intensity was significantly higher (about 0.7-fold) in the cytoplasm (Fig 3E).

By detection of specific RNAs, we determined the localization of specific mRNAs and lncRNA in the oocytes, 2-cell embryos and mouse embryonic fibroblasts.

### Expression and localization of RNA binding proteins in the oocyte and 2-cell embryo

RBPs are essential for RNA metabolism and localization [52–54], and so we accordingly examined the localization of a number of these proteins in the oocytes and early embryos. First, we studied the ubiquitously binding RBPs, heterogeneous nuclear ribonucleoproteins (hnRNP), which participate in pre-mRNA processing and are important determinants of mRNA export localization, translation, and stability [55]. Heterogeneous nuclear ribonucleoprotein A1 (hnRNPA1) was localized mostly in the nucleus of the oocyte (Fig 4A). However, in the embryo, the protein was present throughout the whole volume of the cell (Fig 4A). Next, we analyzed the distribution of the exon junction complex protein eIF4A3, which is deposited onto mRNA during splicing and is released during the first round of translation [26,56]. ICC showed a high abundance of eIF4A3 in the nuclei of both cell types, with a weak presence in the cytoplasm (Fig 4B). Another protein, 5'UTR cap-binding protein 4E-BP1, functions as a repressor of cap dependent translation [19,57,58]. In our experiments, 4E-BP1 showed a granular structure in the cytoplasm with a significant increase of signal in the nucleoplasm (Fig 4C and S2 Fig). RNase A treatment disrupted the granular pattern in the oocyte (S2 Fig). CPEB4 is responsible for meiotic progression between MI and MII and for the regulation of cytostatic factors in the frog oocyte [59]. CPEB4 analysis showed a granular distribution in the whole volume of the cells (Fig 4D). Next, WB was used to validate the antibodies (Fig 4E and 4F and S3 Fig). Expression levels of the hnRNPA1, eIF4A3, 4E-BP1 and CPEB4 showed no significant decrease in the early embryo (Fig 4F). The GAPDH protein was used as a loading control for WB.

### Localization of translational machinery

To characterize the localization and expression of ribosomal proteins in the GV oocyte and 2-cell embryo, we selected several components of the 40S ribosomal subunit–ribosomal

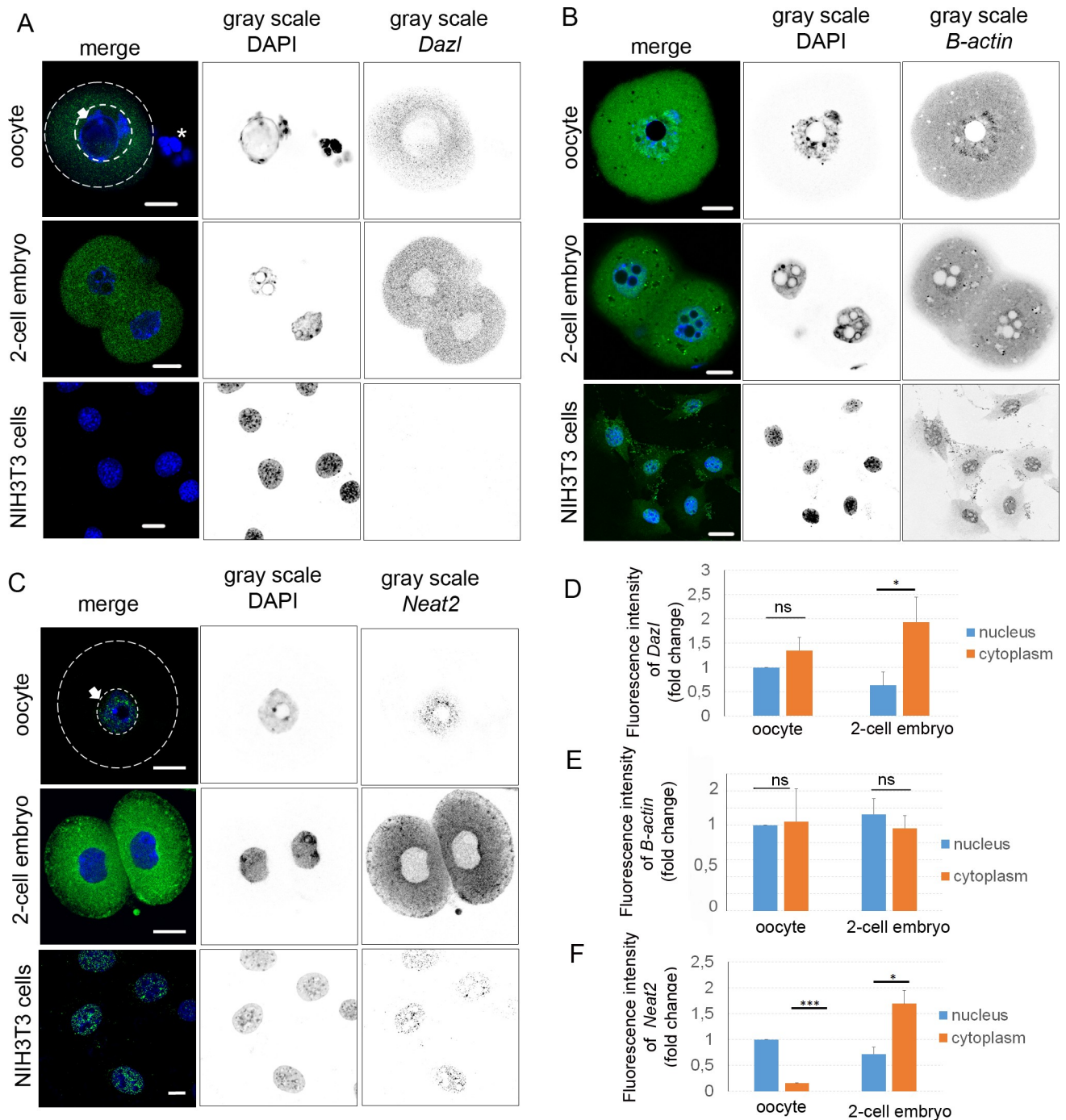


**Fig 3. Localization of specific RNAs in GV oocyte, 2-cell embryo and NIH3T3 cells.** A) Confocal images of smRNA FISH of *Dazl* (green) in GV oocyte, 2-cell embryo and NIH3T3 cells. DNA stained with DAPI (blue). The gray scale shows separated channels. The arrow with the white line indicates the nucleus of the oocyte. The asterisk indicates cumulus cells. The white line indicates the cortex of the oocyte. Scale bars 20  $\mu$ m. The experiment was repeated 3 times, with 15 oocytes/embryos per experiment. B) Confocal images of smRNA FISH of  $\beta$ -actin (green) in GV oocyte, 2-cell embryo and NIH3T3 cells (DNA stained with DAPI (blue)). The gray scale shows separated light channels. Scale bars 20  $\mu$ m. The experiment was repeated 3 times, with 15 oocytes and embryos per experiment. C) Confocal images of smRNA FISH of *Neat2* lncRNA (green) in GV oocyte, 2-cell embryo and NIH3T3 cells. DNA stained with DAPI (blue). The gray scale shows separated channels. The arrow with the white line indicates the nucleus of the oocyte. The white line indicates the cortex of the oocyte. Scale bars 20  $\mu$ m. The experiment was repeated 3 times, with 15 oocytes/embryos per experiment. D) Quantification of fluorescence intensity of *Dazl* mRNA in the nucleus and cytoplasm from equatorial Z-stacks. The value of the oocyte nucleus was set as 1. The experiment was repeated 3 times, with 15 oocytes/embryos per experiment. Data are represented as mean  $\pm$  s.d.; the values bars with ns are not significant, and the asterisk denotes statistically significant differences \*  $p < 0.05$ ; \*\*  $p < 0.01$ ; \*\*\*  $p < 0.001$ . E) Quantification of fluorescence intensity of  $\beta$ -

*actin* mRNA in the nucleus and cytoplasm from equatorial Z-stacks. Value of oocyte nucleus was set as 1. The experiment was repeated 3 times, with 15 oocytes and embryos per experiment. Data are represented as mean  $\pm$  s.d.; the value bars with *ns* are not significant, asterisk denotes statistically significant differences \*  $p < 0.05$ ; \*\*  $p < 0.01$ ; \*\*\*  $p < 0.001$ . F) Quantification of fluorescence intensity of *Neat2* lncRNA in the nucleus and cytoplasm from equatorial Z-stacks. The value of the oocyte nucleus was set as 1. The experiment was repeated 3 times, with 15 oocytes and embryos per experiment. Data are represented as mean  $\pm$  s.d.; the value bars with *ns* are not significant, and the asterisk denotes statistically significant differences \*  $p < 0.05$ ; \*\*  $p < 0.01$ ; \*\*\*  $p < 0.001$ .

<https://doi.org/10.1371/journal.pone.0192544.g003>

proteins S14 (RPS14) and S3 (RPS3) and RPS6 phosphorylated on S235/236 –as well as of the 60S subunit, ribosomal protein L7 (RPL7) and L24 (RPL24). These subunits combine to form the eukaryotic (80S) ribosome [33], a large molecular machine that catalyzes the synthesis of proteins. ICC analysis showed that RPS14 was localized at the cortex of the oocyte and embryo and in the nucleoplasm of the oocyte (Fig 5A). However, in the 2-cell embryo we found a significant decrease of fluorescence in the nucleoplasm and cytoplasm, which was also confirmed by WB analysis (Fig 5A, 5F and 5G). The RPS3 protein was localized evenly in both compartments—nucleus and cytoplasm in the oocyte and the embryo (Fig 5B). The protein level of RPS3 was stable in the oocyte and 2-cell embryo (Fig 5F and 5G). It is known that phosphorylation of RPS6 on S235/236 increases its affinity to the cap structure of RNA, which strongly implies that RPS6 phosphorylation enhances mRNA translation initiation [60]. RPS6 protein phosphorylated on S235/236 was distributed throughout the whole cytoplasm with a decreased signal in the nucleoplasm in both the oocyte and the embryo (Fig 5C). RPS6(S235/236) significantly decreased its presence in the 2-cell embryo (Fig 5C, 5F and 5G). Protein RPL7 was distributed in the cytoplasm of the oocyte and embryo and with higher intensity in the nucleus of the oocyte (Fig 5D) compared to the embryo. Protein levels of RPL7 were stable in the oocyte and 2-cell embryo (Fig 5F and 5G). RPL24 showed more abundant distribution in the cytoplasm than in the nucleus in both cell types (Fig 5E). The quantification of the expression of ribosome components by WB in the oocyte and the embryo showed a significant decrease only for RPS14 (0.67-fold) and RPS6 phosphorylated on S235/236 (0.85-fold) in the 2-cell embryos (Fig 5F and 5G). Other components of ribosome, RPS3, RPL7 and RPL24 showed no significant decrease in the embryo (Fig 5F and 5G). The GAPDH protein was used as a loading control.

We showed different localization and expression of components of 40S and 60S subunits in the mouse oocyte and early embryo.

### Nascent translation in oocyte and 2-cell embryo

In order to detect ongoing protein synthesis, we used the Duolink *in situ* proximity ligation assay (PLA) [61,62] with RPL24 and RPS6 specific antibodies to detect assembled 80S ribosomes in the oocyte and embryo. The positive interaction of the RPL24 and RPS6 ribosomal proteins suggests completion of 80S ribosome and ongoing translation. Through PLA, we detected significant interactions of these two proteins in the cytoplasm of the oocyte and 2-cell embryo (Fig 6A). The quantification of the RPL24 and RPS6 interaction foci showed a similar number of RPL24 and RPS6 interactions in the oocyte and the embryo (Fig 6B). The distribution of interactions was even, with increased intensity at the cortex of blastomeres. The cultivation of oocytes or embryos in the presence of translational inhibitor puromycin (which disrupts translating ribosomes) showed a significant decrease (0.7-fold) in the number of interactions in both cell types (Fig 6A and 6B). Moreover, using RPS6 antibody alone as a negative control of PLA showed 0.98-fold significant decrease (Fig 6A and 6B). In order to detect nascent translation *in situ*, the methionine analog L-homopropargylglycine (HPG) was incorporated into the translated proteins during a short 30-minute cultivation period followed by the Click-IT protocol to fluorescently label HPG in the cell [63]. The fluorescent signals of HPG

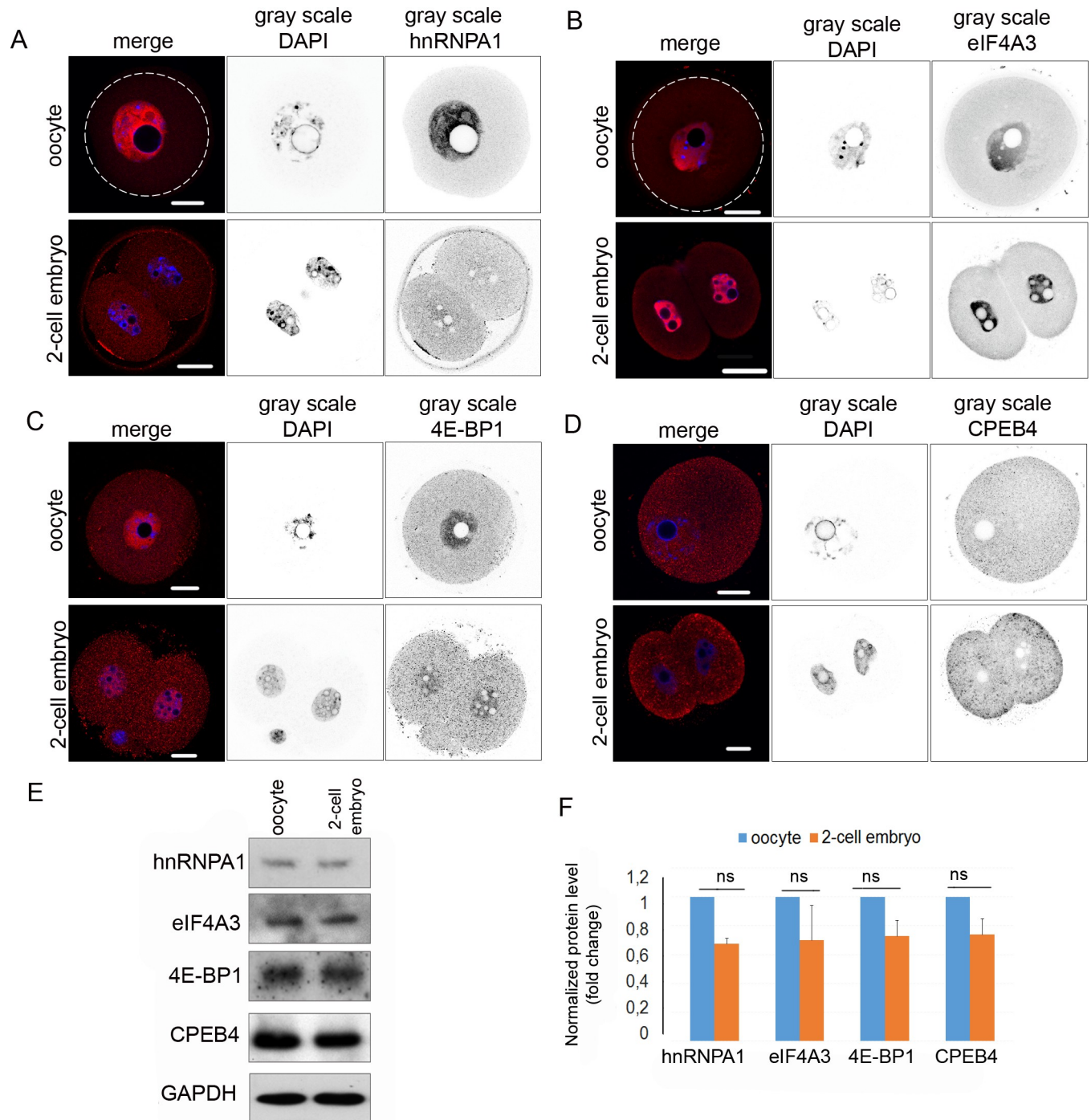


**Fig 4. Localization and expression levels of RNA binding proteins in GV oocyte and 2-cell embryo.** A) Representative confocal images of GV oocyte and 2-cell stage embryo stained with hnRNPA1 antibody (red), DNA stained with DAPI (blue); the gray scale images show separated light channels. The white line indicates the cortex of the oocyte. Scale bars 20  $\mu$ m. The experiment was repeated 3 times, with 25 oocytes/embryos per experiment. B) Representative confocal image of GV oocyte and 2-cell embryo stained with eIF4A3 antibody (red), DNA stained with DAPI (blue); the gray scale images show separated light channels. The white line indicates the cortex of the oocyte. Scale bars 20  $\mu$ m. The experiment was repeated 3 times, with 25 oocytes/embryos per experiment. C) Representative confocal image of GV oocyte and 2-cell embryo stained with 4E-BP1 antibody (red), DNA stained with DAPI (blue); the gray scale images show separated light channels. White line indicate cortex of oocyte. Scale bars 20  $\mu$ m. The experiment was repeated 3 times, with 25 oocytes per experiment. D) Representative confocal image of GV oocytes and 2-cell embryo stained with CPEB4 antibody (red), DNA stained with DAPI (blue); the gray scale images show separated light channels. The white line indicates the cortex of the oocyte. Scale bars 20  $\mu$ m. The experiment was repeated 3 times, with 25 oocytes/embryos per experiment. E) Representative images from WB probed by antibodies for hnRNPA1, eIF4A3, 4E-BP1, and CPEB4 proteins in the GV oocytes and



2-cell stage embryos. GAPDH was used as a loading control. WBs were performed 3 times, with 100 cells per experiment. F) Quantification of hnRNPA1, eIF4A3, 4E-BP1 and CPEB4 expression in the oocytes and embryos. Data were normalized to GAPDH. The values of oocytes were set as 1. Data are represented as mean  $\pm$  s.d.; the value bars with *ns* are not significant, and the asterisk denotes statistically significant differences \*  $p < 0.05$ ; \*\*  $p < 0.01$ ; \*\*\*  $p < 0.001$ .

<https://doi.org/10.1371/journal.pone.0192544.g004>

were observed in the whole oocyte, with an increase in the perinuclear area (S4A Fig), while in the 2-cell embryo we detected strong signals at the dividing ridge of the blastomeres. As expected, the disruption of the ribosomes by puromycin decreased the intensity of the HPG signal in the oocyte by about 95%, and in the 2-cell embryo by about 80% (S4A and S4B Fig). In the presence of cycloheximide (CHX; protein elongation inhibitor) the intensity of the HPG signal in the oocyte and the embryo decreased to 15% and 13% respectively (S4A and S4B Fig).

The combination of PLA and HPG methods provided consistent visualization of the *in situ* translation in the oocyte and 2-cell embryo.

### Visualization of translation of endogenous $\beta$ -actin mRNA in live oocyte

The ReAsH method [42] was used to detect *in situ* translation of the specific transcript  $\beta$ -actin (Fig 7A). The plasmid coding the sequence of the  $\beta$ -actin ORF with tetracysteine (TC) and GFP domain [43] was injected into the nucleus of transcriptionally active oocytes in the presence of cycloheximide (CHX, protein synthesis inhibitor) (Fig 7B). Overnight cultivation of oocytes led to the transcription of the construct, which mimicked the endogenous  $\beta$ -actin mRNA. We found translation of  $\beta$ -actin in patches at the cortex of the oocyte, where ReAsH and GFP fluorescence were localized. GFP visualized mature protein on the cortex and ReAsH showed spots of *in situ* translation of  $\beta$ -actin (Fig 7C). A quantification of the images showed a sevenfold increase of the fluorescent intensity in ReAsH and GFP in the patches in the cortex (Fig 7D) compared with other areas of the cell or with negative control (non-injected oocytes). However, we detected a high presence of the ReAsH dye in the nucleus as well, where GFP was not detected (Fig 7C), which might suggest non-specific incorporation or an unknown process in the oocyte [64].

We were able to detect translation of the endogenous  $\beta$ -actin mRNA in the living oocyte, which resembled the known localization of filamentous actin [65,66], shown also in S5 Fig.

### Localization of global RNA and RBPs in the human oocyte

In order to study the similarity between mouse and human oocytes, a localization of the global transcriptome was determined through the visualization of the poly(A) RNA population. We found that the poly(A) RNA fluorescence signal was distributed evenly throughout the cytoplasm and nucleoplasm with the presence of the abundant poly(A) RNA foci in the cytoplasm and nucleus of the human oocyte (Fig 8A). Next, the ICC labeling of RBPs, 4E-BP1 (green) and eIF4A3 (red) was performed, uncovering a similar localization of these proteins in human oocytes to our previously reported findings in the mouse oocyte [19] (Fig 8B). 4E-BP1 was distributed in both, the cytoplasm and the nucleoplasm. Contrastingly, eIF4A3 was localized in the nucleoplasm only (Fig 8B). Through analyses of the poly(A) RNA population and RBPs, we found similar localization of the selected transcriptome markers in both mammalian species.

### Discussion

Post-transcriptional control of gene expression at the level of translation has been shown to be essential for the regulation of a number of cellular processes during development [19,67].

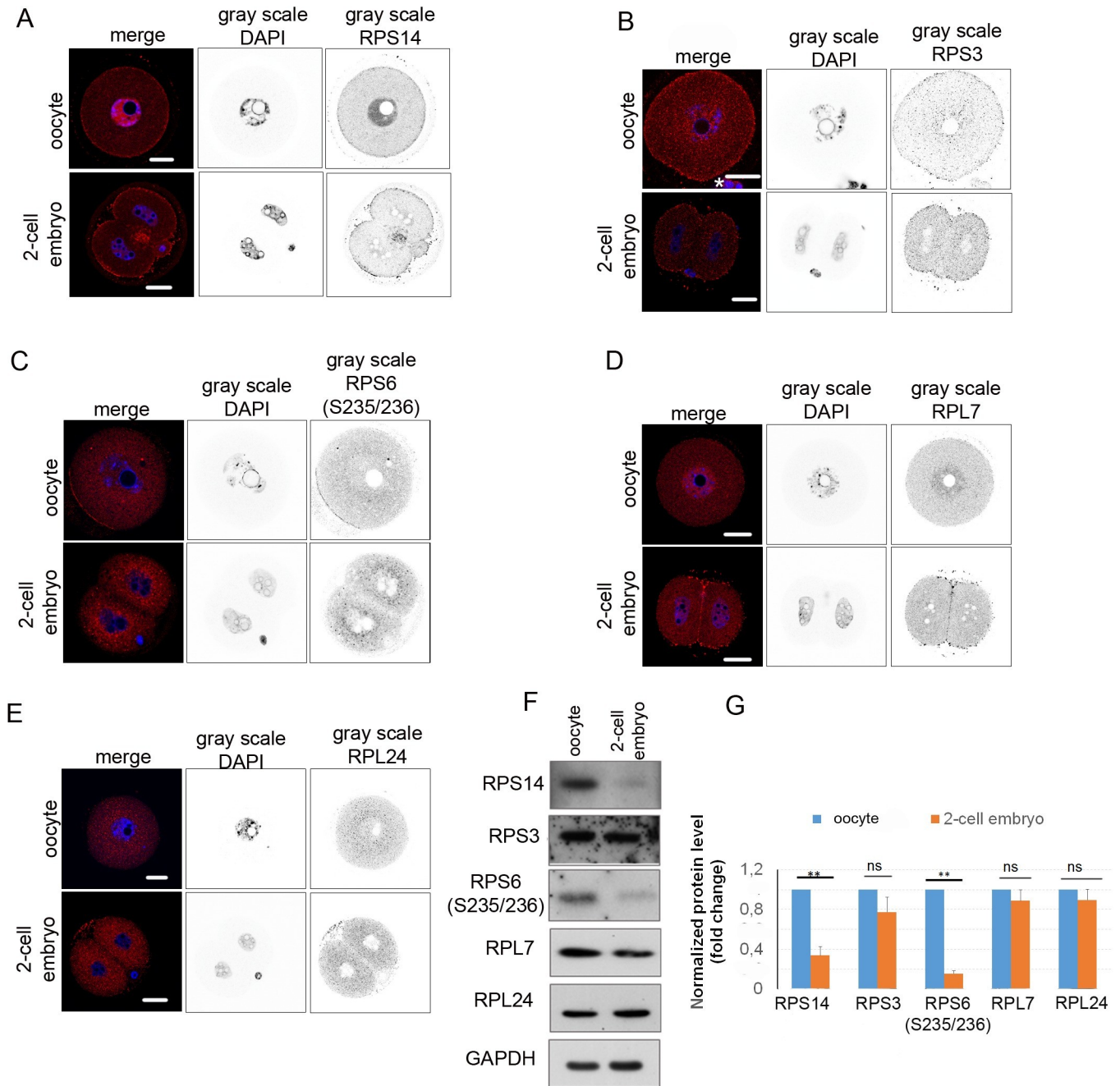


**Fig 5. Localization and expression levels of selected ribosomal proteins.** A) Confocal images of GV oocyte and 2-cell stage embryo probed with RPS14 antibody (red), DNA stained with DAPI (blue); the gray scale shows separated light channels. Scale bars 20  $\mu$ m. The experiment was repeated 3 times, with 25 oocytes/embryos per experiment. B) Confocal images of GV oocyte and 2-cell stage embryo probed with RPS3 antibody (red), DNA stained with DAPI (blue); the gray scale shows separated light channels. The asterisk indicates cumulus cells. Scale bars 20  $\mu$ m. The experiment was repeated 3 times, with 25 oocytes/embryos per experiment. C) Confocal images of GV oocyte and 2-cell stage embryo probed with RPS6(S235/236) antibody (red), DNA stained with DAPI (blue); the gray scale shows separated light channels. Scale bars 20  $\mu$ m. The experiment was repeated 3 times, with 25 oocytes/embryos per experiment. D) Confocal images of GV oocyte and 2-cell stage embryo probed with RPL7 antibody (red); DNA stained with DAPI (blue); the gray scale shows separated light channels. Scale bars 20  $\mu$ m. The experiment was repeated 3 times, with 25 oocytes/embryos per experiment. E) Confocal images of GV oocyte and 2-cell stage embryo probed with RPL24 antibody (red). DNA stained with DAPI (blue); the gray scale images shows separated light channels. Scale bars 20  $\mu$ m. The experiment was repeated 3 times, with 25 oocytes/embryos per experiment. F) Representative images from WBs for RPS14, RPS3, RPS6 (S235/236), RPL7, RPL24 protein expression in GV oocytes and 2-cell stage embryos, and the loading control (GAPDH); WB was repeated 3 times, with 100 oocytes/embryos per experiment. G) Quantification of expression of RPS14, RPS3, RPS6 (S235/236), RPL7 and RPL24 proteins in the oocyte and embryo. Data were normalized to GAPDH. Data are represented as the mean  $\pm$  s.d.; the values obtained from oocytes were set as 1. The value bars with *ns* are not significant, the asterisk denotes statistically significant differences \* $p$ <0.05; \*\* $p$ <0.01; \*\*\* $p$ <0.001.

<https://doi.org/10.1371/journal.pone.0192544.g005>

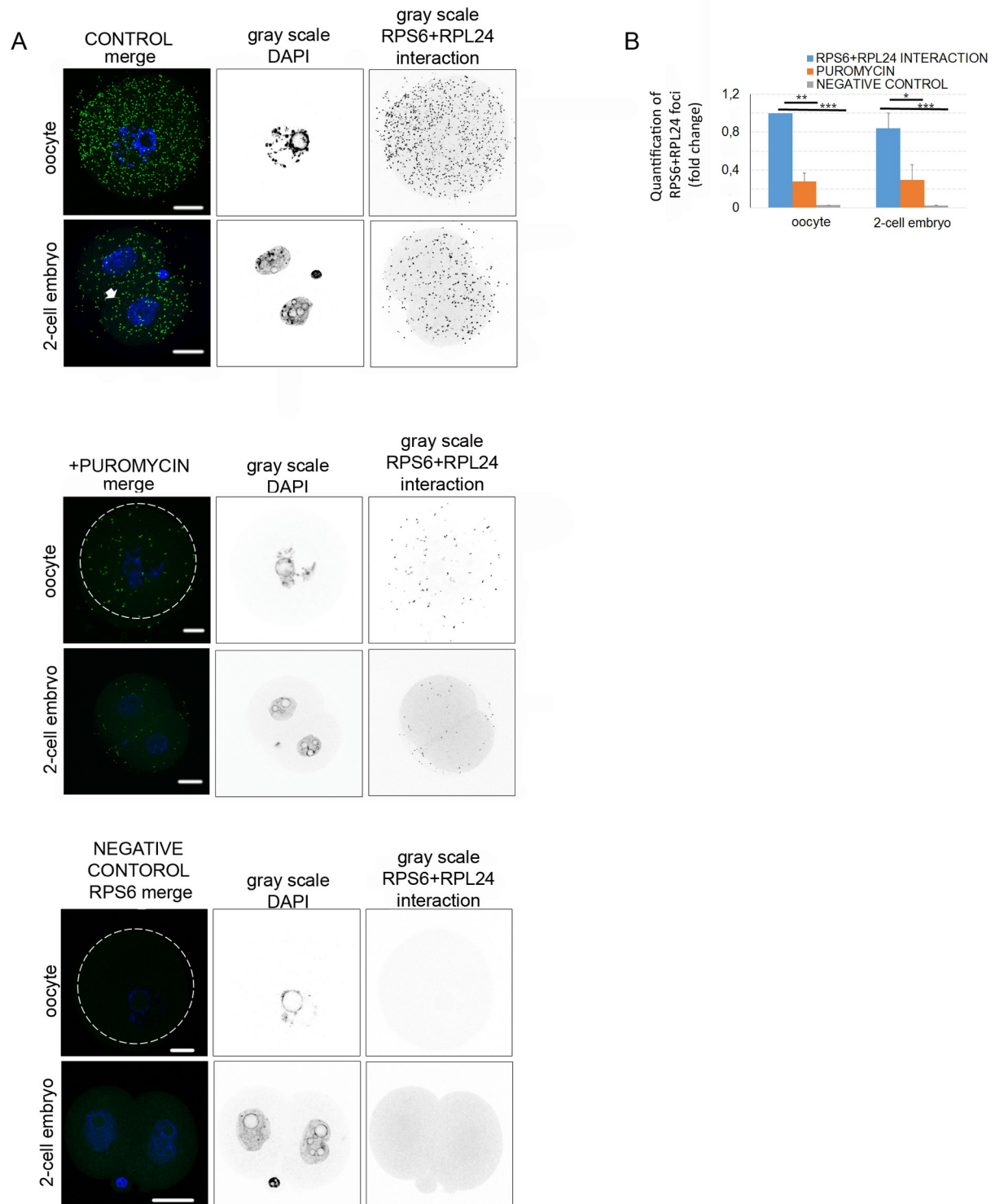


**Fig 6. Detection of in situ translation in oocyte and embryo.** A) Proximity ligation assay (PLA) detects interaction of two translational components RPL24 and RPS6 in the oocyte and 2-cell embryo. Fluorescent foci indicate RPL24 and RPS6 interactions (green) in the oocyte and embryo. As negative controls, oocytes and 2-cell embryos were treated with the translational inhibitor puromycin, or a single RPS6 antibody was used. DNA stained with DAPI (blue); the gray scale shows separated channels. Scale bar 20µm. The experiment was repeated 3 times, with 25 oocytes/embryos per experiment. B) Graph shows quantification of RPL24 and RPS6 interactions in the whole cell volume. The

values obtained from the oocyte were set as 1. The experiment was repeated 3 times, with 25 oocytes/embryos per experiment. Data are represented as mean  $\pm$  s.d.; the value bars with *ns* are not significant, and the asterisk denotes statistically significant differences \* $p$ <0.05; \*\* $p$ <0.01; \*\*\* $p$ <0.001.

<https://doi.org/10.1371/journal.pone.0192544.g006>

Mammalian oocytes are transcriptionally active during their growth period. However, after resumption of meiosis, the oocytes reach a phase of transcriptional quiescence and utilize a store of maternally synthesized RNAs. The progression through meiosis and early embryogenesis is therefore regulated in the oocyte at the level of mRNA stabilization, translation and post-translational modifications. The aim of this study was to detect the global transcriptome present in the mammalian GV oocyte and the 2-cell embryo as a prerequisite for protein synthesis. Using RCA, poly(A) and RNA antibody detection techniques, we observed RNA

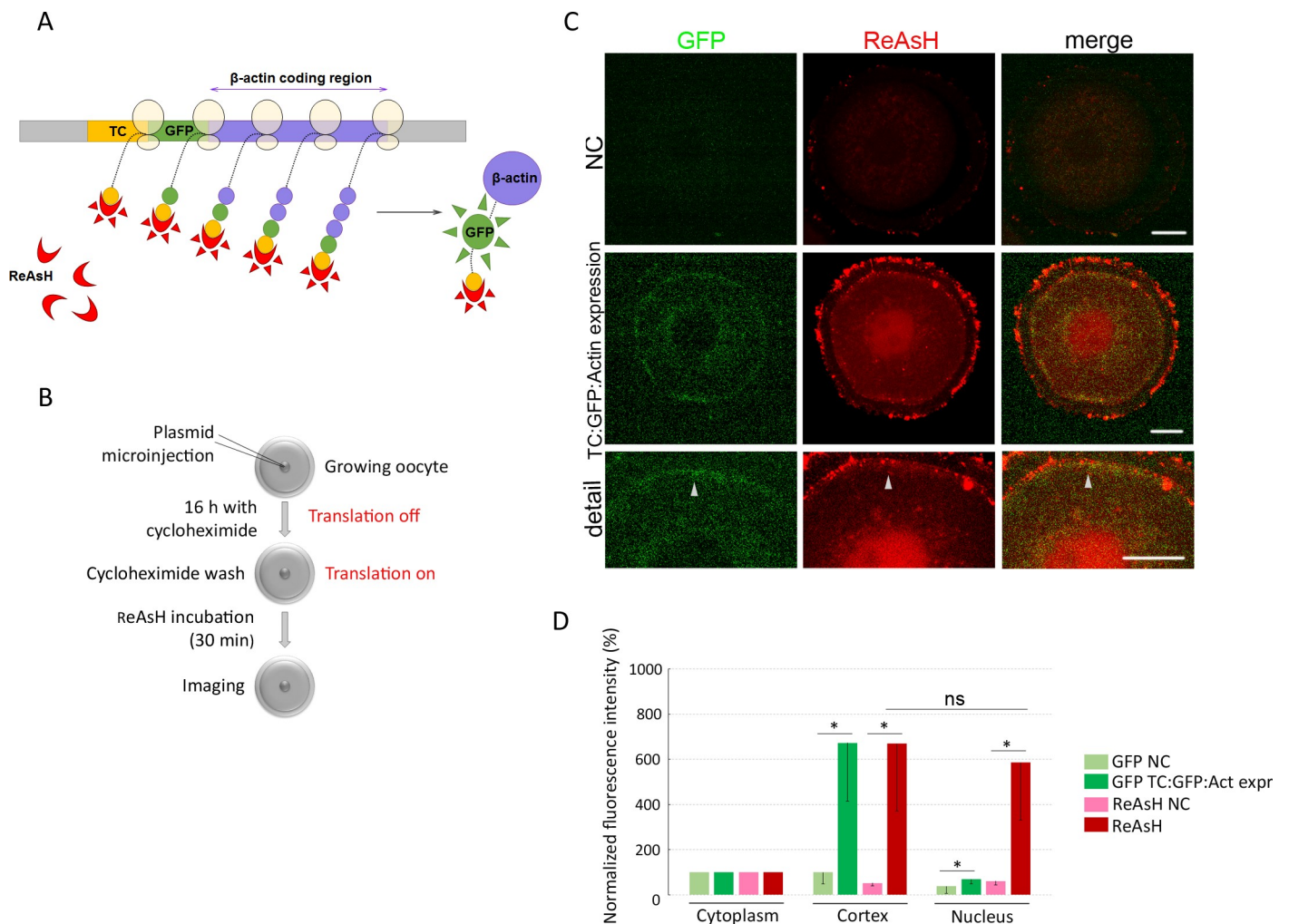


**Fig 7. Visualization of translation of endogenous  $\beta$ -actin mRNA in live oocyte.** A) Scheme of the TC GFP  $\beta$ -actin construct and detection of nascent translation. TC—tetracycline sequence; GFP—green fluorescent protein sequence;  $\beta$ -actin—open reading frame; ReAsH—resorufin arsenical hairpin binder. B) Scheme of the experimental procedures for translational detection of the  $\beta$ -actin RNA in the live oocyte. C) Representative confocal images of the oocyte microinjected with TC GFP  $\beta$ -actin plasmid and of non-injected control. ReAsH dye labels TC tag (red) of newly translated  $\beta$ -actin protein. GFP (green) was used as a marker of fully translated  $\beta$ -actin. The arrowheads depict nascent translation of  $\beta$ -actin RNA. Scale bars 10  $\mu$ m. D) Quantification of the fluorescence intensity in the cytoplasm, cortex and nucleus. The values of the cytoplasm were set as 100%. The experiment was repeated 3 times, with 10 oocytes per experiment. Data are represented as mean  $\pm$  s.d.; the value bars with *ns* are not significant; and the asterisk denotes statistically significant differences \* $p$ <0.05; \*\* $p$ <0.01; \*\*\* $p$ <0.001.

<https://doi.org/10.1371/journal.pone.0192544.g007>



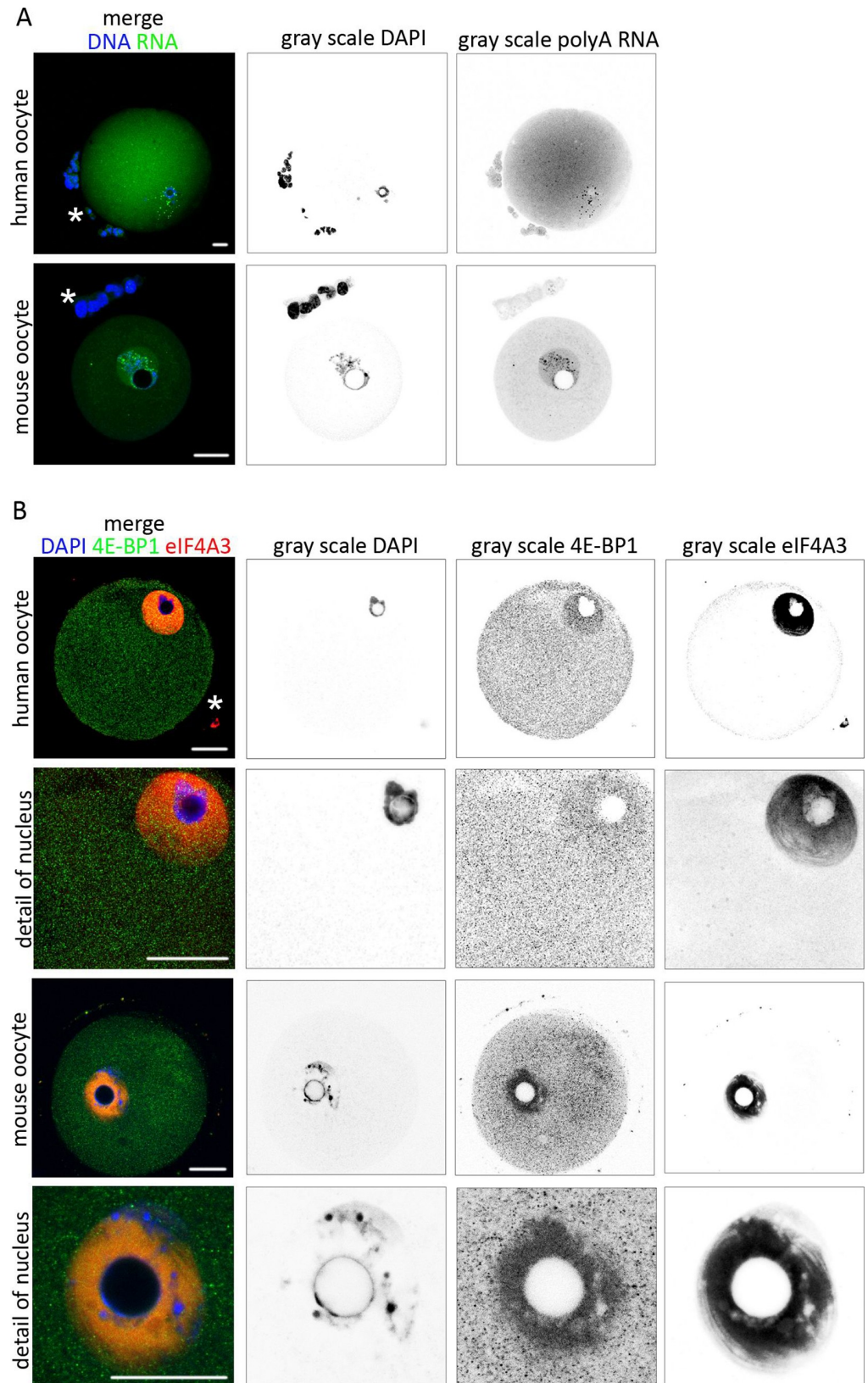


**Fig 8. Localization of poly(A) RNA and RNA binding proteins in human oocyte.** A) Single Z-stack from confocal images of human and mouse GV oocytes. RNA FISH detecting poly(A) RNA subpopulation (green) and DNA (blue). The gray scale shows separated light channels. The asterisk indicates cumulus cells. The experiment was repeated 3 times, with 15 mouse oocytes per experiment and 3 human oocytes per experiment. Scale bars 20  $\mu\text{m}$ . B) Single Z-stack of human and mouse GV oocytes and 2-cell stage mouse embryos probed with 4E-BP1 (green) and eIF4A3 (red) and DAPI (blue). The gray scale shows separated channels. The experiment was repeated 3 times, with 15 mouse oocytes and 3 human oocytes. Scale bars 20  $\mu\text{m}$ . The asterisk indicates cumulus cells.

<https://doi.org/10.1371/journal.pone.0192544.g008>

distribution in both the cytoplasm and the nucleus of transcriptionally inactive oocytes, as well as in active 2-cell stage embryos, consistent with previous analyses [1,8]. Our results lead us to the conclusion that the transcriptionally inactive nucleus might serve as a repository for translationally dormant mRNAs, which may later be translated when the nuclear envelope breaks down after the resumption of meiosis. However, the presence of RNAs in the nucleus of the 2-cell embryo might also be the result of transcription. Our results from RNA FISH and immunocytochemistry analyses positively correlate with previously published results [8,19]. In addition to global RNA found in the nucleus, we detected the partial presence of specific mRNAs *Dazl* and  $\beta$ -*actin* in the nucleoplasm. *Neat2 lncRNA* was present exclusively in the nucleus of the oocyte. In contrast, in the 2-cell embryo, *Neat2* appeared also in the cytoplasm. *Neat2* lncRNA and other RNAs of this class are known to be localized in the nuclei of mouse embryonic fibroblasts and HeLa cells [7,51].

Although findings on translation in the nuclei of cells have been published [68,69], and we detected a number of ribosome components (5.8S rRNA RPS14, RPS3, RPL7) in the nuclei, our other results (absence of phosphorylated RPS6 in the nucleus of the both cell types, and presence of the translational inhibitor 4E-BP1 in the nucleoplasm) indicate that the mRNAs present in the nucleus are translationally dormant [70]. In addition, the translational repressor 4E-BP1 was active in both stages, the oocyte and the embryo (consistently with [19]). The localization of 4E-BP1 in the 2-cell embryo might have a role in the post-transcriptional regulation [71] of the newly synthesized RNA upon embryonic gene activation [72]. The localization of ribosomal components in the nucleoplasm suggests a known mechanism of ribosome biogenesis in the nucleus [73,74]. eIF4A3 is the component of translation initiation complex and also of the exon junction complex, and has a dominant nuclear localization signal sequence [75] which might be responsible for the localization of the protein after the pioneer round of translation [76]. CPEB proteins are key players in the polyadenylation of maternal transcripts [11,20,77] and thus ensure their translation. Our previous work on the mammalian oocyte [21] revealed that CPEB1 was degraded after the resumption of meiosis. Igea and Mendez (2010) proposed that, in the frog oocyte, CPEB4 is accumulated during the second meiotic division and thus can substitute for degraded CPEB1. These authors further suggest that a mechanism is present in *Xenopus* which enables CPEB4 to replace later polyadenylation events in the oocyte. However, we found that CPEB4 was also abundant in the oocyte prior to the resumption of meiosis when CPEB1 was also abundant and functional, suggesting a different mechanism of CPEB regulation in the mammalian oocyte.

We found that selected RBPs, hnRNPA1, eIF4A3, CPEB4 and translational repressor 4E-BP1 were expressed at the same level in the oocyte and in the embryo. However, the ribosomal components RPS14 and phosphorylated RPS6(S235/236) showed significant reduction in the 2-cell embryos. On the other hand, ribosomal components RPS3, RPL7 and RPL24 did not show significant changes in the embryos. We observed different localization of components of ribosomal subunits. During ribosome biogenesis, proteins change their localization, and they also have different localization if they are unbound from ribosomal subunits. We assume that localization of RPS3, RPS14 and RPL7 in the nucleus is necessary for ribosome biogenesis [76,

77, 78, 79] prior to nuclear envelope breakdown to efficiently localize translational machinery to the newly developing spindle [8,9,58].

It is accepted that maternal components (RNA, proteins, organelles) are eliminated after fertilization [32,80]. It is possible that mammalian oocytes and embryos adjust their pool of rRNA and ribosomes to match the mRNA pool and protein requirements, with high levels during oocyte growth, and a relative quiescence in MII stage is accompanied by global reduction of protein synthesis [81–83]. The presence or absence of specific ribosomal proteins in the ribosome is known to control translation of specific subsets of mRNAs [84,85]. This suggests that the elimination of maternal ribosomes might lead to changes in the RNA metabolism between oocyte to embryo transition. Ellederova et al. (2006) and Susor et al. (2008) observed a decrease in global translation during early embryo development, which supports our results generated by PLA showing that 2-cell embryos display a 16% significant decrease in ribosome assembly. In addition, we found that the interaction between RPL24 and RPS6 decreased after the disruption of active ribosomes by puromycin [86], indicating that the interaction foci were active translational sites. We propose that the studied components of the translational machinery are essential for oocyte and embryo development, consistent with [8,19,58]. Monti et al. (2013) discovered that RPL24 and RPS6 are transcribed at the end of the transcriptional activity of the oocyte and are essential for the oocyte to support early embryo development. Ellederova et al. (2006) and Tomek et al. (2002) also observed that despite a decrease in overall protein synthesis in the mammalian oocyte during meiosis, there is a regulatory program that ensures temporal and spatial synthesis of specific proteins that are essential for meiotic progression and embryo development. Similarly with this basic principle we have confirmed the decrease in translation in 2-cell embryos by PLA and HPG methods.

Moreover, we showed *in situ* translation of the well-known cytoskeletal protein  $\beta$ -actin in the live oocyte. A quantification of the images showed a sevenfold increase of fluorescent intensity in ReAsH and GFP in the patches within the cortex. *In vivo* transcription of the construct DNA showed the translation of  $\beta$ -actin RNA in the area of protein localization in the cell.

Although the human oocyte is extremely valuable as the gold standard for assessing clinical relevance, using this cell type is limited in several ways. By starting with the identification of the localization of transcriptome and RBPs in the mouse oocyte and the application of selected markers to the human oocyte, we have found a similar localization of poly(A) RNA and proteins 4E-BP1 and eIF4A3 in both mammalian species, which suggests similar RNA metabolism in human and mouse GV oocytes.

Our findings provide a fundamental insight into the cellular architecture of maternal RNAs in oocytes and embryos from two different mammalian species, mouse and human. We provide a view of the localization of ribosomal proteins, revealing unique and unexpected roles for the translation machinery itself in directing essential aspects of oocyte and early embryo development.

## Supporting information

**S1 Fig. Controls used in the smRNA FISH.** A) Detection of RNA coding GFP in the oocyte. Detection of non-endogenous RNA coding eGFP in the oocyte. Non-endogenous RNA detection was used as a negative control. GFP (green) and DAPI (blue). The gray scale shows separated light channels. The white line indicates the cortex of the oocyte and the arrow with the white line indicates the nucleus of the oocyte. The experiment was repeated 3 times, with 15 mouse oocytes per experiment. Scale bars 20  $\mu$ m. B) As negative controls for smRNA FISH, RNA was digested by RNase A treatment in the fixed oocytes. Oocytes were probed for *Dazl*,

$\beta$ -actin and *Neat2* RNAs. The gray scale shows separated light channels: RNA (green) and DNA (blue). The white line indicates the cortex of the oocyte. The arrow with the white line indicates the nucleus of the oocyte. The asterisk indicates cumulus cells. Scale bars 20  $\mu$ m. (TIF)

**S2 Fig. Localization of RBPs in the mouse oocyte after RNA digestion.** Treatment with RNase A leads to decrease of signal intensity and disruption of granular structure of 4E-BP1. Single Z-stack from confocal images of mouse GV oocytes and detail of nuclei. We used for 4E-BP1 (green) and eIF4A3 (red) antibodies and stained DNA with DAPI (blue). The gray scale shows different light channels. The experiment was repeated 3 times, with 25 oocytes per experiment. Scale bars represent 10  $\mu$ m.

(TIF)

**S3 Fig. Images of whole WBs.** Images of WBs probed for specific proteins with depicted molecular size.

(TIF)

**S4 Fig. Detection of in situ translation in oocyte and embryo.** A) Single Z-stack of confocal image shows nascent translation (red) in GV oocytes and 2-cell embryos. Cells were cultured for 30 minutes in the presence of methionine analog HPG and nascent translation was visualized by Click-IT chemistry. The suppression of translation by potent inhibitors puromycin and cycloheximide (CHX) inhibits the incorporation of HPG to the newly synthesized proteins. The white line indicates the cortex of the oocyte. Representative images of at least three independent experiments are shown. DNA stained with DAPI (blue). The gray scale shows light channel for HPG. The arrow indicates the ridge of blastomeres. The asterisk indicates cumulus cells. Scale bars 20 $\mu$ m.

B) Quantification of fluorescence intensity of HPG signal after treatment by puromycin or CHX in GV oocytes and 2-cell stage embryos. The experiment was repeated 3 times, with 25 oocytes per experiment. Data are represented as mean  $\pm$  s.d.; the values bars with *ns* are not significant, and the asterisk denotes statistically significant differences \* $p < 0.05$ ; \*\* $p < 0.01$ ; \*\*\* $p < 0.001$ .

(TIF)

**S5 Fig. Visualization of actin microfilaments in oocyte and 2-embryo.** Single Z-stack of confocal images. Actin filaments visualized by phalloidin (green) and DNA stained with DAPI (blue). Representative images of at least three independent experiments are shown. Scale bars represent 10  $\mu$ m.

(TIF)

## Acknowledgments

We thank Jaroslava Supolikova and Marketa Hancova for their exceptional technical assistance with experiments and also to Lenka Gahurova, PhD for valuable advices and comments. We are also grateful to the members of the Obstetrics and Gynecology Clinic of the General University Hospital in Prague—Mgr. Martina Moosova, Dr. Karel Rezabek and Dr. Jana Pavelkova—for obtaining human oocytes.

## Author Contributions

**Conceptualization:** Denisa Jansova.

**Data curation:** Denisa Jansova.



**Formal analysis:** Denisa Jansova.

**Funding acquisition:** Denisa Jansova, Michal Kubelka.

**Investigation:** Denisa Jansova, Anna Tetkova.

**Methodology:** Marketa Koncicka.

**Supervision:** Andrej Susor.

**Validation:** Denisa Jansova, Anna Tetkova.

**Writing – original draft:** Denisa Jansova.

**Writing – review & editing:** Anna Tetkova, Michal Kubelka, Andrej Susor.

## References

1. Schultz RM. Regulation of zygotic gene activation in the mouse. *BioEssays News Rev Mol Cell Dev Biol.* 1993; 15: 531–538. <https://doi.org/10.1002/bies.950150806>
2. Ellederova Z, Kovarova H, Melo-Sterza F, Livingstone M, Tomek W, Kubelka M. Suppression of translation during in vitro maturation of pig oocytes despite enhanced formation of cap-binding protein complex eIF4F and 4E-BP1 hyperphosphorylation. *Mol Reprod Dev.* 2006; 73: 68–76. <https://doi.org/10.1002/mrd.20368> PMID: 16211600
3. Tomek W, Melo Sterza FA, Kubelka M, Wollenhaupt K, Torner H, Anger M, et al. Regulation of translation during in vitro maturation of bovine oocytes: the role of MAP kinase, eIF4E (cap binding protein) phosphorylation, and eIF4E-BP1. *Biol Reprod.* 2002; 66: 1274–1282. PMID: 11967187
4. Flemr M, Ma J, Schultz RM, Svoboda P. P-body loss is concomitant with formation of a messenger RNA storage domain in mouse oocytes. *Biol Reprod.* 2010; 82: 1008–1017. <https://doi.org/10.1095/biolreprod.109.082057> PMID: 20075394
5. Femino AM, Fay FS, Fogarty K, Singer RH. Visualization of single RNA transcripts in situ. *Science.* 1998; 280: 585–590. PMID: 9554849
6. Trcek T, Chao JA, Larson DR, Park HY, Zenklusen D, Shenoy SM, et al. Single-mRNA counting using fluorescent in situ hybridization in budding yeast. *Nat Protoc.* 2012; 7: 408–419. <https://doi.org/10.1038/nprot.2011.451> PMID: 22301778
7. Cabili MN, Dunagin MC, McClanahan PD, Bjaesch A, Padovan-Merhar O, Regev A, et al. Localization and abundance analysis of human lncRNAs at single-cell and single-molecule resolution. *Genome Biol.* 2015; 16: 20. <https://doi.org/10.1186/s13059-015-0586-4> PMID: 25630241
8. Susor A, Jansova D, Cerna R, Danylevska A, Anger M, Toralova T, et al. Temporal and spatial regulation of translation in the mammalian oocyte via the mTOR-eIF4F pathway. *Nat Commun.* 2015; 6: 6078. <https://doi.org/10.1038/ncomms7078> PMID: 25629602
9. Susor A, Kubelka M. *Translational Regulation in the Mammalian Oocyte.* Oocytes. Springer, Cham; 2017. pp. 257–295. [https://doi.org/10.1007/978-3-319-60855-6\\_12](https://doi.org/10.1007/978-3-319-60855-6_12)
10. Blower MD, Feric E, Weis K, Heald R. Genome-wide analysis demonstrates conserved localization of messenger RNAs to mitotic microtubules. *J Cell Biol.* 2007; 179: 1365–1373. <https://doi.org/10.1083/jcb.200705163> PMID: 18166649
11. Groisman I, Huang Y-S, Mendez R, Cao Q, Theurkauf W, Richter JD. CPEB, Maskin, and Cyclin B1 mRNA at the Mitotic Apparatus: Implications for Local Translational Control of Cell Division. *Cell.* 2000; 103: 435–447. [https://doi.org/10.1016/S0092-8674\(00\)00135-5](https://doi.org/10.1016/S0092-8674(00)00135-5) PMID: 11081630
12. VerMilyea MD, Maneck M, Yoshida N, Blochberger I, Suzuki E, Suzuki T, et al. Transcriptome asymmetry within mouse zygotes but not between early embryonic sister blastomeres. *EMBO J.* 2011; 30: 1841–1851. <https://doi.org/10.1038/emboj.2011.92> PMID: 21468028
13. Becalska AN, Gavis ER. Lighting up mRNA localization in *Drosophila* oogenesis. *Dev Camb Engl.* 2009; 136: 2493–2503. <https://doi.org/10.1242/dev.032391>
14. Johnstone O, Lasko and P. Translational Regulation and RNA Localization in *Drosophila* Oocytes and Embryos. *Annu Rev Genet.* 2001; 35: 365–406. <https://doi.org/10.1146/annurev.genet.35.102401.090756> PMID: 11700288
15. King ML, Messitt TJ, Mowry KL. Putting RNAs in the right place at the right time: RNA localization in the frog oocyte. *Biol Cell.* 2005; 97: 19–33. <https://doi.org/10.1042/BC20040067> PMID: 15601255
16. Kloc M, Etkin LD. RNA localization mechanisms in oocytes. *J Cell Sci.* 2005; 118: 269–282. <https://doi.org/10.1242/jcs.01637> PMID: 15654016

17. Medioni C, Mowry K, Besse F. Principles and roles of mRNA localization in animal development. *Dev Camb Engl*. 2012; 139: 3263–3276. <https://doi.org/10.1242/dev.078626>
18. Müller-McNicol M, Neugebauer KM. How cells get the message: dynamic assembly and function of mRNA-protein complexes. *Nat Rev Genet*. 2013; 14: 275–287. <https://doi.org/10.1038/nrg3434> PMID: [23478349](https://pubmed.ncbi.nlm.nih.gov/23478349/)
19. Jansova D, Koncicka M, Tetkova A, Cerna R, Malik R, Del Llano E, et al. Regulation of 4E-BP1 activity in the mammalian oocyte. *Cell Cycle Georget Tex*. 2017; 1–13. <https://doi.org/10.1080/15384101.2017.1295178>
20. Richter JD. CPEB: a life in translation. *Trends Biochem Sci*. 2007; 32: 279–285. <https://doi.org/10.1016/j.tibs.2007.04.004> PMID: [17481902](https://pubmed.ncbi.nlm.nih.gov/17481902/)
21. Komrskova P, Susor A, Malik R, Prochazkova B, Liskova L, Supolikova J, et al. Aurora kinase A is not involved in CPEB1 phosphorylation and cyclin B1 mRNA polyadenylation during meiotic maturation of porcine oocytes. *PLoS One*. 2014; 9: e101222. <https://doi.org/10.1371/journal.pone.0101222> PMID: [24983972](https://pubmed.ncbi.nlm.nih.gov/24983972/)
22. Görlach M, Burd CG, Portman DS, Dreyfuss G. The hnRNP proteins. *Mol Biol Rep*. 1993; 18: 73–78. PMID: [8232298](https://pubmed.ncbi.nlm.nih.gov/8232298/)
23. Piñol-Roma S, Dreyfuss G. Shuttling of pre-mRNA binding proteins between nucleus and cytoplasm. *Nature*. 1992; 355: 730–732. <https://doi.org/10.1038/355730a0> PMID: [1371331](https://pubmed.ncbi.nlm.nih.gov/1371331/)
24. Burd CG, Dreyfuss G. RNA binding specificity of hnRNP A1: significance of hnRNP A1 high-affinity binding sites in pre-mRNA splicing. *EMBO J*. 1994; 13: 1197–1204. PMID: [7510636](https://pubmed.ncbi.nlm.nih.gov/7510636/)
25. Jean-Philippe J, Paz S, Caputi M. hnRNP A1: The Swiss Army Knife of Gene Expression. *Int J Mol Sci*. 2013; 14: 18999–19024. <https://doi.org/10.3390/ijms140918999> PMID: [24065100](https://pubmed.ncbi.nlm.nih.gov/24065100/)
26. Chan CC, Dostie J, Diem MD, Feng W, Mann M, Rappsilber J, et al. eIF4A3 is a novel component of the exon junction complex. *RNA*. 2004; 10: 200–209. <https://doi.org/10.1261/ra.5230104> PMID: [14730019](https://pubmed.ncbi.nlm.nih.gov/14730019/)
27. Wang Z, Murigneux V, Le Hir H. Transcriptome-wide modulation of splicing by the exon junction complex. *Genome Biol*. 2014; 15. <https://doi.org/10.1186/s13059-014-0551-7>
28. Inoue K, Ohno M, Sakamoto H, Shimura Y. Effect of the cap structure on pre-mRNA splicing in *Xenopus* oocyte nuclei. *Genes Dev*. 1989; 3: 1472–1479. PMID: [2606355](https://pubmed.ncbi.nlm.nih.gov/2606355/)
29. Monti M, Zanoni M, Calligaro A, Ko MSH, Mauri P, Redi CA. Developmental Arrest and Mouse Antral Not-Surrounded Nucleolus Oocytes. *Biol Reprod*. 2013; 88: 2. <https://doi.org/10.1095/biolreprod.112.103887> PMID: [23136301](https://pubmed.ncbi.nlm.nih.gov/23136301/)
30. Clegg KB, Pikó L. RNA synthesis and cytoplasmic polyadenylation in the one-cell mouse embryo. *Nature*. 1982; 295: 342–345. <https://doi.org/10.1038/295342a0>
31. Zeng F, Baldwin DA, Schultz RM. Transcript profiling during preimplantation mouse development. *Dev Biol*. 2004; 272: 483–496. <https://doi.org/10.1016/j.ydbio.2004.05.018> PMID: [15282163](https://pubmed.ncbi.nlm.nih.gov/15282163/)
32. Su Y-Q, Sugiura K, Woo Y, Wigglesworth K, Kamdar S, Affourtit J, et al. Selective degradation of transcripts during meiotic maturation of mouse oocytes. *Dev Biol*. 2007; 302: 104–117. <https://doi.org/10.1016/j.ydbio.2006.09.008> PMID: [17022963](https://pubmed.ncbi.nlm.nih.gov/17022963/)
33. Ben-Shem A, Garreau de Loubresse N, Melnikov S, Jenner L, Yusupova G, Yusupov M. The structure of the eukaryotic ribosome at 3.0 Å resolution. *Science*. 2011; 334: 1524–1529. <https://doi.org/10.1126/science.1212642> PMID: [22096102](https://pubmed.ncbi.nlm.nih.gov/22096102/)
34. Krieg J, Hofsteenge J, Thomas G. Identification of the 40 S ribosomal protein S6 phosphorylation sites induced by cycloheximide. *J Biol Chem*. 1988; 263: 11473–11477. PMID: [3403539](https://pubmed.ncbi.nlm.nih.gov/3403539/)
35. Rosner M, Fuchs C, Dolznig H, Hengstschläger M. Different cytoplasmic/nuclear distribution of S6 protein phosphorylated at S240/244 and S235/236. *Amino Acids*. 2011; 40: 595–600. <https://doi.org/10.1007/s00726-010-0684-2> PMID: [20625781](https://pubmed.ncbi.nlm.nih.gov/20625781/)
36. Ruvinsky I, Meyuhas O. Ribosomal protein S6 phosphorylation: from protein synthesis to cell size. *Trends Biochem Sci*. 2006; 31: 342–348. <https://doi.org/10.1016/j.tibs.2006.04.003> PMID: [16679021](https://pubmed.ncbi.nlm.nih.gov/16679021/)
37. Meyuhas O, Drazan A. Ribosomal protein S6 kinase from TOP mRNAs to cell size. *Prog Mol Biol Transl Sci*. 2009; 90: 109–153. [https://doi.org/10.1016/S1877-1173\(09\)90003-5](https://doi.org/10.1016/S1877-1173(09)90003-5) PMID: [20374740](https://pubmed.ncbi.nlm.nih.gov/20374740/)
38. Kim T-H, Leslie P, Zhang Y. Ribosomal proteins as unrevealed caretakers for cellular stress and genomic instability. *Oncotarget*. 2014; 5: 860–871. <https://doi.org/10.18632/oncotarget.1784> PMID: [24658219](https://pubmed.ncbi.nlm.nih.gov/24658219/)
39. Zhou X, Hao Q, Liao J, Zhang Q, Lu H. Ribosomal Protein S14 Unties the MDM2-p53 Loop Upon Ribosomal Stress. *Oncogene*. 2013; 32: 388–396. <https://doi.org/10.1038/onc.2012.63> PMID: [22391559](https://pubmed.ncbi.nlm.nih.gov/22391559/)
40. Jansova D. Single Molecule RNA FISH in the Mammalian Oocyte. *Bio-protocol*. 2015; 2015: e1666. <https://doi.org/10.21769/BioProtoc.1666>

41. Lee JH, Daugharthy ER, Scheiman J, Kalhor R, Ferrante TC, Terry R, et al. Fluorescent in situ sequencing (FISSEQ) of RNA for gene expression profiling in intact cells and tissues. *Nat Protoc.* 2015; 10: 442–458. <https://doi.org/10.1038/nprot.2014.191> PMID: [25675209](#)
42. Machleidt T, Robers M, Hanson GT. Protein labeling with FIAsH and ReAsH. *Methods Mol Biol Clifton NJ.* 2007; 356:209–220.
43. Rodriguez AJ, Shenoy SM, Singer RH, Condeelis J. Visualization of mRNA translation in living cells. *J Cell Biol.* 2006; 175: 67–76. <https://doi.org/10.1083/jcb.200512137> PMID: [17030983](#)
44. Tetkova A, Hancova M. Mouse Oocyte Isolation, Cultivation and RNA Microinjection. *BIO-Protoc.* 2016;6. <https://doi.org/10.21769/BioProtoc.1729>
45. Jambor H, Surendranath V, Kalinka AT, Mejsirik P, Saalfeld S, Tomancak P. Systematic imaging reveals features and changing localization of mRNAs in *Drosophila* development. *eLife.* 2015;4. <https://doi.org/10.7554/eLife.05003>
46. Clegg KB, Pikó L. Poly(A) length, cytoplasmic adenylation and synthesis of poly(A)+ RNA in early mouse embryos. *Dev Biol.* 1983; 95: 331–341. PMID: [6186546](#)
47. Larsson C, Grundberg I, Söderberg O, Nilsson M. In situ detection and genotyping of individual mRNA molecules. *Nat Methods.* 2010; 7: 395–397. <https://doi.org/10.1038/nmeth.1448> PMID: [20383134](#)
48. Bochnig P, Reuter R, Bringmann P, Lührmann R. A monoclonal antibody against 2,2,7-trimethylguanosine that reacts with intact, class U, small nuclear ribonucleoproteins as well as with 7-methylguanosine-capped RNAs. *Eur J Biochem.* 1987; 168: 461–467. PMID: [2959477](#)
49. Elela SA, Nazar RN. Role of the 5.8S rRNA in ribosome translocation. *Nucleic Acids Res.* 1997; 25: 1788–1794. <https://doi.org/10.1093/nar/25.9.1788> PMID: [9108162](#)
50. Lerner EA, Lerner MR, Janeway CA, Steitz JA. Monoclonal antibodies to nucleic acid-containing cellular constituents: probes for molecular biology and autoimmune disease. *Proc Natl Acad Sci U S A.* 1981; 78: 2737–2741. PMID: [6789322](#)
51. Miyagawa R, Tano K, Mizuno R, Nakamura Y, Ijiri K, Rakwal R, et al. Identification of cis- and trans-acting factors involved in the localization of MALAT-1 noncoding RNA to nuclear speckles. *RNA.* 2012; 18: 738–751. <https://doi.org/10.1261/rna.028639.111> PMID: [22355166](#)
52. Deshler JO, Hightett MI, Abramson T, Schnapp BJ. A highly conserved RNA-binding protein for cytoplasmic mRNA localization in vertebrates. *Curr Biol.* 1998; 8: 489–496. [https://doi.org/10.1016/S0960-9822\(98\)70200-3](https://doi.org/10.1016/S0960-9822(98)70200-3) PMID: [9560341](#)
53. Tolino M, Köhrmann M, Kiebler MA. RNA-binding proteins involved in RNA localization and their implications in neuronal diseases. *Eur J Neurosci.* 2012; 35: 1818–1836. <https://doi.org/10.1111/j.1460-9568.2012.08160.x> PMID: [22708593](#)
54. Zhang Z, Wang Y, Jiang Y, Lin P, Jia X, Zou Z. Ribosomal protein L24 is differentially expressed in ovary and testis of the marine shrimp *Marsupenaeus japonicus*. *Comp Biochem Physiol B Biochem Mol Biol.* 2007; 147: 466–474. <https://doi.org/10.1016/j.cbpb.2007.02.013> PMID: [17462931](#)
55. Dreyfuss G, Kim VN, Kataoka N. Messenger-RNA-binding proteins and the messages they carry. *Nat Rev Mol Cell Biol.* 2002; 3: 195–205. <https://doi.org/10.1038/nrm760> PMID: [11994740](#)
56. Shibuya T, Tange TØ, Sonenberg N, Moore MJ. eIF4AIII binds spliced mRNA in the exon junction complex and is essential for nonsense-mediated decay. *Nat Struct Mol Biol.* 2004; 11: 346–351. <https://doi.org/10.1038/nsmb750> PMID: [15034551](#)
57. Gingras AC, Gygi SP, Raught B, Polakiewicz RD, Abraham RT, Hoekstra MF, et al. Regulation of 4E-BP1 phosphorylation: a novel two-step mechanism. *Genes Dev.* 1999; 13: 1422–1437. PMID: [10364159](#)
58. Romasko EJ, Amarnath D, Midic U, Latham KE. Association of maternal mRNA and phosphorylated EIF4EBP1 variants with the spindle in mouse oocytes: localized translational control supporting female meiosis in mammals. *Genetics.* 2013; 195: 349–358. <https://doi.org/10.1534/genetics.113.154005> PMID: [23852387](#)
59. Igea A, Méndez R. Meiosis requires a translational positive loop where CPEB1 ensues its replacement by CPEB4. *EMBO J.* 2010; 29: 2182–2193. <https://doi.org/10.1038/emboj.2010.111> PMID: [20531391](#)
60. Roux PP, Shahbazian D, Vu H, Holz MK, Cohen MS, Taunton J, et al. RAS/ERK Signaling Promotes Site-specific Ribosomal Protein S6 Phosphorylation via RSK and Stimulates Cap-dependent Translation. *J Biol Chem.* 2007; 282: 14056–14064. <https://doi.org/10.1074/jbc.M700906200> PMID: [17360704](#)
61. Benesova V, Kinterova V, Kanka J, Toralova T. Characterization of SCF-Complex during Bovine Preimplantation Development. *PLoS One.* 2016; 11: e0147096. <https://doi.org/10.1371/journal.pone.0147096> PMID: [26824694](#)
62. Söderberg O, Leuchowius K-J, Gullberg M, Jarvius M, Weibrecht I, Larsson L-G, et al. Characterizing proteins and their interactions in cells and tissues using the in situ proximity ligation assay. *Methods San Diego Calif.* 2008; 45: 227–232. <https://doi.org/10.1016/j.ymeth.2008.06.014>



63. Dieterich DC, Hodas JJJ, Gouzer G, Shadrin IY, Ngo JT, Triller A, et al. In situ visualization and dynamics of newly synthesized proteins in rat hippocampal neurons. *Nat Neurosci*. 2010; 13: 897–905. <https://doi.org/10.1038/nn.2580> PMID: [20543841](https://pubmed.ncbi.nlm.nih.gov/20543841/)
64. Reid DW, Nicchitta CV. The enduring enigma of nuclear translation. *J Cell Biol*. 2012; 197: 7–9. <https://doi.org/10.1083/jcb.201202140> PMID: [22472436](https://pubmed.ncbi.nlm.nih.gov/22472436/)
65. Azoury J, Verlhac M-H, Dumont J. Actin filaments: key players in the control of asymmetric divisions in mouse oocytes. *Biol Cell Auspices Eur Cell Biol Organ*. 2009; 101: 69–76.
66. Schuh M, Ellenberg J. Self-Organization of MTOCs Replaces Centrosome Function during Acentrosomal Spindle Assembly in Live Mouse Oocytes. *Cell*. 2007; 130: 484–498. <https://doi.org/10.1016/j.cell.2007.06.025> PMID: [17693257](https://pubmed.ncbi.nlm.nih.gov/17693257/)
67. Curtis D, Lehmann R, Zamore PD. Translational regulation in development. *Cell*. 1995; 81: 171–178. PMID: [7736569](https://pubmed.ncbi.nlm.nih.gov/7736569/)
68. Belgrader P, Cheng J, Maquat LE. Evidence to implicate translation by ribosomes in the mechanism by which nonsense codons reduce the nuclear level of human triosephosphate isomerase mRNA. *Proc Natl Acad Sci U S A*. 1993; 90: 482–486. PMID: [8421679](https://pubmed.ncbi.nlm.nih.gov/8421679/)
69. Reid DW, Nicchitta CV. Primary role for endoplasmic reticulum-bound ribosomes in cellular translation identified by ribosome profiling. *J Biol Chem*. 2012; 287: 5518–5527. <https://doi.org/10.1074/jbc.M111.312280> PMID: [22199352](https://pubmed.ncbi.nlm.nih.gov/22199352/)
70. Ford CL, Randal-Whitis L, Ellis SR. Yeast proteins related to the p40/laminin receptor precursor are required for 20S ribosomal RNA processing and the maturation of 40S ribosomal subunits. *Cancer Res*. 1999; 59: 704–710. PMID: [9973221](https://pubmed.ncbi.nlm.nih.gov/9973221/)
71. Siemer C, Smiljakovic T, Bhojwani M, Leiding C, Kanitz W, Kubelka M, et al. Analysis of mRNA associated factors during bovine oocyte maturation and early embryonic development. *Mol Reprod Dev*. 2009; 76: 1208–1219. <https://doi.org/10.1002/mrd.21096> PMID: [19697362](https://pubmed.ncbi.nlm.nih.gov/19697362/)
72. Hamatani T, Carter MG, Sharov AA, Ko MSH. Dynamics of Global Gene Expression Changes during Mouse Preimplantation Development. *Dev Cell*. 2004; 6: 117–131. [https://doi.org/10.1016/S1534-5807\(03\)00373-3](https://doi.org/10.1016/S1534-5807(03)00373-3) PMID: [14723852](https://pubmed.ncbi.nlm.nih.gov/14723852/)
73. David A, Dolan BP, Hickman HD, Knowlton JJ, Clavarino G, Pierre P, et al. Nuclear translation visualized by ribosome-bound nascent chain puromycylation. *J Cell Biol*. 2012; 197: 45–57. <https://doi.org/10.1083/jcb.201112145> PMID: [22472439](https://pubmed.ncbi.nlm.nih.gov/22472439/)
74. Xue S, Barna M. Specialized ribosomes: a new frontier in gene regulation and organismal biology. *Nat Rev Mol Cell Biol*. 2012; 13: 355–369. <https://doi.org/10.1038/nrm3359> PMID: [22617470](https://pubmed.ncbi.nlm.nih.gov/22617470/)
75. SHIBUYA T, TANGE TØ, STROUPE ME, MOORE MJ. Mutational analysis of human eIF4AIII identifies regions necessary for exon junction complex formation and nonsense-mediated mRNA decay. *RNA*. 2006; 12: 360–374. <https://doi.org/10.1261/rna.2190706> PMID: [16495234](https://pubmed.ncbi.nlm.nih.gov/16495234/)
76. Maquat LE, Tarn W-Y, Isken O. The Pioneer Round of Translation: Features and Functions. *Cell*. 2010; 142: 368–374. <https://doi.org/10.1016/j.cell.2010.07.022> PMID: [20691898](https://pubmed.ncbi.nlm.nih.gov/20691898/)
77. Eliscovich C, Peset I, Vernos I, Méndez R. Spindle-localized CPE-mediated translation controls meiotic chromosome segregation. *Nat Cell Biol*. 2008; 10: 858–865. <https://doi.org/10.1038/ncb1746> PMID: [18536713](https://pubmed.ncbi.nlm.nih.gov/18536713/)
78. Meyuhas O, Klein A. The mouse ribosomal protein L7 gene. Its primary structure and functional analysis of the promoter region. *J Biol Chem*. 1990; 265: 11465–11473. PMID: [2365680](https://pubmed.ncbi.nlm.nih.gov/2365680/)
79. Hemmerich P, von Mikecz A, Neumann F, Sözeri O, Wolff-Vorbeck G, Zobelein R, et al. Structural and functional properties of ribosomal protein L7 from humans and rodents. *Nucleic Acids Res*. 1993; 21: 223–231. PMID: [8441630](https://pubmed.ncbi.nlm.nih.gov/8441630/)
80. Alizadeh Z, Kageyama S-I, Aoki F. Degradation of maternal mRNA in mouse embryos: selective degradation of specific mRNAs after fertilization. *Mol Reprod Dev*. 2005; 72: 281–290. <https://doi.org/10.1002/mrd.20340> PMID: [16094646](https://pubmed.ncbi.nlm.nih.gov/16094646/)
81. Schultz RM, Wassarman PM. Biochemical studies of mammalian oogenesis: Protein synthesis during oocyte growth and meiotic maturation in the mouse. *J Cell Sci*. 1977; 24: 167–194. PMID: [893541](https://pubmed.ncbi.nlm.nih.gov/893541/)
82. Susor A, Jelínková L, Karabinová P, Torner H, Tomek W, Kovárová H, et al. Regulation of cap-dependent translation initiation in the early stage porcine parthenotes. *Mol Reprod Dev*. 2008; 75: 1716–1725. <https://doi.org/10.1002/mrd.20913> PMID: [18386287](https://pubmed.ncbi.nlm.nih.gov/18386287/)
83. Ellederová Z, Cais O, Susor A, Uhlířová K, Kovárová H, Jelínková L, et al. ERK1/2 map kinase metabolic pathway is responsible for phosphorylation of translation initiation factor eIF4E during in vitro maturation of pig oocytes. *Mol Reprod Dev*. 2008; 75: 309–317. <https://doi.org/10.1002/mrd.20690> PMID: [17290414](https://pubmed.ncbi.nlm.nih.gov/17290414/)
84. Kondrashov N, Pusic A, Stumpf CR, Shimizu K, Hsieh AC, Xue S, et al. Ribosome-mediated specificity in Hox mRNA translation and vertebrate tissue patterning. *Cell*. 2011; 145: 383–397. <https://doi.org/10.1016/j.cell.2011.03.028> PMID: [21529712](https://pubmed.ncbi.nlm.nih.gov/21529712/)

85. Kang SA, Pacold ME, Cervantes CL, Lim D, Lou HJ, Ottina K, et al. mTORC1 Phosphorylation Sites Encode Their Sensitivity to Starvation and Rapamycin. *Science*. 2013; 341: 1236566. <https://doi.org/10.1126/science.1236566> PMID: [23888043](https://pubmed.ncbi.nlm.nih.gov/23888043/)
86. Azzam ME, Algranati ID. Mechanism of Puromycin Action: Fate of Ribosomes after Release of Nascent Protein Chains from Polysomes. *Proc Natl Acad Sci U S A*. 1973; 70: 3866–3869. PMID: [4590173](https://pubmed.ncbi.nlm.nih.gov/4590173/)



Article

# Increased Expression of Maturation Promoting Factor Components Speeds Up Meiosis in Oocytes from Aged Females

Marketa Koncicka <sup>1,2</sup>, Anna Tetkova <sup>1,2</sup>, Denisa Jansova <sup>1</sup>, Edgar Del Llano <sup>1,2,3</sup>, Lenka Gahurova <sup>1,4</sup>, Jana Kracmarova <sup>1</sup>, Sarka Prokesova <sup>1</sup>, Tomas Masek <sup>3</sup>, Martin Pospisek <sup>3</sup>, Alexander W. Bruce <sup>4</sup>, Michal Kubelka <sup>1</sup> and Andrej Susor <sup>1,\*</sup>

<sup>1</sup> Laboratory of Biochemistry and Molecular Biology of Germ Cells, Institute of Animal Physiology and Genetics, CAS, Rumburska 89, 277 21 Libechov, Czech Republic; Koncicka@iapg.cas.cz (M.K.); tetkova@iapg.cas.cz (A.T.); jansova@iapg.cas.cz (D.J.); Llano@iapg.cas.cz (E.D.L.); lveselovska@prf.jcu.cz (L.G.); kracmarova@iapg.cas.cz (J.K.); prokesovas@af.czu.cz (S.P.); kubelka@iapg.cas.cz (M.K.)

<sup>2</sup> Department of Cell Biology, Faculty of Science, Charles University in Prague, Albertov 6, 128 43 Prague, Czech Republic

<sup>3</sup> Department of Genetics and Microbiology, Faculty of Science, Charles University in Prague, Albertov 6, 128 43 Prague, Czech Republic; masek@natur.cuni.cz (T.M.); martin.pospisek@natur.cuni.cz (M.P.)

<sup>4</sup> Laboratory of early mammalian development, Department of Molecular Biology and Genetics, Faculty of Science, University of South Bohemia, Branisovska 1760, 370 05 Ceske Budejovice, Czech Republic; awbruce@prf.jcu.cz

\* Correspondence: susor@iapg.cas.cz

Received: 17 August 2018; Accepted: 17 September 2018; Published: 19 September 2018



**Abstract:** The rate of chromosome segregation errors that emerge during meiosis I in the mammalian female germ line are known to increase with maternal age; however, little is known about the underlying molecular mechanism. The objective of this study was to analyze meiotic progression of mouse oocytes in relation to maternal age. Using the mouse as a model system, we analyzed the timing of nuclear envelope breakdown and the morphology of the nuclear lamina of oocytes obtained from young (2 months old) and aged females (12 months old). Oocytes obtained from older females display a significantly faster progression through meiosis I compared to the ones obtained from younger females. Furthermore, in oocytes from aged females, lamin A/C structures exhibit rapid phosphorylation and dissociation. Additionally, we also found an increased abundance of MPF components and increased translation of factors controlling translational activity in the oocytes of aged females. In conclusion, the elevated MPF activity observed in aged female oocytes affects precocious meiotic processes that can multifactorially contribute to chromosomal errors in meiosis I.

**Keywords:** aging; oocyte; MPF; meiosis; translation; lamin A/C

## 1. Introduction

The development of female germ cells (oocytes) is essential for sexual reproduction. Oocytes, arrested in meiotic prophase, undergo a major growth phase during their development in ovarian follicles. During this phase, they actively transcribe their genome; however, most derived mRNAs are stored in ribonucleoprotein particles to be used much later during the final stages of meiosis and early embryonic development. A unique property of the oocyte is that the final stages of meiosis (after prophase I) occur in the absence of de novo transcription. Consequently, regulation of mRNA stability and translation serves as the main driving forces behind oogenesis and early embryogenesis [1].

Mammalian oocytes undergo two successive cell divisions without an intermediate replicative phase. This brief period is called “meiotic maturation” and is crucial for the formation of an egg capable of being fertilized and for the generation of viable and euploid offspring. At the onset of meiosis I, the nuclear lamina is phosphorylated (namely lamin A/C; LMN A/C) and disassembled, leading to nuclear envelope break down (NEBD), chromosome condensation, and progressive reorganization of microtubules into a bipolar spindle [2]. At the end of meiosis I, the first asymmetric division occurs.

Human and mouse oocytes are vulnerable to aging as the incidence of chromosome segregation errors (aneuploidy) reaches high levels in females/mothers of advanced age [3–5]. For example, in 20-year-old women, aneuploidy occurs in ~2% of matured oocytes; however, after 35 years of age aneuploidy increases to 35% [6,7]. Similarly, oocytes from aged mice display a significant increase in the incidence of aneuploidy. In three-month-old mice, aneuploidy occurs in 5% of cases; however, by 12 months of age this figure increases to 30–50% [4,8,9]. The majority of chromosome segregation errors are known to arise during the first meiotic cytokinesis [6,10]; however, the reasons why female meiosis shows this peculiar vulnerability to aging remains unclear.

In this study, we present evidence for the aberrant timing of meiosis I in the oocytes derived from female mice of advanced age. Such age-associated abnormalities present as aberrations in nuclear envelope morphology as well as the precocious timing of NEBD and the formation of kinetochore-microtubule (K-MT) attachments, resulting in accelerated first polar body extrusion (PBE). Furthermore, we reveal that it is the overexpression of metaphase promoting factor (MPF) components associated with impaired translational machinery that leads to this phenotype.

## 2. Results

### 2.1. Meiosis I Is Accelerated in Oocytes from Females of Advanced Age

It is well known that increased maternal age negatively affects oocyte quality [3,5]. We isolated oocytes from antral follicles and obtained an average of 22 fully grown GV oocytes per young mouse (YF; 2 months old) compared to 3 oocytes per aged female (AF; 12 months old). Following removal of IBMX from the culture medium, to restart meiosis I, 98.75% of selected oocytes from young females and 98.53% oocytes from aged females resumed meiosis (NEBD; Student's *t*-test  $p = 0.9985$ ). Of the cells that resumed meiosis, 84% of the young oocytes extruded polar body and reached MII in the 12 h period compared to 94% of AF oocytes (Student's *t*-test  $p = 0.010809$ ). Measurement of oocyte diameter did not show any differences between age groups ( $71.73 \pm 1.5$  and  $72.31 \pm 1.6$   $\mu\text{m}$ , respectively, Student's *t*-test  $p = 0.99743$ ). To analyze the effect of maternal age on the progress of meiosis I, we compared the maturation of mouse oocytes from young females (YF; 2 months old) and aged females (AF; 12 months old). Time-lapse microscopy revealed that the oocytes from AF progress through meiosis I significantly 30 min faster than oocytes from YF ( $p < 0.05$ ; Figure 1a,b). The oocytes in the AF group initiate nuclear envelope breakdown (NEBD) earlier (Figure 1a) and consequently polar body extrusion (PBE) also occurs earlier than in the YF group ( $p < 0.05$ ; Figure 1b); manifest as a shortening of time between NEBD and PBE (Figure 1b). Next, we scored the attachment of individual cold-stable microtubules (MT) with end-on kinetochores in both age groups. We found that, during metaphase I, 6 h after releasing oocytes from prophase I (6 h post-IBMX-wash), the AF group had a higher number of stably attached kinetochores (95.5%) than the YF group (75.8%,  $p < 0.01$ ) (Figure 1c,d). The larger number of stably end-on attached kinetochores in the AF group demonstrates that the progression through meiosis I was accelerated in the oocytes from the AF group.

### 2.2. Dissociation of Nuclear Envelope Is Accelerated in the Oocytes from Aged Females

The abundant components of the nuclear envelope are lamin A and C (LMN A/C) [11]. Phosphorylation of these lamins at Serine-22 (Ser22) triggers the disassembly of the nuclear lamina, which is a prerequisite for nuclear envelope breakdown [12]. Therefore, we analyzed the phosphorylation of LMN A/C (Ser22) as a marker of meiotic progression. Oocytes from both age

groups were analyzed by Western blotting at various time points relative to their initial isolation (i.e., after 0, 1, 3, 6, and 12 h). We found that the AF group had a significantly increased level of phosphorylated LMN A/C 1 h post-IBMX-wash ( $p < 0.05$ ; Figure 2a,b). On the contrary, the YF group only had an abundant level of phosphorylated LMN A/C 3 h post-IBMX-wash (Figure 2a,b). Despite the observed different timing of LMN A/C phosphorylation between these two groups, the total/eventual level of LMN A/C remained constant (Figure 2a,c).

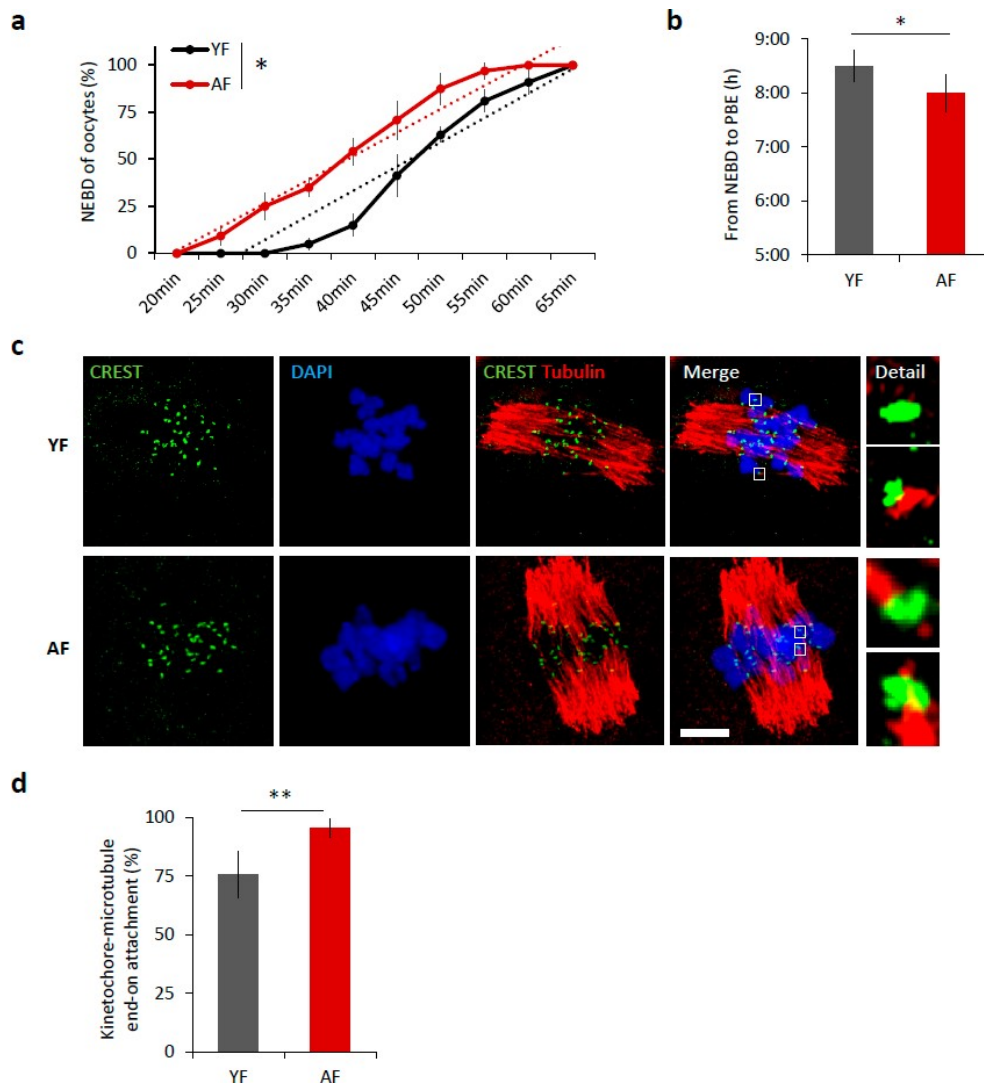


**Figure 1.** Meiosis I is accelerated in oocytes from females of advanced age. **(a)** Timing of nuclear envelope breakdown (NEBD) of oocytes isolated from young females (YF,  $n = 80$ ; black line) and aged females (AF,  $n = 68$ ; red line). Trend line is depicted by dot line. Data represent mean  $\pm$  SD,  $n = 6$ , \*  $p < 0.05$ , Student's  $t$ -test. **(b)** Time from NEBD to polar body extrusion (PBE) in oocytes from YF ( $n = 80$ ;  $t = 8:30$  h) and AF ( $n = 68$ ;  $t = 8$  h). Data represent mean  $\pm$  SD and data are from at least three experiments of biologically different samples. \*  $p < 0.05$ , Student's  $t$ -test. **(c)** Representative Z-projections from the assessment of cold stable attachments of kinetochore (KT) to microtubule (MT) imaged by confocal microscopy using CREST (green) and Tubulin (red) antibodies. Representative images from three experiments of biologically different samples are presented (scale bar, 10  $\mu$ m). **(d)** The percentage of cold stable end-on MT to KT attachments in each age group averaged over multiple cells ( $n \geq 15$ ) 6 h post-IBMX-wash. Kinetochore-MT end-on attachments were quantified. The morphology of kinetochores analyzed is specified in detail. Data represent mean  $\pm$  SD. \*\*  $p < 0.01$ , Student's  $t$ -test.



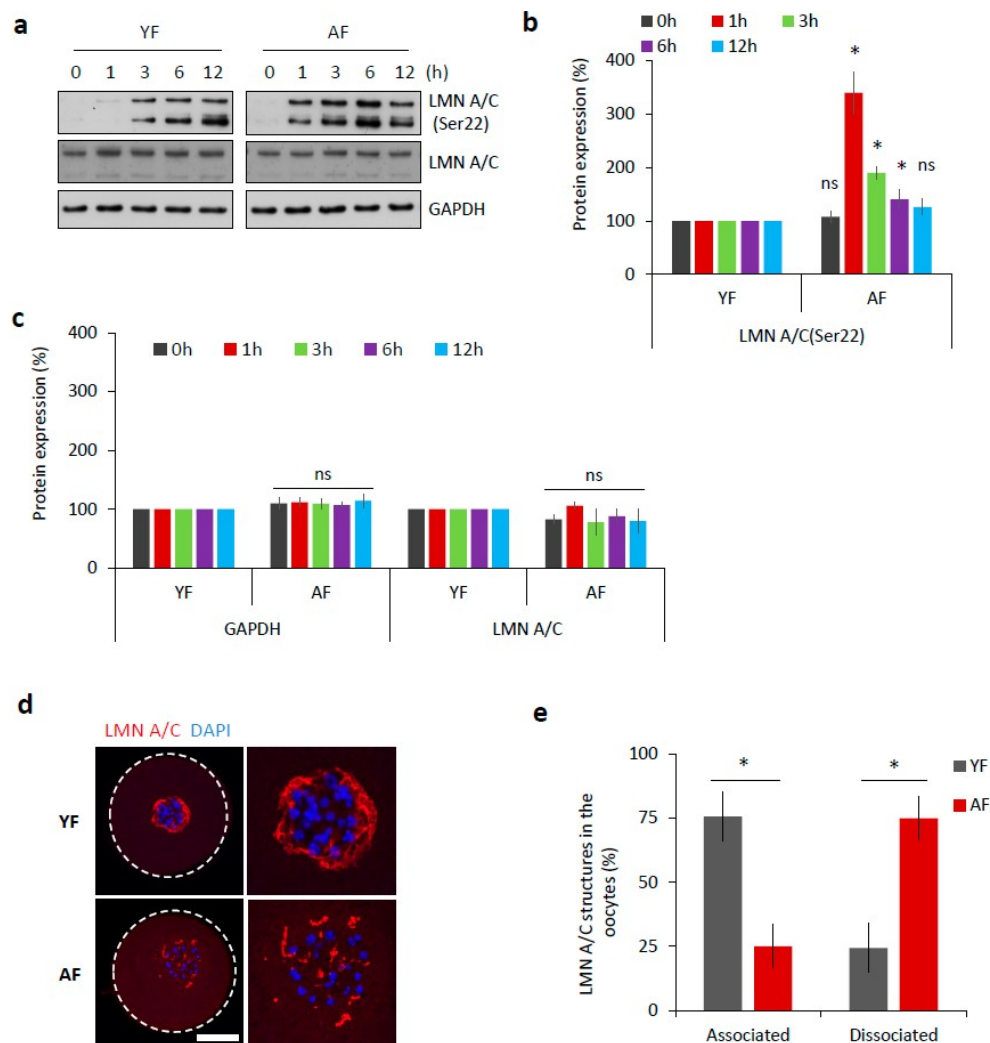


**Figure 2.** Dissociation of nuclear lamina is accelerated in the oocytes from the AF group. **(a)** Western blot analysis of phosphorylation status of LMN A/C (Ser22) at different time points during meiotic progression (0 h, GV; 1 h, post-NEBD; 3 h, post-NEBD; 6 h, post-NEBD/metaphase I; 12 h, post-NEBD/metaphase II). Antibodies against LMN A/C and GAPDH were used as loading controls. Representative images are from three experiments of biologically different samples. **(b)** Quantification of LMN A/C phosphorylation (Ser22) at different time points during meiotic maturation. Data are from three experiments of biologically different samples. Values obtained for the YF group were set as 100%. AF values from each antibody was compared between groups and same oocyte stage. Data represent mean  $\pm$  SD. \*  $p < 0.05$ , bars with ns are non-significant, Student's *t*-test. **(c)** Quantification of GAPDH and LMN A/C protein expression at different time points during meiotic maturation. Data are from three experiments of biologically different samples. Values obtained for the YF group were set as 100%. AF values from each antibody was compared between groups and same oocyte stage. Data represent mean  $\pm$  SD. \*  $p < 0.05$ , bars with ns are non-significant, Student's *t*-test. **(d)** Representative images of LMN A/C structures 3 h post-IBMX-wash (post-NEBD, scale bar 20  $\mu$ m). The cortex of the oocyte indicated by the white dashed line. See Figure S1 for the LMN A/C localization and phosphorylation during oocyte meiotic progression and Figure S2 for electron microscopy images of the nuclear lamina. **(e)** Quantification of LMN A/C structures in the oocytes from different age groups post-NEBD ( $n \geq 33$  and three independent biological replicates). Data represent mean  $\pm$  SD. \*  $p < 0.05$ , Student's *t*-test.

It has been previously documented [13,14] that nuclear lamina structures can be still present at least a few hours after NEBD in mouse oocytes. By immunocytochemistry (ICC), we visualized LMN A/C structures during oocyte meiotic maturation (Figure S1a,b). Using specific antibodies,

both total LMN A/C as well as phosphorylated LMN A/C (Ser22) were detected within the disrupted nuclear lamina structures in NEBD stage oocytes, 3 h post-IBMX-wash (Figure S1a,b). The observed lamina structures surrounded the chromosomal area, where the new spindle was due to be assembled (Figure S1c), but disappeared as meiosis progressed (Figure S1). When we compared 3 h post-IBMX-wash oocytes from both age groups, we found that the dissociation of the described LMN A/C structures was completed significantly faster in the AF group, at a time-point at which they still persisted in the YF oocytes ( $p < 0.05$ ; Figure 2d,e).

Additionally, we imaged GV stage oocytes (oocytes with intact nucleus designated as germinal vesicle, GV) from both age groups by transmission electron microscopy and we were able to distinguish visible differences in the structure of the nuclear envelope in both groups. The nuclear membrane of AF oocytes presented an unique characteristic series of invaginations and decreased compactness (Figure S2a,b). The distinct morphology of the nuclear envelope in the AF oocyte group resulted in a significant increase in the circumference of the nuclear envelope ( $p < 0.01$ ; Figure S2b). Moreover, the observed ultrastructural morphology of the nuclear lamina in AF oocytes resembled that reported in the nuclear phenotypes of other aged cells [15,16].

To conclude, in addition to the above-mentioned precocious timing in meiosis, observed in AF oocytes, we also observed a comparatively earlier phosphorylation of LMN A/C that was associated with a faster disassembly of nuclear lamina, thus affecting the timing of nuclear membrane breakdown, when compared to oocytes from the YF group.

### 2.3. CDK1 Activity Is Responsible for NEBD in Mouse Oocytes

NEBD is reported to be driven by CDK1 (MPF) activity via phosphorylation of lamin proteins and subsequent lamina disassembly at the onset of meiotic resumption or mitosis [17,18]. To test whether LMN A/C were phosphorylated in a CDK1-dependent manner, we treated mouse oocytes with 20  $\mu$ M Roscovitine (Rosco), a potent inhibitor of CDK1 activity, for 2 h after NEBD. We found significantly decreased levels of LMN A/C (Ser22) phosphorylation in oocytes treated with Rosco ( $p < 0.05$ ; Figure 3a,b) versus controls, a result that is consistent with findings of [17].

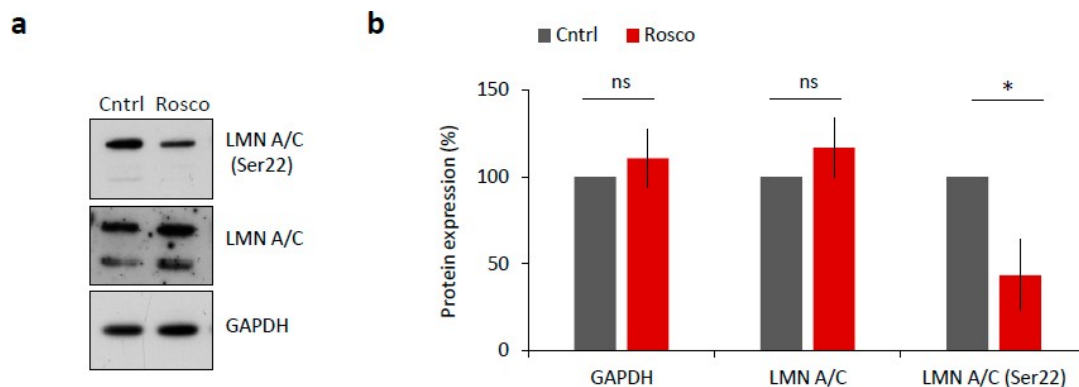


**Figure 3.** CDK1 is responsible for LMN A/C phosphorylation in mouse oocyte. (a) Western blot analysis of oocyte samples treated for 2 h after NEBD with 20  $\mu$ M CDK1 inhibitor, Roscovitine (Rosco). Phosphorylation status of LMN A/C (Ser22) was detected using a specific antibody. Antibodies against LMN A/C and GAPDH were used as a loading control. (b) Quantification of total and phosphorylated LMN A/C after Roscovitine (Rosco) treatment. Protein levels were normalized in a way that non-treated controls are 100%. Data was derived from three experiments containing biologically different samples. Columns represent mean,  $\pm$  SD; ns non-significant; \*  $p < 0.05$ , Student's *t*-test.

Thus, our data confirm the functional involvement of the activated MPF in nuclear lamina disassembly through regulation of LMN A/C phosphorylation status.



#### 2.4. CDK1 Activity Is Increased in Mouse Oocytes from Aged Females

We next examined, whether the expression of MPF components, that directly affect meiotic progression [19], differs between the YF and AF groups of mouse oocytes. Firstly, we isolated total RNA from transcriptionally silent GV staged oocytes from each group and performed quantitative RT-PCR mRNA expression analysis of the MPF component genes *Cdk1* and the B-type *Cyclins*. We found significantly increased levels of both *Cdk1* and *Cyclin B* transcripts in the oocytes from the AF group (Figure 4a) that were not reflected in the total RNA content (Figure S3a) nor in the expression level of *Gapdh* mRNA (Figure 4a). Next we analyzed the expression of MPF components at the protein level via Western blotting, and again we discovered a significant increase in the expression levels of CCNB and CDK1 proteins, specifically in the AF group of oocytes (Figure 4b,c). In addition to the use of a pan-CDK1 antibody, we also probed the oocyte samples with an antibody that specifically recognized phosphorylated (Thr161) CDK1, the enzymatically active form of the protein that is required for a functional MPF activity [19–22]. Again, we found increased phosphorylation status of CDK1 in the AF group versus the YF group of oocytes (Figure 4d,e). Consistently, an analysis of MPF activity, using a standard kinase assay, also revealed a significant increase in CDK1 activity at 1 h in the AF oocytes compared with the YF oocytes, at the time of NEBD (Figure 4d,e).

Taking these results together, we conclude that the activation of the MPF is significantly accelerated in the oocytes from aged females.

#### 2.5. Translation of Positive Regulators of Translation Is Increased in the Oocytes from Aged Females

De novo transcription in fully grown oocytes ceased, so we wondered whether the elevated levels of CCNB and CDK1 proteins in the oocytes from aged females were only due to higher transcript abundance or could also be related to higher translational activity. To experimentally address this question, we compared the incorporation of <sup>35</sup>S-Methionine into nascently translated proteins in both the YF and AF groups of oocytes during maturation (Figure S3b), but we found no significant difference in the levels of global translation (Figure S3b,c). However, we also derived an RNA-seq dataset of mRNA polyribosomal occupancy that allowed us to detect and identify actively translated mRNAs in the two studied age groups of oocytes. Whilst the polysome occupancy was unchanged for mRNAs encoding GAPDH, CDK1, and CCNB1, we did intriguingly identify *Ccnb2*-derived transcripts enriched over 11-fold in polysomal fractions from AF compared to YF oocytes (Figure 5a). A further GO-term (gene ontology) enrichment analysis of polysome-bound mRNAs indicated a significant enrichment of mRNA coding for protein factors belonging to GO functional categories associated with translation initiation and regulation, specifically in the AF oocyte group ( $p$ -value =  $4.76\text{--}6.34 \times 10^{-6}$  for 38 individual mRNAs) (Figure 5b). Generally, this enrichment was higher and the respective categories contained more mRNAs in the AF group over the YF oocytes. We therefore systematically examined the polysome-bound mRNAs whose products are involved in the regulation of translation and revealed increased levels of mRNA coding for positive translation regulators, namely, eukaryotic translation initiation factors (eIF2D, eIF3E, eIF4B, eIF4E3, and eIF4G1), polyadenylation factors (PABPN1L and PABPN1), elongation factor (eEF2), and the number of ribosomal proteins (60S-RPL6, RPL10, RPL10A, RPL17, RPL19, RPL23A, RPL24, RPL37, RPL38; 40S-RPS6, RPS8, RPS9, RPS13, RPS16, and RPS25) in the AF group of oocytes (Figure 5c). Contrarily, we detected a decreased level of mRNA-polysome association for the elongation factor kinase (eEF2K), which is known to act as a suppressor of translational elongation (Figure 5c).

Overall, these results suggest that the translation of individual MPF components and of specific translational factors is elevated in AF oocytes, which is likely to result in changes in the physiology of oocytes from aged female mice.

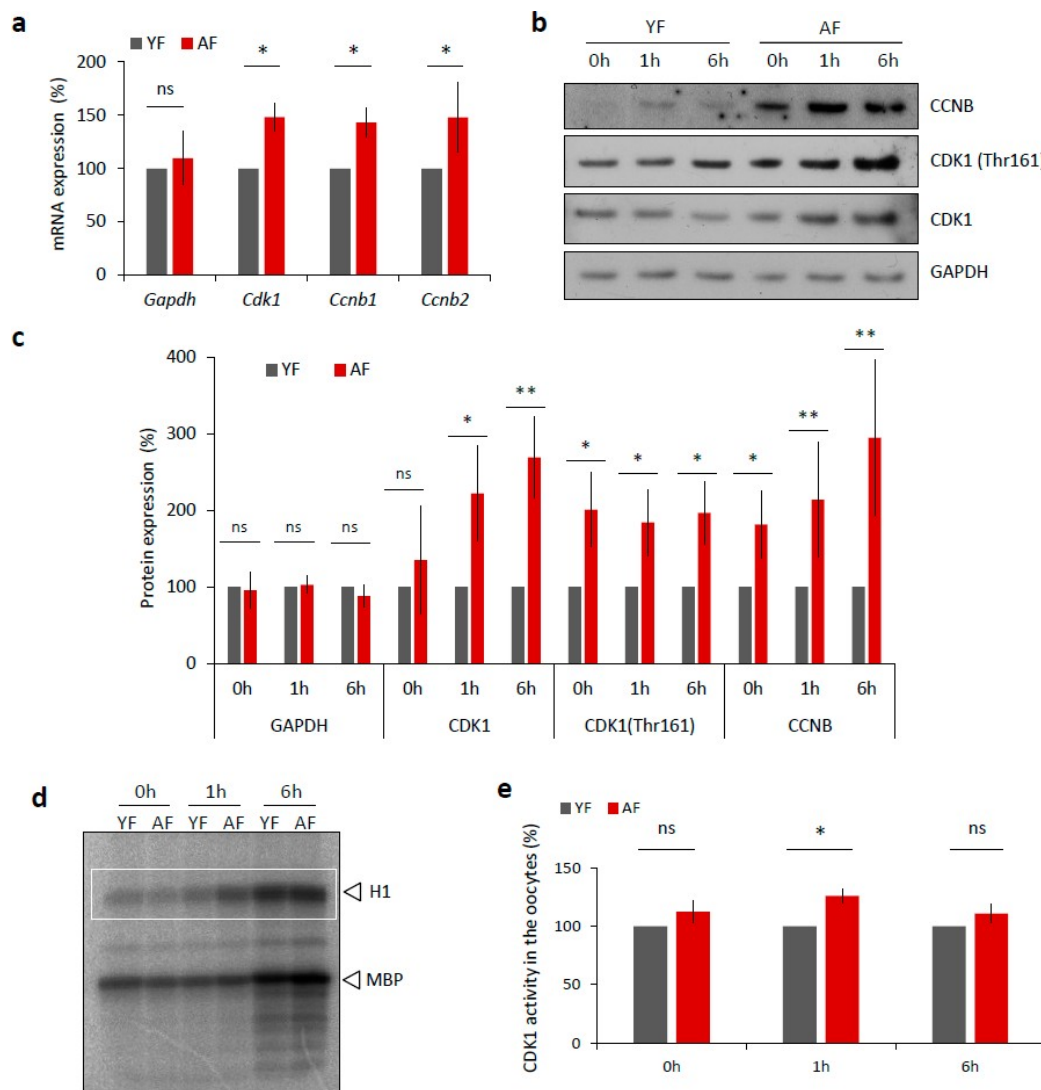


**Figure 4.** Expression of MPF components and its activity is increased in the oocytes from aged females. (a) RT-PCR quantification of mRNA coding for CDK1 and B-type cyclins, as well as loading control *Gapdh* in the GV oocytes (0 h) from different age groups. For quantification of total RNA content in oocytes from YF and AF groups see Figure S3a. Values obtained for the YF group were set as 100%. Data was derived from at least four experiments of biologically different samples. Columns represent mean; error bars  $\pm$  SD; ns non-significant; \*  $p < 0.05$ , Student's *t*-test. (b) Western blot analysis of CDK1, CDK1 (Thr161) and CCNB during oocyte maturation (0 h, 1 h and 6 h) in the both age groups. See Figure S3b,c for the assessment of global translation in oocytes from YF and AF groups. (c) Quantification of MPF components, CDK1, its phosphorylation (Thr161), CCNB and GAPDH as a loading control. Values obtained for the YF group were set as 100%. From at least three experiments of biologically different samples. Columns represent mean  $\pm$  SD; \*  $p < 0.05$ ; \*\*  $p < 0.01$ ; bars with ns are non-significant; Student's *t*-test. (d) Representative image of analysis of CDK1 activity (H1) in the oocytes after isolation (0 h), NEBD (1 h) and at metaphase I (6 h). Kinase assay was done with oocytes of both female age groups. CDK1 activity was measured towards histone H1 as external substrate, marked by white rectangle. (e) Quantification of CDK1 (H1 substrate) activity during oocyte maturation from YF and AF groups. Measurements originated from four experiments of biologically different samples. Values obtained for the YF group were set as 100%. Columns represent mean; error bars  $\pm$  SD; ns non-significant; \*  $p < 0.05$ ; Student's *t*-test.

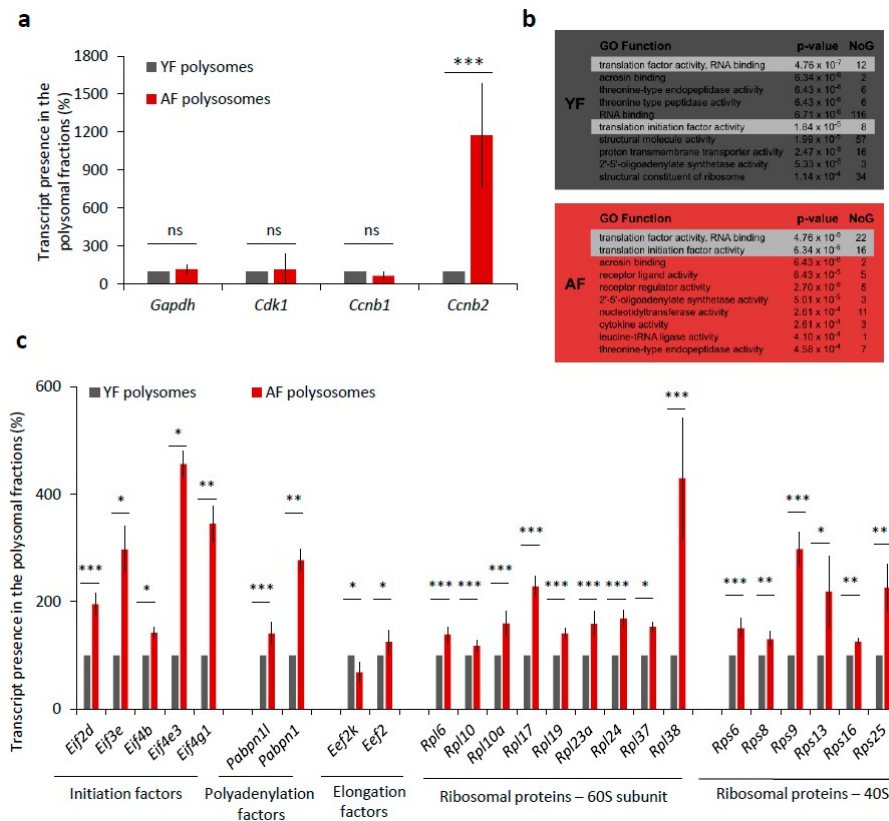


**Figure 5.** Translation of a number of translational factor components is increased in the oocytes from aged females. **(a)** mRNA abundance of MPF components, *Cdk1* and *Cyclins B* as well as *Gapdh* used as the control in the polyribosomal fractions. Percentage of reads from RNA-Seq. See Figure S3a for quantification of total RNA in oocytes from YF and AF groups. Three independent experimental datasets from biologically different samples. Values obtained for the YF group were set as 100%. Data columns represent mean; error bars,  $\pm$  SEM; ns non-significant; \*\*\*  $p < 0.001$ ; Student's *t*-test. **(b)** Top 10 most enriched GO Function categories in polysome-bound mRNAs in YF (grey) and AF (red) oocytes determined by Gorilla. NoG (Number of Genes) denotes the number of genes in enriched categories. Highlighted lines represent translational functional categories. **(c)** Translational regulation of mRNA coding for different translational factors from polysomal fractions of YF and AF oocytes. Values obtained for the YF group were set as 100%. Data represent mean  $\pm$  SEM; \*  $p < 0.05$ ; \*\*  $p < 0.01$ ; \*\*\*  $p < 0.001$ ; Student's *t*-test.

## 2.6. Elevated CDK1 Activity Is Responsible for Faster Meiosis I in Mouse Oocytes

It is known that the expression of CCNB is the limiting factor for the activation of MPF in oocytes prior to resumption of meiosis I [23,24]. It has been reported [25] that the slow increase in CDK1 activity during meiosis I acts as an intrinsic timing mechanism that ensures the appropriate stabilization of kinetochore attachments and thus guards the oocyte against chromosomal segregation errors. We examined whether the overexpression of CCNB affects the timing of meiotic progression. We overexpressed CCNB by microinjecting a cRNA encoding GFP-fused to CCNB into YF oocytes at the GV (0 h) stage (Figure S4). We also microinjected other GV oocytes with *Gfp* cRNA as a negative control. We found that, when experimenting with oocytes derived from the YF cohort, there was a significant increase ( $p < 0.05$ ) in the levels of phosphorylated LMN A/C (Ser22) and phosphorylated CDK1 (Thr161) when microinjected with *Ccnb:gfp* cRNA, as measured 3 h post-IBMX-wash compared to the control group (Figure 6a,b). Live cell imaging of meiotic progression/maturation of such oocytes revealed that the increased expression of CCNB was also able to significantly accelerate overall meiotic progression, as evaluated by the timing of the NEBD and PBE ( $p < 0.05$ ; Figure 6c,d). Specifically, oocytes injected with *Ccnb:gfp* extruded the polar body significantly earlier compared to the control

group (Figure 6c). Thus, they mimicked the phenotype observed in the AF oocytes (Figure 1). Moreover, we also visualized cold-stable kinetochore-microtubule end-on attachments [25,26] and found that the oocytes overexpressing CCNB had a significantly higher rate of the kinetochore-microtubule end-on attachment than the controls at the 6 h post-IBMX-wash ( $p < 0.05$ ; Figure 6e,f). These results suggest that artificially increasing MPF activity leads to a notably more rapid progression through meiosis I as exemplified by the production of stable kinetochore-microtubule attachments.

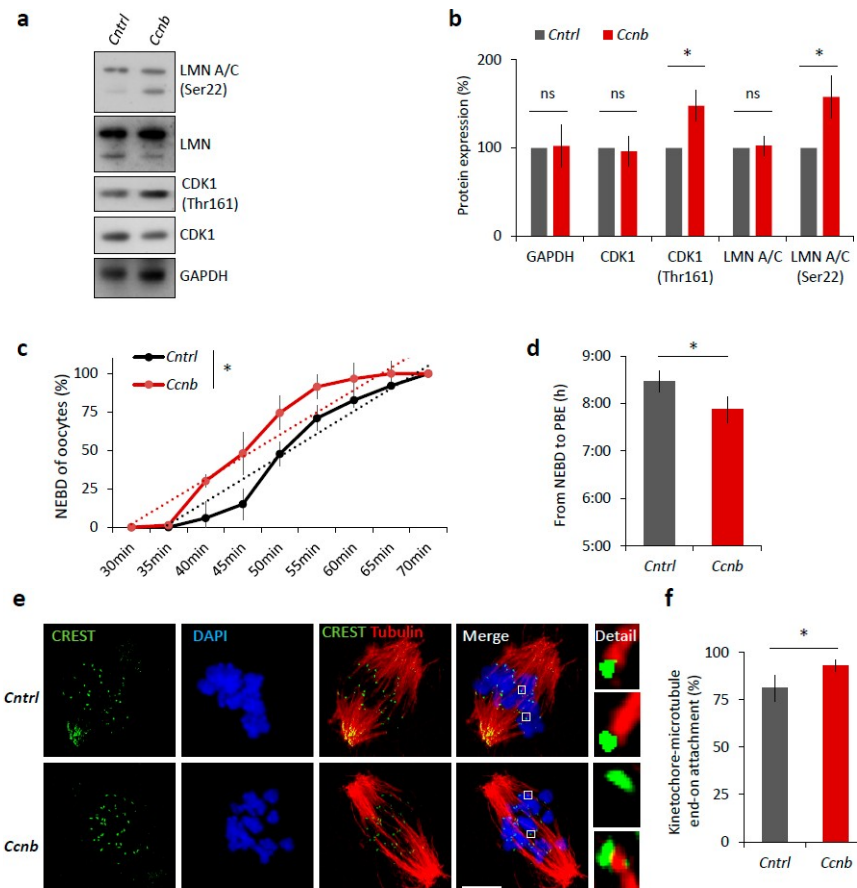


**Figure 6.** Elevated MPF activity is responsible for meiosis I acceleration in oocytes. **(a)** Western blot analysis of LMN A/C (Ser22), LMN A/C, CDK1 (Thr161), CDK1, and GAPDH in the post-NEBD oocytes (3 h) injected with *Ccnb* RNA or control *Gfp* RNA (*Cntrl*). See Figure S4 for the over-expression of CCNB in oocytes. Representative images from at least three experiments of biologically different samples. **(b)** Quantification of protein expression, LMN A/C, and CDK1 phosphorylation. From three experiments of biologically different samples. Values obtained for the YF group were set as 100%. Data represent mean  $\pm$  SD; ns non-significant; \*  $p < 0.05$ ; Student's *t*-test. **(c)** Timing of NEBD of YF oocytes microinjected with *Gfp* ( $n = 46$ ; black line) and *Ccnb* cRNA ( $n = 51$ ; red line). From three experimental data sets of biologically different samples. Trend line is depicted by dot lines. Data represent mean  $\pm$  SD. \*  $p < 0.05$ , Student's *t*-test. **(d)** Time from NEBD to PBE in oocytes from YF injected with RNA coding for *Gfp* ( $n = 46$ ;  $t = 8:25$  h) and *Ccnb* ( $n = 51$ ;  $t = 7:52$  h). Data represent mean  $\pm$  SD and data are from at least three experiments of biologically different samples. Student's *t*-test. **(e)** Representative Z-projections from the assessment of cold stable attachments of kinetochores (KT, CREST, green) to microtubule (MT, tubulin, red) of oocytes microinjected with control *Gfp* and *Ccnb* cRNA. Representative images are from three experiments of biologically different samples (scale bar, 10  $\mu$ m). **(f)** The percentage of cold stable end-on MT to KT attachments in each group averaged over multiple cells ( $n \geq 28$ ) 6 h post-IBMX-wash. Kinetochore-MT end-on attachments were quantified. The morphology of kinetochores analyzed is specified in detail. Data represent mean  $\pm$  SD. \*  $p < 0.05$ , Student's *t*-test.



Taken together, these experiments show we were able to mimic the faster meiotic progression observed in the AF oocytes, that itself stems from higher MPF activity.

### 3. Discussion

Here we have addressed the question of how meiosis I differs in oocytes from females of advanced reproductive age versus those originating from young females. The precise timing of the cell cycle is a prerequisite for the appropriate propagation of genomes. It is well accepted that, in human and mouse oocytes, the incidence of genomic instability and aneuploidy increases with maternal age [5,7,27–30]. Age-associated increase in aneuploidy [27–30] has been attributed, at least in part, to a faster progression through the first meiotic division in oocytes from aged females, which would affect the time available for proper chromosome congression prior to chromosome segregation [27]. The mouse is a useful model in which to study the effect of age on egg quality, including the molecular basis for observed age-associated increase in aneuploidy.

We have found that oocytes from aged females resume meiosis and progress through meiosis I faster than the oocytes from young females. Our finding is consistent with findings of others [5,27,31–33] but opposes other findings reporting a lack of timing in oocytes from aged females [34,35]. In addition, we found that oocytes from aged females are significantly more meiotically competent than from young females, a further consistent observation [36]. The underlying reasons for the reported discrepancies related to the length of meiosis I in aged oocytes are not clear; however, they may have their origin in the methodologies employed to select meiotically competent GV oocytes and/or further differences in oocyte manipulation (e.g., the removal of cumulus cells and microinjection). Relating to our own data, we conclude that an increase in MPF activity during meiosis I temporarily regulates acceleration of NEBD, the attachment of chromosomes, and cytokinesis events in aged oocytes. Moreover, our results are in agreement with previous findings [25] in which it is reported that premature increases of CDK1 kinase activity, induced by cyclin-B microinjection, are responsible for the precocious formation of stable kinetochore-microtubule attachments and lagging chromosomes during anaphase I, a condition that leads to aneuploidy. Thus, the increased presence of MPF components, as observed in our AF oocyte cohort, could clearly act in a similar manner to result in chromosome segregation errors during meiosis I.

Surprisingly, we have also found that transcripts coding for MPF components are significantly overexpressed in the oocytes from aged females. However, it is important to recognize that the abundance of mRNA only represents one part of the regulation of gene expression and that selective translational regulation of transcripts can play a pivotal role. It has been previously reported that CCNB2 has a functional role during the prophase/metaphase transition of mouse oocyte maturation [37], and these data support our findings showing that the increased translational rate of CCNB2 transcripts in the oocytes from aged females might be associated with faster meiotic progression. Consistent with this prevailing view, we have also demonstrated elevated phosphorylation levels of CDK1 (Thr161), that in turn contributes to its MPF activity [38], in AF oocytes. Notwithstanding this observation, the upregulation of Cyclin B clearly plays a positive role in reinforcing CDK1/MPF activity and thus driving meiotic cycle progression. As such, our study correlates the resumption of meiosis with the synthesis of the regulatory subunit of MPF, namely cyclin B1/2, as supported by the fact that the level of MPF activity is known to depend on the amount of cyclin B present [22,39,40]. Thus, the fact that the MPF components in aged GV oocytes are apparently more expressed (but not necessarily fully active) and that they are then rapidly activated during their maturation (in AF versus YF oocytes) contributes to the observed acceleration of the AF oocytes meiotic progression.

We show that both cyclins B are expressed and differentially occupy polyribosomes in the AF group. In addition to the increased expression of MPF components, which leads to accelerated meiotic progression, we also demonstrate that the key components of the translational machinery are more translated (associated with polysome fractions), which in turn is likely to positively affect general translation in AF oocytes. Indeed, our findings are in good agreement with published

data describing increased numbers of ribosomes in oocytes from older females [41]. However, in connection to increased number of ribosomes, we have not observed increased rates of global translation. Nonetheless, our results suggest that there is increased translation of specific mRNAs related to specific translational machinery activity in AF oocytes, which may contribute to amplifying the roles of specific regulators [13,42]; mechanisms that could target specific mRNAs for translation and consequently affect meiotic progression rates. In addition to the increased number of ribosomes and translational regulators in oocytes from females of advanced age, it has also been reported [43,44] that the number of mitochondria is also increased in the oocytes and embryos derived from aged mouse and human subjects.

We have also shown that the GV oocytes from female mice of advanced age have aberrantly formed nuclear envelopes, which strongly resemble the morphology of those in aged somatic cells [15,45]. In association with described precocious meiotic progression and increased MPF activity, we have shown that the nuclear lamina is also precociously dispersed in aged oocytes. We have previously reported that LMN A/C structures surround oocyte chromosomes post-NEBD, resembling an organelle-exclusion “spindle envelope” that acts as a diffusion barrier structure [46–48]. Such spindle envelopes are thought to confine spindle assembly and their mechanical disruption is reported to compromise precise and appropriate chromosome segregation in mitosis [47]. It is therefore possible that the lack of such a functioning spindle envelope in AF-derived oocytes contributes to increased aneuploidy rates observed.

Taken together, our results can provide at least a partial explanation for the commonly recognized multifactorial phenomenon of age-related increase in oocyte aneuploidy on a molecular level. In addition, our study significantly contributes to the overall knowledge base concerning the molecular physiology of aged cells, including but not restricted to oocytes, and provides a solid foundation for further work related to the observed translational discrepancies between young and aged oocytes identified herein, and their functional interplay with meiotic progression/maturation.

## 4. Material and Methods

### 4.1. Oocyte Cultivation, Treatment, and Microinjection

GV oocytes were obtained from CD1 mice 46 h after injection by 5 IU pregnant mare serum gonadotropin (PMSG, HOR 272, ProSpec, Rehovot, Israel). Oocytes were obtained from females in two distinct age categories: young females (YF) group (2 months old) and aged females (AF) group (12 months old). Oocytes were isolated in germinal vesicle stage (GV; 0 h) in transfer medium [49] supplemented with 100  $\mu$ M 3-isobutyl-1-methylxanthine (IBMX, I5879, Sigma-Aldrich, Darmstadt, Germany) to prevent NEBD. Selected fully grown GV oocytes were denuded by pipetting and cultured in M16 medium (M7292, Sigma-Aldrich, Darmstadt, Germany) without IBMX at 37 °C, 5% CO<sub>2</sub>. Post-IBMX-wash (PIW) oocytes undergo nuclear envelope breakdown (NEBD) within 1 h; they reach metaphase I in 6 h and metaphase II in 12 h. For oocytes treatment, 20  $\mu$ M roscovitin (186692-46-6, Cayman Chemical, Ann Arbor, MI, USA) was added 1 h PIW. GV oocytes were microinjected in the presence of the IBMX on inverted microscope Leica DMI 6000B (Leica Microsystems, Wetzlar, Germany) using TransferMan NK2 (Eppendorf, Hamburg, Germany) and FemtoJet (Eppendorf). Oocytes were injected with 20 ng/ $\mu$ L of in vitro transcribed (mMessage, Ambion, Thermo Fisher Scientific, Waltham, MA, USA) RNAs from plasmids (GFP, [50]; CCNB1, Dr. Martin Anger, Laboratory of Cell Division Control, IAPG, CAS) diluted in RNase free water. Approximately 5 pL of RNA solution were injected into one oocyte. Microinjected oocytes were used for time-lapse microscopy, cold tubulin stability testing, and immunoblotting. All animal work was conducted according to Act No 246/1992 for the protection of animals against cruelty; from 25.09.2014 number CZ02389, issued by Ministry of agriculture.

#### 4.2. Time-Lapse Microscopy

Oocytes were scanned with an inverted wide field microscope, Leica DMI 6000B (Leica Microsystems, Wetzlar, Germany), equipped with a chamber system (Pecon, Erbach, Germany), a Tempcontroller 2000-2 (Pecon), and a CO<sub>2</sub> controller (Pecon). Cover-glass-based 4-well chambers (94.6190.402, Sarstedt, Nümbrecht, Germany) were used for live oocytes imaging. Oocytes were put into a 10 µL drop of M16 medium without IBMX and covered by approximately 1 mL of mineral oil (M8410, Sigma-Aldrich). The chamber was pre-tempered to 37 °C and 5% CO<sub>2</sub>. Images were captured every 5 min. Timing of the NEBD and polar body extrusion (PBE) were evaluated through time lapse movies.

#### 4.3. Immunoblotting

Oocytes were washed in phosphate buffer saline (PBS, Sigma-Aldrich) with polyvinyl alcohol (PVA, Sigma-Aldrich) and frozen to −80 °C. An exact number of oocytes (15–30) were lysed in 10 µL of 1× Reducing SDS Loading Buffer (lithium dodecyl sulfate sample buffer NP 0007 and reduction buffer NP 0004, Thermo Fisher Scientific, Waltham, MA, USA) and heated at 100 °C for 5 min. Proteins were separated by gradient precast 4–12% SDS-PAGE gel (NP 0323, Thermo Fisher Scientific) and transferred to Immobilon P membrane (IPVD 00010, Millipore, Merck group, Darmstadt, Germany) using a semidry blotting system (Biometra GmbH, Analytik Jena, Jena, Germany) for 25 min at 5 mA cm<sup>−2</sup>. Membranes were blocked by 5% skimmed milk dissolved in 0.05% Tween-Tris buffer saline (TTBS), pH 7.4 for 1 h. After a brief washing in TTBS, membranes were incubated at 4 °C overnight with the primary antibodies diluted in 1% milk/TTBS (see Table S1). Secondary antibody Peroxidase Anti-Rabbit Donkey (711-035-152) or Peroxidase Anti-Mouse Donkey (715-035-151, Jackson ImmunoResearch, West Grove, PA, USA) was diluted 1:7500 in 1% milk/TTBS. The membranes were incubated in the secondary antibodies for 1 h at room temperature. Immunodetected proteins were visualized on films using ECL (Amersham, GE Healthcare Life Sciences, Barcelona, Spain). Films were scanned using a GS-800 calibrated densitometer (Bio-Rad Laboratories, CA, USA) and quantified using ImageJ (<http://rsbweb.nih.gov/ij/>).

#### 4.4. Measurement of Overall Protein Synthesis

To measure the overall protein synthesis, 50 µCi of <sup>35</sup>S-methionine (Hartmann Analytics, Braunschweig, Germany) was added to methionine-free culture medium. Ten oocytes per sample were labeled for 2 h, then lysed in SDS-buffer, and loaded to SDS-polyacrylamide gel electrophoresis and transferred to an Immobilon P membrane using the semidry blotting system for 25 min at 5 mA cm<sup>−2</sup> (the same materials as in Immunoblotting). The labeled proteins were visualized by autoradiography on FujiFilm (incubated at least 14 days in −80 °C), scanned using BAS-2500 Photo Scanner (FujiFilm Life Science, Tokyo, Japan) and quantified by ImageJ. GAPDH antibody was used as a loading control.

#### 4.5. Immunocytochemistry and Cold-Stable MT Assay

After cultivation, oocytes were fixed for 15 min in 4% paraformaldehyde (PFA, Alfa Aesar, Thermo Fisher Scientific, Waltham, MA, USA) in PBS/PVA. Oocytes were permeabilized in 0.1% Triton (X-100, Sigma-Aldrich) in PBS/PVA for 10 min, washed in PBS/PVA, and incubated overnight at 4 °C with primary antibodies (see Table S1). After washing in PBS/PVA, detection of the primary antibodies was performed by cultivation of the oocytes with relevant Highly Cross-Adsorbed Secondary Antibodies, Alexa Fluor 488, 594 or 647 conjugates (Thermo Fisher Scientific) diluted 1:250 for 1 h at room temperature. Oocytes were then washed two times for 15 min in PBS/PVA and mounted using a Vectashield Mounting Medium with DAPI (H-1200, Vector Laboratories, Burlingame, CA, USA). For the cold-stable MT assay, oocytes were matured for 6 h post-IBMX-wash and then were incubated for 15 min in 4 °C, fixed in 4% PFA/PVA, and stained for tubulin and CREST according to the immunocytochemistry protocol. Confocal images were collected as Z stacks at 0.3 µm intervals



to visualize the entire meiotic spindle region. Samples were visualized using a Leica SP5 inverted confocal microscope (Leica Microsystems, Wetzlar, Germany). To classify kinetochore attachment status, images were scored around the same Z plane using the merged two-color confocal stack of CREST and MT images. Images were assembled in software LAS X (Leica Microsystems).

#### 4.6. Transmission Electron Microscopy

Mouse oocytes in GV were washed three times in PBS/PVA and one time in 0.1 M Sorenson's phosphate buffer (pH = 7.2) with PVA. Oocytes were fixed in 2.5% glutaraldehyde (G5882, Sigma-Aldrich) in 0.1 M Sorenson's phosphate buffer for 1 h at room temperature. Fixed oocytes were transported to the Electron Microscopy facility at the Microscopy Centre of the Institute of Molecular Genetics, CAS. Fixative was removed and oocytes were centrifuged ( $5000\times g/5$  min) in 1% low-temperature melting agarose. Oocytes were embedded to Epon blocks and sliced by UltraCut6 (Leica Microsystems) to ultra-thin sections. Oocyte sections were imaged at 80 kV using FEI Morgagni 268 Transmission Electron Microscope with Olympus Megaview III Digital Camera EM (FEI Company, Hillsboro, OR, USA).

#### 4.7. RNA Isolation and RT-PCR

RNA was extracted using a RNeasy Plus Micro kit (74034, Qiagen, Hilden, Germany) and genomic DNA was depleted using gDNA Eliminator columns. The quality and quantity of the isolated RNA was analyzed using the Bioanalyzer 2100 (Agilent, Santa Clara, CA, USA) system employing the RNA 6000 Pico kit (5067-1513, Agilent). RT-PCR was then carried out using the Rotor-Gene 3000 (Biocompare, South San Francisco, CA, USA) and the OneStep RT-PCR Kit (210210, Qiagen) and SybrGreen I (S7563, Thermo Fisher Scientific) according to manufacturers' provided protocols. Gene/transcript specific RT-PCR primers were designed with an annealing temperature of 58 °C (see Table S2). The reaction condition for reverse transcription was as follows: 50 °C/30 min, then initial activation at 95 °C/15 min, followed by 40 PCR amplification cycles (95 °C/15 s, 58 °C/20 s, 72 °C/30 s) and 72 °C/10 min. Quantification analyses were performed using a dynamic amplification efficiency determination for each amplification run as provided in the comparative quantification function with the Rotor-Gene RG-3000 software. The exact amplification efficiencies were assessed in each tube, and a mathematic model was applied for the derived calculation of the relative gene expression in the control (YF).

#### 4.8. Polysome Fractionation and RNA Extraction

Prior to oocyte collection, 100 µg/mL of cycloheximide (CHX, 01810, Sigma-Aldrich) was added for 10 min. Next, 200 oocytes (per sample) were washed three times in PBS/PVA supplemented with CHX and frozen at -80 °C in low-binding tube (Eppendorf). To disrupt the zona pellucida and lysate the oocytes, 250 µL of zirconia-silica beads (11079110z, BioSpec, Bartlesville, OK, USA) were added to the tube with frozen oocytes together with 350 µL of lysis buffer (10 mM Hepes, pH 7.5; 62.5 mM KCl; 5 mM MgCl<sub>2</sub>; 2 mM DTT; 1% TritonX-100; 100 µg/mL of CHX supplemented with Complete-EDTA-free Protease Inhibitor (05 056 489 001 3, Roche Diagnostics GmbH, Mannheim, Germany) and Ribolock 20 U/mL (EO0381, Thermo Fisher Scientific)). Oocytes were disrupted in the mixer mill apparatus MM301 (shake frequency 30, total time 45 s, Retsch, Haan, Germany). Lysates were clarified by centrifugation at  $8000\times g$  for 5 min at 4 °C. Supernatants were loaded onto 10–50% linear sucrose gradients containing 10 mM Hepes, pH 7.5; 100 mM KCl; 5 mM MgCl<sub>2</sub>; 2 mM DTT; 100 µg/mL CHX; Complete EDTA-free (1 tablet/100 mL); and 5 U/mL Ribolock. Centrifugation was carried out using Optima L-90 ultracentrifuge (Beckman Coulter, Brea, CA, USA) at  $35,000\times g$  for 65 min at 4 °C. Polysome profiles were recorded using ISCO UA-5 UV absorbance reader. We monitored the overall quality of the polysome fractionation experiment by an inclusion of a parallel HEK293 cells sample. Ten equal fractions were recovered from each sample and subjected to RNA isolation by Trizol reagent (Sigma-Aldrich). Each fraction was then tested by qPCR with 18S and 28S rRNA-specific primers in

LightCycler480 (Roche) to reconstruct a distribution of non-polysomal and polysomal RNA complexes in each oocyte – specific profile.

#### 4.9. Library Preparation, RNA Sequencing and Data Analysis

Fractions corresponding to polysomal and non-polysomal part, respectively, were pulled together. These sub-samples were concentrated to 16  $\mu$ L of Clean & Concentrator-5 (R1014, Zymo Research, Irvine, CA, USA) and ribosomal RNA was removed from them by Ribozero-Gold (MRZG12324, Illumina, San Diego, CA, USA). Afterwards, RNA was turned into cDNA and amplified by using the REPLI-g WTA Single Cell Kit (150063, Qiagen). Finally, cDNA was tagged and libraries were prepared using the Nextera DNA Library Prep Kit (FC-121-1030, Illumina). Sequencing was performed in Centro Nacional de Analisis Genomico facility (CNAG, Barcelona, Spain). Samples were sequenced by HiSeq 2500 (Illumina) as 150 bp paired-end. Reads were trimmed using Trim Galore! v0.4.1 and mapped to the mouse GRCm38 genome assembly using Hisat2 v2.0.5. Gene expression was quantified as fragments per kilobase per million (FPKM) values in Seqmonk v1.40.0. Functional annotation was performed using GOrilla [51,52] with ranked lists of genes detected in polysomal fractions (FPKM > 0.1).

#### 4.10. Kinase Assay

Kinase activities of CDK1 (H1) and MAPK (MBP) were determined in a single assay via their capacity to phosphorylate external substrates histone H1 and myelin basic protein (MBP), respectively [53]. Fifteen oocytes per sample were collected and lysed in 5  $\mu$ L of lysis buffer (10  $\mu$ g/mL leupeptin, 10  $\mu$ g/mL aprotinin, 10 mM p-nitrophenyl phosphate, 20 mM  $\beta$ -glycerophosphate, 0.1 mM  $\text{Na}_3\text{VO}_4$ , 5 mM EGTA, 1 mM benzamidine, 1 mM AEBSF) by three cycles of freezing/thawing. Next, 5  $\mu$ L of double kinase buffer (60  $\mu$ g/mL leupeptin, 60  $\mu$ g/mL aprotinin, 24 mM p-nitrophenyl phosphate, 90 mM  $\beta$ -glycerophosphate, 4.6 mM  $\text{Na}_3\text{VO}_4$ , 24 mM EGTA, 2 mM benzamidine, 2 mM AEBSF, 24 mM  $\text{MgCl}_2$ , 0.2 mM EDTA, 4 mM NaF, 1.6 mM DTT, 0.2% (*w/v*) polyvinyl alcohol, 40 mM MOPS pH 7.2, 2.2  $\mu$ M protein kinase inhibitor (P0300, Sigma-Aldrich), 1 mg/mL MBP (M1891, Sigma-Aldrich), 0.5 mg/mL histone H1 (10223549001, Roche), 0.6 mM ATP, 1 mCi/mL [ $\gamma$ - $^{32}\text{P}$ ] ATP (Hartmann Analytic, Braunschweig, Germany) was incubated with the lysed sample for 30 min at 30 °C. The reaction was terminated by addition of 12.5  $\mu$ L of double-strength concentrated reducing sample buffer [54]. The phosphorylated substrates were resolved on 15% SDS-PAGE gel, the gel was stained with Coomassie Brilliant Blue R250 (27816, Sigma-Aldrich), dried and exposed to an intensifying screen in the exposure cassette for 20 h. Phosphorylated substrates were visualized using a FujiFilm BAS-2500 Photo Scanner and the kinase activity was quantified using Aida Image Analyzer software (Elysia Raytest, Angleur, Belgium).

#### 4.11. Statistical Analysis

Mean and standard deviation ( $\pm$ SD) values were calculated using MS Excel. Statistical significance of the differences between the groups was tested using Student's *t*-test (PrismaGraph5) and  $p < 0.05$  was considered as statistically significant (marked by asterisks: \*  $p < 0.05$ ; \*\*  $p < 0.01$ ; \*\*\*  $p < 0.001$ ).

**Supplementary Materials:** Supplementary materials can be found at <http://www.mdpi.com/1422-0067/19/9/2841/s1>. Figure S1. Localization of LMN A/C during oocyte maturation. (a) Representative confocal images from immunocytochemistry (ICC) showed localization of LMN A/C (red) and phosphorylated LMN A/C Ser22 (green) during oocyte maturation (GV 0 h; NEBD 3 h; MI 6 h, MII 12 h). Cortex of oocytes is depicted by white dashed line. DNA, blue and scale bar, 10  $\mu$ m. (b) Co-localization of LMN A/C (Ser22) (green) and the spindle (tubulin, red). DNA, blue and scale bar 10  $\mu$ m. (c) Localization of LMN A/C (red) during oocyte meiotic maturation. DNA, blue and scale bar 10  $\mu$ m. Arrowhead marks polar body. Figure S2. Transmission electron microscopy of oocyte nuclei from females of different age. (a) Representative images of the nucleus from YF and AF oocytes. The images in the right panels show nuclear membrane highlighted with red line. Scale bar 10  $\mu$ m. (b) Measurement of nuclear membrane circumference of oocytes from the YF and the AF group. From two experiments of biologically different samples ( $n \geq 8$ ). Data represent mean  $\pm$ SD. \*\*  $p < 0.01$ , Student's *t*-test. (c) Detail of nuclear lamina from AF and YF oocytes. Representative images are from two experiments from biologically different samples (bar, 1  $\mu$ m).

The images in the right panels show nuclear membrane highlighted with red line. Figure S3. Total RNA amount and global translational activity is not different between YF and AF groups. (a) Quantification of total RNA by Agilent 2100 Bioanalyzer in the oocytes from different age groups. From 10 experiments of biologically different samples. Data represent mean  $\pm$ SD. ns, non-significant, Student's *t*-test. (b) <sup>35</sup>S-Methionine incorporation during meiotic progression of oocytes from YF and AF groups. Representative images are from three experiments of biologically different samples. (c) Quantification of <sup>35</sup>S-Methionine incorporation in the oocytes from different groups. From three experiments of biologically different samples. Values obtained for the YF group were set as 100%. Data represent mean  $\pm$ SD, ns, non-significant, Student's *t*-test. Figure S4. Induced expression of the CCNB in the oocytes. Oocytes injected with control *Gfp* (*Ctrl*) and *Ccnb* RNA. See Figure 6a for the effect of the overexpression. WB analysis of samples using CCNB antibody. Arrowhead depicts endogenous CCNB and arrow GFP tagged CCNB protein. GAPDH was used as a loading control. From three experiments of biologically different samples. Table S1. Primary antibodies used for WB and ICC in the study. Table S2. Primers used in the study for RT-PCR.

**Author Contributions:** A.S. designed research; M.K. (Marketa Koncicka), A.T., S.P., D.J., J.K., T.M., M.P., L.G., and A.S. performed research; A.S., M.K. (Marketa Koncicka), L.G., A.W.B., D.J., E.D.L., T.M. and M.P. analyzed data; A.S., A.W.B., M.K. (Marketa Koncicka) and M.K. (Michal Kubelka) wrote the paper.

**Funding:** This research was funded by MSMT (EXCELLENCE CZ.02.1.01/0.0/0.0/15\_003/0000460 OP RDE) and GACR (18-19395S) and GACR (15-22765S) and MC (EIF-708,255; to L.G.) and GACR (18-02891S; to A.W.B.) and Institutional Research Concept RVO67985904 and Development, and Innovations Infrastructures" (CESNET LM2015042).

**Acknowledgments:** We thank Jaroslava Supolikova and Marketa Hancova for their exceptional assistance with experiments and Martin Anger for kindly providing the GFP and CCNB plasmid.

**Conflicts of Interest:** The authors declare no conflict of interest.

## References

1. Colegrove-Otero, L.J.; Devaux, A.; Standart, N. The Xenopus ELAV protein ElrB represses Vg1 mRNA translation during oogenesis. *Mol. Cell. Biol.* **2005**, *25*, 9028–9039. [[CrossRef](#)] [[PubMed](#)]
2. Schuh, M.; Ellenberg, J. Self-organization of MTOCs replaces centrosome function during acentrosomal spindle assembly in live mouse oocytes. *Cell* **2007**, *130*, 484–498. [[CrossRef](#)] [[PubMed](#)]
3. Hassold, T.; Jacobs, P.; Kline, J.; Stein, Z.; Warburton, D. Effect of maternal age on autosomal trisomies. *Ann. Hum. Genet.* **1980**, *44*, 29–36. [[CrossRef](#)] [[PubMed](#)]
4. Pan, H.; Ma, P.; Zhu, W.; Schultz, R.M. Age-associated increase in aneuploidy and changes in gene expression in mouse eggs. *Dev. Biol.* **2008**, *316*, 397–407. [[CrossRef](#)] [[PubMed](#)]
5. Sebestova, J.; Danylevska, A.; Novakova, L.; Kubelka, M.; Anger, M. Lack of response to unaligned chromosomes in mammalian female gametes. *Cell Cycle* **2012**, *11*, 3011–3018. [[CrossRef](#)] [[PubMed](#)]
6. Hassold, T.; Hunt, P. To err (meiotically) is human: The genesis of human aneuploidy. *Nat. Rev. Genet.* **2001**, *2*, 280–291. [[CrossRef](#)] [[PubMed](#)]
7. Hunt, P. Oocyte Biology: Do the Wheels Fall Off with Age? *Curr. Biol.* **2017**, *27*, R266–R269. [[CrossRef](#)] [[PubMed](#)]
8. Chiang, T.; Duncan, F.E.; Schindler, K.; Schultz, R.M.; Lampson, M.A. Evidence that weakened centromere cohesion is a leading cause of age-related aneuploidy in oocytes. *Curr. Biol.* **2010**, *20*, 1522–1528. [[CrossRef](#)] [[PubMed](#)]
9. Merriman, J.A.; Jennings, P.C.; McLaughlin, E.A.; Jones, K.T. Effect of aging on superovulation efficiency, aneuploidy rates, and sister chromatid cohesion in mice aged up to 15 months. *Biol. Reprod.* **2012**, *86*. [[CrossRef](#)] [[PubMed](#)]
10. Chiang, T.; Schultz, R.M.; Lampson, M.A. Meiotic Origins of Maternal Age-Related Aneuploidy. *Biol. Reprod.* **2012**, *86*. [[CrossRef](#)] [[PubMed](#)]
11. Dechat, T.; Pflieger, K.; Sengupta, K.; Shimi, T.; Shumaker, D.K.; Solimando, L.; Goldman, R.D. Nuclear lamins: Major factors in the structural organization and function of the nucleus and chromatin. *Genes Dev.* **2008**, *22*, 832–853. [[CrossRef](#)] [[PubMed](#)]
12. Heald, R.; McKeon, F. Mutations of phosphorylation sites in lamin A that prevent nuclear lamina disassembly in mitosis. *Cell* **1990**, *61*, 579–589. [[CrossRef](#)]
13. Susor, A.; Jansova, D.; Cerna, R.; Danylevska, A.; Anger, M.; Toralova, T.; Malik, R.; Supolikova, J.; Cook, M.S.; Oh, J.S.; et al. Temporal and spatial regulation of translation in the mammalian oocyte via the mTOR-eIF4F pathway. *Nat. Commun.* **2015**, *6*. [[CrossRef](#)] [[PubMed](#)]

14. Sanfins, A.; Plancha, C.E.; Overstrom, E.W.; Albertini, D.F. Meiotic spindle morphogenesis in in vivo and in vitro matured mouse oocytes: Insights into the relationship between nuclear and cytoplasmic quality. *Hum. Reprod.* **2004**, *19*, 2889–2899. [[CrossRef](#)] [[PubMed](#)]
15. Haithcock, E.; Dayani, Y.; Neufeld, E.; Zahand, A.J.; Feinstein, N.; Mattout, A.; Gruenbaum, Y.; Liu, J. Age-related changes of nuclear architecture in *Caenorhabditis elegans*. *Proc. Natl. Acad. Sci. USA* **2005**, *102*, 16690–16695. [[CrossRef](#)] [[PubMed](#)]
16. Righolt, C.H.; van 't Hoff, M.L.R.; Vermolen, B.J.; Young, I.T.; Raz, V. Robust nuclear lamina-based cell classification of aging and senescent cells. *Aging* **2011**, *3*, 1192–1201. [[CrossRef](#)] [[PubMed](#)]
17. Adhikari, D.; Zheng, W.; Shen, Y.; Gorre, N.; Ning, Y.; Halet, G.; Kaldis, P.; Liu, K. Cdk1, but not Cdk2, is the sole Cdk that is essential and sufficient to drive resumption of meiosis in mouse oocytes. *Hum. Mol. Genet.* **2012**, *21*, 2476–2484. [[CrossRef](#)] [[PubMed](#)]
18. Peter, M.; Nakagawa, J.; Dorée, M.; Labbé, J.C.; Nigg, E.A. In vitro disassembly of the nuclear lamina and M phase-specific phosphorylation of lamins by cdc2 kinase. *Cell* **1990**, *61*, 591–602. [[CrossRef](#)]
19. Jones, K.T. Turning it on and off: M-phase promoting factor during meiotic maturation and fertilization. *Mol. Hum. Reprod.* **2004**, *10*, 1–5. [[CrossRef](#)] [[PubMed](#)]
20. Morgan, D.O. Principles of CDK regulation. *Nature* **1995**, *374*, 131–134. [[CrossRef](#)] [[PubMed](#)]
21. Ducommun, B.; Brambilla, P.; Félix, M.A.; Franza, B.R.; Karsenti, E.; Draetta, G. cdc2 phosphorylation is required for its interaction with cyclin. *EMBO J.* **1991**, *10*, 3311–3319. [[CrossRef](#)] [[PubMed](#)]
22. Solomon, M.J. Activation of the various cyclin/cdc2 protein kinases. *Curr. Opin. Cell Biol.* **1993**, *5*, 180–186. [[CrossRef](#)]
23. Hampl, A.; Eppig, J.J. Translational regulation of the gradual increase in histone H1 kinase activity in maturing mouse oocytes. *Mol. Reprod. Dev.* **1995**, *40*, 9–15. [[CrossRef](#)] [[PubMed](#)]
24. Lévesque, J.T.; Sirard, M.A. Resumption of meiosis is initiated by the accumulation of cyclin B in bovine oocytes. *Biol. Reprod.* **1996**, *55*, 1427–1436. [[CrossRef](#)] [[PubMed](#)]
25. Davydenko, O.; Schultz, R.M.; Lampson, M.A. Increased CDK1 activity determines the timing of kinetochore-microtubule attachments in meiosis I. *J. Cell Biol.* **2013**, *202*, 221–229. [[CrossRef](#)] [[PubMed](#)]
26. Rieder, C.L. The structure of the cold-stable kinetochore fiber in metaphase PtK1 cells. *Chromosoma* **1981**, *84*, 145–158. [[CrossRef](#)] [[PubMed](#)]
27. Eichenlaub-Ritter, U.; Boll, I. Age-related non-disjunction, spindle formation and progression through maturation of mammalian oocytes. *Prog. Clin. Biol. Res.* **1989**, *318*, 259–269. [[PubMed](#)]
28. Zuccotti, M.; Boiani, M.; Garagna, S.; Redi, C.A. Analysis of aneuploidy rate in antral and ovulated mouse oocytes during female aging. *Mol. Reprod. Dev.* **1998**, *50*, 305–312. [[CrossRef](#)]
29. Liu, L.; Keefe, D.L. Ageing-associated aberration in meiosis of oocytes from senescence-accelerated mice. *Hum. Reprod.* **2002**, *17*, 2678–2685. [[CrossRef](#)] [[PubMed](#)]
30. Cukurcam, S.; Betzendahl, I.; Michel, G.; Vogt, E.; Hegele-Hartung, C.; Lindenthal, B.; Eichenlaub-Ritter, U. Influence of follicular fluid meiosis-activating sterol on aneuploidy rate and precocious chromatid segregation in aged mouse oocytes. *Hum. Reprod.* **2007**, *22*, 815–828. [[CrossRef](#)] [[PubMed](#)]
31. Chiang, T.; Schultz, R.M.; Lampson, M.A. Age-Dependent Susceptibility of Chromosome Cohesion to Premature Separase Activation in Mouse Oocytes. *Biol. Reprod.* **2011**, *85*, 1279–1283. [[CrossRef](#)] [[PubMed](#)]
32. Eichenlaub-Ritter, U.; Chandley, A.C.; Gosden, R.G. The CBA mouse as a model for age-related aneuploidy in man: Studies of oocyte maturation, spindle formation and chromosome alignment during meiosis. *Chromosoma* **1988**, *96*, 220–226. [[CrossRef](#)] [[PubMed](#)]
33. Eichenlaub-Ritter, U.; Boll, I. Nocodazole sensitivity, age-related aneuploidy, and alterations in the cell cycle during maturation of mouse oocytes. *Cytogenet. Genome Res.* **1989**, *52*, 170–176. [[CrossRef](#)] [[PubMed](#)]
34. Duncan, F.E.; Chiang, T.; Schultz, R.M.; Lampson, M.A. Evidence That a Defective Spindle Assembly Checkpoint Is Not the Primary Cause of Maternal Age-Associated Aneuploidy in Mouse Eggs1. *Biol. Reprod.* **2009**, *81*, 768–776. [[CrossRef](#)] [[PubMed](#)]
35. Lister, L.M.; Kouznetsova, A.; Hyslop, L.A.; Kalleas, D.; Pace, S.L.; Barel, J.C.; Nathan, A.; Floros, V.; Adelfalk, C.; Watanabe, Y.; et al. Age-Related Meiotic Segregation Errors in Mammalian Oocytes Are Preceded by Depletion of Cohesin and Sgo2. *Curr. Biol.* **2010**, *20*, 1511–1521. [[CrossRef](#)] [[PubMed](#)]
36. Cui, L.-B.; Zhou, X.-Y.; Zhao, Z.-J.; Li, Q.; Huang, X.-Y.; Sun, F.-Z. The Kunming mouse: As a model for age-related decline in female fertility in human. *Zygote* **2013**, *21*, 367–376. [[CrossRef](#)] [[PubMed](#)]

37. Gui, L.; Homer, H. Hec1-dependent cyclin B2 stabilization regulates the G2-M transition and early prometaphase in mouse oocytes. *Dev. Cell* **2013**, *25*, 43–54. [[CrossRef](#)] [[PubMed](#)]
38. De Smedt, V.; Poulhe, R.; Cayla, X.; Dessauge, F.; Karaiskou, A.; Jesus, C.; Ozon, R. Thr-161 phosphorylation of monomeric Cdc2. Regulation by protein phosphatase 2C in *Xenopus* oocytes. *J. Biol. Chem.* **2002**, *277*, 28592–28600. [[CrossRef](#)] [[PubMed](#)]
39. Félix, M.A.; Cohen, P.; Karsenti, E. Cdc2 H1 kinase is negatively regulated by a type 2A phosphatase in the *Xenopus* early embryonic cell cycle: Evidence from the effects of okadaic acid. *EMBO J.* **1990**, *9*, 675–683. [[CrossRef](#)] [[PubMed](#)]
40. Li, J.; Tang, J.-X.; Cheng, J.-M.; Hu, B.; Wang, Y.-Q.; Aalia, B.; Li, X.-Y.; Jin, C.; Wang, X.-X.; Deng, S.-L.; et al. Cyclin B2 can compensate for Cyclin B1 in oocyte meiosis I. *J. Cell Biol.* **2018**. [[CrossRef](#)] [[PubMed](#)]
41. Duncan, F.E.; Jasti, S.; Paulson, A.; Kelsh, J.M.; Fegley, B.; Gerton, J.L. Age-associated dysregulation of protein metabolism in the mammalian oocyte. *Aging Cell* **2017**, *16*, 1381–1393. [[CrossRef](#)] [[PubMed](#)]
42. Xue, S.; Barna, M. Specialized ribosomes: A new frontier in gene regulation and organismal biology. *Nat. Rev. Mol. Cell Biol.* **2012**, *13*, 355–369. [[CrossRef](#)] [[PubMed](#)]
43. Tao, X.; Landis, J.N.; Krisher, R.L.; Duncan, F.E.; Silva, E.; Lonczak, A.; Scott, R.T.; Zhan, Y.; Chu, T.; Scott, R.T.; et al. Mitochondrial DNA content is associated with ploidy status, maternal age, and oocyte maturation methods in mouse blastocysts. *J. Assist. Reprod. Genet.* **2017**, *34*, 1587–1594. [[CrossRef](#)] [[PubMed](#)]
44. Fragouli, E.; Spath, K.; Alfarawati, S.; Kaper, F.; Craig, A.; Michel, C.-E.; Kokocinski, F.; Cohen, J.; Munne, S.; Wells, D. Altered Levels of Mitochondrial DNA Are Associated with Female Age, Aneuploidy, and Provide an Independent Measure of Embryonic Implantation Potential. *PLoS Genet.* **2015**, *11*. [[CrossRef](#)] [[PubMed](#)]
45. Raz, V.; Vermolen, B.J.; Garini, Y.; Onderwater, J.J.M.; Mommaas-Kienhuis, M.A.; Koster, A.J.; Young, I.T.; Tanke, H.; Dirks, R.W. The nuclear lamina promotes telomere aggregation and centromere peripheral localization during senescence of human mesenchymal stem cells. *J. Cell. Sci.* **2008**, *121*, 4018–4028. [[CrossRef](#)] [[PubMed](#)]
46. Maiato, H.; Hergert, P.J.; Moutinho-Pereira, S.; Dong, Y.; Vandenbeldt, K.J.; Rieder, C.L.; McEwen, B.F. The ultrastructure of the kinetochore and kinetochore fiber in *Drosophila* somatic cells. *Chromosoma* **2006**, *115*, 469–480. [[CrossRef](#)] [[PubMed](#)]
47. Schweizer, N.; Pawar, N.; Weiss, M.; Maiato, H. An organelle-exclusion envelope assists mitosis and underlies distinct molecular crowding in the spindle region. *J. Cell Biol.* **2015**, *210*, 695–704. [[CrossRef](#)] [[PubMed](#)]
48. Katsani, K.R.; Karess, R.E.; Dostatni, N.; Doye, V. In vivo dynamics of *Drosophila* nuclear envelope components. *Mol. Biol. Cell* **2008**, *19*, 3652–3666. [[CrossRef](#)] [[PubMed](#)]
49. Tetkova, A.; Hancova, M. Mouse Oocyte Isolation, Cultivation and RNA Microinjection. *Bio-Protocol* **2016**, *6*. [[CrossRef](#)]
50. McGuinness, B.E.; Anger, M.; Kouznetsova, A.; Gil-Bernabé, A.M.; Helmhart, W.; Kudo, N.R.; Wuensche, A.; Taylor, S.; Hoog, C.; Novak, B.; et al. Regulation of APC/C activity in oocytes by a Bub1-dependent spindle assembly checkpoint. *Curr. Biol.* **2009**, *19*, 369–380. [[CrossRef](#)] [[PubMed](#)]
51. Eden, E.; Lipson, D.; Yogeve, S.; Yakhini, Z. Discovering Motifs in Ranked Lists of DNA Sequences. *PLoS Comput. Biol.* **2007**, *3*, e39. [[CrossRef](#)] [[PubMed](#)]
52. Eden, E.; Navon, R.; Steinfeld, I.; Lipson, D.; Yakhini, Z. GOrilla: A tool for discovery and visualization of enriched GO terms in ranked gene lists. *BMC Bioinform.* **2009**, *10*, 48. [[CrossRef](#)] [[PubMed](#)]
53. Motlík, J.; Sutovský, P.; Kalous, J.; Kubelka, M.; Moos, J.; Schultz, R.M. Co-culture with pig membrana granulosa cells modulates the activity of cdc2 and MAP kinase in maturing cattle oocytes. *Zygote* **1996**, *4*, 247–256. [[CrossRef](#)] [[PubMed](#)]
54. Laemmli, U.K. Cleavage of structural proteins during the assembly of the head of bacteriophage T4. *Nature* **1970**, *227*, 680–685. [[CrossRef](#)] [[PubMed](#)]









22 **ABSTRACT**

23 CKS proteins bind cyclin-dependent kinases (CDKs) and play important roles in cell division  
24 control and development, though their precise molecular functions are not fully understood.  
25 Mammals express two closely related paralogs called CKS1 and CKS2, but only CKS2 is  
26 expressed in the germ line indicating it is solely responsible for regulating CDK functions in  
27 meiosis. Using *cks2*<sup>-/-</sup> knockout mice, we show that CKS2 is a crucial regulator of MPF (CDK1-  
28 Cyclin A/B) activity in meiosis. *cks2*<sup>-/-</sup> oocytes display reduced and delayed MPF activity during  
29 meiotic progression, leading to defects in germinal vesicle breakdown (GVBD), anaphase-  
30 promoting complex/cyclosome (APC/C) activation, and meiotic spindle assembly. *cks2*<sup>-/-</sup> germ  
31 cells express significantly reduced levels of MPF components CDK1 and Cyclins A1/B1.  
32 Additionally, injection of MPF + CKS2, but not MPF alone, restored normal GVBD in *cks2*<sup>-/-</sup>  
33 oocytes demonstrating GVBD is driven by a CKS2-dependent function of MPF. Moreover, we  
34 generated *cks2*<sup>*cks1/cks1*</sup> knock-in mice and found CKS1 can compensate for CKS2 in meiosis *in*  
35 *vivo*, but homozygous embryos arrested development at the 2-5-cell stage. Collectively, our  
36 results show that CKS2 is a crucial regulator of MPF functions in meiosis and its paralog CKS1  
37 must be excluded from the germ line for proper embryonic development.

38

39       **INTRODUCTION**

40       Cell division cycle (Cdc) kinase subunit (CKS) proteins were originally identified through their  
41       ability to genetically suppress defective cyclin-dependent kinase (CDK) alleles in both fission (*S.*  
42       *pombe*) and budding (*S. cerevisiae*) yeast <sup>1-3</sup>. Subsequent investigations demonstrated these  
43       small (9-18kD), highly conserved proteins are ubiquitous in eukaryotes and physically interact  
44       with CDKs. Whereas lower eukaryotes express one CKS protein, humans, mice, and possibly  
45       other vertebrates, express two CKS paralogs that are highly similar at the amino acid level <sup>4</sup>.

46               Genetic and biochemical studies mostly in lower eukaryotes have shown that CKS proteins  
47       play important roles in mitosis (M phase), though other molecular functions have been suggested  
48       <sup>5,6</sup>. Genetic disruption of *cks1* in *S. pombe* leads to condensed but unsegregated chromosomes,  
49       an extended spindle structure, and elevated CDK1-Cyclin B kinase activity, consistent with an M  
50       phase arrest <sup>7</sup>. In *Xenopus*, the CKS ortholog Xe-p9 performs multiple essential functions in  
51       both M phase entry and the metaphase-to-anaphase transition <sup>8</sup>.

52               In both mitotic and meiotic cell division cycles M phase is regulated by maturation-  
53       promoting factor (MPF), which is composed of CDK1, Cyclin A/B, and CKS. However, the  
54       precise molecular function(s) of CKS proteins in regulating MPF activity remain unclear. CKS  
55       proteins have been proposed to function as adaptors that physically link CDK-Cyclins to  
56       partially phosphorylated substrates for further phosphorylation <sup>9</sup>. For example, Xe-p9 promotes  
57       CDK1-dependent phosphorylation of CDC25, MYT1, and WEE1 leading to MPF activation <sup>10</sup>,  
58       and MPF-mediated phosphorylation of the anaphase-promoting complex/cyclosome (APC/C)  
59       ubiquitin ligase, which is essential for M phase exit <sup>11</sup>. In *S. cerevisiae*, CKS proteins also  
60       stimulate transcription of APC/C regulator CDC20 by recruiting the 26S proteasome to the  
61       *cdc20* promoter <sup>12</sup>.

62 Mouse knockout studies demonstrate that CKS1/2 perform both redundant and specialized  
63 roles in cell division control and development. *cks1<sup>-/-</sup>* mice are viable and fertile, however adult  
64 mice are ~25% smaller compared to *wild-type (wt)* littermates<sup>13</sup>. *cks1<sup>-/-</sup>* mouse embryo  
65 fibroblasts (MEFs) also grow poorly in culture and senesce prematurely. These physiological  
66 and cellular defects were attributed to a paralog-specific function of CKS1 as an essential  
67 cofactor of the SCF<sup>SKP2</sup> ubiquitin ligase, which promotes the ubiquitin-dependent proteolysis of  
68 several CDK inhibitors including p27<sup>KIP1</sup>, p21<sup>CIP1</sup>, p57<sup>KIP2</sup>, and p130<sup>13,14</sup>. In contrast, *cks2<sup>-/-</sup>*  
69 knockout mice are sterile for both sexes with germ cells failing to progress past metaphase of  
70 meiosis division I<sup>15</sup>. Interestingly, CKS2 is the only CKS paralog that is expressed in oocytes  
71 and spermatocytes, though microinjection of either *cks1* or *cks2* mRNA into *cks2<sup>-/-</sup>* oocytes was  
72 shown sufficient to rescue the metaphase I arrest<sup>15</sup>. Therefore, it is unclear as to why CKS2 is  
73 solely responsible for regulating CDK functions in meiosis. *cks1<sup>-/-</sup> cks2<sup>-/-</sup>* double knockout  
74 (DKO) mice die early in embryogenesis at or before the morula stage (<E3.5), indicating an  
75 essential role for CKS proteins in mammalian development<sup>16</sup>.

76 In the present study, we sought to define the role of CKS2 in regulating MPF functions in  
77 meiosis and determine why CKS2 is the sole CKS paralog expressed in the germ line. Our study  
78 demonstrates that *cks2<sup>-/-</sup>* oocytes exhibit reduced/delayed MPF activity that is attributed to  
79 reduced MPF component expression, leading to defects in germinal vesicle breakdown (GVBD),  
80 APC/C activation, and meiotic spindle assembly. Furthermore, we generated *cks2<sup>cks1/cks1</sup>* knock-  
81 in mice and found that CKS1 can compensate for CKS2 in meiosis *in vivo*, but its expression in  
82 the germ line causes arrest of embryonic development at the 2-5-cell stage.

83

## 84 RESULTS

85 ***cks2*<sup>-/-</sup> oocytes exhibit delayed GVBD and reduced MPF/MAPK kinase activities**

86 CKS2 is required for progression through metaphase of meiosis division I<sup>15</sup>. Therefore, we  
87 investigated whether upstream meiotic events might also be affected by CKS2 deficiency.  
88 Germinal vesicle (GV)-stage oocytes isolated from *cks2*<sup>-/-</sup> mice displayed no obvious defects in  
89 maturation, including the presence of condensed chromatin, when compared to *wt* oocytes (Fig.  
90 1A). However, following resumption of meiosis, *cks2*<sup>-/-</sup> oocytes demonstrated a significant delay  
91 in GVBD (Fig. 1B). Microscopic examination of the GVs revealed that GVBD was delayed  
92 approximately 2 hours in the *cks2*<sup>-/-</sup> oocytes compared to *wt* oocytes (*wt*- 1.05 hours, *cks2*<sup>-/-</sup>- 3.10  
93 hours; *P* < 0.001) (Fig. 1C). Next, analyzed the timing and level of MPF kinase activity in *cks2*<sup>-/-</sup>  
94 oocytes following meiotic resumption using *in vitro* kinase assays with HISTONE H1 as  
95 substrate. Whereas *wt* oocytes exhibited detectable MPF activity within 2 hours following the  
96 resumption of meiosis and maximal activity at approximately 4 hours, MPF activity was detected  
97 in *cks2*<sup>-/-</sup> oocytes at 6 hours with maximal activity at 8 hours (Fig. 1D). In addition, MPF kinase  
98 activity in *cks2*<sup>-/-</sup> oocytes was reduced at all time points compared to *wt* oocytes (Fig. 1D). MPF  
99 activity was previously shown to induce expression of oocyte maturation factor MOS, which  
100 stimulates MAPK activity to promote meiotic spindle assembly<sup>17</sup>. Consistent with this, *in vitro*  
101 kinase assays showed MAPK activity was delayed (*wt*- 4 hours, *cks2*<sup>-/-</sup>- 6 hours) and reduced at  
102 all time points in *cks2*<sup>-/-</sup> oocytes (Fig. 1D). Immunoblot analysis demonstrated that MAPK  
103 phosphorylation, a marker of its activation, was absent in *cks2*<sup>-/-</sup> oocytes at 3 hours post-meiotic  
104 resumption (Fig. 1E). We then analyzed *cks2*<sup>-/-</sup> oocytes for defects in MPF-dependent  
105 downstream processes during meiotic maturation. One target of MPF kinase activity is CDC27,  
106 which activates APC/C ubiquitin ligase activity leading to degradation of Securin and  
107 stimulation of chromatid segregation<sup>18,19</sup>. Immunocytochemical (ICC) analysis demonstrated

108 that CDC27 phosphorylation was absent and Securin persisted at 8 hours post-meiotic  
109 resumption in *cks2<sup>-/-</sup>* oocytes, consistent with a defect in MPF activation (Fig. 1F and 1G).  
110 Collectively, these data demonstrated that *cks2<sup>-/-</sup>* oocytes exhibit delayed GVBD, likely  
111 attributed to delayed and/or reduced MPF/MAPK kinase activities.

## 112 ***cks2<sup>-/-</sup>* germ cells display reduced expression of CDK1 and Cyclins A and B1**

113 To investigate the underlying mechanism(s) for the reduced MPF activity in *cks2<sup>-/-</sup>* oocytes, we  
114 analyzed the expression of MPF components and regulatory factors by qRT-PCR. GV-stage  
115 *cks2<sup>-/-</sup>* oocytes were found to contain significantly reduced levels of *cdk1*, *ccnb1* (Cyclin B1), and  
116 *ccna1* (Cyclin A1) compared to stage matched *wt* oocytes (Fig. 2A). The levels of *cdk2* and  
117 *cdc20* were also reduced in *cks2<sup>-/-</sup>* oocytes. Moreover, *cdk1* expression was found reduced in  
118 *cks2<sup>-/-</sup>* spermatocytes and MEFs (Fig. 2B). Of note, the reduced *cdk1* expression in *cks2<sup>-/-</sup>* MEFs  
119 could be rescued by transduction of cells with CKS2-expressing retroviruses, confirming the  
120 defect was caused by the absence of CKS2 (Fig. 2B). The reduced CDK1 in *cks2<sup>-/-</sup>* oocytes and  
121 spermatocytes was further confirmed by immunoblotting (Fig. 2C and 2D). Furthermore, we  
122 found *cks2<sup>-/-</sup>* oocytes contained increased inhibitory phosphorylation of CDK1 at Tyrosine 15  
123 (Tyr15), which when normalized to total CDK1 levels represented an approximate 40% increase  
124 compared to *wt* oocytes (Fig. 2C and 2E). To explore the potential cause(s) of the reduced  
125 CDK1 expression/activity in *cks2<sup>-/-</sup>* oocytes, we analyzed the expression of CDK1-activating  
126 kinase *wee1* and its transcriptional regulators *e2F1* and *bmyb* by qRT-PCR. Whereas expression  
127 of *wee1*, *e2F1*, and *bmyb* were all reduced in *cks2<sup>-/-</sup>* MEFs and spermatocytes, *wee1* and *e2F1*  
128 were significantly increased in *cks2<sup>-/-</sup>* oocytes (Fig. 2F-2H). Furthermore, retroviral-mediated  
129 expression of CKS2 in *cks2<sup>-/-</sup>* MEFs restored the expression of *wee1* and *e2F1* comparable to *wt*  
130 MEFs (Fig. 2F and 2G). These results suggested that the reduced and delayed MPF activity

131 observed in *cks2*<sup>-/-</sup> germ cells was likely attributed to decreased *cdk1* expression and  
132 dysregulation of CDK1 activation, and CDK1 expression in oocytes may be differentially  
133 regulated compared to other cell types.

#### 134 ***cks2*<sup>-/-</sup> oocytes display defective MI spindle assembly**

135 MPF and MAPK play crucial roles in regulating meiotic spindle assembly<sup>20</sup>. Since *cks2*<sup>-/-</sup>  
136 oocytes exhibited delayed and reduced MPF and MAPK kinase activities, we next determined  
137 whether these cells were also defective in MI spindle assembly. As expected, ICC analysis of  
138 microtubules showed normal spindles formed in *wt* oocytes arrested at metaphase I (Fig. 3A). In  
139 contrast, *cks2*<sup>-/-</sup> oocytes displayed defective spindles with chromosomes failing to align on the  
140 metaphase plate (Fig. 3A). Moreover, *cks2*<sup>-/-</sup> oocytes that arrested in metaphase of MI exhibited  
141 non-separated chromosomes, suggesting a failure to properly resolve chiasmata (Fig. 3B). To  
142 determine whether the spindle assembly defect in *cks2*<sup>-/-</sup> oocytes was caused by reduced MPF  
143 activity, we microinjected inactive or active MPF into *cks2*<sup>-/-</sup> oocytes and examined MI spindle  
144 assembly by ICC. Whereas microinjection of inactive MPF could not rescue the MI spindle  
145 assembly defect, *cks2*<sup>-/-</sup> oocytes microinjected with active MPF displayed partially rescued  
146 spindles (Fig. 3C). We confirmed the inactive and active status of the microinjected MPF by *in*  
147 *vitro* kinase assays (Fig. 3D). These results demonstrated that the MI spindle assembly defect in  
148 *cks2*<sup>-/-</sup> oocytes was likely caused by reduced MPF activity.

#### 149 **Microinjection of active MPF + CKS2 rescues the GVBD delay in *cks2*<sup>-/-</sup> oocytes**

150 We next sought to determine the molecular cause(s) of the GVBD delay in *cks2*<sup>-/-</sup> oocytes. GV-  
151 stage oocytes from *cks2*<sup>-/-</sup> mice were microinjected with various MPF components and the ability  
152 to rescue the GVBD delay assessed by microscopic evaluation. As expected, *cks2*<sup>-/-</sup> oocytes  
153 microinjected with inactive MPF demonstrated delayed GVBD comparable to non-injected *cks2*<sup>-/-</sup>



154 <sup>-/-</sup> oocytes (Fig. 4). In contrast, microinjection of active MPF or recombinant CKS2 protein alone  
155 into *cks2*<sup>-/-</sup> oocytes reduced GVBD delay by nearly 1 hr. However, microinjection of active MPF  
156 + CKS2 protein completely rescued the GVBD delay, comparable to the timing of non-injected  
157 *wt* oocytes. Interestingly, we found that microinjection of recombinant CKS1 protein into *cks2*<sup>-/-</sup>  
158 oocytes rescued the GVBD delay more effectively than CKS2 protein, and was nearly  
159 comparable to *cks2*<sup>-/-</sup> oocytes microinjected with active MPF + CKS2 protein. These results  
160 demonstrated that CKS2-dependent MPF functions mediate GVBD in mammalian oocytes.

### 161 **CKS1 can compensate for CKS2 in mammalian meiosis but is deleterious for early** 162 **embryonic development**

163 Previously it was shown that microinjection of *cks1* mRNA into *cks2*<sup>-/-</sup> oocytes could rescue the  
164 metaphase I arrest<sup>15</sup>. Additionally, our data above shows that microinjection of CKS1 protein  
165 into *cks2*<sup>-/-</sup> oocytes rescues the GVBD delay more effectively than CKS2 (Fig. 4). It is therefore  
166 perplexing as to why CKS1 is excluded from the germ line if it can compensate for CKS2  
167 functions in meiosis *in vitro*. To address this question, we generated knock-in (KI) mice that  
168 express *cks1* from the endogenous *cks2* promoter by homologous recombination (designated  
169 *cks2*<sup>*cks1/cks1*</sup>) (Fig. 5A). Heterozygous *cks2*<sup>*cks1/+*</sup> ES cells were injected into mouse blastocysts to  
170 generate chimeras and germ line transmission confirmed by PCR (Fig. 5B). *cks2*<sup>*cks1/+*</sup> mice were  
171 interbred and produced *cks2*<sup>*cks1/+*</sup> and *cks2*<sup>*+/+*</sup> mice at approximately the expected 2:1 ratio,  
172 however no homozygous *cks2*<sup>*cks1/cks1*</sup> mice were detected out of 283 adult mice genotyped (Fig.  
173 5C). We also failed to detect *cks2*<sup>*cks1/cks1*</sup> mid-gestation embryos between E7.5 and E13.5 from  
174 83 embryos genotyped (Fig. 5C). These results suggested that *cks2*<sup>*cks1/cks1*</sup> mice were not viable.  
175 In support of this, *cks2*<sup>*cks1/+*</sup> intercrosses demonstrated a 25% frequency of embryo reabsorption  
176 *in utero*, compared to only 2% for *wt* intercrosses (Fig. 5D and 5E). We therefore examined

177 *cks2<sup>cks1/+</sup>* intercrosses for blastocyst formation at E3.5. Whereas 69% of embryos from *cks2<sup>cks1/+</sup>*  
178 intercrosses matured to form normal blastocysts at E3.5, 15% arrested development at the 2-cell  
179 stage and 16% arrested at the 4-5-cell stage (Fig. 5F). By comparison, the frequency of 2-5-cell  
180 stage E3.5 embryos from *wt* intercrosses was only 2% (data not shown). Genotyping of the 2-5-  
181 cell stage embryos from *cks2<sup>cks1/+</sup>* intercrosses revealed they were homozygous for the *cks2<sup>cks1</sup>*  
182 allele (Fig. 5G). In contrast, normal blastocysts isolated from the *cks2<sup>cks1/+</sup>* intercrosses were  
183 either *wt* or *cks2<sup>cks1/+</sup>* genotypes (Fig. 5G). These data demonstrated that CKS1 could  
184 compensate for CKS2 in meiosis and *cks2<sup>cks1</sup>* oocytes could be appropriately fertilized. To  
185 investigate why the *cks2<sup>cks1/cks1</sup>* embryos arrested development, we molecularly analyzed MEFs  
186 derived from *cks2<sup>cks1/+</sup>* embryos. *cks2<sup>cks1/+</sup>* MEFs were contained reduced CDK1 expression and  
187 increased inhibitory pTyr15-CDK1 compared to *wt* MEFs (Fig. 5H). In addition, *cks2<sup>cks1/+</sup>*  
188 MEFs contained increased CDK2 and reduced p27<sup>KIP1</sup>, a substrate of SCF<sup>SKP2-CKS1</sup>-mediated  
189 degradation. These results demonstrated that although CKS1 could compensate for CKS2 in  
190 mammalian meiosis, its expression in the germ line was deleterious for early embryonic  
191 development.

## 193 **DISCUSSION**

### 194 **Delayed GVBD in *cks2<sup>-/-</sup>* oocytes**

195 MPF regulates various cellular and molecular events during meiotic maturation, including  
196 GVBD, APC/C-mediated degradation of Cyclin B1 and Securin, polar body extrusion, and  
197 spindle assembly<sup>21,22</sup>. KKS proteins are a component of MPF, but their precise role(s) in  
198 regulating MPF functions during meiosis had not been fully delineated. Previously it was shown  
199 that *cks2<sup>-/-</sup>* oocytes arrest maturation at metaphase of meiosis division I<sup>15</sup>. In the present study,

200 we extended these observations and now show that *cks2*<sup>-/-</sup> oocytes exhibit delayed GVBD. In  
201 mouse oocytes, GVBD is promoted by a surge in MPF-associated kinase activity that plateaus as  
202 oocytes approach metaphase of MI<sup>23,24</sup>. Consistent with the observed delay in GVBD we found  
203 that MPF-associated kinase activity was delayed and reduced at all time points in *cks2*<sup>-/-</sup> oocytes  
204 following meiotic resumption. A similar delay was also observed for MAPK-associated kinase  
205 activity, which is stimulated by MPF<sup>17</sup>. However, we found that microinjection of active MPF  
206 into *cks2*<sup>-/-</sup> oocytes could not completely rescue the GVBD delay, though the delay was rescued  
207 by MPF + CKS2. These data suggest that CKS2-dependent functions of MPF promote GVBD in  
208 mammalian oocytes.

209 It has been reported that deletion of CDK1 promotes the permanent arrest of oocytes at the  
210 GV stage, indicating CDK1 is the sole CDK that is required and sufficient for the resumption of  
211 meiosis in mouse oocytes<sup>23</sup>. Moreover, microinjection of CDK1 into *cdk1*<sup>-/-</sup> oocytes leads to  
212 progression and arrest in metaphase I<sup>25</sup>. Our finding that GVBD is delayed in *cks2*<sup>-/-</sup> oocytes  
213 suggests the absence of CKS2 could compromise CDK1 functions, possibly altering MPF's  
214 ability to target substrates whose phosphorylation promote GVBD. The substrates of MPF-  
215 CKS2 that promote GVBD in mammalian oocytes are currently not known.

### 216 **Defects in MPF expression in *cks2*<sup>-/-</sup> germ and somatic cells**

217 During meiotic maturation cellular events are ordered in a timely manner, which is regulated by  
218 the level of Cyclin B<sup>26</sup>. Previously it was shown in budding yeast that CKS plays a direct role in  
219 transcriptional regulation by promoting the recruitment of CDK1 and the proteasome to coding  
220 regions<sup>27</sup>. In mammalian cells, depletion of CKS1 + CKS2 impairs the transcription of *ccnb1*,  
221 *ccna2*, and *cdk1*<sup>16</sup>. CKS2 was shown to associate with the promoters and open-reading frames  
222 (ORFs) of these genes in G<sub>2</sub> phase cells, possibly contributing to their transcriptional activation,

223 though the precise mechanism of action has not been delineated. We found that the levels of  
224 *ccna1*, *ccnb1*, *cdc20*, *cdk1* and *cdk2* mRNAs were all downregulated in *cks2*<sup>-/-</sup> oocytes.  
225 Interestingly, the corresponding genes that encode these mRNAs harbor cell cycle-dependent  
226 element and cell cycle genes homology regions (CDE/CHR) repressive promoter elements,  
227 which allow for expression in G<sub>2</sub>-M phase of the cell division cycle <sup>28</sup>. Our finding that *cks2*<sup>-/-</sup>  
228 oocytes, spermatocytes, and MEFs all contain reduced levels of *cdk1* mRNA suggests that CKS2  
229 is an important transcriptional regulator of *cdk1* in germ and somatic cells. It will be of interest  
230 to determine whether CKS2 associates with the promoters of these genes during oocyte and  
231 spermatocyte maturation and whether CDE/CHR promoter elements play a role in regulating  
232 gene expression during meiosis.

### 233 **CKS1 can compensate for CKS2 in meiosis *in vitro***

234 CKS1 and CKS2 have been shown to have both redundant and specialized roles in cell division  
235 control. For example, both CKS1 and CKS2 can bind CDK1 in human somatic cells <sup>4</sup>.  
236 Additionally, the viability of *cks1*<sup>-/-</sup> and *cks2*<sup>-/-</sup> mice demonstrates that either CKS homolog can  
237 drive mitotic cell division cycles and development <sup>13,15</sup>. However, CKS1 accumulates in G<sub>1</sub>/S  
238 phase and CKS2 in G<sub>2</sub>/M in human cells, suggesting differential functions. One specialized  
239 function of CKS1 that has been identified is its role as an essential co-factor of the SCF<sup>SKP2</sup>  
240 ubiquitin ligase, which mediates the degradation of several CDK2 inhibitors at the G<sub>1</sub>/S phase  
241 transition. Since CKS2 is the only CKS paralog expressed in mouse oocytes and spermatocytes,  
242 it is suggested that CKS2 performs a specialized role in regulating CDK functions in mammalian  
243 meiosis <sup>15</sup>. Though, previously it was shown that microinjection of *cks1* mRNA into *cks2*<sup>-/-</sup>  
244 oocytes could rescue the metaphase I arrest <sup>15</sup>. In the current study, we also found that  
245 microinjection of CKS1 into prophase-arrested germinal vesicle (GV) stage *cks2*<sup>-/-</sup> oocytes

246 promoted GVBD. Collectively, these results demonstrate that although CKS1 is excluded from  
247 the germ line it can compensate for CKS2 functions in meiotic progression *in vitro*.

### 249 **CKS1 is deleterious for early mammalian development**

250 The exclusion of CKS1 from the mouse germ line is perplexing since CKS1 rescues the GVBD  
251 delay and metaphase I arrest in *cks2*<sup>-/-</sup> oocytes. Analysis of *cks2*<sup>*cks1/cks1*</sup> mice showed that CKS1  
252 could compensate for CKS2 in meiosis *in vivo*, since *cks2*<sup>*cks1*</sup> oocytes were generated and could  
253 be fertilized. However, homozygous *cks2*<sup>*cks1/cks1*</sup> embryos arrested development at the 2-5-cell  
254 stage, indicating that although CKS1 can compensate for CKS2 function in meiosis its  
255 expression in the germ line and early embryonic cell division cycles is deleterious for  
256 development. The fact that both *cks1*<sup>-/-</sup> and *cks2*<sup>-/-</sup> mice are viable indicates the premature  
257 expression of CKS1 in *cks2*<sup>*cks1/cks1*</sup> germ cells and embryos is likely responsible for the observed  
258 developmental arrest.

259 At the molecular level, the arrest of *cks2*<sup>*cks1/cks1*</sup> embryos at the 2-5-cell stage could be  
260 caused by CKS1 blocking the activation of MPF in early cell division cycles. In *Xenopus*, CKS  
261 homolog Xe-p9 promotes CDK1-dependent phosphorylations of CDC25, MYT1, and WEE1,  
262 which in turn promote MPF activation<sup>10</sup>. It might be possible that CKS1 expressed from the  
263 *cks2* promoter, which displays differential strength and cell cycle regulation, could block these  
264 phosphorylations leading to defective CDK1 activation. In support of this, we observed  
265 significantly increased pThr15-CDK1 in *cks2*<sup>*cks1/+*</sup> MEFs. Alternatively, CKS1 could interfere  
266 with the phosphorylation of substrate(s) that are required for early embryonic cell division cycles  
267 that are normally mediated by MPF or MPF-CKS2. Another possibility is the expression of  
268 CKS1 in the germ line could promote the premature activation of CDK2 and initiation of somatic

269 cell division cycles as was previously suggested <sup>29</sup>. *cdk2*<sup>-/-</sup> mice of both sexes are sterile with  
270 oocytes failing to transition from the pachytene to diplotene stage of prophase I <sup>30,31</sup>. In contrast,  
271 oocyte-specific deletion of *cdk2* from the primordial follicle stage showed that CDK2 is not  
272 required for oocyte maturation and female fertility <sup>23</sup>. These results suggest that CDK2 is  
273 dispensable for meiotic resumption of GV-stage oocytes. Very little is known regarding the  
274 precise functions of CDK2 in the transition from meiotic to somatic cell division cycles. We  
275 found that *cks2*<sup>*cks1/+*</sup> MEFs contained significantly reduced levels of p27<sup>KIP1</sup>, a CDK2 inhibitor  
276 whose degradation is dependent on CDK2 activity and the SCF<sup>SKP2-CKS1</sup> ubiquitin ligase <sup>13,14</sup>.  
277 This data suggests that *cks1* expressed from the *cks2* promoter could drive the degradation of  
278 CDK2 inhibitors, resulting in the premature activation of CDK2-associated kinase activity.  
279 CKS1 could also promote the premature paralog-specific phosphorylation of CDK2 substrates  
280 during meiosis or early embryonic cell cycles, leading to the observed developmental arrest.  
281 Further studies will be needed to determine if the developmental arrest of *cks2*<sup>*cks1/cks1*</sup> embryos is  
282 CDK2-dependent, and if so, what substrates are prematurely targeted by CDK2-CKS1.

283 In summary, our study shows that CKS2 is a crucial regulator of MPF activity during  
284 meiosis and its deletion in oocytes results in delayed MPF activation and GVBD, and defective  
285 spindle assembly. Furthermore, *cks2*<sup>*cks1/cks1*</sup> knock-in mice revealed that CKS1 could compensate  
286 for CKS2 in mammalian meiosis *in vivo*, but its expression in the germ line is deleterious for  
287 early embryonic development.



289 **MATERIALS AND METHODS**

290 **Oocyte collection, culture, and microinjection**

291 All animal work was conducted according to Act No. 246/1992 for the protection of animals  
292 against cruelty. All institutional and national guidelines for the care and use of laboratory  
293 animals were followed accordingly. Oocytes were obtained from 8-12 week old *cks2<sup>-/-</sup>* and *wt*  
294 female mice after injection with 5 IU of pregnant mare serum gonadotropin 43-48 hours prior to  
295 scarification by cervical dislocation. Oocytes were collected in preheated M2 medium  
296 supplemented with 2.5  $\mu$ M milrinone (Sigma-Aldrich) or 100 nM 3-isobutyl-1-metyl-xanthine  
297 (IBMX, Sigma-Aldrich) to prevent meiotic maturation, denuded by pipetting, washed and  
298 cultured in M16 medium (Sigma-Aldrich) supplemented with 0.22 mM sodium pyruvate,  
299 4 mg/ml BSA (Sigma-Aldrich), and 1% penicillin/streptomycin (Sigma-Aldrich) at 37°C in 5%  
300 CO<sub>2</sub> atmosphere. After a IBMX/milirinone wash, at least 90% of oocytes resumed meiosis  
301 (GVBD) within 70 min.

302 GV stage oocytes were microinjected in transfer medium (Hancova/Tetkova, bioprotocols)  
303 with IBMX on an inverted Leica DMI 6000B microscope with Transferman NK2 and Femtojet  
304 (Eppendorf). Approximately 5 pl of solution of active CDK1-Cyclin B1 cocktail (SRP5009,  
305 Sigma) and/or recombinant proteins diluted in RNase-free water was microinjected. Inactivated  
306 MPF cocktail was obtained by denaturation at 95°C for 5 min.

307

308 **Spermatocyte isolation and separation**

309 A pool of spermatogenic cells were isolated from the testes of mice. Testes were decapsulated  
310 and transferred to 20 ml of TIM (testis isolation medium; 0.1 M NaCl, 0.05 M KCl, 1.2 mM  
311 CaCl<sub>2</sub>, 1.2 mM MgSO<sub>4</sub>, 6 mM Na<sub>2</sub>HPO<sub>4</sub>, 0.7 mM KH<sub>2</sub>PO<sub>4</sub>, 0.1% glucose, 0.04% L-glutamine, 1

312 mM sodium pyruvate, 6 mM sodium-DL-lactate and antibiotics). The seminiferous tubules were  
313 dispersed by incubation with 2 mg/ml collagenase followed by 0.35 mg/ml trypsin and the  
314 reaction stopped by addition of 1% BSA. Pachytene spermatocytes were separated by STA-PUT  
315 velocity sedimentation. Different cell types were sedimented through a linear BSA gradient  
316 according to their cell size. Pachytene spermatocytes were collected and optionally cultured in  
317 medium with 2-5  $\mu$ M oocadaic acid (Sigma-Aldrich) for 2 hours to induce meiotic maturation.

### 319 **Kinase assays**

320 CDK1 and MAP kinase activities were measured by their capability to phosphorylate external  
321 substrates HISTONE H1 and MBP, respectively<sup>32</sup>. Ten oocytes per sample were collected at the  
322 indicated times and lysed in 5  $\mu$ l of homogenization buffer (40 mM MOPS (pH 7.2), 20 mM  
323 NaF, 20 mM para-nitrophenyl phosphate, 40 mM  $\beta$ -glycerophosphate, 0.2 mM  $\text{Na}_3\text{VO}_4$ , 10 mM  
324 EGTA, 0.2 mM EDTA, 2 mM benzamidine, 20  $\mu$ g/ml leupeptin and 20  $\mu$ g/ml aprotinin, 1 mM  
325 phenyl-methylsulphonyl fluoride) by three to five cycles of freezing/thawing in liquid nitrogen.  
326 Next, 2.5  $\mu$ l of 4x kinase buffer (50 mM MOPS (pH 7.2), 10 mM  $\text{MgCl}_2$ , 5 mM EGTA, 0.1 mM  
327 EDTA, 1 mM DTT, 0.4  $\mu$ M protein kinase C inhibitor 1, and cocktail of phosphatases and  
328 proteases inhibitors) containing 10 mg/ml HISTONE H1, and 5 mg/ml MBP was mixed with 1.5  
329  $\mu$ l of 0.1 mM ATP and 1  $\mu$ l of 10 mCi/ml [ $\gamma$ -<sup>32</sup>P] ATP (Amersham Pharmacia Biotech) and  
330 incubated with the lysed sample for 30 min at 37 °C. Reactions were terminated by the addition  
331 of SDS-PAGE loading buffer and incubation at 95°C for 5 min. Samples were then run on 12%  
332 SDS-PAGE gels, dried, and subjected to autoradiography.

### 334 **qRT-PCR analysis**

335 RNA was isolated from mouse oocytes by adding 10 µl of lysis buffer and 1 µl of enhancer,  
336 incubated for 10 min at 75°C, followed by DNase treatment for 10 min at room temperature.  
337 RNA from MEFs and spermatocytes was isolated using the RNeasy Plus Minikit (Qiagen). qRT-  
338 PCR reactions were performed using standard techniques. Primers were designed on the intron  
339 borders to eliminate potential DNA amplifications. Sequences of primers used were: *cdk1* (5'-  
340 CTCGGCTCGTTACTCCACTC-3', 5'-ACTCGACTTCTGGCCACACT-3'); *ccnb1* (5'-  
341 CTTGGAGAGGGATTATCA-3', 5'-ACCAGAGGTGGAAGTTGCTG-3'); *ccna1* (5'-  
342 GTGGTGATTCAAACTGCCA-3', 5'-GGCCAGCTGAGCTTAAAGAA-3'); *cdk2* (5'-  
343 GAAATTCTTCTGGGCTGCAA-3', 5'-CGAAAGATCCGGAAGAGTTG-3'); *e2f1* (5'-  
344 CAGCATGTTGTCAGTGGCTT-3', 5'-GGGATCGCAGAGACCATAGA-3'); *bmyb* (5'-  
345 TCTGGATGAGTTACACTACCAGG-3', 5'-GTGCGGTTAGGAAAGTGACTG-3'); *cdc20*  
346 (5'-CTGGAGGTGACCGCTTTATCC-3', 5'-TCAAACCGTTCAGGTTGAGAGA-3'); and  
347 *gapdh* (5'-TTGAGGTCAATGAAGGGGTC-3', 5'-TCGTCCCGTAGACAAAATGG-3').

348

### 349 **Immunocytochemistry (ICC)**

350 Oocytes were fixed in 4% paraformaldehyde (PFA) in PBS for 30 min, permeabilized for 15 min  
351 in PBS with 0.1% Triton X-100, and incubated overnight at 4 °C with primary antibodies (1:100)  
352 against p-CDC27 (Abcam, ab12281), SECURIN, acetylated TUBULIN (Sigma-Aldrich, T6793),  
353 CREST (Thermo Fisher) and LAMIN A/C (Sigma-Aldrich, SAB4200236). Cortical ACTIN was  
354 visualized by ACTIN Green Phalloidin 488 (Thermo Fisher). After washing, the oocytes were  
355 incubated for 1 hour at room temperature with Alexa Fluor-conjugated antibodies (1:250;  
356 Molecular Probes). DAPI was used for chromosome staining (Vectashield). Samples were

357 visualized using an inverted confocal microscope in 16 bit depth (Leica, TCS SP5). Images were  
358 assembled in Photoshop CS3.

359

### 360 **Live-cell imaging**

361 Oocytes at 1-2 hours post-microinjection were washed in transfer medium and transferred in  
362 M16 medium to a Leica AF6000 wide-field automated microscope equipped with a conditioned  
363 chamber of 37°C and 5% CO<sub>2</sub> atmosphere. Time lapse imaging was performed for 16 hours  
364 using Leica LAS AF software. Progression of meiotic maturation was analyzed manually.

365

### 366 **MEF isolation and retroviral infections**

367 MEFs (*wt*, *cks2*<sup>-/-</sup>, *cks2*<sup>*cks1*+/+</sup>) were derived by incubating E13.5 embryos, devoid of internal  
368 organs or head, in 0.5% trypsin for 3 hours at 37°C and then seeding cells in DMEM medium  
369 supplemented with 10% FBS. At least 3 embryos of the same genotype were pooled and cells  
370 passaged for 2-3 population doublings before performing the described experiments. MEFs were  
371 infected with retroviruses (pBABE) that express Flag-*cks2* using standard techniques.

372

### 373 **SDS-PAGE and western blot analysis**

374 Cells were lysed in RIPA buffer (150 mM NaCl, 5 mM EDTA, 0.05% NP-40, 1% sodium  
375 deoxycholate, 0.1% SDS, 1% Triton X-100, 50 mM Tris-HCl (pH 7.4) with phosphatase and  
376 protease inhibitors), sonicated, and centrifuged at 10,000 x g for 10 min at 4°C. Samples were  
377 adjusted to the total number of oocytes or total protein (10 µg of total protein per sample) and  
378 loaded onto 12% or 15% Tris-acetate gels. Gels were transferred onto PVDF membranes,  
379 blocked in 5% skimmed milk in 1x TBST, and probed overnight at 4°C with antibody diluted in

380 5% milk in 1x TBST. The following antibodies were used: anti-p-Tyr15 CDK1 (Cell Signaling,  
381 cs-4539); anti-CDK1 (Santa Cruz Biotechnology, sc-8395); anti-CDK2 (Santa Cruz  
382 Biotechnology, sc-6248); anti-p27<sup>KIP1</sup> (BD Biosciences, 610241); anti-ACTIN (Santa Cruz  
383 Biotechnology, sc-58673); anti-p-p44/42 MAPK (Thr202/Tyr204) (Cell Signaling, cs-9101); and  
384 anti-p44/42 MAPK (Cell Signaling, cs-9102). Secondary antibodies conjugated with HRP (anti-  
385 mouse, Jackson ImmunoResearch, #711-035-152, or anti-rabbit, Jackson ImmunoResearch,  
386 #711-035-152) were used. The signals were revealed by chemiluminescence (ECL, APCzech,  
387 #28980926).

388

### 389 **Generation of *cks2<sup>cks1</sup>* knock-in mice**

390 A *cks2<sup>cks1</sup>* replacement vector was constructed based on the vector pBKSII-FRT-mc/Neo. DNA  
391 fragments of 1.8 kb and 5.5 kb in length corresponding to sequences immediately upstream and  
392 downstream of the mouse *cks2* coding region, respectively, were amplified using a high-fidelity  
393 polymerase, verified by DNA sequencing, and sub-cloned into the cloning sites flanking the Frt-  
394 mc/Neo-Frt cassette. *cks1* cDNA containing a stop codon was then cloned into the vector such  
395 that proper homologous recombination would result in *cks1* expression under control of the *cks2*  
396 promoter, with the appropriate upstream and 3' UTR sequences. A *pgk-dta* cassette was  
397 included for negative selection. The *cks2<sup>cks1</sup>* knock-in vector was then electroporated into  
398 *129svj* embryonic stem (ES) cells and neomycin-resistant (Neo<sup>r</sup>) clones isolated. Positive ES  
399 cell clones were identified by southern blotting and then subsequently injected into *c57bl/6j*  
400 blastocysts to generate chimeric mice. Germline transmission of the *cks2<sup>cks1</sup>* allele was followed  
401 by PCR. The Mc/Neo cassette was then excised by crossing *cks2<sup>cks1/+</sup>* mice with *frt*-expressing  
402 transgenic mice.

403

#### 404 **Southern blotting and genotyping**

405 Southern blot analysis was performed using an 1138 bp probe corresponding to a DNA sequence  
406 adjacent to the *cks2* mouse locus that was amplified with primers 5'-  
407 ACTCTGCTCATGACCCACCT-3' and 5'-TTTGGTTTTCAAATGCACCA-3'. DNA from  
408 Neo<sup>f</sup> ES clones was cut with EcoRI. A 9.9 kb band was predicted for the *wt* allele and a 8.7 kb  
409 band indicated proper homologous recombination. PCR-based genotyping of adult mice and  
410 embryos was performed using a multiplexed PCR with primers 5'-  
411 GCAACAGGCTTCTGATTGGT-3', 5'-ACATGACATGCCGGTATTTCG-3', and 5'-  
412 TAACGACTCCCCATCTCCTG-3'. A 293 bp product corresponded to the *cks2<sup>cks1</sup>* allele and a  
413 424 bp product to the *wt cks2* allele. Deletion of the FRT cassette was determined by inclusion  
414 of primer 5'-ACGAATGTGGCACCTGAACT-3'. DNA was isolated from blastocysts and early  
415 embryos by adding 5 µl of 10 mM Tris and 5 mM EDTA and boiling for 3 min. Proteinase K (1  
416 µg/µl solution) was added and incubated overnight at 56°C and then heat inactivated.

417 DNA (5 µl) was then genotyped using a nested PCR protocol with external primers 5'-  
418 GAGCAATTCATCCACTGCAA-3' and 5'-TCAACAATGGTGATATAAATGCAA-3' and  
419 internal primers 5'-TGATCCCGCTTACTCCTCTG, 5'-ATCCCTGACTCTGCTGAACG-3',  
420 and 5'-CCATCTAACGACTCCCCATC-3'. The *cks2<sup>cks1</sup>* allele corresponded to a 198 bp PCR  
421 product and *wt cks2* allele a 333 bp product.

422

#### 423 **Embryo/blastocyst isolations**

424 Two month old female *cks2<sup>cks1/+</sup>* mice from the same litter were injected with 5 IU of pregnant  
425 mare serum gonadotropin and 5 IU of human chorionic gonadotropin (hCG) 43-48 hours prior to



426 mating with males. The next morning, females positive for vaginal plugs were separated. Mice  
427 were sacrificed at day E3.5 for blastocyst isolations and day E7.5 or later for embryo isolations.  
428 Blastocysts were then flushed from oviducts with preheated M2 media (Sigma-Aldrich),  
429 photographed, and subsequently used for genotyping or ICC analysis.

### 431 **Statistical analysis**

432 All experiments were repeated at least three times unless otherwise indicated. Mean and SD  
433 values were calculated using MS Excel and statistical significance tested using the Student's t-  
434 test (PrismaGraph5), with a  $P < 0.05$  considered statistically significant.

### 436 **ACKNOWLEDGEMENTS**

437 We thank Dr. Silvia Evans (University of California at San Diego) for plasmid pBKSII-FRT-  
438 mc/Neo and Frt-expressing transgenic mice. We thank Jaroslava Supolikova, Marketa Hancova,  
439 and Marie Valova for their exceptional assistance with experiments. This work was supported  
440 by NIH/NICHD grant 7RO1HD049539 to C.S. and by the National Sustainability Programme  
441 Project number LO1609 (Czech Ministry of Education, Youth and Sports) and GACR15-22765S  
442 and 18-19395S EXCELLENCE CZ.02.1.01/0.0/0.0/15\_003/0000460 OP RDE and Institutional  
443 Research Concept RVO67985904.

### 445 **REFERENCES**

- 446 1 Hayles J, Beach D, Durkacz B, Nurse P. The fission yeast cell cycle control gene  
447 *cdc2*: isolation of a sequence *suc1* that suppresses *cdc2* mutant function. *Mol Gen*  
448 *Genet* 1986;**202**:291–3.

- 449           2     Hadwiger JA, Wittenberg C, Mendenhall MD, Reed SI. The *Saccharomyces*  
450                    *cerevisiae* CKS1 gene, a homolog of the *Schizosaccharomyces pombe* *suc1+* gene,  
451                    encodes a subunit of the Cdc28 protein kinase complex. *Mol Cell Biol*  
452                    1989;**9**:2034–41.
- 453           3     Reed SI, Hadwiger JA, Richardson HE, Wittenberg C. Analysis of the Cdc28  
454                    protein kinase complex by dosage suppression. *J Cell Sci Suppl* 1989;**12**:29–37.
- 455           4     Richardson HE, Stueland CS, Thomas J, Russell P, Reed SI. Human cDNAs  
456                    encoding homologs of the small p34Cdc28/Cdc2-associated protein of  
457                    *Saccharomyces cerevisiae* and *Schizosaccharomyces pombe*. *Genes Dev*  
458                    1990;**4**:1332–44.
- 459           5     Tang Y, Reed SI. The Cdk-associated protein Cks1 functions both in G1 and G2 in  
460                    *Saccharomyces cerevisiae*. *Genes Dev* 1993;**7**:822–32.
- 461           6     Reynard GJ, Reynolds W, Verma R, Deshaies RJ. Cks1 is required for G(1)  
462                    cyclin-cyclin-dependent kinase activity in budding yeast. *Mol Cell Biol*  
463                    2000;**20**:5858–64.
- 464           7     Moreno S, Hayles J, Nurse P. Regulation of p34cdc2 protein kinase during mitosis.  
465                    *Cell* 1989;**58**:361–72.
- 466           8     Patra D, Dunphy WG. Xe-p9, a *Xenopus* Suc1/Cks homolog, has multiple  
467                    essential roles in cell cycle control. *Genes Dev* 1996;**10**:1503–15.
- 468           9     Bourne Y, Watson MH, Hickey MJ, Holmes W, Rocque W, Reed SI, *et al.* Crystal  
469                    structure and mutational analysis of the human CDK2 kinase complex with cell  
470                    cycle-regulatory protein CksHs1. *Cell* 1996;**84**:863–74.
- 471           10    Patra D, Wang SX, Kumagai A, Dunphy WG. The *xenopus* Suc1/Cks protein

- 472 promotes the phosphorylation of G(2)/M regulators. *J Biol Chem* 1999;**274**:36839–  
473 42.
- 474 11 Patra D, Dunphy WG. Xe-p9, a *Xenopus* Suc1/Cks protein, is essential for the  
475 Cdc2-dependent phosphorylation of the anaphase-promoting complex at mitosis.  
476 *Genes Dev* 1998;**12**:2549–59.
- 477 12 Morris MC, Kaiser P, Rudyak S, Baskerville C, Watson MH, Reed SI. Cks1-  
478 dependent proteasome recruitment and activation of CDC20 transcription in  
479 budding yeast. *Nature* 2003;**423**:1009–13. <https://doi.org/10.1038/nature01720>.
- 480 13 Spruck C, Strohmaier H, Watson M, Smith AP, Ryan A, Krek TW, *et al.* A CDK-  
481 independent function of mammalian Cks1: targeting of SCF(Skp2) to the CDK  
482 inhibitor p27Kip1. *Mol Cell* 2001;**7**:639–50.
- 483 14 Ganoth D, Bornstein G, Ko TK, Larsen B, Tyers M, Pagano M, *et al.* The cell-  
484 cycle regulatory protein Cks1 is required for SCF(Skp2)-mediated ubiquitinylation  
485 of p27. *Nat Cell Biol* 2001;**3**:321–4. <https://doi.org/10.1038/35060126>.
- 486 15 Spruck CH, de Miguel MP, Smith APL, Ryan A, Stein P, Schultz RM, *et al.*  
487 Requirement of Cks2 for the first metaphase/anaphase transition of mammalian  
488 meiosis. *Science* 2003;**300**:647–50. <https://doi.org/10.1126/science.1084149>.
- 489 16 Martinsson-Ahlzen H-S, Liberal V, Grunenfelder B, Chaves SR, Spruck CH, Reed  
490 SI. Cyclin-Dependent Kinase-Associated Proteins Cks1 and Cks2 Are Essential  
491 during Early Embryogenesis and for Cell Cycle Progression in Somatic Cells. *Mol*  
492 *Cell Biol* 2008;**28**:5698–709. <https://doi.org/10.1128/MCB.01833-07>.
- 493 17 Minshull J, Sun H, Tonks NK, Murray AW. A MAP kinase-dependent spindle  
494 assembly checkpoint in *Xenopus* egg extracts. *Cell* 1994;**79**:475–86.

- 495 18 Kotani S, Tanaka H, Yasuda H, Todokoro K. Regulation of APC activity by  
496 phosphorylation and regulatory factors. *J Cell Biol* 1999;**146**:791–800.
- 497 19 Huang J-Y, Morley G, Li D, Whitaker M. Cdk1 phosphorylation sites on Cdc27  
498 are required for correct chromosomal localisation and APC/C function in syncytial  
499 *Drosophila* embryos. *J Cell Sci* 2007;**120**:1990–7.  
500 <https://doi.org/10.1242/jcs.006833>.
- 501 20 Brunet S, Pahlavan G, Taylor S, Maro B. Functionality of the spindle checkpoint  
502 during the first meiotic division of mammalian oocytes. *Reproduction*  
503 2003;**126**:443–50.
- 504 21 Choi T, Aoki F, Mori M, Yamashita M, Nagahama Y, Kohmoto K. Activation of  
505 p34cdc2 protein kinase activity in meiotic and mitotic cell cycles in mouse oocytes  
506 and embryos. *Development* 1991;**113**:789–95.
- 507 22 Verlhac MH, Kubiak JZ, Clarke HJ, Maro B. Microtubule and chromatin behavior  
508 follow MAP kinase activity but not MPF activity during meiosis in mouse oocytes.  
509 *Development* 1994;**120**:1017–25.
- 510 23 Adhikari D, Zheng W, Shen Y, Gorre N, Ning Y, Halet G, *et al.* Cdk1, but not  
511 Cdk2, is the sole Cdk that is essential and sufficient to drive resumption of meiosis  
512 in mouse oocytes. *Hum Mol Genet* 2012;**21**:2476–84.  
513 <https://doi.org/10.1093/hmg/dds061>.
- 514 24 Adhikari D, Liu K. The regulation of maturation promoting factor during prophase  
515 I arrest and meiotic entry in mammalian oocytes. *Mol Cell Endocrinol*  
516 2014;**382**:480–7. <https://doi.org/10.1016/j.mce.2013.07.027>.
- 517 25 Santamaría D, Barrière C, Cerqueira A, Hunt S, Tardy C, Newton K, *et al.* Cdk1 is

- 518 sufficient to drive the mammalian cell cycle. *Nature* 2007;**448**:811–5.  
519 <https://doi.org/10.1038/nature06046>.
- 520 26 Polanski Z, Ledan E, Brunet S, Louvet S, Verlhac MH, Kubiak JZ, *et al.* Cyclin  
521 synthesis controls the progression of meiotic maturation in mouse oocytes.  
522 *Development* 1998;**125**:4989–97.
- 523 27 Yu VPCC, Baskerville C, Grünenfelder B, Reed SI. A kinase-independent function  
524 of Cks1 and Cdk1 in regulation of transcription. *Mol Cell* 2005;**17**:145–51.  
525 <https://doi.org/10.1016/j.molcel.2004.11.020>.
- 526 28 Müller GA, Engeland K. The central role of CDE/CHR promoter elements in the  
527 regulation of cell cycle-dependent gene transcription. *FEBS J* 2010;**277**:877–93.  
528 <https://doi.org/10.1111/j.1742-4658.2009.07508.x>.
- 529 29 Donovan PJ, Reed SI. Germline exclusion of Cks1 in the mouse reveals a  
530 metaphase I role for Cks proteins in male and female meiosis. *Cell Cycle*  
531 2003;**2**:275–6.
- 532 30 Berthet C, Aleem E, Coppola V, Tessarollo L, Kaldis P. Cdk2 knockout mice are  
533 viable. *Curr Biol* 2003;**13**:1775–85.
- 534 31 Ortega S, Prieto I, Odajima J, Martín A, Dubus P, Sotillo R, *et al.* Cyclin-  
535 dependent kinase 2 is essential for meiosis but not for mitotic cell division in mice.  
536 *Nat Genet* 2003;**35**:25–31. <https://doi.org/10.1038/ng1232>.
- 537 32 Motlík J, Sutovský P, Kalous J, Kubelka M, Moos J, Schultz RM. Co-culture with  
538 pig membrana granulosa cells modulates the activity of cdc2 and MAP kinase in  
539 maturing cattle oocytes. *Zygote* 1996;**4**:247–56.
- 540  
541

542 **FIGURE LEGENDS**

543 **Figure 1. Delayed GVBD and delayed/reduced MPF/MAPK activities in *cks2*<sup>-/-</sup> oocytes.**

544 (A) GV-stage *cks2*<sup>-/-</sup> oocytes display normal development. ICC analysis shows staining of DNA  
545 (DAPI- blue), cortical ACTIN (green), and LAMIN A/C (red) in *wt* and *cks2*<sup>-/-</sup> GV-stage  
546 oocytes. Scale bar, 30  $\mu$ m. (B) Delayed GVBD in *cks2*<sup>-/-</sup> oocytes. (C) Graphical representation  
547 of data in B. Timing of GVBD was 1.05 hours for *wt* oocytes and 3.10 hours for *cks2*<sup>-/-</sup> oocytes.  
548  $n \geq 18$  oocytes were analyzed. Data represent mean  $\pm$  SD. \*\*\* $P < 0.001$ , Student's t-test. (D)  
549 MPF and MAPK kinase activities are delayed and reduced in *cks2*<sup>-/-</sup> oocytes. GV-stage oocytes  
550 were stimulated to resume meiosis, harvested at the indicated times, and extracts subjected to *in*  
551 *vitro* kinase assays using HISTONE H1 (MPF) and MBP (MAPK) as substrates. (E)  
552 Immunoblots showing reduced p-MAPK, a marker of activation, in *cks2*<sup>-/-</sup> oocytes at 3 hours  
553 post-meiotic resumption. (F) ICC analysis showing the absence of phosphorylation of APC/C  
554 component CDC27 in *cks2*<sup>-/-</sup> oocytes at 7 hours post-meiotic resumption. Scale bar, 15-25  $\mu$ m.  
555 (G) ICC analysis demonstrating the persistence of SECURIN in *cks2*<sup>-/-</sup> oocytes at 8 hours post-  
556 meiotic resumption. Scale bar, 25  $\mu$ m.

557

558 **Figure 2. Reduced expression of MPF components *cdk1*, *ccna1*, and *ccnb1* in *cks2*<sup>-/-</sup> oocytes.**

559 (A) qRT-PCR analysis showing reduced expression of MPF components in *cks2*<sup>-/-</sup> oocytes.  
560 Expression of *cdk2* and *cdc20* are also shown. Data represent mean  $\pm$  SD. \*\*\*\* $P < 0.0001$ ,  
561 \*\*\* $P < 0.001$ , \*\* $P < 0.01$ , Student's t-test. (B) Reduced *cdk1* expression in *cks2*<sup>-/-</sup> oocytes,  
562 spermatocytes, and MEFs. Expression of *cks2* in *cks2*<sup>-/-</sup> MEFs restored the expression of *cdk1* to  
563 *wt* level. Data represent mean  $\pm$  SD. \*\*\* $P < 0.001$ , \* $P < 0.05$ , Student's t-test. (C)  
564 Immunoblots confirming reduced CDK1 in *cks2*<sup>-/-</sup> oocytes. ACTIN is shown as a loading

565 control. (D) Immunoblots showing reduced CDK1 in *cks2*<sup>-/-</sup> spermatocytes. (E) Immunoblot of  
566 p-Tyr15 CDK1 in *wt* and *cks2*<sup>-/-</sup> oocytes. GV-stage oocytes and oocytes at 3 hours post-meiotic  
567 resumption were analyzed. Normalized p-Tyr15 CDK1 is 1:1.40, *wt:cks2*<sup>-/-</sup>. (F-H) qRT-PCR  
568 analysis of *wee1* (F), *e2f1* (G), and *bmyb* (H) in *wt* and *cks2*<sup>-/-</sup> oocytes, spermatocytes, and MEFs.  
569 *wee1* and *e2f1* expression are restored in *cks2*<sup>-/-</sup> MEFs by enforced *cks2* expression. Data  
570 represent mean ± SD. \*\*\*\**P* < 0.0001, \*\*\**P* < 0.001, \*\**P* < 0.01, \**P* < 0.05, Student's t-test.

571

572 **Figure 3. Aberrant MI spindle assembly in *cks2*<sup>-/-</sup> oocytes can be rescued by MPF.** (A) ICC  
573 images showing aberrant MI spindles in *cks2*<sup>-/-</sup> oocytes, as indicated by TUBULIN (red) and  
574 DNA (DAPI- blue) staining. Scale bar, 10 μm. (B) Absence of appropriately resolved chiasmata  
575 in *cks2*<sup>-/-</sup> oocytes. ICC image shows TUBULIN (red), DNA (blue), and kinetochores (CREST -  
576 green). Scale bar, 5 μm. (C) Microinjection of active MPF into *cks2*<sup>-/-</sup> oocytes rescues the MI  
577 spindle defect. Scale bar, 10 μm. (D) *In vitro* kinase assays confirming the activities of  
578 microinjected MPF samples. Data represent mean ± SD. \*\*\**P* < 0.001, Student's t-test.

579

580 **Figure 4. Microinjection of MPF + CKS2 or CKS1 alone rescues the GVBD delay in *cks2*<sup>-/-</sup>**  
581 **oocytes.** Oocytes were injected with the indicated proteins and the timing of GVBD assessed by  
582 microscopic examination. Data represent mean ± SD. \**P* < 0.05, \*\**P* < 0.01, \*\*\**P* < 0.001,  
583 Student's t-test.

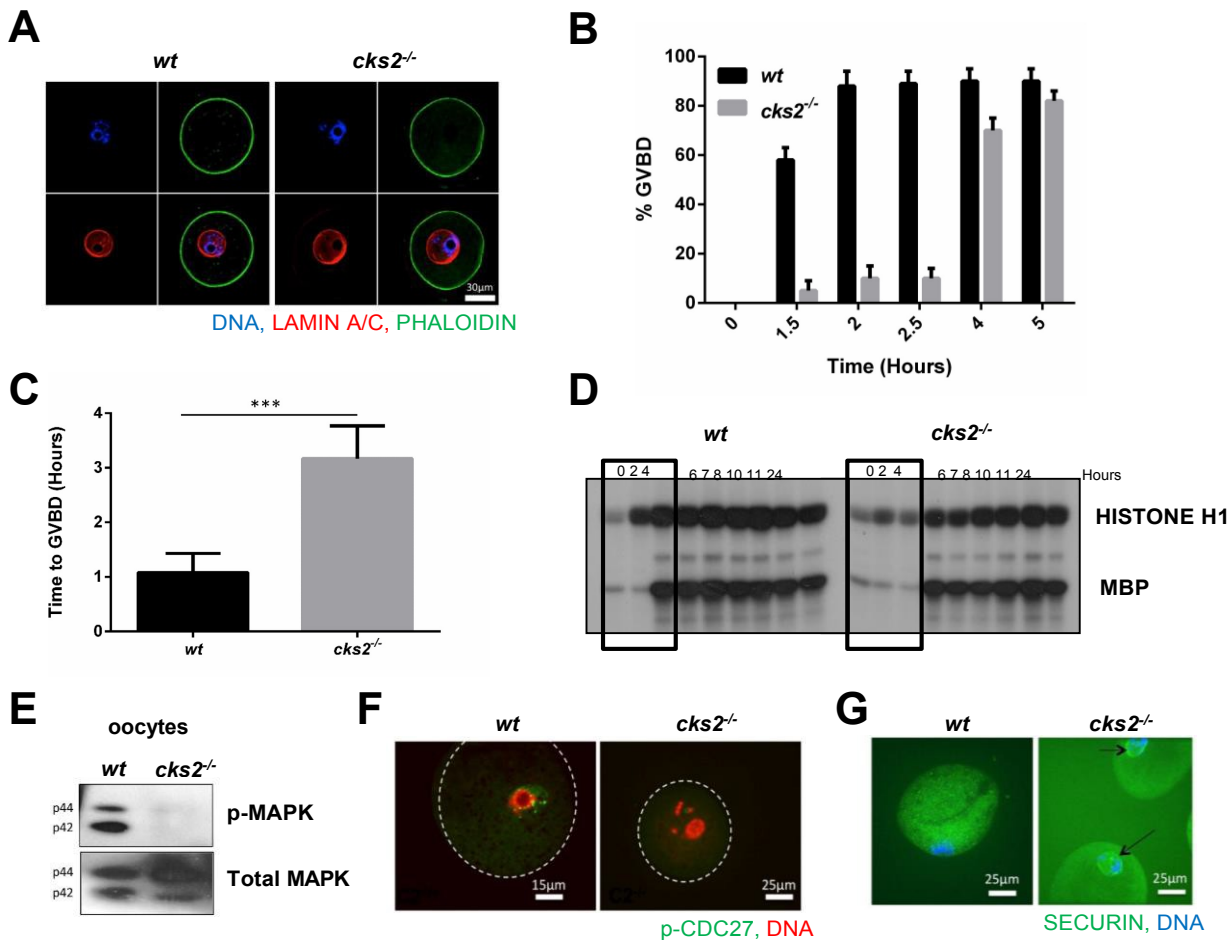
584

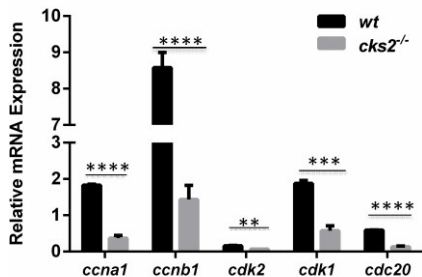
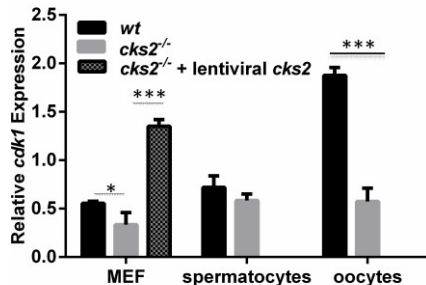
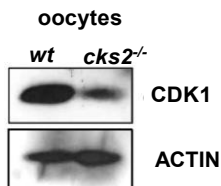
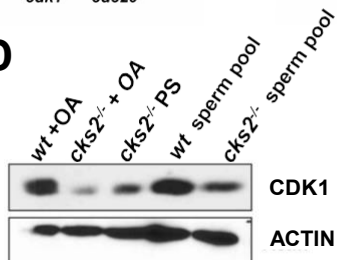
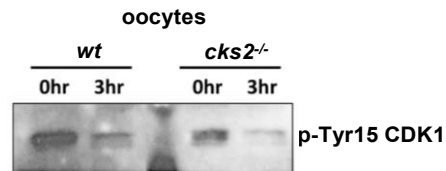
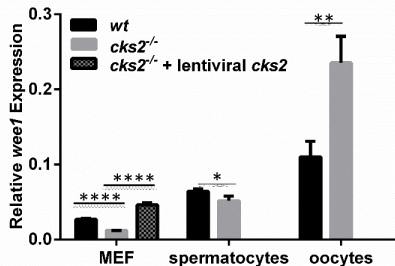
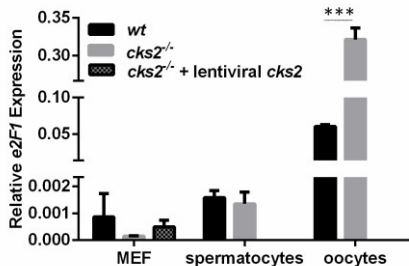
585 **Figure 5. *cks2*<sup>*cks1/cks1*</sup> knock-in mice arrest embryonic development at the 2-5-cell stage.** (A)  
586 Schematic showing the homologous recombination targeting strategy used to generate  
587 *cks2*<sup>*cks1/cks1*</sup> knock-in mice. (B) Genetic screening of ES clones for proper homologous



588 recombination events by southern blotting (top) and germline transmission of the *cks2<sup>cks1</sup>* allele  
589 by PCR (bottom). (C) Genotyping results of adult progeny and E7.5-E13.5 embryos from  
590 *cks2<sup>cks1/+</sup>* intercrosses showing the absence of homozygous mice and embryos. (D) Comparison  
591 of absorbed embryos from *wt* and *cks2<sup>cks1/+</sup>* intercrosses at E6.5. (E) Image showing absorbed  
592 embryos at E6.5 from *cks2<sup>cks1/+</sup>* intercrosses. Scale bar, 8  $\mu$ m. (F) *cks2<sup>cks1/+</sup>* intercrosses  
593 produce a prevalence of embryos arrested at the 2-cell- (15%) and 4-5-cell (16%) stage. Scale  
594 bar, 100  $\mu$ m. (G) Images of blastocysts and 2-5-cell embryos (left) and representative PCR  
595 genotyping showing the 2-5-cell stage embryos from *cks2<sup>cks1/+</sup>* intercrosses are *cks2<sup>cks1/cks1</sup>*. N, no  
596 DNA. Scale bar, 100  $\mu$ m. (H) Immunoblots showing reduced CDK1, increased p-Tyr15 CDK1,  
597 increased CDK2, and reduced p27<sup>KIP1</sup> in *cks2<sup>cks1/+</sup>* MEFs.

598



**A****B****C****D****E****F****G****H**